Raúl Periáñez

Modelling the Dispersion of Radionuclides in the Marine Environment

An Introduction

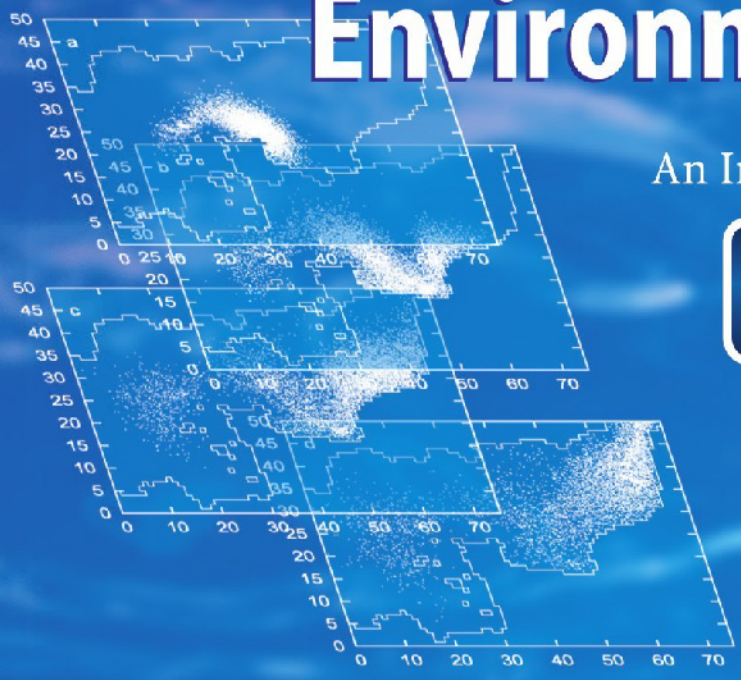

EXTRA MATERIALS
extras.springer.com

Springer

Raúl Periáñez

Modelling the Dispersion of Radionuclides in the Marine Environment

An Introduction

Raúl Periáñez

Modelling the Dispersion of Radionuclides in the Marine Environment

An Introduction

With 71 Figures

Springer

Dr. Raúl Periáñez
University of Seville, EUITA, Dept. of Applied Physics I
Ctra Utrera km 1, 41013 Seville
Spain
E-mail: *rperianez@us.es*

Library of Congress Control Number: 2005920454

ISBN 3-540-24875-7 **Springer Berlin Heidelberg New York**

Springer is a part of Springer Science+Business Media
springeronline.com

Printed in The Netherlands

Cover design: Erich Kirchner
Production: Luisa Tonarelli
Typesetting: Camera-ready by the author
Printing: Krips bv, Meppel
Binding: Litges + Dopf, Heppenheim

Printed on acid-free paper 30/2132/LT – 5 4 3 2 1 0

Dedicated to Pablo

Contents

The original version of appendix A was revised.
Equation A.8 on page 160 should read $\varepsilon = \frac{C_1 E^{\frac{3}{2}}}{\ell}$

1

Introduction

1.1 General objectives of the book

This is an introductory text on the topic of modelling radioactivity dispersion in the marine environment. It has been oriented in a very practical sense. Thus, we are not going in deep into all the theory that is behind equations and numerical schemes used to solved them. Also, this text may serve as a bibliography compilation about the topic, from the earliest box models to the most recent developments. Thus, we are citing only the most accesible documents (books and papers in well known international journals), and avoiding citations to internal institute reports, project reports etc...

Our intention is that the readers learn the basic principles on building a numerical dispersion model for the marine environment and, at the same time, know where to find more detailed information that may be useful in the future to develop more complex modelling applications.

In general, a marine dispersion model requires water currents to solve the transport equation for radionuclides. These currents are generally obtained from a hydrodynamic model. As a consequence, it is essential to have some knowledge on hydrodynamic modelling as well.

The most important processes governing radionuclide dispersion in the sea are reviewed in chapter 2. The transport equation is described in chapter 3, and some methods to solve it in a simple one-dimensional case are shown. These methods can be extended latter to more general 2D or 3D situations. The necessary hydrodynamic modelling is described in chapter 4 and, in chapter 5, hydrodynamic and dispersion models are linked. Other processes that affect the fate of radionuclide discharges in the sea, like interactions with solid particles (suspended matter and bottom sediments) and redox reactions (very important in the case of plutonium) are presented in chapter 6.

Another option for simulating dispersion consists of the use of a Lagrangian, or particle tracking, model. Instead of solving the dispersion equation, a discharge is modelled by a number of discrete particles whose tracks are followed individually, turbulent diffusion being described by a Monte Carlo

random walk process. These models are very useful for decision-making purposes, since give very fast answers. They are presented in chapter 7.

A practical case of a modelling study carried out to simulate the dispersion of ^{226}Ra (enhanced because the operation of fertilizer processing plants) in an estuarine system in southwest Spain is described in chapter 8. Generally speaking, modelling techniques for estuaries are the same as described before for the marine environment. Some ideas on sensitivity analysis are given in chapter 9, since this is the last stage in all modelling studies. Finally, in chapter 10, a brief review on some published radionuclide dispersion models for the marine environment is presented.

1.2 Why modelling radioactivity dispersion in the marine environment?

A model can be defined as a mathematical tool that simulates the behaviour of a given system. It is a huge simplification of an usually very complex reality and, consequently, models are imprecise. The modeller must select the most relevant processes to be included in the model, and derive or select the appropriate mathematical equations that describe such processes. Such equations are, usually, differential equations that have to be solved numerically in most of the cases. Thus, a computational code has to be developed to carry out the integration of the equations.

A model can predict the behaviour of the modelled system in response to a given external forcing. Thus, they can be used to provide inputs to decision-making processes. Also, a model can be used to test hypotheses concerning the environmental behaviour of a system when direct observations cannot be carried out or, for instance, are too expensive.

A model for radioactivity dispersion in the environment is a good example concerning the comments given above. The model describes the behaviour of a given radionuclide in a given environmental system. The model will include the most relevant processes governing the behaviour of the radionuclide, probably both physical and biogeochemical. These models can be used to assess the radioactive impact arising from deliberate or routine releases of radioactivity into the environment in a quantitative manner. They may provide concentrations of radionuclides in several environmental compartments, also including biota and the foodchain. Thus, can be used in the prediction of doses for radiological assessments. As discussed in [154], the objectives of any modelling study for radionuclide dispersion can be classified as:

- Description and characterisation of the environment.
- Prediction of the state of the environment as a result of an action. For instance, in the case of an accident where there is only limited data available in the early stages, a model can be used to predict concentrations of radionuclides and whether they will exceed defined limits.

- Monitoring. Models are used in a regulatory situation, to demonstrate compliance with standards set to protect man, biota and the environment.

A model should also give an insight into the processes responsible for the observed behaviour, not only a set of radionuclide concentrations at certain locations, compartments or instants of time. A general discussion on radionuclide dispersion models in the environment may be seen in [154, 164, 173].

A particular case would be a model for simulating radioactivity dispersion in the marine environment, which is the subject of this book. Frequently, they are used as tools to forecast the consequences of accidental releases and to support decision-making concerning remedial counter-measures. Model forecasts can help to detect and observe areas of high contamination, but may also serve for further dose assessments. They also help to monitor areas that are affected by permanent releases from reprocessing plants or other nuclear facilities.

But it is not only radioecology that benefits from numerical modelling of dispersion. Oceanographers are also interested in radionuclide dispersion modelling results: anthropogenic radioactivity can be a valuable oceanic tracer of currents and ocean circulation. Releases from nuclear fuel reprocessing plants are specially useful for this purpose since the input function is usually well known. Also, isotopic ratios for certain elements are constant and source specific. Thus, water is labeled and its transit through the ocean can be followed.

The process of building a model has several stages. First, environmental processes to be simulated must be selected, as well as model structure (temporal and spatial resolution etc). This is followed by the creation of a set of differential equations that captures the selected processes and model structure. This mathematical model must be translated into a computational code. Model calibration follows. It consists of selecting the appropriate parameter values that allow the reproduction of measurements. In some cases, it has to be done through simple trial and error. The model must be verified through the comparison of model output with a set of observations different to that used for model calibration. Finally, sensitivity analysis has to be carried out to study the model response to changes in input parameters. These stages will be studied along the book. However, it has to be pointed out that we will remain in the physico-chemical processes affecting radionuclide dispersion in the marine environment. Thus, neither radionuclide transfer to biological compartments nor dose calculations are studied.

1.3 Marine dispersion models: from box models to full 3D dispersion models for non conservative radionuclides

The first models developed to simulate the dispersion of radioactivity in the marine environment were compartment (or box) models for long-term dispersion [66]. Box models can be used for modelling radiological consequences of

radioactivity releases in the sea with spatial and temporal scales of several thousand kilometres and millenniums, respectively. In these models, the marine area to be studied is divided into a number of boxes which exchange radioactivity by means of effective transfer coefficients. These coefficients combine different transport mechanisms and are usually derived from basic oceanographic information. The box modelling approach uses two general assumptions for dispersion of radionuclides in oceanic space: (i) uniform and (ii) instantaneous mixing in each box. Exchanges of radionuclides between the water column and sediments are also included in these models by means of equilibrium distribution coefficients, since temporal resolution allows to assume that equilibrium is reached into each time step. The distribution coefficient, k_d, is defined as the ratio of specific activity in the solid and dissolved phases:

$$k_d = \frac{C_s}{C_d} \tag{1.1}$$

where C_s (Bq/kg) is activity concentration in the solid phase and C_d (Bq/m^3) is concentration in the dissolved phase at equilibrium. Thus the k_d is expressed in m^3/kg. The distribution coefficient describes the partitioning of radionuclides between the liquid and solid phases when the system is at equilibrium. Although conceptually very simple, these models are still being used for radiological assessment purposes [108, 75].

As an example, the computational domain of the compartment model described in [75] can be seen in figure 1.1, where the boxes are shown. The equations for the transfer of radionuclides between the boxes are of the form:

$$\frac{dA_i}{dt} = \sum_{j=1}^{n} k_{ji} A_j - \sum_{j=1}^{n} k_{ij} A_i - k_i A_i + Q_i \tag{1.2}$$

where $k_{ii} = 0$ for all i, A_i and A_j are activities (Bq) at time t in boxes i and j; k_{ij} and k_{ji} are transfer rates (y^{-1}) between boxes i and j; k_i is the effective activity transfer rate (y^{-1}) from box i taking into account loss of material from the compartment without transfer to another, for example radioactive decay; Q_i is a source of activity into box i (Bq/y) and finally n is the number of boxes in the system.

A box model for simulating ^{137}Cs dispersion in the Mediterranean Sea is described in [152]. The sea was divided into 40 boxes (10 horizontal regions with 4 layers each) shown in figure 1.2. Source terms include global fallout, Chernobyl, nuclear industry releases and river runoff. ^{137}Cs concentrations were predicted during the period 1954-1994.

In the model of Abril and García-León [2], a compartment approach is applied, although transfer coefficients between boxes are derived from the so-called stream function, related to the average water transport. The model also includes exchanges of radionuclides between water, suspended particulate matter and bed sediments described in terms of equilibrium distribution

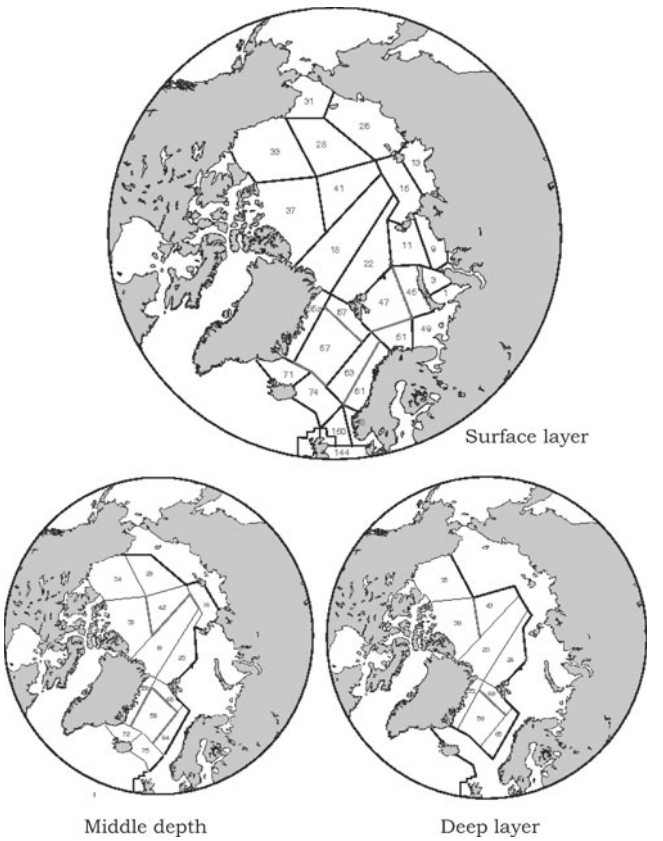

Fig. 1.1. Box structure for surface, mid-depth and deep waters of the Artic Ocean region in the model described in [75]

coefficients. It was applied to simulate the dispersion of ^{137}Cs and ^{239,240}Pu released from Sellafield reprocessing plant into the Irish Sea.

More recently, modellers have started including time-dependent flow fields. Thus, the hydrodynamic equations are solved to calculate currents at each point of the model domain and at each time step. These computed currents are then used to solve the advection-diffusion dispersion equation for radionuclide concentrations. This kind of dynamic models were first applied to conservative radionuclides, remaining dissolved [140, 114, 120, 122, 119, 63, 70, 9, 24]. An

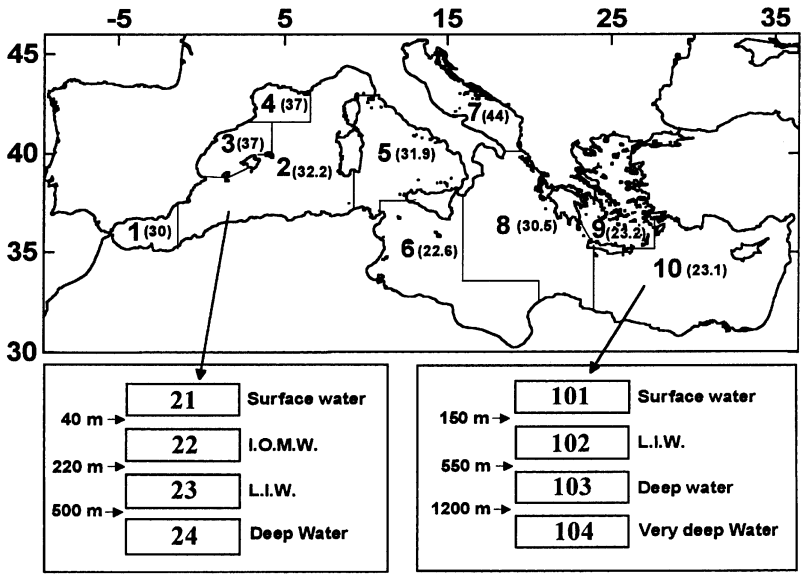

Fig. 1.2. Box structure for the model describing the Mediterranean Sea [152]

example of a computed current field is shown in figure 1.3. This model was developed to simulate the dispersion of radionuclides released from Sellafield nuclear fuel reprocessing plant into the eastern Irish Sea.

Obviously, the next step was to include the exchanges of radionuclides between the dissolved and solid phase in dynamic models. As commented before, in the case of box models this was achieved through the use of equilibrium distribution coefficients. This approach was also used in the model of Abril and García-León [2] and in [67, 169], that are not box models. However, if distribution coefficients are used, it is supposed that uptake/release reactions quickly reach an equilibrium. In coastal environments, geochemical, physical and sedimentological processes often occur on time scales that are of the order of one tidal cycle. These rapid coastal processes are likely to influence the outcome of interactions between sediments and contaminated waters. For instance, if contact time between water and sediments in a bay is shorter than the time required by uptake/release reactions to reach equilibrium, the dispersion away of dissolved radionuclides will be greater than predicted by these equilibrium models. At the same time, these models will be overestimating the activity fixed to the solid phase. In consequence, a kinetic approach is more adequate than an equilibrium one to describe the distribution of radionuclides between particles and solution [109]. Indeed, more recent dispersion models use the kinetic approach [94, 6, 12, 137, 85, 65, 115, 121, 123, 127, 130]. In this approach, it is considered that the exchanges of radionuclides between the

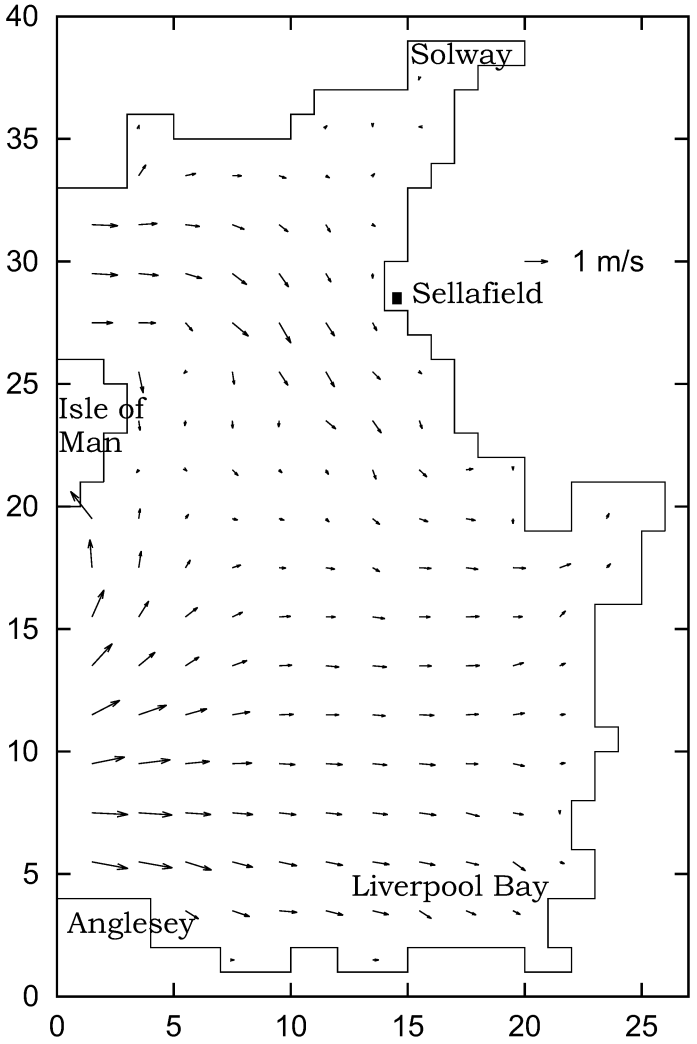

Fig. 1.3. Computed tidal currents in the Irish Sea when water level is increasing at Anglesey. Only one of each four vectors are shown. Each unit in the axis is the grid cell number. The Irish Sea model is described in [120, 122]

liquid and solid phases are described by a reversible reaction. A kinetic rate k_1 governs the transfer of radionuclides from water to particles and a kinetic coefficient k_2 governs the inverse process.

In recent times, more complex processes have been incorporated. For instance, the Irish Sea plutonium dispersion model described in [124] includes two different plutonium oxidation states, as well as redox reactions transforming each one into the other. Also, more complex kinetic models involving several parallel or consecutive reactions have been used to describe adsorption/desorption reactions. These models have been proposed by several authors to fit their adsorption laboratory experiments. The behaviour of several of these kinetic models when included into a marine dispersion model of the English Channel has been tested and compared in [131].

The spatial resolution of models has also evolved with time: from the coarse box models as shown for instance in figure 1.1, to fine finite difference grids with a resolution of a few kilometers or less. Some of the most recent models are also three-dimensional, thus they are able to provide information on the distribution of radionuclides in the water column. Examples of 3D models for conservative radionuclides are those described in [63, 70]. Several 3D models for non conservative radionuclides have also been described [94, 121, 126, 129]. Some 3D models for non conservative radionuclides can finally be applied in stratified waters (water density is not uniform along the water column). These density differences have to be included in the hydrodynamic equations since have strong influence on water circulation. Maybe they are the most sophisticated models. Examples are those in [94, 85], applied to an estuary in the Black Sea, and the model of the Rhone River plume presented in [132].

As commented previously, there is another kind of model: the Lagrangian or particle tracking model. In this type of model, water currents must be obtained as well from, generally, a hydrodynamic model. However, dispersion is solved in a different way. A discharge of radionuclides is simulated by a number of discrete particles. The path followed by each particle is then calculated, turbulent diffusion being simulated by a random walk method. Radionuclide concentrations can be calculated from the density of particles per water volume unit. Particle-tracking models have been used to simulate the dispersion of passive tracers [69, 64], oil spills [145, 146], radionuclides [153, 102, 103, 125, 133] and even contaminated milk [55] in coastal waters. The first particle tracking models could be applied only to dissolved contaminants. However, algorithms for including exchanges of radionuclides between the liquid and solid phases have recently been described [103, 125]. In reference [125], a particle tracking model for simulating radionuclide dispersion in the English Channel is described. As an example, the position of particles (dissolved) at several times after an instantaneous release from La Hague reprocessing plant are shown in figure 1.4. It can be seen that the cloud of particles moves towards Dover Strait due to the residual (average) circulation in the Channel.

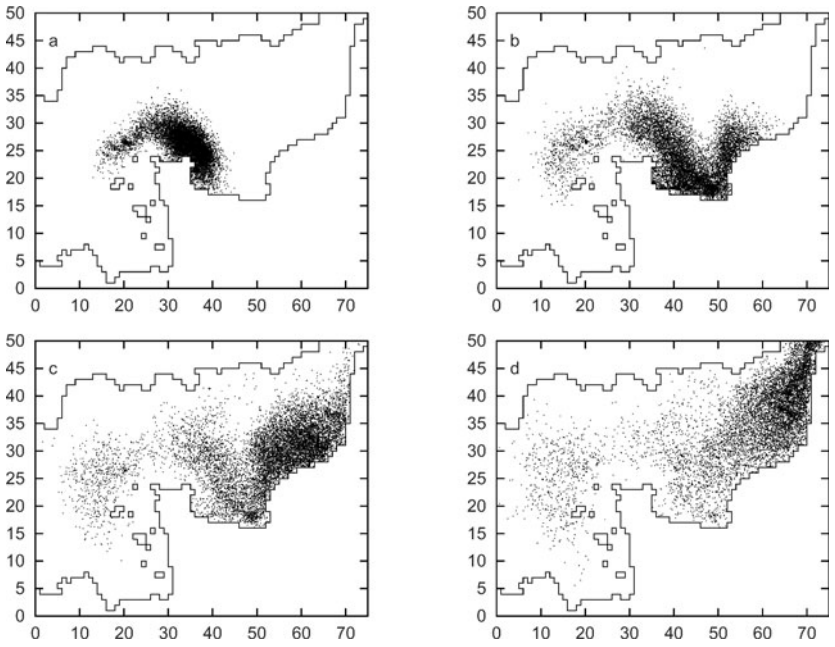

Fig. 1.4. Position of dissolved particles 20, 40, 60 and 80 days (a, b, c and d respectively) after an instantaneous release from La Hague. 50000 particles are used in the simulation

Finally, areas covered by recent models are very variable, from local models covering an estuary or a shelf sea, as for instance in [85, 67, 94, 12, 121, 123, 127], to models designed to simulate dispersion over an ocean or the whole oceanic space (global models) [102, 103, 70, 63, 169].

This increase in model resolution (both spatial and temporal), as well as in the complexity of simulated processes (for instance stratification and chemical reactions), has been possible because of the increase in computing power produced during the last times.

2

Model structure and processes

2.1 Processes governing radionuclide dispersion

The essential processes governing the dispersion of radionuclides in the marine environment are advective and diffusive transport. The advective transport is determined by the water circulation, whereas diffusion represents the subgrid scale turbulent mixing. Advection is contaminant transport due to the movement of water. Water movement may be caused by tides, wind or density differences. Due to diffusion, a patch of contamination increases its size and, simultaneously, maximum concentrations are reduced.

In a general form, the time evolution of radionuclide concentration dissolved in water, C, is given by the transport advection/diffusion equation:

$$\frac{\partial C}{\partial t} + \frac{\partial uC}{\partial x} + \frac{\partial vC}{\partial y} + \frac{\partial wC}{\partial z} = K_h \left(\frac{\partial^2 C}{\partial x^2} + \frac{\partial^2 C}{\partial y^2} \right) + K_v \frac{\partial^2 C}{\partial z^2} \tag{2.1}$$

where u, v and w are the components of water velocity at each point in the x, y and z directions respectively, and K_h and K_v are the horizontal and vertical diffusion coefficients, assumed to be constant.

There are two basic approaches for solving the transport equation: the Eulerian approach calculates the exchange of radionuclides between adjacent grid boxes for each time step. The Lagrangian approach applies a particle tracking method to follow the path of particles in time, as has been commented before.

If a 2D depth averaged model is used, it is assumed that radionuclide concentration is constant through the water column, and the transport equation is reduced to:

$$\frac{\partial C}{\partial t} + \frac{\partial uC}{\partial x} + \frac{\partial vC}{\partial y} = K_h \left(\frac{\partial^2 C}{\partial x^2} + \frac{\partial^2 C}{\partial y^2} \right) \tag{2.2}$$

These transport equations are valid for conservative radionuclides, that move in a dissolved form without being significantly fixed to suspended sediments, bottom sediments or biota.

Decay of radionuclides, described by the radioactive decay constant λ, is easily included in the transport equation by adding the term

$$-\lambda C \tag{2.3}$$

to the right hand side of equations 2.1 and 2.2. A source term can also be added if a specific release must be simulated.

The conservative behaviour of a radionuclide depends on its k_d distribution coefficient. Thus, radionuclides are generally considered as conservative if $k_d < 10^4$ L/kg. For instance, the average value for the distribution coefficient of Cs given in [74] is 3×10^3 L/kg. However, depending on the intention of the investigation, even for a low k_d radionuclide, the use of a conservative approach may be critical. For instance, Cs has been considered as conservative in several modelling works [102, 63, 169]. However, several models have also been proposed to describe Cs uptake by sediment particles [131] since this process may be relevant in environments with high suspended matter concentrations or in shallow waters, where radionuclide adsorption by bed sediments may also be significant. Thus, the conservative character of a radionuclide depends not only on its geochemical behaviour, but on environmental conditions as well (including water salinity, temperature, pH etc...). Consequently, k_d values for a given radionuclide generally vary over several orders of magnitude [74].

The first models for non conservative radionuclides [2] were based upon the equilibrium distribution coefficient, or the partition coefficient. The last gives the fraction of the total activity in a parcel of water that remains dissolved [107, 67]:

$$PC_w = \frac{1}{1 + k_d m} \tag{2.4}$$

where k_d is the distribution coefficient of the corresponding radionuclide and m is the suspended load concentration. However, if distribution or partition coefficients are used it is supposed that uptake/release reactions quickly reach an equilibrium [48]. This approach is valid in the case of long term box models, due to the large time steps used. However, if the interest lies on short term processes, for instance tidal dispersion, equilibrium is not reached inside each time step (that may be of the order of the minute or less). In this case, it is more appropriate to use a kinetic approach to describe the transfers of radionuclides between the liquid and solid phases [109].

Radionuclides are fixed to suspended particles and the bed sediment. Radionuclides in the dissolved phase and suspended particles are transported by advection and diffusion processes. Suspended particles may be deposited on the bed and, depending on the magnitude of the currents, the bed sediment may be eroded. This implies a transfer of radionuclides from the bed sediment to the suspended particle phase. At the same time, desorption of radionuclides from the bed and suspended particles occurs. Adsorption is described by a kinetic coefficient k_1 and desorption by a coefficient k_2. All these processes are

summarized in figure 2.1, taken from [115], where a grid cell incorporating these processes is shown. In this model, two grain size fractions are considered in the bed sediment: only the small particles can be resuspended and incorporated into the water column as suspended matter.

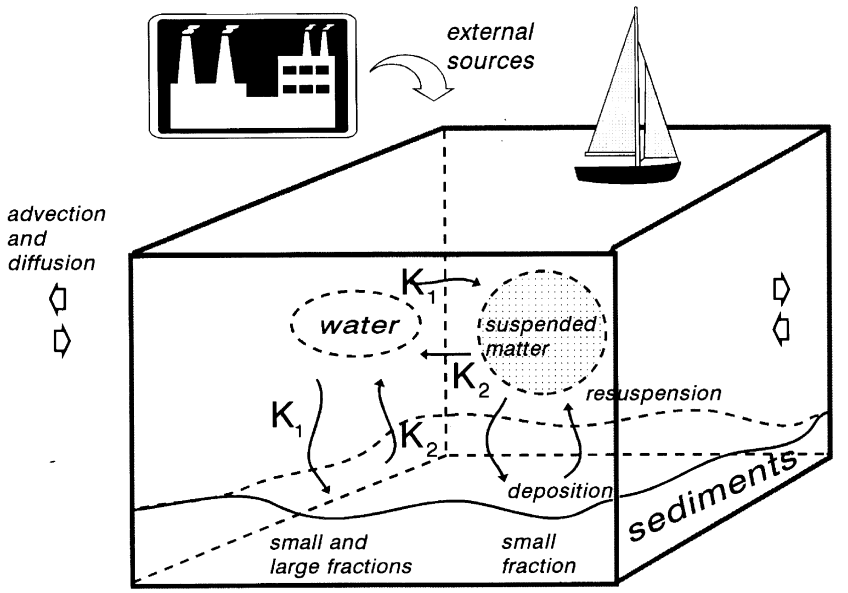

Fig. 2.1. Grid cell showing processes affecting the dispersion of non conservative radionuclides

These processes can be described by appropriate differential equations. The suspended load in the water column must also be known. This requires solving additional equations for the transport of suspended matter. Some more detail will be given in chapter 6.

Some other processes may be relevant for specific radionuclides. For instance, the behaviour of plutonium in aquatic systems is of considerable complexity due to the fact that it can exist in different oxidation states simultaneously. Thus, Pu (III) and Pu (IV) predominate as the reduced and Pu (V) and Pu (VI) as the oxidized forms. The reduced Pu is highly particle reactive and has been shown to possess a distribution coefficient that is two orders of magnitude higher than that of the more soluble oxidized Pu [100]. Hence the values observed in field measurements represent the properties of the mixture of oxidation states that is present in the particular sample. To overcome this problem, Irish Sea models described in [3, 121] used a mean distribution

coefficient and mean kinetic transfer coefficients, respectively. Nevertheless, the main difficulty is that the oxidation state of Pu changes with time: Pu is released from Sellafield in a reduced form and after some days an equilibrium in the partition of Pu between the reduced and oxidized species is achieved. In the Irish Sea model presented in [124] redox reactions are described in terms of reaction velocities. Thus, the rate at which plutonium is oxidized is considered to be proportional to the concentration of reduced plutonium at each particular point. The proportionality factor is the oxidation velocity β_1. Similarly, the rate at which plutonium is reduced is considered to be proportional to the concentration of oxidized Pu. The proportionality factor will be now the reduction velocity, denoted as β_2. A scheme showing the processes included in the model is presented in figure 2.2. It can be seen that different kinetic coefficients for adsorption are used for each Pu oxidation state, since they present different affinities for the solid phase. However, the same coefficient k_2 is used to describe release from the solid particle. Of course, the number of equations to be solved is doubled since it is necessary to solve separately the dispersion of each plutonium specie.

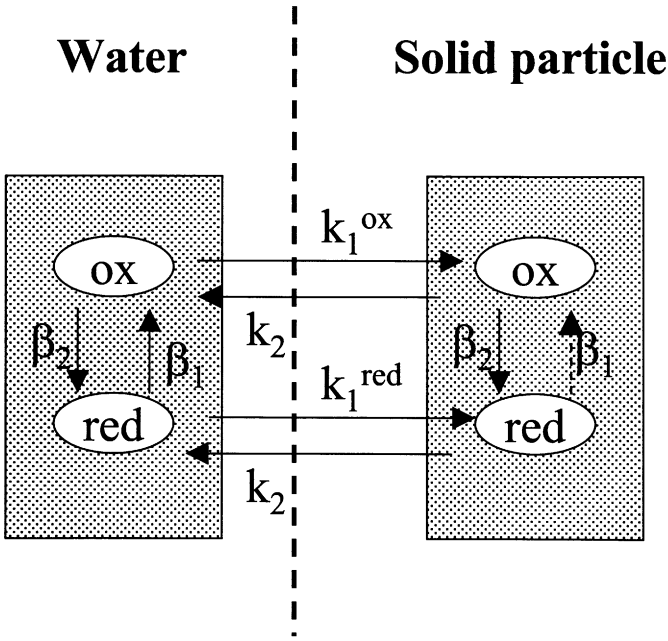

Fig. 2.2. Scheme of the interactions between the dissolved and solid phases in the Irish Sea plutonium dispersion model described in [124]

2.2 Model configuration. Resolution

Numerical models consists of a set of equations which are solved at discrete time steps on a regular or irregular grid that covers the area of interest. A modelling study starts with the selection of the model domain (area covered), the definition of the grid used to solve the equations (for instance 2D or 3D) and the determination of the grid size and time step. The spatial extension of the model is the most obvious difference between different modelling approaches. Following this aspect, dispersion models based on hydrodynamic models (long term box models will not be discussed) have been classified as follows in [154]:

- Near field or local applications that deal with estuaries, fjords, bays or straits. Typical size of the model domain is 1-100 km and typical grid size is 0.01 to 5 km.
- Medium range or regional scale applications that deal with shelf areas or semi-enclosed seas like the North Sea, Black Sea or Kara Sea. Typical size of the model domain is 100-1000 km and typical grid size is 5 to 50 km.
- Far field or global/basin scale applications that deal with large ocean basins or whole oceans like for instance the Artic or Pacific. Global ocean models (cover all oceans) also belong to this class. Typical size of the model domain is 1000 km - global scale and typical grid size is 10 to 500 km.

The selection of the model domain and grid can also be influenced by the source of radionuclides to be considered. Atmospheric sources like fallout from bomb testing or accidents (Chernobyl) use to be very diffuse and affect waters on a large spatial scale. This would require large model domains and coarse grids. On the other hand, marine sources discharge directly into the sea, as is the case of nuclear fuel reprocessing plants (Sellafield or Cap de La Hague, in UK and France respectively) or sunken nuclear ship reactors. These represent point sources allowing for near field or medium range modelling applications.

The physical characteristics of the studied area will affect the type of model to be used. For instance, in areas well mixed in the vertical, a 2D depth averaged model can be a good approach since radionuclide distribution along the water column will be homogeneous. This is generally the case in shallow areas like the Irish Sea or in very energetic environments like the English Channel, where tides produce an effective mixing in the vertical. In deep or stratified waters, where there may be significant gradients in the vertical direction, a full 3D model should be used. For instance, in the case of the Rhone River mouth, the low mixing of the discharge waters gives place to a well-identified surface freshwater plume in which a thin upper layer (1 or 2 m) is separated from the ambient seawater by a sharp density gradient. This plume extends 20 or 30 km offshore. Numerical modelling of these plumes is a difficult task that requires the inclusion of density differences in the full 3D hydrodynamic equations, since water circulation in the plume is essentially governed by such density gradients. Salinity changes also affect the behaviour

of radionuclides, which tend to be redissolved as salinity increases. These processes have been considered in a model developed to simulate the transport of Cs and Pu by the Rhone River plume [132].

Of course, a 3D model is a much more computationally expensive approach than a 2D depth averaged model. In this sense, the temporal discretisation of the model should be as coarse as possible to save computational time. The maximum time step size, Δt, is limited (unless implicit methods are used to solve the equations; we are going to describe only explicit schemes) by several stability conditions imposed by the hydrodynamic equations and the advection and diffusion terms in the transport equation. This will be discussed in detail later. Moreover, time step must be smaller than the characteristic time of the process in which we are interested. For instance, if the model is designed to simulate tidal dispersion, it has no sense to use a time step of, say, 1 day, since tidal period is shorter than a single time step.

If the interest lies on temporal scales much longer than tidal cycles, residual circulation can be used. This is the average water circulation obtained by averaging the flows computed from the hydrodynamic equations over a time longer than cyclic fluctuations. The transport equation is then solved using this average circulation. This way, the stability condition imposed by the solution of the hydrodynamic equations is avoided and we are limited only by those due to the transport equation (which are less restrictive than the first). As a consequence, a longer time step can be used. Simultaneously, water currents have not to be computed for each time step, which is increasing computation speed as well.

Finally, a new stability condition is due to the terms describing the exchanges of radionuclides between the liquid and solid phases in the case of non conservative radionuclides. This condition is less restrictive than those derived from the advection and diffusion terms, but may be relevant in the case of very reactive radionuclides. This was the case in the Rhone River plume model when applied to simulate plutonium dispersion [132]. It will be described in chapter 6.

2.3 Mixing time scales

Several time scales have been introduced to quantify the transport processes within a water body. Sometimes different definitions and formulations in terms of calculations appear between different authors. The following definitions are those given by Prandle [140].

If a radioactive release (or any material in general) is introduced at point (x_0, y_0) within a sea region, then at any position (x, y) the following time scales may be defined:

Age: time required to travel from (x_0, y_0) to (x, y).
Residence time: time required to travel from (x, y) to the boundary of the region.

Transit time: time required to travel from (x_0, y_0) to the boundary of the region.

In references [123, 151], transit times from La Hague to different points in the English Channel and North Sea were calculated. However, these transit times actually correspond to the definition of age given above.

Age is not easy to calculate. Since dissolved material moves both by advection and diffusion, a patch becomes rapidly distorted and the age is not simple to obtain, both experimentally and numerically. Salomon et al. [151] defined the transit time (age) between two points as the lapse of time which gives the best similarity between signals (concentrations versus time) in the two locations. This similarity is quantified by the cross correlation function between the two local series, that is defined as:

$$\theta(\tau) = \frac{< C_1(t)C_2(t+\tau) >}{\sqrt{< C_1(t)^2 >}\sqrt{< C_2(t)^2 >}} \tag{2.5}$$

where θ is the cross correlation function, C_1 and C_2 are concentrations at the two locations and $<>$ means time averaging. The maximum of the cross correlation function occurs for a given value of τ, which is a statistical evaluation of the transit time between the two points.

This definition was used in [151] and [123] to calculate age from La Hague to Dover Strait in the English Channel. In the first reference a long term dispersion model was used. In the second one tides were explicitly solved. However, ages obtained from both models, for a conservative radionuclide, were in good agreement. In the case of ^{239,240}Pu, computed age was significantly larger than for conservative radionuclides [123] due to the higher reactivity of this radionuclide, which tends to remain fixed to suspended matter and bed sediments.

More rigorous definitions are introduced in references [20, 46], which are beyond our scope. They were used to estimate age and residence time in a tidal estuary by means of a three dimensional hydrodynamic model [156].

The turn over time for a bounded region is defined as the time for the total mass of material initially within the region to be reduced by a factor e^{-1}. The flushing time is defined exactly the same in [142]. In general, the value of the turn over time increases with the dimensions of the initial region considered.

3

Introduction to the transport equation

3.1 Introduction

The advection/diffusion dispersion equation has been presented in the previous chapter. Now it will be studied in more detail. In particular, some of the numerical methods used to solve it are described in the case of a one-dimensional dispersion problem in a fluid with constant and homogeneous flow. These methods can be extended to the cases of 2D or 3D dispersion and variable flow. Equations are solved by finite differences: the differential equation is discretized on a regular grid and transformed into an algebraic equation. Then, the values of the concentrations at the new time level are obtained from their vales at the previous one.

The advection and diffusion terms are studied separately in the following sections. Stability conditions imposed by these terms are also discussed.

3.2 Advection

Let us start with the one dimensional advection problem described by the following equation:

$$\frac{\partial C}{\partial t} + u\frac{\partial C}{\partial x} = 0 \tag{3.1}$$

where C is the concentration of radionuclides, $u > 0$ is the water velocity and $0 \leq x \leq \infty$. This equation describes the variations of concentrations along the x axis due to advection by an uniform and constant velocity u. As a simplification, we have initially assumed that the velocity is directed to the right (positive).

To construct a finite difference scheme to solve this equation, the one dimensional grid shown in figure 3.1 is applied. The one-dimensional fluid is divided into a number of cells with length Δx numbered from left to right. The concentration of the radionuclide is defined at the centre of each cell,

and the velocity of the fluid at the right side. This is not relevant in what follows since it is assumed, to construct the finite difference scheme, that the velocity is uniform over the grid. However, it has to be taken into account if the velocity is not uniform over the model domain.

The differential equation is then transformed into an algebraic equation. From this equation, the values of the concentrations at each cell are obtained from their values in the previous time level.

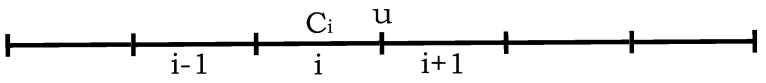

Fig. 3.1. One dimensional grid used to solve the dispersion equation. Velocity is assumed to be constant and positive. C is defined at the centre of each cell and u at the right side of the cell

A simple finite difference form of equation 3.1 is the following:

$$\frac{C_i^* - C_i}{\Delta t} = -u\frac{C_i - C_{i-1}}{\Delta x} \tag{3.2}$$

where C_i^* is concentration at cell i at the new time level and Δt is the time step used for the integration. This scheme is explicit since concentrations appearing at the right side are known from the old time level. Thus C_i^* can be easily obtained.

It can be noted that the spatial derivative has been written in a backwards form:

$$\frac{\partial C}{\partial x} = \frac{C_i - C_{i-1}}{\Delta x} \tag{3.3}$$

instead of using the forward formulae

$$\frac{\partial C}{\partial x} = \frac{C_{i+1} - C_i}{\Delta x} \tag{3.4}$$

The time derivative is defined at the centre of the grid cell, where C is defined. However, the spatial derivative is centered at the left side of the cell (is shifted to the direction where the current comes from, i.e., upstream). This is the reason why this numerical scheme is denoted as *upstream advection scheme*. Indeed, if the water current is directed to the left ($u < 0$), the numerical scheme would be

$$\frac{C_i^* - C_i}{\Delta t} = -u\frac{C_{i+1} - C_i}{\Delta x} \tag{3.5}$$

where it can be seen that again the spatial derivative is shifted upstream (in this case is centered at the right side of the cell).

The time step used in the calculations cannot be arbitrarily large, but is restricted by the following stability condition:

$$\Delta t < \frac{\Delta x}{u} \tag{3.6}$$

It means that the amount of radioactivity extracted from a grid cell by the current in a time step must be smaller than the total radioactivity content into the cell, which is obvious.

This stability condition can be avoided if an implicit scheme is applied. This will not be described here, although may be consulted in [84]. Essentially, in an implicit scheme the spatial derivative is defined at the new time level. In consequence, C_i^* cannot be worked out directly.

There are also other schemes that can be applied to the advection equation, as those based on centered derivative and angular derivative. Discussion may be found in [84].

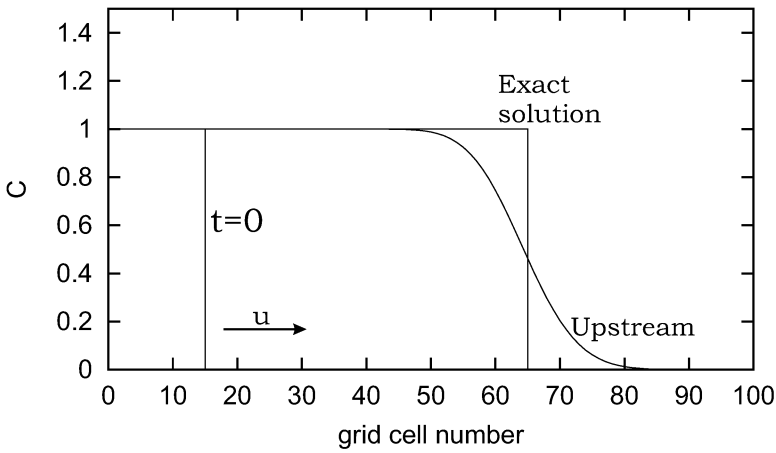

Fig. 3.2. Solution of the advection equation with the upstream scheme and exact solution. The field of concentrations at $t = 0$ is also shown

The upstream scheme may be implemented in such a way that the stability condition 3.6 is satisfied, buy anyway very often does not provide a correct solution of the advection process. The main problem arises from the so-called numerical diffusion. As a consequence of numerical diffusion, gradients of concentrations are not only advected with velocity u, but also their shapes change in time in such a way that the gradients are progressively smoothed. It can be clearly seen with the help of figure 3.2, where the advection of a vertical front using the upstream scheme is shown together with the exact solution. After some iterations the front is not vertical. Instead there is a continuous decrease in concentrations from 1 to 0.

Numerical diffusion is due to the fact that a finite difference scheme is always only an approximation to the real differential equation describing the advection problem. Expressions for the derivatives shown above are indeed obtained from Taylor's series from which only a finite number of terms are retained. Thus, some error is always introduced since many terms are neglected. Indeed, the upstream scheme is only a first order accuracy scheme. It can be seen in figure 3.2 that the effect of numerical diffusion is exactly the same as if we add a real diffusion to the exact solution. The magnitude of the diffusion coefficient that produces the present numerical diffusion is [140]:

$$K_{num} = \frac{1}{2}(u\Delta x - u^2\Delta t) \tag{3.7}$$

Thus, depending on the particular problem (grid size, time step and typical velocities), numerical diffusion may be more or less relevant. Ideally, if an upstream scheme is applied, K_{num} should be much smaller than the real turbulent diffusion coefficient. In our example $\Delta x = 100$ m, $\Delta t = 10$ s and u=1 m/s. Thus, the numerical diffusion coefficient is $K_{num} = 45$ m^2/s.

A method to reduce excessive numerical diffusion consists of the use of a higher order scheme for advection. In general, an advection scheme must be monotonic (or positive definite). It means that concentrations are conserved (negative values nor artificial maximum are produced). The upstream method is positive definite, as can be seen in figure 3.2. In other schemes, dispersive waves are generated (artificial oscillations in the solution).

A second order accuracy scheme that works rather well is the MSOU scheme (Monotonic Second Order Upstream), described in [171]. It is, obviously, monotonic and does not generate dispersive waves. The advection equation is written in the following form:

$$\frac{C_j^* - C_j}{\Delta t}\Delta x = T_{j-1} - T_j \tag{3.8}$$

with

$$T_j = F_j u_j \tag{3.9}$$

The first order upstream scheme is obtained if $F_j = C_j$. In the MSOU:

$$F_j = C_j + \frac{1}{2}\psi_j \Delta C_j \tag{3.10}$$

where $\Delta C_j = C_j - C_{j-1}$ and

$$\psi_j = \max[0, \min(2r_j, 1), \min(r_j, 2)] \tag{3.11}$$

with

$$r_j = \frac{C_{j+1} - C_j}{C_j - C_{j-1}} \tag{3.12}$$

This is valid in the case of flow in the positive direction. The space index must be switched if the flow is in the opposite direction. The MSOU scheme is a

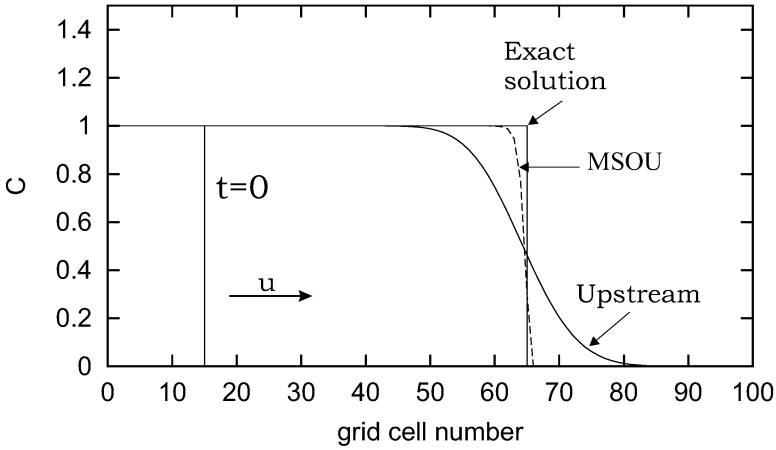

Fig. 3.3. Solution of the advection equation with the upstream scheme, MSOU (dashed line) and exact solution. The field of concentrations at $t = 0$ is also shown

second order correction to the upstream scheme. Later, it will be extended to flow in arbitrary direction and to a 2D form.

The same advection problem in figure 3.2 has been solved with the MSOU scheme. Results are presented in figure 3.3, where the upstream and exact solutions are also shown. It can be seen that the MSOU scheme introduces much less numerical diffusion than the upstream, approaching better the exact solution. Of course, it is computationally more expensive and a little more difficult to program (indeed, the upstream scheme is rather easy to implement).

3.3 Diffusion

The diffusion part of the transport equation will be treated now. It accounts for the reduction of the maximum concentrations and the size increase of a patch of contamination due to molecular diffusion (random movement of particles inside a fluid). However, in real marine dispersion problems, turbulence produces a mixing that is much larger than that due to pure molecular diffusion. The intensity of mixing is characterized through the diffusion coefficient K. The effective diffusion coefficient due to turbulent mixing is many orders of magnitude larger than the pure molecular diffusion coefficient ($K \sim 10^{-6}$ m^2/s). As a consequence, molecular diffusion is neglected when studying dispersion in the sea. Indeed, the time required by a contaminant patch to travel a distance s due to diffusion is given by $t = s^2/K$. Thus, if the only process is molecular diffusion, transit over a 100 km distance would require $\sim 10^8$ years. Typical values for turbulent diffusion coefficients used in shelf sea models are of the order of $10^0 - 10^1$ m^2/s. Thus, travel time for the same distance is re-

duced to $\sim 10^1 - 10^2$ years because of turbulent mixing. A review on diffusion may be seen in [72].

Again, in a simple one-dimensional problem, the diffusion equation can be written as:

$$\frac{\partial C}{\partial t} = K \frac{\partial^2 C}{\partial x^2} \tag{3.13}$$

where the diffusion coefficient K is assumed to be constant. This equation can be written in finite differences using the same grid as for the advection equation (figure 3.1). A second order accuracy can be obtained centering the second derivative at the center of the grid cell where equation is solved:

$$\frac{\partial^2 C}{\partial x^2} = \frac{1}{\Delta x}\left(\frac{C_{i+1} - C_i}{\Delta x} - \frac{C_i - C_{i-1}}{\Delta x}\right) = \frac{C_{i+1} + C_{i-1} - 2C_i}{\Delta x^2} \tag{3.14}$$

Thus the diffusion equation is written if finite differences, for constant K, in the following way:

$$\frac{C_i^* - C_i}{\Delta t} = K \frac{C_{i+1} + C_{i-1} - 2C_i}{\Delta x^2} \tag{3.15}$$

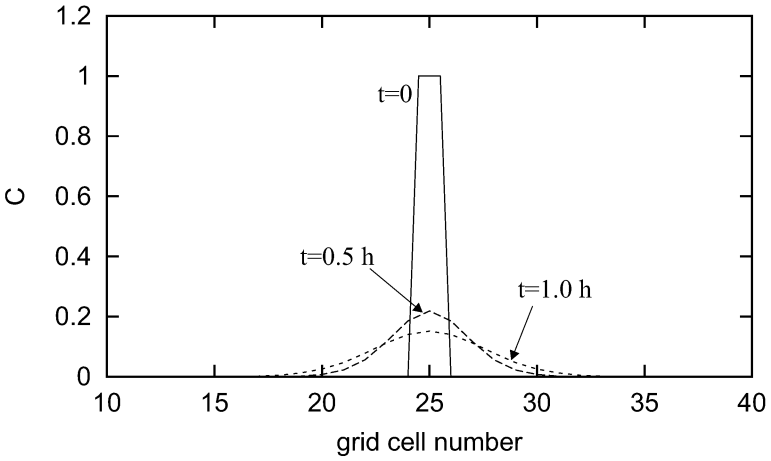

Fig. 3.4. Computed concentrations at several times resulting from the solution of the diffusion equation

An example of the solution of the diffusion equation with this scheme is shown in figure 3.4. The same computation grid as in figures 3.2 and 3.3 is used. Initial concentrations over the grid are zero except for cell $i = 25$, where $C = 1.0$. Concentrations at $t = 0$, $t = 0.5$ h and $t = 1.0$ h are shown. It can be seen that the magnitude of the peak decreases with time while the patch size

increases. In this simulation an arbitrary diffusion coefficient $K = 10\ \mathrm{m}^2/\mathrm{s}$ is used.

The finite difference scheme for diffusion given in equation 3.15 can be easily extended to the general case in which the diffusion coefficient is not constant with the help of the finite difference form of the second derivative (equation 3.14). The diffusion coefficient is defined on the grid at the right side of the cell (the same point as the velocity). For a non constant diffusion coefficient, the diffusion equation must be written in a slightly different way:

$$\frac{\partial C}{\partial t} = \frac{\partial}{\partial x}\left(K\frac{\partial C}{\partial x}\right) \tag{3.16}$$

Using the finite difference form of the second derivative given by the first part of equation 3.14, this equation is discretized as follows:

$$\frac{C_i^* - C_i}{\Delta t} = \frac{1}{(\Delta x)^2}[K_i(C_{i+1} - C_i) - K_{i-1}(C_i - C_{i-1})] \tag{3.17}$$

The diffusion term introduces a stability condition, as occurred with advection. For a one-dimensional diffusion problem this condition is:

$$\Delta t < \frac{(\Delta x)^2}{2K} \tag{3.18}$$

This condition is generally less restrictive than the imposed by the advection equation. Thus, in our example, the stability condition due to advection is

$$\Delta t < \frac{\Delta x}{u} = \frac{100}{1} = 100\,\mathrm{s}$$

while that due to diffusion is

$$\Delta t < \frac{(\Delta x)^2}{2K} = \frac{100^2}{2 \times 10} = 500\,\mathrm{s}.$$

However, the last condition may be relevant if a very fine grid is used. This is the case, for instance, to solve vertical diffusion in the water column where a high resolution is required (when there is stratification and a high resolution is needed to solve mixing at the pycnocline, i.e., the density jump). In this case an implicit scheme should be used. Some of them are described in [84], although a numerical scheme that is easy to implement is the Saul'ev one.

In the Saul'ev method the direction in which the numerical grid is swept alternates for each time step. In the first time step (and all subsequent odd time steps) the grid is swept from low to high i. The difference equation in this case is:

$$\frac{C_i^* - C_i}{\Delta t} = \frac{K}{(\Delta x)^2}[(C_{i+1} - C_i^*) - (C_i - C_{i-1}^*)] \tag{3.19}$$

At the following time step (and all even time steps) the grid is swept from high to low i and the difference equation is:

$$\frac{C_i^* - C_i}{\Delta t} = \frac{K}{(\Delta x)^2}[(C_{i+1}^* - C_i) - (C_i^* - C_{i-1})] \tag{3.20}$$

Although this scheme is implicit in the notation (values of the concentrations at the new time level appear at the right side of the equations), it can be solved explicitly (C_i^* can be worked out) since C_{i-1}^* and C_{i+1}^* in equations 3.19 and 3.20 respectively have been calculated immediately before the calculation of C_i^*.

A common problem when a real model is being developed consists of the selection of appropriate diffusion coefficients. Actually, the diffusion term represents sub-grid scale turbulent mixing: eddies smaller than the grid size that, as a consequence, can not be solved. The value of the diffusion coefficient should depend on the grid size: coarse grids require large diffusion coefficients and viceversa. In other words, turbulent diffusion is advection that can not be solved by the numerical scheme due to the finite grid size. As the grid size is reduced, smaller and smaller eddies can be explicitly solved as advection, and the diffusion coefficient must be reduced. After some experiments, the following parameterization for the diffusion coefficient has been proposed and used in some models [110, 45]:

$$K = 0.2055 \times 10^{-3} \Delta x^{1.15} \tag{3.21}$$

As an example, this equation gives a diffusion coefficient of 1.3 m^2/s for a grid size equal to 2 km.

Turbulent mixing is also affected by the so-called shear dispersion. The water current is not uniform along the water column. It has a maximum value at the surface and is reduced with increasing depth. Finally velocity is zero at the sea bed due to friction with the bottom. This velocity profile is the origin of the shear dispersion. If a patch is released at the surface, it is partially transported downwards the water column due to diffusion. But radionuclides at the surface are advected faster than radionuclides at deeper positions since velocity at the surface is larger. Thus, the patch suffers a deformation as indicated in figure 3.5, towards the direction of the current in the upper part of the water column. Then a larger diffusion in the vertical direction is produced since it depends on the concentration gradient, that is higher in the direction of the current. The overall result of these processes is an enhanced dispersion (due to vertical shear in currents) and a lengthening of the patch in the current direction. Shear dispersion is automatically considered in 3D models, since they solve the vertical current profile, but not in the case of 2D depth averaged models.

Horizontal shear of currents also produces shear dispersion. In the case of a channel, for instance, currents are larger at the centre than along shores due to friction with them. Shear effect will enhance mixing along the channel. If the channel is solved with a 2D model, this horizontal shear is included since the hydrodynamic model automatically produces the current distribution commented above. However, if a 1D model is applied, the effective diffusion coefficient must be increased to account for this horizontal shear. This

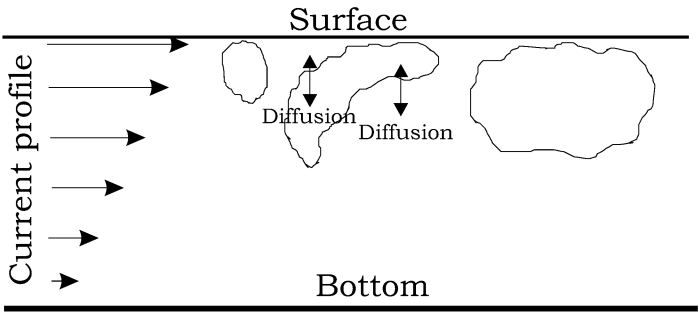

Fig. 3.5. Shear dispersion. A patch at the surface deforms in the current direction near the surface due to the higher velocities here. Vertical mixing then occurs. The final result is a higher effective diffusion

was the situation when a 1D model was applied to simulate dispersion in the Suez Canal [9].

3.3.1 Vertical diffusion in the sea

A vertical diffusion coefficient must be defined as well if the dispersion model is three dimensional, as for instance generally occurs in particle-tracking models. The vertical diffusion coefficient depends on the water depth and on the stability of the water column. Thus, it is usually higher close to the surface because of the generation of turbulence by winds and surface waves. On the other hand, in a sea with stable stratification (density increases as depth increases) vertical turbulent movement of particles is inhibited because more energy is required to transfer more dense water to a higher level and viceversa. As a consequence, the generation of turbulence, and hence turbulent diffusion is precluded. Moreover, if there exists a halocline or a thermocline (a sharp salinity or temperature gradient respectively), a sharp density gradient is also generated (a pycnocline). The pycnocline acts as a barrier for vertical mixing. Indeed, vertical diffusion coefficients in this area may be close to the molecular diffusion coefficient. In practice, the two water masses separated by the pycnocline do not mix one with the other.

Of course, the simplest way to parameterize the vertical diffusion coefficient consists of using a constant value. Typical diffusion coefficients are of the order of 10^{-3} m^2/s. This approach is usually applied in particle tracking models, in which rapid computations are generally required.

Actually, turbulence is characterized by the coefficient of vertical eddy viscosity A_v. The vertical diffusion coefficient may be obtained from it [84]:

$$\frac{K_v}{A_v} = \sigma \tag{3.22}$$

where the non-dimensional number σ ranges from 0.1 to 0.5. Nevertheless, it is also usual to take the vertical diffusion coefficient equal to the vertical eddy viscosity. Vertical eddy viscosity describes diffusion of momentum, while the diffusion coefficient describes the diffusion of salt, temperature and dissolved tracers.

Eddy viscosity is not a function of the fluid, but of the flow. A simple approach consists of taking it as:

$$A_v = C_V \sqrt{\bar{u}^2 + \bar{v}^2}\ H \tag{3.23}$$

where C_V is a dimensionless experimentally measured coefficient, $\bar{u}$ and $\bar{v}$ are depth mean currents along the x and y axis respectively and H is water depth. This formulation has given good results for tidal flow studies [79] and has been applied in the Irish Sea radionuclide dispersion model described in [120, 121, 129].

In the Kolmogorov-Prandtl formulation, eddy viscosity is written as a function of a mixing length and turbulent kinetic energy:

$$A_v = C_0 \ell E^{1/2} \tag{3.24}$$

where C_0 is a numeric constant obtained from calibration, ℓ is mixing length and E is turbulent kinetic energy. Different approaches vary in the way that ℓ and E are obtained. These methods are denoted as turbulence closure models.

In the simplest closure model, both ℓ and E are obtained from algebraic expressions. More complex approaches consist of using 1-equation or 2-equation closure models. In the 1-equation model ℓ is determined from an algebraic expression while kinetic energy is determined from a balance equation that must be solved over the model domain:

$$\frac{\partial E}{\partial t} = \text{production} + \text{diffusion} - \text{dissipation} \tag{3.25}$$

This kind of turbulence model is described with some more detail in appendix A. In the 2-equation model an additional equation is used to determine ℓ. A more detailed description of turbulence models is beyond the scope of this book. More details may be seen, for instance, in [38, 41, 42].

4

Solving hydrodynamics

4.1 Introduction

The hydrodynamic equations will be presented and a method to solve them is described. The solution of these equations provides the magnitude of the water currents at each point of the model domain, which are required to solve the advective terms in the transport equation.

Several model configurations may be adopted. The most general equations are the full 3D hydrodynamic equations, also including baroclinic terms (density differences. These density differences may generate currents that also affect the transport of radionuclides). A 2D vertical model can also be used: they are useful in case of fjords, for instance, in which circulation in the transverse direction is negligible. However, the most popular model is the 2D depth-averaged one. Depth averaged models can be applied when the water column is well mixed in the vertical. The model provides the magnitude of the depth-averaged current and, when the transport equation is solved, the radionuclide concentrations are assumed to be homogeneous through the water column. Examples of 2D depth-averaged hydrodynamic models may be seen in [60, 139, 122, 62, 61, 167, 163, 133], although in some of them, covering very large areas, the hydrodynamic equations are written using spherical coordinates (latitude change is automatically included in this coordinate system).

If the time scale in which we are interested must solve explicitly tidal mixing, the hydrodynamic equations will provide currents and water surface elevations over the model domain and for each time step, which must be smaller than the tidal period. These instantaneous currents are used to solve the transport equation. However, if our interest lies on a scale much longer than tidal periods (say years), average currents may be used to solve the transport equations. This is the so-called residual circulation.

The 2D depth-averaged hydrodynamic equations and an easy method to solve them are described. Boundary conditions must be specified to solve the equations. Thus, several boundary conditions commonly used are presented.

Some comments about tides are also included. Next, residual transport is described briefly. Full 3D hydrodynamic equations are presented in appendix A.

4.2 Hydrodynamic equations

The most general equations for describing water circulation in the marine environment are the Navier-Stokes equations, although it is not clear if they should be denoted as Saint-Venant equations. The reason is that a set of equations equivalent to that of Navier-Stokes was published earlier by Saint-Venant, although it seems that he only obtained the 1D equations. The French scientific community generally prefers the Saint-Venant denomination. Two approximations are used in most hydrodynamic models, that are:

- Hydrostatic: it ignores the vertical accelerations of water since are very small when compared to the acceleration due to gravity. Thus, if vertical acceleration is small and the flow is essentially horizontal, the equation of vertical motion is replaced by a simple hydrostatic pressure law.
- Boussinesq: considers that water density variations are small. Thus, an average density is used in all terms of the hydrodynamic equations except in the terms describing explicitly the horizontal pressure gradients.

The 2D depth-averaged hydrodynamic equations (obtained through integration of the hydrostatic and Boussinesq 3D equations in the vertical direction) may be written in the following form for an incompressible and homogeneous sea (constant density):

$$\frac{\partial z}{\partial t} + \frac{\partial}{\partial x}(Hu) + \frac{\partial}{\partial y}(Hv) = 0 \tag{4.1}$$

$$\frac{\partial u}{\partial t} + u\frac{\partial u}{\partial x} + v\frac{\partial u}{\partial y} + g\frac{\partial z}{\partial x} - \Omega v + \frac{\tau_u}{\rho_w H} = A\left(\frac{\partial^2 u}{\partial x^2} + \frac{\partial^2 u}{\partial y^2}\right) \tag{4.2}$$

$$\frac{\partial v}{\partial t} + u\frac{\partial v}{\partial x} + v\frac{\partial v}{\partial y} + g\frac{\partial z}{\partial y} + \Omega u + \frac{\tau_v}{\rho_w H} = A\left(\frac{\partial^2 v}{\partial x^2} + \frac{\partial^2 v}{\partial y^2}\right) \tag{4.3}$$

where u and v are the depth averaged water velocities along the x and y axis, D is the depth of water below the mean sea level, z is the displacement of the water surface above the mean sea level measured upwards, $H = D + z$ is the total water depth, Ω is the Coriolis parameter ($\Omega = 2w \sin\beta$, where w is the Earth rotational angular velocity and β is latitude), g is acceleration due to gravity, ρ_w is water density and A is the horizontal eddy viscosity. τ_u and τ_v are sea bed friction stresses that are usually written in terms of a quadratic friction law:

$$\begin{aligned} \tau_u &= k\rho_w u\sqrt{u^2 + v^2} \\ \tau_v &= k\rho_w v\sqrt{u^2 + v^2} \end{aligned} \tag{4.4}$$

where k is the bed friction coefficient, obtained from model calibration. This means that the friction coefficient is changed, by trial and error, until computed currents and elevations reproduce measurements.

These equations are written in rectangular coordinates. Their transformation into spherical coordinates may be seen, for instance, in [84]. However, we will limit our analysis to rectangular coordinates.

The second and third terms in 4.2 and 4.3 are the non-linear or advective terms. The next is the gravity term: it generates currents when the sea surface is not horizontal. The Coriolis term accounts for the rotation of the Earth. In these equations, it is assumed that atmospheric pressure acting on the sea surface is constant.

In many shallow water models, tidal currents are strong (of the order of 1 m/s) and bottom friction is large. In these conditions, it is possible to obtain a stable solution of the hydrodynamic equations without including the horizontal friction terms ($A = 0$). However, in deep water and in regions with abrupt bottom topography (the shelf edge for instance), it is necessary to retain the horizontal viscous terms to have a stable solution.

The effect of wind can be incorporated by adding the terms

$$-\frac{\tau_x^w}{\rho_w H} \tag{4.5}$$

$$-\frac{\tau_y^w}{\rho_w H} \tag{4.6}$$

to the left hand side of equations 4.2 and 4.3 respectively. The components of the wind stress along the x and y axis are:

$$\tau_x^w = C_D \rho_a |W| W \cos\theta \tag{4.7}$$

$$\tau_y^w = C_D \rho_a |W| W \sin\theta \tag{4.8}$$

where ρ_a is air density, W is wind velocity and θ is the direction to which the wind blows measured counter clockwise from east. C_D is a dimensionless drag coefficient. An acceptable value for C_D is [147]:

$$C_D = (0.63 + 0.066W) \times 10^{-3} \tag{4.9}$$

if W is given in m/s and measured 10 m above the sea surface.

It is finally possible to include the influence of horizontal density gradients by adding the following terms to the left hand side of equations 4.2 and 4.3 respectively [140]:

$$\frac{Hg}{2\rho_w}\frac{\partial \rho_w}{\partial x} \tag{4.10}$$

$$\frac{Hg}{2\rho_w}\frac{\partial \rho_w}{\partial y} \tag{4.11}$$

The density of water may be obtained from the water salinity and temperature through a standard equation of state, as for instance in appendix A and as described in [84]. In the Boussinesq approximation, a constant reference value for the density ρ_w is used in all terms in the hydrodynamic equations except in the partial derivatives in 4.10 and 4.11. The water density derived from the equation of state is used only to evaluate such derivatives.

4.3 Numerical solution

The hydrodynamic equations will be solved using finite differences. Thus, the differential equations are transformed into a set of algebraic equations. The values of elevations and currents at the present time level are obtained from their values in the previous one, as with the transport equation. An explicit scheme can be used. It means that the equations can be rearranged to work out the value of the current or elevation at the present time level, as commented before. In particular, the scheme used in [60] will be described.

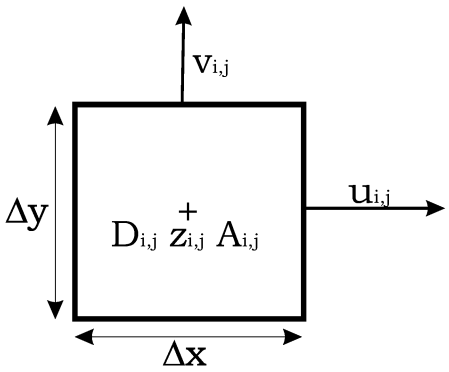

Fig. 4.1. Grid cell i, j showing where the different magnitudes are defined

The area of interest is covered by a grid in which the equations are solved. A grid cell is represented in figure 4.1. All magnitudes must be defined in a particular point of the grid cell. Thus, water depth, horizontal viscosity and elevations are defined at the centre of the cell, the u component of the current is defined at the centre of the right side and the v current component at the centre of the top side. Each grid cell is denoted by its grid coordinates (i, j), and grid size in the x and y direction is Δx and Δy respectively.

Solution starts by the continuity equation 4.1. The time derivative is written in the following form:

$$\frac{\partial z}{\partial t} = \frac{z^*_{i,j} - z_{i,j}}{\Delta t} \tag{4.12}$$

where z^* is the value of the surface elevation at the present time level, to be calculated, and z is its value at the old time level. Since this equation is used to calculate z^*, that is defined at the centre of the grid cell, all derivatives must be centered at the grid cell center. Thus, the following term in equation 4.1 is written as:

$$\frac{\partial}{\partial x}(Hu) = \frac{H_1 u_{i,j} - H_2 u_{i-1,j}}{\Delta x} \tag{4.13}$$

where H_1 and H_2 are water depths at the right and left sides of the grid cell respectively. They are defined as:

$$H_1 = 0.5(H_{i,j} + H_{i+1,j}) \tag{4.14}$$

$$H_2 = 0.5(H_{i,j} + H_{i-1,j}) \tag{4.15}$$

The last term is written in a similar way:

$$\frac{\partial}{\partial y}(Hv) = \frac{H_3 v_{i,j} - H_4 v_{i,j-1}}{\Delta y} \tag{4.16}$$

with

$$H_3 = 0.5(H_{i,j} + H_{i,j+1}) \tag{4.17}$$

$$H_4 = 0.5(H_{i,j} + H_{i,j-1}) \tag{4.18}$$

Once that the new values of the surface elevation, z^*, have been obtained over the whole model domain, the equation for the u current component is solved. The time derivative is again:

$$\frac{\partial u}{\partial t} = \frac{u^*_{i,j} - u_{i,j}}{\Delta t} \tag{4.19}$$

Since u is defined at the right side of the grid cell, all derivatives must be centered at this point. The gravity term is written as:

$$\frac{\partial z}{\partial x} = \frac{z^*_{i+1,j} - z^*_{i,j}}{\Delta x} \tag{4.20}$$

Note that the new values of the elevations are used since they have been previously calculated. The Coriolis term must be defined at the right side of the grid cell. Thus v is obtained through averaging:

$$\Omega v = \Omega v_p \tag{4.21}$$

where

$$v_p = \frac{1}{4}(v_{i,j} + v_{i,j-1} + v_{i+1,j-1} + v_{i+1,j}) \tag{4.22}$$

Similarly, the friction term must be defined at the same point again. Thus, it is:

$$k\frac{u^*_{i,j}\sqrt{u^2_{i,j} + v^2_p}}{H^*_1} \tag{4.23}$$

Note that again v is defined as v_p and that the new values of H_1 and of the velocity, outside the root, are used. This improves the solution stability.

Several approaches may be used for treating the nonlinear terms, which are described in detail in [60]. However, the simplest option will be presented here. The first derivative is written as:

$$u\frac{\partial u}{\partial x} = u_{i,j}\frac{u_{i+1,j} - u_{i-1,j}}{2\Delta x} \tag{4.24}$$

again defined at the cell right side. The second derivative must be centered at the same point, of course. The following approach may be used:

$$v\frac{\partial u}{\partial y} = \frac{0.5(v_{i,j} + v_{i+1,j})u_{i,j+1} - 0.5(v_{i,j-1} + v_{i+1,j-1})u_{i,j-1}}{2\Delta y} \tag{4.25}$$

The horizontal friction term, assuming that A is constant (which is the usual), is expressed in the form:

$$\begin{aligned} &A\left(\frac{\partial^2 u}{\partial x^2} + \frac{\partial^2 u}{\partial y^2}\right) \\ &= A\left(\frac{u_{i+1,j} + u_{i-1,j} - 2u_{i,j}}{\Delta x^2} + \frac{u_{i,j+1} + u_{i,j-1} - 2u_{i,j}}{\Delta y^2}\right) \end{aligned} \tag{4.26}$$

It may be noted that the non linear and horizontal friction terms, when evaluated close to an open boundary (see next section), require velocities not defined since correspond to points outside the model domain. A solution proposed in [60] consists of omitting these terms within a distance from the open boundary equal to the grid size.

Thus, the differential equation is transformed into an algebraic equation that can be arranged to calculate $u^*_{i,j}$. A similar treatment is used for the v equation, that is finally solved. When defining u_p for the Coriolis and friction terms, the u^* values are used since they have already been calculated.

A question is how to select the time step to solve the equations. It cannot have any arbitrarily large value, but is limited by a stability condition. In the case of gravity waves (tides), the stability condition is denoted as the CFL (Courant-Friedrichs-Lewy) criterion. In a 2D flow, and if the grid size is the same in the x and y directions ($\Delta x = \Delta y$), it is written as

$$\Delta t < \frac{\Delta x}{\sqrt{2gH}} \tag{4.27}$$

and means that the time step must be shorter than the travel time of the tide wave over one grid cell. There are ways to avoid this limitation (the use of implicit methods). These methods are outside our scope and some discussion may be found in [84, 172].

4.4 Computing tidal currents. Boundary conditions

We have studied in the previous section how the hydrodynamic equations can be written in finite differences. These equations are solved over the grid covering the model domain. However, to obtain a solution, boundary conditions must be defined. Initial conditions must be provided as well to start calculations.

Two different boundary types have to be considered: closed boundaries (coastline) and open boundaries appearing since the model domain is finite, covering only a portion of a sea. Along the coastline, the normal component of the velocity is set to zero.

Open boundaries are artificial in the sense that have no physical meaning. They are just a line drawn in a map. Water elevations or normal currents are prescribed along the open boundaries from observations. These boundary conditions represent the *outside world* and usually we only have limited information on what is happening there. This will be a source of error. Errors in boundary data propagate inside the computational domain and the solution cannot be better than the boundary data. Also, boundary conditions will lead to a partial reflection of waves traveling outside the grid. This will be discussed below.

As an example, the computational grid for the Gibraltar Strait model described in [133] is shown in figure 4.2. We have two closed boundaries along the Spain and Morocco coasts and two N-S open boundaries. If we want to calculate tidal circulation in the Strait, tidal forcing must be prescribed along the open boundaries. The simplest way is usually to prescribe tidal elevations as a function:

$$z(t) = h\cos(wt - g) \tag{4.28}$$

where h and g are amplitude and phase (relative to some defined time zero) of the tide, respectively, and w is the tide angular speed. This way the tide is described by a harmonic wave. However, real tides consist of many harmonics with different amplitudes, phases and angular speeds. Thus, several functions in the form of equation 4.28 have to be used.

The current component that is normal to the boundary must also be provided somehow. There are several ways to estimate it, which are described in detail in [76]. Let us denote ϕ the normal current component to be estimated. The simplest condition is the clamped, in which the magnitude does not change in time:

$$\frac{\partial \phi}{\partial t} = 0 \tag{4.29}$$

For instance, in the west open boundary in figure 4.2, it would be written as:

$$u^*_{0,j} = u_{0,j} \tag{4.30}$$

Note that the boundary condition provides the velocity for $i = 0$. This is because velocity for $i = 1$ can be calculated directly from the hydrodynamic

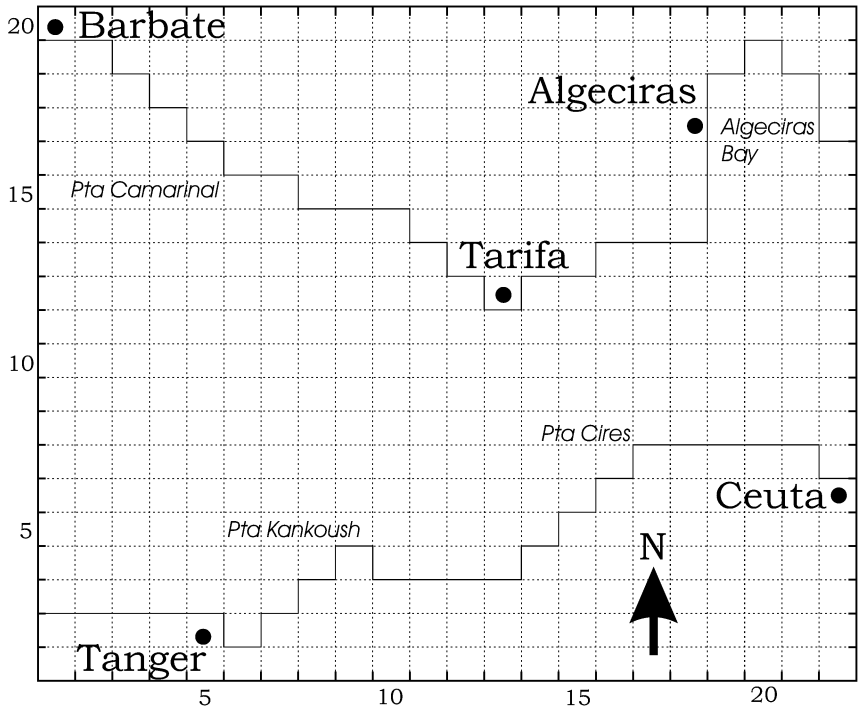

Fig. 4.2. Example of a computational grid covering the Strait of Gibraltar. Each unit in the axis denote the grid cell number. The size of the grid cell is $\Delta x = \Delta y = 2500$ m

equations, without requiring any boundary data. Thus, care must be taken when dimensions of matrixes are defined in the computational code.

In tidal flows this condition has no sense since the currents change during the tidal cycle. Nearly as simple is the zero gradient condition:

$$\frac{\partial \phi}{\partial n} = 0 \tag{4.31}$$

where the derivative is taken normal to the open boundary. In our example it is written in the form:

$$u^*_{0,j} = u^*_{1,j} \tag{4.32}$$

These conditions are fully reflective for gravity waves. Adding both equations leads to an improved condition:

$$\frac{\partial \phi}{\partial t} + \frac{\partial \phi}{\partial n} = 0 \tag{4.33}$$

which radiates out waves with a non-dimensional phase speed of 1. The numerical form is found by inserting values for the gradient at the new time

level or by adding equations 4.30 and 4.32:

$$u^*_{0,j} = \frac{1}{2}(u_{0,j} + u^*_{1,j}) \tag{4.34}$$

The most sophisticated boundary conditions are the so-called radiation conditions, that assume a free propagation of waves outside the domain. They are based upon the one-dimensional wave equation

$$\frac{\partial \phi}{\partial t} + c\frac{\partial \phi}{\partial n} = 0 \tag{4.35}$$

where c is the non-dimensional phase speed. Following [111], and as explained in detail in [84], the phase speed is calculated, if it is directed outward from the computational domain, in this way:

$$c = -\frac{\partial \phi / \partial t}{\partial \phi / \partial n} \tag{4.36}$$

In this equation, the derivatives are known from the previous time level. Estimation of c is performed one grid cell distance from the boundary. Computation proceeds as follows. First, the non dimensional phase velocity is calculated from:

$$c = \begin{cases} -\frac{\phi^*_{b-1} - \phi_{b-1}}{\phi_{b-1} - \phi_{b-2}} & 0 \leq c \leq 1 \\ 1 & c > 1 \\ 0 & c < 0 \end{cases} \tag{4.37}$$

Next, the new value of ϕ at the boundary, ϕ^*_b, is calculated:

$$\phi^*_b = (1 - c)\phi_b + c\phi_{b-1} \tag{4.38}$$

This way, in our example, the boundary u values are obtained from the following equations:

$$u^*_{22,j} = cu_{21,j} + (1 - c)u_{22,j} \tag{4.39}$$

with

$$c = \begin{cases} -\frac{u^*_{21} - u_{21}}{u_{21} - u_{20}} & 0 \leq c \leq 1 \\ 1 & c > 1 \\ 0 & c < 0 \end{cases} \tag{4.40}$$

and

$$u^*_{0,j} = (1 + c)u_{0,j} - cu_{1,j} \tag{4.41}$$

with

$$c = \begin{cases} -\frac{u^*_1 - u_1}{u_2 - u_1} & -1 \leq c \leq 0 \\ -1 & c < -1 \\ 0 & c > 0 \end{cases} \tag{4.42}$$

If the denominator of the fraction appearing in the calculation of c is zero, the sign of the numerator must be taken into account to decide if $c = 0$ or

is equal to 1 or -1 (depending if we are in the right or left boundary). These expressions can be extended to the cases of north and south open boundaries.

A simple option for progressive waves, that often works well [84, 120] and does not require additional calculations, consists of writing the normal component of the current, ϕ, as a function of tidal elevation just inside the grid:

$$\phi = \pm\sqrt{\frac{g}{D}}\, z \tag{4.43}$$

the sign is selected so that the water current has the correct direction according to the water level (positive or negative).

As commented before, initial conditions have to be prescribed as well. The simplest and most usual initial condition assumes that the water is initially at rest and with a horizontal water level, although this does not occur in reality. The influence of these wrong initial data gradually fades out due to wave damping by bottom friction (and if boundary conditions do not reflect, by radiation to the *outside world*). In the meantime the flow gets more and more influence by external forces or incoming waves so that it forgets the initial situation. To determine whether the influence of initial conditions has been sufficiently reduced, a possibility (in the case of periodic tides) consists of checking whether the results for two consecutive tidal periods coincide. Otherwise, a good check is obtained by starting the model from two different initial conditions and observing convergence of the results.

Water depths must be finally provided to start calculations. They are often taken from bathymetric maps through interpolation of iso-depth lines. Data are stored in a file that will be read by the code before starting computations.

As a summary, calculations are carried out in the following sequence:

1. Read water depths.
2. Prescribe elevations along open boundaries.
3. Solve the equation for z^* sweeping the computational grid.
4. Solve the equation for u^*.
5. Give open boundary conditions for u^*
6. Solve the equation for v^*.
7. Give open boundary conditions for v^*.
8. Make $z = z^*$, $u = u^*$ and $v = v^*$.
9. Jump to step 2 to continue time integration.

An example of results from the hydrodynamic model of the English Channel described in [122] is presented in figure 4.3, where computed and measured current magnitude and direction at a point in the central part of the Channel are shown for a situation of medium tides. Another example of results obtained from a hydrodynamic model was given in figure 1.3, where a map of computed currents in the Irish Sea is shown.

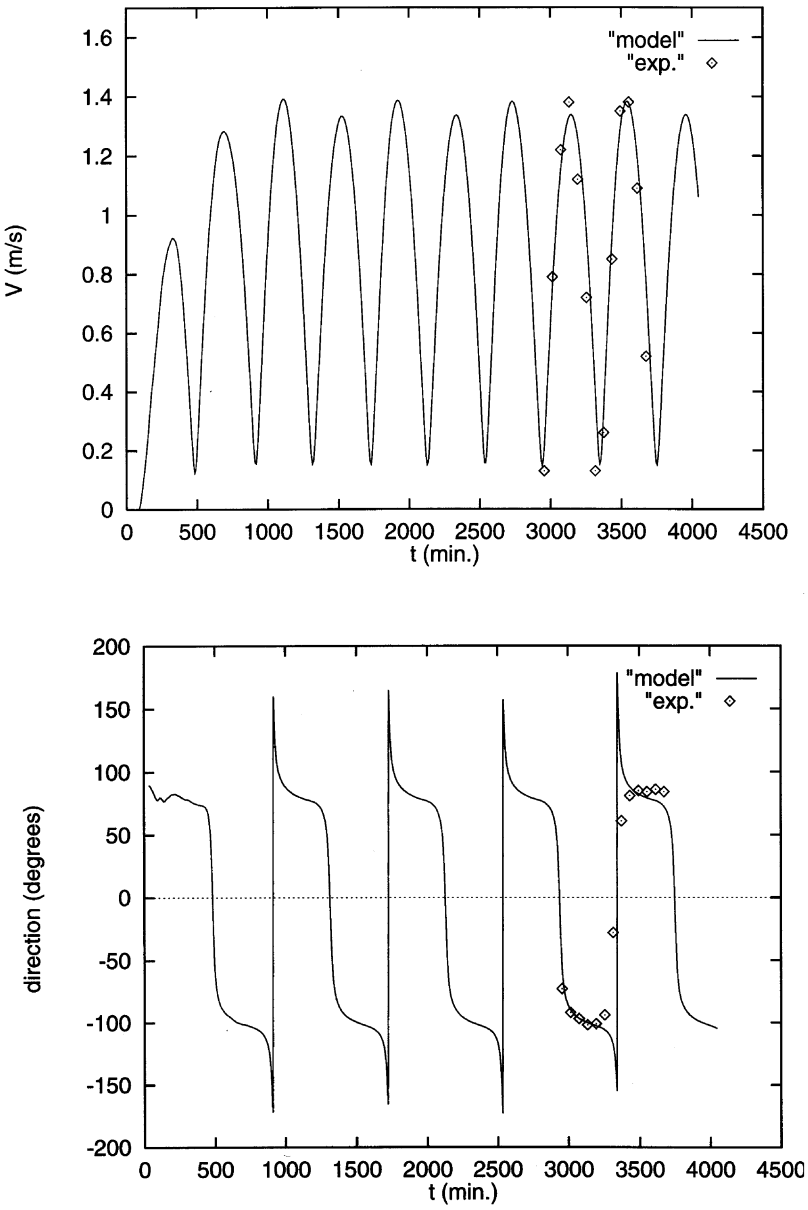

Fig. 4.3. Observed (points) and computed (lines) time evolution of current magnitude and direction at a point in the central English Channel. Direction is measured clockwise from north

4.5 Something about tides

As commented before, tidal elevations must be prescribed along open boundaries to compute tidal currents inside the computational domain. A few lines about tides must be included here. A detailed description of the origin and characteristics of tides may be found in [99] and, mainly, in [147].

Tides are generated by the gravitational attraction of the Earth, Sun and Moon. The simplest model for understanding tides assumes that the Earth is completely covered by water (no continents). This theory, known as the equilibrium tide model, was developed by Newton. Initially, only the Earth-Moon system will be considered. Both bodies revolve around their common centre of mass (figure 4.4) with a period of 27.32 days, denoted as a sidereal month. In this rotation, all the points on the Earth surface describe a circle of the same radius, thus all points suffer the same centrifugal force (figure 4.5) and experience the same acceleration. However, the attraction force at the Earth surface due to the Moon will be larger in a point immediately below the Moon than in a point on the Earth surface located at the opposed side (figure 4.6). Thus, below the Moon, there is a net force directed to the Moon due to an excess of attraction force respect to the centrifugal force. At the opposed side of the Earth, the centrifugal force is larger than the force due to Moon attraction. As a consequence, there is a net force directed as the centrifugal force. These net forces generate tides. Nevertheless, these vertical forces are too weak to have any effect on water. It is the tangential components (parallel to the Earth surface) of these forces at mid latitudes which produce accelerations large enough to induce water movements (figure 4.6). Newton created an image consisting of two tidal bulges, that are shown in figure 4.7. Water level is higher directly below the Moon and at the opposed side of the Earth. Thus, two areas of high water are apparent at each instant of time.

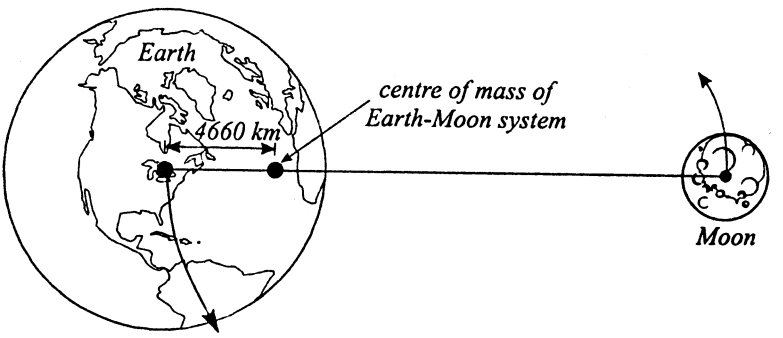

Fig. 4.4. Rotation of the Earth and Moon around their common centre of mass

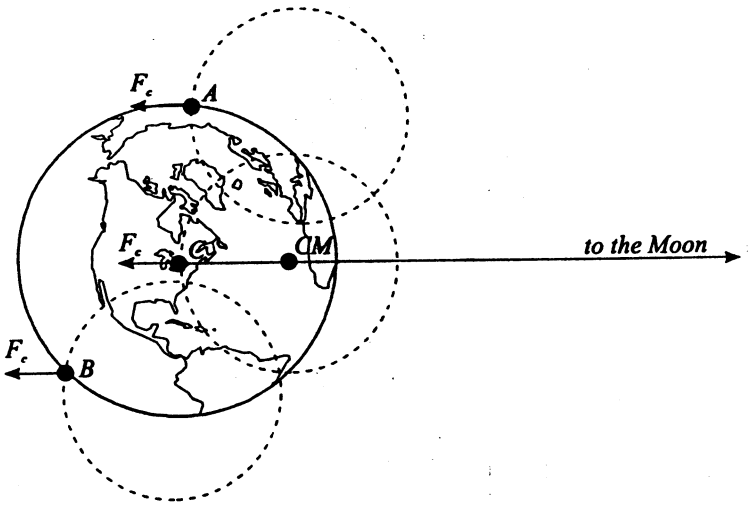

Fig. 4.5. All points on the Earth surface describe circles of the same radius and thus experience the same centrifugal force F_c

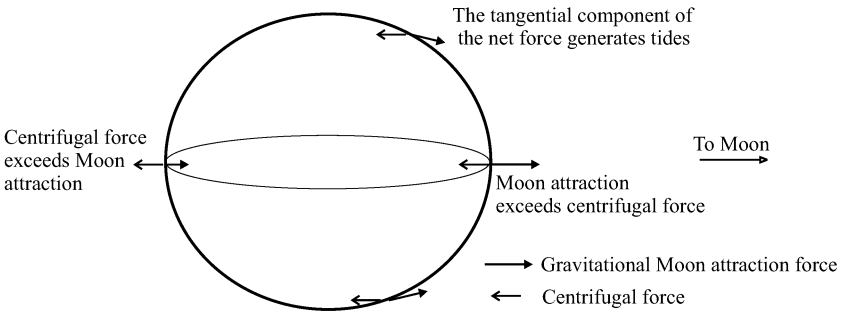

Fig. 4.6. Gravitational and centrifugal forces acting on the Earth surface

A point on the Earth surface passes once each day below the Moon and the opposed side to the Moon, as can be deduced from figure 4.4, thus there are two tides each day. However, the period of the Earth rotation with respect to the Moon is 24 hours and 50 minutes, period denoted as a lunar day. This is longer than the solar day (24 hours). In other words, high water and low water levels are about one hour later each successive day.

The Sun generates tides in the same way, although there is not such 1 hour delay each day. The solar tidal forces are a factor 0.46 weaker due to the greater Sun-Earth distance. The other planets in the Solar System generate negligible tides.

Moon and Sun tides are additive. When Earth, Sun and Moon are in a straight line (Full Moon and New Moon) high and low water for both tides occur at the same time, thus the resulting tide will be higher than average (high water level will be higher and low water level will be lower). This is the spring tide. When the Earth-Sun-Moon system forms a right angle (quadratures) the tide will be smaller than average. This tide is known as neap tide. The time from one spring tide to the next is 14.8 days. Currents associated with spring tides will be stronger than currents during neap tides. Thus spring-neap cycles have a strong influence on the dispersion of radionuclides in the sea and should be considered [133].

Tides are affected by changes in the declinations of the Moon and Sun and changes in their distances to the Earth. As the Moon or Sun are nearer to the Earth, their corresponding tides will be stronger. Declinations generate diurnal tides (figure 4.7): high water level at point P will be higher than when this point moves to P'. Thus, there are two high and two low water levels each day, but their amplitudes are different, unless P is located on the Earth equator. This can be considered as a combination of two tides: one with a period of about 12 hours (semidiurnal tide, two cycles each day) and one with a period of about one day (diurnal tide, one cycle each day). Maximum diurnal tidal ranges occur when declination is the greatest. Spatially, diurnal tides have maximum amplitudes at latitude $\pm 45°$ and zero amplitude at the equator and poles.

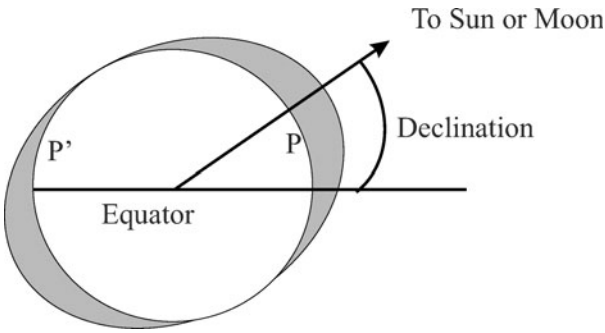

Fig. 4.7. Generation of diurnal tides: high water level at P is higher than at P'

However, real tides do not agree with the predictions of Newton's equilibrium tide theory, although it allows understanding how tides are generated. There are several reasons: tidal bulges predicted by Newton's theory cannot

travel around the Earth due to the presence of continents, and complex ocean bathymetry limits the possible directions of tidal flows. Flows are also affected by Earth rotation (Coriolis acceleration). As the tide propagates into shallower regions and finds the coastal line, it suffers reflection. The combination of the incoming and reflected wave produces the observed tides, whose amplitudes are larger than those deduced from the equilibrium tide. If a wave propagates into a rectangular bay and is reflected at the closed end without energy loss, a pattern of standing waves is generated. If Earth rotation is neglected, the pattern alternates lines across the bay where the water levels do not change (node lines) with lines where tide amplitudes are maximum (antinode lines).

If rotation is included the pattern is a little more complex: node lines are replaced by single nodal points denoted as amphidromes. The amplitude of the tide is zero at each amphidrome. The crest of the tidal wave rotates around the amphidrome (counter clockwise in the northern hemisphere and clockwise in the southern one), and the tide amplitude increases with increasing distance from the amphidrome.

Finally, the sea basins have their own natural modes of oscillations, with resonant frequencies. The whole ocean is near to resonance at semidiurnal tidal frequency, thus semidiurnal tides are also larger than predicted by the equilibrium tide because of this effect.

Tides can be represented by tidal charts, composed of corange and cotidal lines. Corange lines join points of equal tide amplitude. They are almost concentric circles around each amphidrome. Lines joining points where tides occur at the same time are denoted as cotidal lines, which radiate outside each amphidrome. As an example, the tide chart in the European continental shelf for the M_2 tide (see below) computed with the model described in [40] is presented in figure 4.8. Two clear amphidromic systems may be seen in the North Sea, other in the English Channel (close to the British coast) and other in the Irish Sea between Wales and Ireland. These two last amphidromic points are actually inside land, thus they are denoted as virtual or degenerate amphidromes.

The computed [167] corange chart for the same tide in the Mediterranean Sea is presented in figure 4.9. In the western basin the tide is affected by the wave incoming through the Strait of Gibraltar, and an amphidromic system is developed close to the Spanish coast. There is another amphidrome in the Strait of Sicily, separating the western and eastern basins, and a third in the Adriatic Sea. There is not agreement between different authors with respect a possible degenerate amphidrome at Crete. The situation in the Aegean Sea is rather complex due to the shallow waters, but no amphidrome can be detected. Although tide amplitudes are rather small in the Mediterranean, strong currents can be observed in the straits of Gibraltar and Messina.

Observed tides at a given point can be given as the addition of a number of harmonic functions as equation 4.28, each of them defined by an amplitude, a phase and an angular speed. Each harmonic is denoted as a tide constituent. All effects described above (cyclic variations in the Moon and Sun position

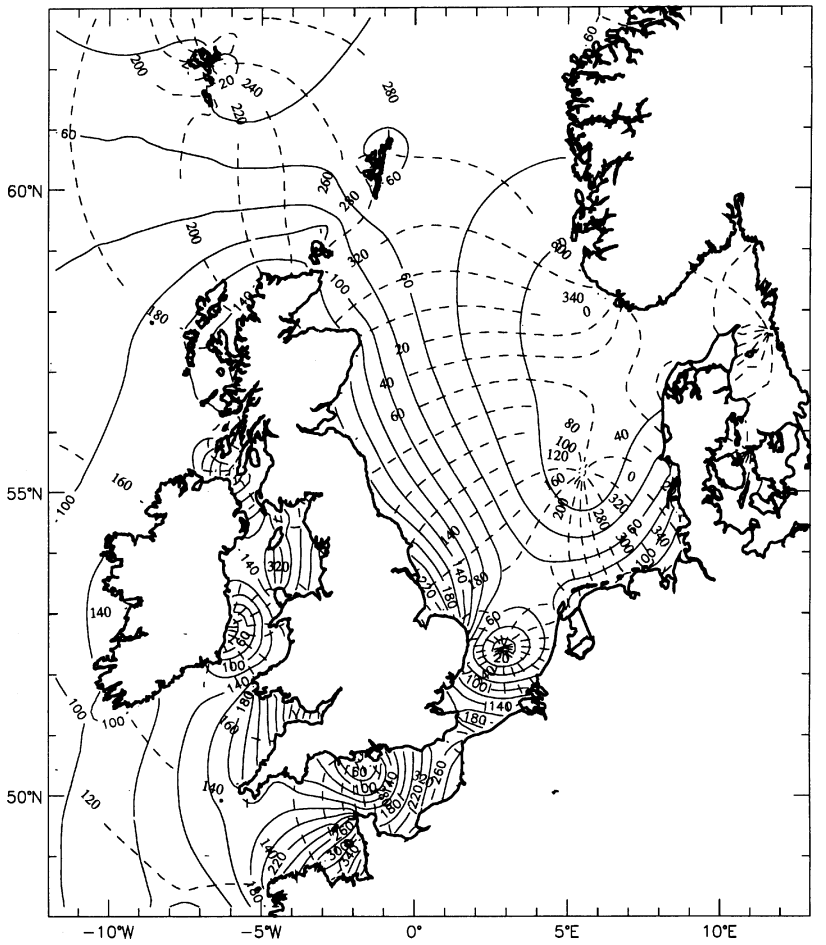

Fig. 4.8. Computed [40] M_2 tide chart for the European continental shelf. Corange lines (solid) show amplitudes in cm and cotidal lines (dashed) show phases in degrees

with respect to the Earth, changing distances between them, changing declinations), produce tides (constituents) with largely varying periods and amplitudes. As many as 390 constituents have been identified. The most important ones are given in table 4.1. Thus, if N constituents are evident, the observed tide can be described as:

$$z(t) = \sum_{i=1}^{N} h_i \cos(w_i t - g_i) \tag{4.44}$$

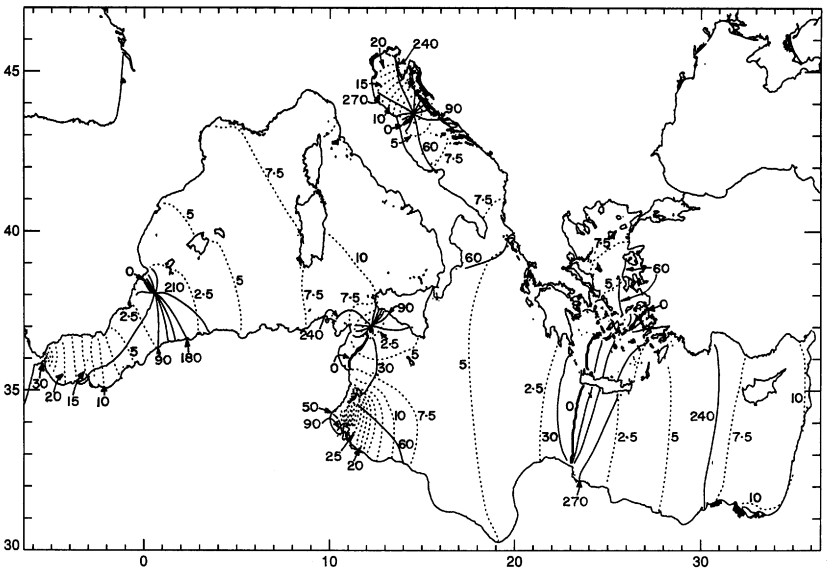

Fig. 4.9. Computed [167] M_2 tide chart for the Mediterranean Sea. Corange lines (dashed) show amplitudes in cm and cotidal lines (solid) show phases in degrees

where h_i, g_i and w_i are amplitude, phase and angular speed of each constituent. Amplitudes and phases of tidal constituents are denoted as tidal constants.

Table 4.1. Main tidal constituents. Amplitudes are given with respect to the main M_2 constituent (100.0)

Name	Symbol	Period (h)	Amplitude	Description
Main lunar	M_2	12.42	100.0	Earth rotation
Main Solar	S_2	12.00	46.6	Earth rotation
Larger lunar elliptic	N_2	12.66	19.2	Variation in Earth-Moon distance
Luni-solar semidiurnal	K_2	11.97	12.7	Changes in declination of Sun and Moon
Luni-solar diurnal	K_1	23.93	58.4	solar-lunar diurnal constituent

Constituents with index 2 are the semidiurnal tides and constituents with index 1 are the diurnal ones. For practical dispersion problems, it is generally enough to include in calculations only the two main constituents M_2 and S_2 [122, 127, 133]. It allows accounting for spring-neap cycles, described above.

4.6 Residual transport

Sometimes, it may be of interest to study the dispersion of radionuclides over long time scales. Here long means a period of time much longer than tidal cycle duration (say from months to decades or even more). These long-term transport processes may be described by the so-called residual circulation. The residual circulation is obtained by averaging the hydrodynamic equation results over a time longer than cyclic fluctuations. The transport equation for radionuclides is then solved using a steady flow which represents the residual circulation.

Of course, the hydrodynamic equations could be integrated for the desired time (say one year) and the dispersion equation solved with currents provided by them. However, the small time step required to solve tidal periods would lead to prohibitive computing times. Thus, the residual circulation approach is more adequate for long term dispersion problems. Examples of application may be seen, for instance, in [140, 24, 130].

Nevertheless, the residual circulation has to be defined with care, and a good review is given in [47]. For instance, it is not adequate to simply average in time the depth-averaged currents for each point since the so obtained circulation does not satisfy mass conservation [47]. Instead, the Eulerian residual transport velocity, $\overline{u}$, must be used:

$$\overline{u} = \frac{< U >}{< H >} \tag{4.45}$$

where $<>$ is the time averaging operator and $U = uH$ is the instantaneous Eulerian transport. Here the meaningful variable is not the mean velocity but the mean transport. For instance, the flow rate across a strait is associated with the mean transport, not the mean velocity. As an example, the computed residual transport velocity in the English Channel [130] is shown in figure 4.10. This velocity field was used to simulate the long term dispersion of non conservative radionuclides released from Cap de La Hague nuclear fuel reprocessing plant.

Lagrangian residuals can also be defined, but will not be presented here since the approach given by equation 4.45 is enough for our purposes. A detailed description may be seen in [47].

Instead of using a constant residual transport, it is possible to calculate monthly averages, for instance, to reflect seasonal variations in wind patterns, that also affect the net transport of radionuclides. Thus, a catalogue of residual transports is obtained. Breton and Salomon [24] ran a hydrodynamic model

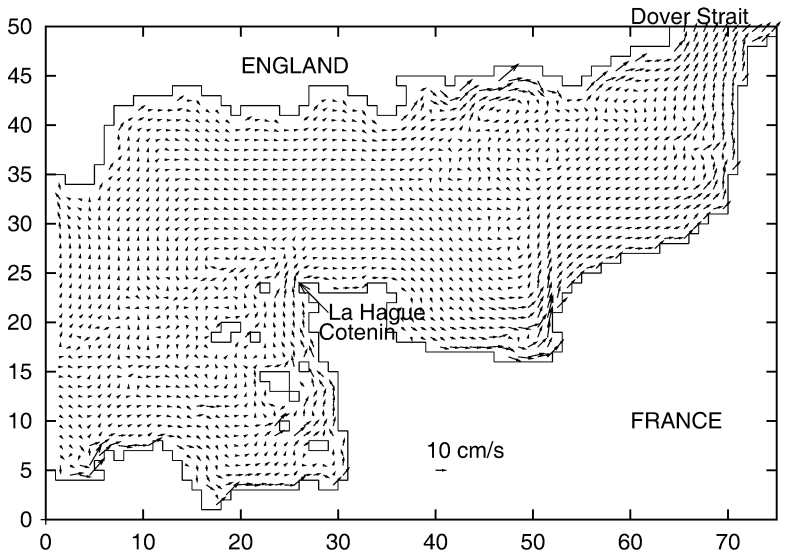

Fig. 4.10. Residual transport velocity computed for the English Channel. Each unit in the axis corresponds to 5 km

for various combinations of tide amplitudes and wind speeds and directions to obtain such a catalogue of residuals. Currents at any position were obtained through interpolation from the catalogue for any tide and wind.

5

Solving hydrodynamics and dispersion

5.1 Introduction

In the previous chapter the hydrodynamic equations have been presented and a finite difference method to solve them has also been described. The dispersion equation was treated in a simple one dimensional form in chapter 3. Now, the solution of the hydrodynamic equations together with dispersion will be discussed. Also, the dispersion equation is generalized to a 2D depth-averaged form with variable water depth and to an arbitrary direction of the flow. Some discussion on boundary conditions for the dispersion equation is finally included.

5.2 Hydrodynamics on-line and off-line

As has already been pointed out, modelling radioactivity dispersion in the marine environment involves two models: a hydrodynamic model and a transport model. The hydrodynamic model calculates the water flows required by the transport model to calculate tracer dispersion according to such flows. Both models can be linked in a way that they run simultaneously, using the same time step. This coupling is called the *on-line* mode. However, it is also possible to run the models separately. The transport model uses in this case time series of flows that have been previously calculated by the hydrodynamic model and stored in files. This coupling is called the *off-line* mode. A scheme showing both approaches can be seen in figure 5.1, taken from [154].

The off-line mode has a clear advantage over the on-line mode: the stability conditions imposed by the transport equation are much less restrictive than the CFL condition due to the hydrodynamic equations. Thus, a larger time step can be used. This, together with the fact that hydrodynamic calculations have all been carried out in advance, and thus only the transport equation is solved each time step, implies that computation is much faster. An off-line dispersion model can use flows derived from different hydrodynamic

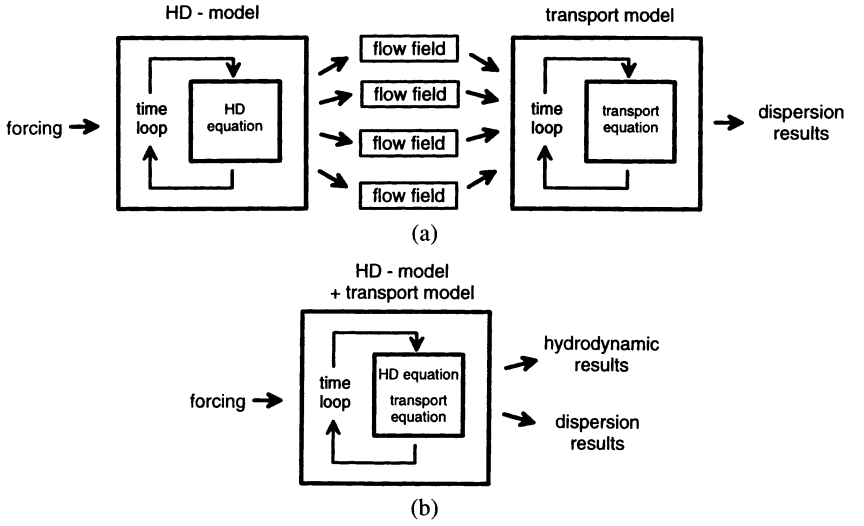

Fig. 5.1. Coupling of the hydrodynamic and dispersion models in the off-line (a) and on-line (b) modes (from [154])

models, or use the same flow field for different source terms, radionuclides or parameters in a much faster way. It is also possible to combine tidal residuals with wind induced flows, as has been done by Breton and Salomon [24]. The drawback is that currents fields are stored at time intervals much larger than the hydrodynamic model time step. Time interpolation between these flow fields cuts off variability at short temporal scale.

In the on-line mode the transport equations are integrated with the hydrodynamic equations, and thus are solved with the same time step. This approach is computationally much more expensive, but the transport equation is receiving flow fields with the highest possible temporal resolution.

Both methods have strengths and weaknesses, but anyway, the flow fields have to be provided to the transport equation in time intervals that allows the reproduction of the dominant flow variability. This time resolution depends on the model area and objective of the work. Studying tidal dispersion in a coastal area requires solving tidal cycles. This will require a much higher resolution than studying long term dispersion in a whole sea or ocean basin.

Another possibility for running a dispersion model off-line and, at the same time, maintaining temporal resolution high enough to solve tidal mixing consists of using standard tidal analysis. As was explained in chapter 4, tides can be represented as a number of harmonics in the form of equation 4.28. Tidal analysis consists of determining, by a standard fitting algorithm, the amplitude and phase (tidal constants) for each constituent included in the model

and for each grid cell. These tidal constants have to be calculated for both components of the flow, u and v, and for water elevation z. Tidal constants, for each tide constituent, are calculated by the same hydrodynamic code and are stored in files that will be read by the dispersion model. Once that tidal constants are known, computation of flow and water elevation at any cell and time just involves the evaluation and addition of a few cosine terms. This is very fast, and simultaneously, the dispersion model is not limited by the CFL condition. The net residual current has to be evaluated by the hydrodynamic model and added to the current obtained from tidal analysis since a net transport cannot be obtained from the pure harmonic currents provided by the tidal analysis. It has to be clearly pointed out that tidal analysis is carried out running the hydrodynamic model for each constituent separately. This technique is usually applied in rapid response Lagrangian models (see chapter 7), although has also been used in finite difference dispersion models [127]. It has the clear advantage of joining the strengths of the off-line mode with a temporal resolution that is high enough to solve tidal processes.

5.3 The transport equation in non constant water flows and depths

The transport equation, in a 2D depth averaged form and for a constant diffusion coefficient and a constant water depth, has already been presented in chapter 2:

$$\frac{\partial C}{\partial t} + \frac{\partial uC}{\partial x} + \frac{\partial vC}{\partial y} = K_h \left(\frac{\partial^2 C}{\partial x^2} + \frac{\partial^2 C}{\partial y^2} \right) \tag{5.1}$$

However, depth will not be constant over the model domain due to changes in bed topography. These changes in depth have to be considered in the transport equation in order that tracer mass is conserved. The transport equation can be generalized to the case in which depth is constant in time for each point but changes from one point in the domain to another. Also, a variable diffusion coefficient can be considered. The new form of the equation would be:

$$\begin{aligned} &\frac{\partial C}{\partial t} + \frac{1}{H} \left\{ \frac{\partial (uHC)}{\partial x} + \frac{\partial (vHC)}{\partial y} \right\} \\ &= \frac{1}{H} \left\{ \frac{\partial}{\partial x} \left(K_x H \frac{\partial C}{\partial x} \right) + \frac{\partial}{\partial y} \left(K_y H \frac{\partial C}{\partial y} \right) \right\} \end{aligned} \tag{5.2}$$

where K_x and K_y are the diffusion coefficients in the directions of x and y respectively, although in practical applications they are generally assumed to be equal and constant.

If water depths also change in time due to tidal oscillations, the transport equation would be written in the following form:

$$\frac{\partial(HC)}{\partial t} + \frac{\partial(uHC)}{\partial x} + \frac{\partial(vHC)}{\partial y} = \frac{\partial}{\partial x}\left(K_x H \frac{\partial C}{\partial x}\right) + \frac{\partial}{\partial y}\left(K_y H \frac{\partial C}{\partial y}\right) \tag{5.3}$$

This is the most general case, and a numerical scheme to solve it will be discussed. The advection terms will be initially treated with the upstream method already presented in chapter 3. The treatment of diffusion is essentially the same as in equation 3.17. The equation will be solved in the same computational grid as the hydrodynamic equations (figure 4.1). Concentration C is defined at the centre of the cell and the diffusion coefficients at the same points as the velocities.

Let us start with the advective terms. In the upstream method the spatial derivative is shifted to the direction where the current comes from, as was explained in chapter 3. Thus, the form of the derivative depends on the current direction. The upstream scheme given by equations 3.2 and 3.5 can be extended to an arbitrary current direction and changing depth. The finite difference form of the transport equation would result as follows:

$$\begin{aligned} &\frac{H^*_{i,j}C^*_{i,j} - H_{i,j}C_{i,j}}{\Delta t} \\ &= \frac{-n_1 u_{i,j} H_1 C_{i,j} - (1-n_1) u_{i,j} H_1 C_{i+1,j}}{\Delta x} \\ &+ \frac{n_2 u_{i-1,j} H_2 C_{i-1,j} + (1-n_2) u_{i-1,j} H_2 C_{i,j}}{\Delta x} \\ &+ \text{y derivative} + \text{diffusion terms} \end{aligned} \tag{5.4}$$

In this equation H_1 and H_2 are water depths at the right and left sides of cell i,j respectively, as described in chapter 4, and numbers n are defined in the following way:

$$n_1 = \begin{cases} 1 & \text{if} \quad u_{i,j} > 0 \\ 0 & \text{if} \quad u_{i,j} < 0 \end{cases} \tag{5.5}$$

and

$$n_2 = \begin{cases} 1 & \text{if} \quad u_{i-1,j} > 0 \\ 0 & \text{if} \quad u_{i-1,j} < 0 \end{cases} \tag{5.6}$$

From this equation $C^*_{i,j}$ is obtained since depth at the new time level, $H^*_{i,j}$, is known from the previous solution (either on- or off-line) of the hydrodynamic equations. It can be noted that the advective flux through a land boundary is automatically zero since the current component normal to the boundary is defined as zero when solving hydrodynamics. The treatment of the y derivative is the same.

The diffusion terms will be written now using the numerical scheme for non constant K given by equation 3.17:

$$\begin{aligned}&\text{diffusion terms}\\&= \frac{1}{\Delta x}\left\{ n_5 K_{i,j} H_1 \frac{C_{i+1,j} - C_{i,j}}{\Delta x} - n_6 K_{i-1,j} H_2 \frac{C_{i,j} - C_{i-1,j}}{\Delta x} \right\}\\&+ \text{y derivative}\end{aligned} \tag{5.7}$$

Here $n_5 = 0$ if $H_{i+1,j} = 0$ to avoid diffusion through a land boundary. Else, $n_5 = 1$. Similarly, $n_6 = 0$ if $H_{i-1,j} = 0$. The treatment for the y derivative is exactly the same. These boundary conditions are mathematically expressed as

$$\frac{\partial C}{\partial n} = 0 \tag{5.8}$$

where n is the direction normal to the land boundary. From these schemes it is easy to obtain the finite difference form of the dispersion equation when depths are constant in time (equation 5.2).

The stability condition due to diffusion terms is different to the one dimensional case (equation 3.18): the factor 2 appearing at the denominator must be 4. In a three dimensional case it would be 6.

The application of the MSOU scheme in the case of flow in arbitrary direction is more tedious. The advective part of the dispersion equation is now written as:

$$\begin{aligned}&\frac{H^*_{i,j} C^*_{i,j} - H_{i,j} C_{i,j}}{\Delta t}\\&= \frac{-n_1 u_{i,j} H_1 F_1 - (1 - n_1) u_{i,j} H_1 F_2}{\Delta x}\\&+ \frac{n_2 u_{i-1,j} H_2 F_3 + (1 - n_2) u_{i-1,j} H_2 F_4}{\Delta x}\\&+ \text{y derivative}\end{aligned} \tag{5.9}$$

where factors F include the second order correction to the upstream scheme:

$$F_1 = C_{i,j} + \frac{1}{2}\psi(C_{i,j} - C_{i-1,j}) \tag{5.10}$$

with

$$\psi = \max\left(0, \min\left(2r, 1\right), \min\left(r, 2\right)\right) \tag{5.11}$$

where

$$r = \frac{C_{i+1,j} - C_{i,j}}{C_{i,j} - C_{i-1,j}} \tag{5.12}$$

$$F_2 = C_{i+1,j} - \frac{1}{2}\psi(C_{i+1,j} - C_{i,j}) \tag{5.13}$$

but now

$$r = \frac{C_{i+2,j} - C_{i+1,j}}{C_{i+1,j} - C_{i,j}} \tag{5.14}$$

$$F_3 = C_{i-1,j} + \frac{1}{2}\psi(C_{i-1,j} - C_{i-2,j}) \tag{5.15}$$

$$r = \frac{C_{i,j} - C_{i-1,j}}{C_{i-1,j} - C_{i-2,j}} \tag{5.16}$$

and finally,

$$F_4 = C_{i,j} - \frac{1}{2}\psi(C_{i,j} - C_{i-1,j}) \tag{5.17}$$

$$r = \frac{C_{i+1,j} - C_{i,j}}{C_{i,j} - C_{i-1,j}} \tag{5.18}$$

In all F factors ψ is defined as in equation 5.11. It must be taken into account that r may diverge if the denominator tends to zero. This has always to be checked and, if occurs, an arbitrary large value is given to r (for instance 10). Thus ψ would be 2 automatically and overflow errors are not generated.

Some additional control is required in the vicinity of land boundaries since it may be necessary to remove the second order correction. The following conditions are included in the code:

$$F_1 = C_{i,j} \quad \text{if} \quad H_{i-1,j} = 0 \tag{5.19}$$

$$F_2 = C_{i+1,j} \quad \text{if} \quad H_{i+2,j} = 0 \tag{5.20}$$

$$F_3 = C_{i-1,j} \quad \text{if} \quad H_{i-2,j} = 0 \tag{5.21}$$

$$F_4 = C_{i,j} \quad \text{if} \quad H_{i+1,j} = 0 \tag{5.22}$$

It can be easily realized that the inclusion of a second order scheme is more complicated and computationally expensive than the simple upstream scheme. However, it is worth making such effort given the results obtained with both methods: an example of the solution of a 2D advection problem with both the upstream and MSOU methods is presented in figure 5.2. Water depths are considered as constants, equal to 5 m, as well as velocities, $u = 0.5$ and $v = 0.15$ m/s. Temporal and spatial resolution are $\Delta t = 180$ s and $\Delta x = \Delta y = 5000$ m. The advection equation has been integrated for 100 hours, that means 2000 time steps. An initial concentration equal to 1.0×10^5 units/m^3 is assumed at cell $(5, 10)$. It can be seen that the upstream scheme produces a very high numerical diffusion. Indeed, concentrations obtained with this method are an order of magnitude smaller than those obtained by the MSOU scheme, which reflects much better the advective transport process. Nevertheless, as expected, the position of the center of the patch is the same with both numerical schemes.

5.4 Open boundary conditions

As for the case of the hydrodynamic equations, open boundary conditions have to be prescribed to solve the transport equation. A review of boundary conditions for the transport equation may be seen in [35]; a brief summary is included here.

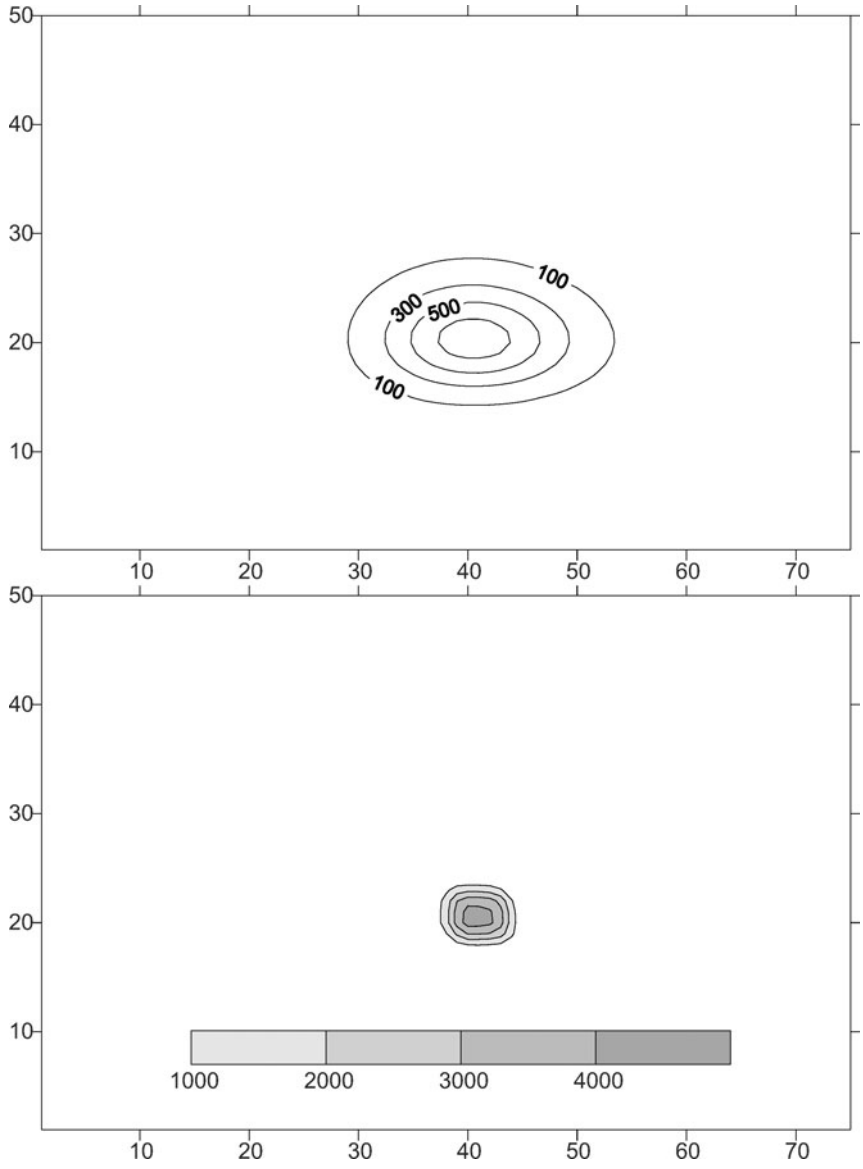

Fig. 5.2. Solution of a 2D advection problem with the upstream scheme (up) and MSOU scheme (down). Contour line units are concentrations, given in arbitrary units per m^3, and numbers in the axis indicate grid cell number

The Dirichlet boundary condition is applied when the concentration at the boundary is given at each time step:

$$C_b(t) = A(t) \tag{5.23}$$

where C_b is concentration at the boundary and A is a function giving the time evolution of such concentration. Of course, as a particular case, A may be a constant.

The Cauchy condition is applied when the total incoming flux of material is prescribed as a function of time at the boundary:

$$-q_n HC + K_n H \frac{\partial C}{\partial n} = f_b(t) \tag{5.24}$$

where n is the direction normal to the boundary, q_n is the current component normal to the boundary and f_b is the prescribed flux per unit length along the boundary.

A variable boundary condition can also be used. It consists of checking if the flow is coming into the domain from outside or if it is going out from inside. This condition may be interesting when tides are the dominant effect in controlling dispersion. It has been used in [114, 115]. If the flow is going out a decay in concentrations can specified to account for the decrease in concentrations with increasing distance from the source:

$$C_b = \Gamma C_{b-1} \tag{5.25}$$

where C_{b-1} is concentration just inside the domain and Γ is a non dimensional number obtained from calibration. A value that can be used is, for instance, $\Gamma = 0.99$.

If flow is incoming, it can be specified as in the Cauchy condition or, alternatively, a Dirichlet condition can be applied, specifying concentration at the boundary.

In the tidal models of the Irish Sea and English Channels [121, 122], where the distance traveled by radionuclides during a single flood or ebb period is very small compared with the model domain and open boundaries are far from the radioactive source, condition given by equation 5.25 is always applied with $\Gamma < 1$. This simulates the observed general decrease in concentrations with increasing distance from the source. Equation 5.25 has also been used in the long-term model of the English Channel [130] and in the Irish Sea model described in [65].

6

Modelling the dispersion of non conservative radionuclides

6.1 Introduction

Non-conservative radionuclides are not transported in a dissolved form by pure advection and diffusion processes. Instead, as was commented in chapter 2, they are partially fixed to the solid phases (suspended matter particles and bottom sediments). Radionuclides dissolved and fixed to suspended matter particles are transported by advection and diffusion processes. Erosion of the bed sediment and deposition of suspended particles produce an exchange of radionuclides between the bed sediment and suspended matter. Sorption and release reactions produce an exchange of radionuclides between the liquid and both solid phases. All these processes were represented in figure 2.1.

It is clear that the suspended matter concentration in the water column must be known to compute the dispersion of non conservative radionuclides. This also implies the calculations of deposition and bed sediment erosion. Since the basic ideas on modelling the dispersion of non conservative radionuclides are given in this chapter, an introduction to sediment transport modelling will be presented first. Kinetic models for sortion/release reactions are described later. As an example, a brief description of a model for simulating the dispersion of non conservative radionuclides in the Rhone River plume, developed at the University of Seville, is given.

6.2 Modelling the transport of suspended sediments

By convention, particulate matter in suspension is defined as the material that is retained on a 0.4 to 0.5 μm pore size filter. Smaller material is considered to be dissolved. Muddy sediments consists of clays with some variable silt content and particle diameter is [147] < 62.5 μm. Larger particles such as sands settle much more rapidly out of suspension in water than mud particles and bed load transport is the most important mechanism in moving this

coarse sediments. Usually, only particles with a diameter < 62.5 μm are considered when modelling suspended matter dynamics [4, 116, 106]. Indeed, it has been pointed out [49] that for all practical purposes mud can be regarded as synonymous of suspended matter. Also, radionuclides have little affinity for coarse materials. A general and good review on suspended matter in the aquatic environment is the book of Eisma [50].

Suspended sediment transport is described here in a 2D depth averaged form, but can be easily extended to a 3D formulation (see appendix A). Essentially, the time evolution of suspended matter concentration, m, is governed by an advection/diffusion equation to which the deposition and erosion terms are added:

$$\begin{aligned} &\frac{\partial(Hm)}{\partial t} + \frac{\partial(uHm)}{\partial x} + \frac{\partial(vHm)}{\partial y} \\ &= \frac{\partial}{\partial x}\left(HK_h\frac{\partial m}{\partial x}\right) + \frac{\partial}{\partial y}\left(HK_h\frac{\partial m}{\partial y}\right) \\ &+ ER - DEP \end{aligned} \tag{6.1}$$

where H is water depth, u and v are depth averaged currents, K_h is the horizontal diffusion coefficient and ER and DEP are the erosion and deposition terms respectively.

The deposition term is usually written in the following form [71, 90, 92, 175, 143, 26]:

$$DEP = w_s m\left(1 - \frac{\tau}{\tau_{cd}}\right) \tag{6.2}$$

where w_s is the suspended particle settling velocity, τ is friction stress (solved in τ_u and τ_v; equations 4.4) and τ_{cd} is a critical deposition stress above which no deposition occurs since particles are kept in suspension by turbulence. The settling velocity of particles can be obtained from Stokes's law:

$$w_s = \frac{\rho - \rho_w}{\rho_w}\frac{gD^2}{18\nu} \tag{6.3}$$

where ρ and D are suspended particle density and diameter respectively, and ρ_w and ν are density and kinematic viscosity of water. It is also possible to include the process of aggregation in the model through a classic relationship [50] in the form:

$$w_s = a_1 m^{a_2} \tag{6.4}$$

where a_1 and a_2 are empirical constants depending on the type of particle and water turbulence. Equation 6.4 expresses the idea that flocculation results in the formation of larger particles that settle faster than the original particles. Flocculation increases as the suspended matter concentration increases since individual particles have a larger probability of colliding and forming an aggregate. The values in a_2 range from 1 to 2 [50]. Equation 6.4 is valid until m reaches a value of some 5 g/L. From this point, the settling velocity decreases

with m due to hindered settling (each particle is hindered by the others in the cloud).

This approach has been used in some suspended sediment models [26, 34, 106, 92] and also in radionuclide dispersion models [121, 123]. Other authors [56, 90, 77, 155, 71, 91] directly calculate the settling velocity from Stokes's law. Tattersall et al. [162] have used a mixed approach. At each time step the settling velocity resulting from equation 6.4 is calculated and compared with that obtained from Stokes's law. Then the higher value is used. Wu et al. [175] use equation 6.4 or Stokes's law depending on the suspended matter concentration to take into account if hindered settling occurs. A problem of equation 6.4 is to find adequate or site-specific values for constants a_1 and a_2.

The erosion rate is generally written in terms of the erodability constant, see for instance references [90, 91, 26, 143, 71, 106]:

$$ER = Ef\left(\frac{\tau}{\tau_{ce}} - 1\right) \tag{6.5}$$

where E is the erodability constant, f gives the fraction of small particles (diameter less than 62.5 μm) in the bed sediment (that are particles that may be resuspended) and τ_{ce} is a critical erosion stress below which no erosion occurs. It is also possible to calculate sedimentation rates as the balance between the deposition and erosion terms.

Other formulations for the erosion term may be found in literature, for instance the presented in [141]:

$$ER = Eq^M \tag{6.6}$$

where M is some power of the water current $q = \sqrt{u^2 + v^2}$ typically in the range 2-5. This formulation has been used in [123, 128] but adding the factor f to take into account the fraction of sediments that can really be eroded. However, the formulation described by equation 6.5 is now more commonly used.

Finally, it may be necessary to include a source term to the suspended matter equation for some points in the domain. It would represent the input of particles from continental runoff, river discharge or industrial releases.

Some models for suspended matter characterize particles by an average size [4, 128, 56, 143]. However, it is also possible to deal with several particle classes simultaneously [91, 77, 71, 162]. Each particle class comprises particles between a minimum and a maximum size. The class is defined by its average particle size and each of the classes possesses a different settling velocity (obtained for instance from Stokes's law applied to the average particle size of the class). This may be relevant for the transport of non conservative radionuclides since they are predominantly adsorbed on the smaller particles. The Rhone River plume radionuclide dispersion model described in [132, 135] includes four particle classes, as well as the model of Piasecki [137]. Of course, a dispersion equation with the corresponding deposition and erosion terms must be solved for each class.

A review on the values generally given to the critical deposition and erosion stresses and erodability may be found through the references cited in this section. The critical deposition stress ranges between 0.04 and 0.1 N/m^2, while the critical erosion stress ranges 0.1-1.5 N/m^2, depending on the model. The critical stress for erosion is larger than that for deposition for cohesive sediments. Thus, in any model for cohesive sediments it should be verified that $\tau_{cd} < \tau_{ce}$. In contrast, for non-cohesive sediments it is assumed that the erosion and deposition thresholds are equal.

Clarke and Elliott [34] made the erodability constant, as well as the deposition and erosion thresholds, functions of the spring-neap cycles in their suspended sediment model of the Firth of Forth (Scotland).

Generally, in models including several particle classes, the same sediment parameters are used for all of them. However, a experimental protocol has been described [51] to determine the critical erosion stress, erodability constant and settling velocity for different particle classes.

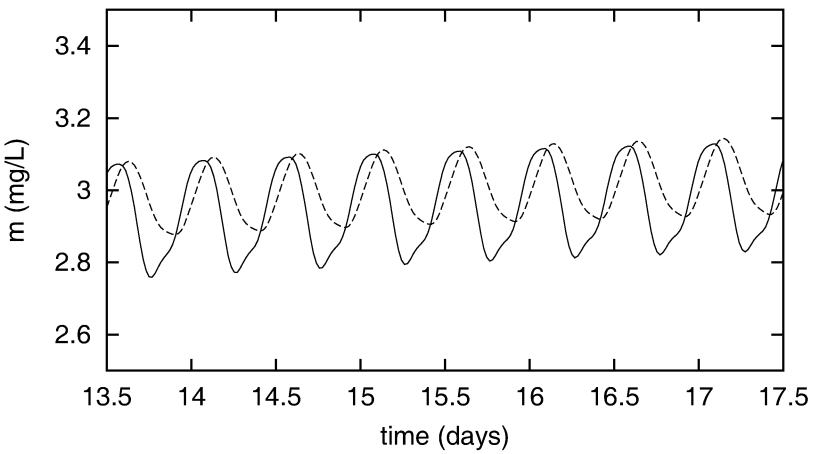

Fig. 6.1. Time evolution of computed suspended matter concentrations (mg/L) at the surface (solid line) and bottom (dashed line) at a point in the Irish Sea

Some examples of results obtained with the three dimensional suspended sediment transport model for the Irish Sea presented in [128] are now described. This model was part of a plutonium dispersion model of this area [121, 124, 126, 129]. Only a particle class with maximum diameter equal to 62.5 μm is considered. The time evolution of surface and bottom suspended matter concentration during several days at a point in the sea is presented in figure 6.1. It can be seen that surface and bottom concentrations are essentially the same, although the bottom ones are slightly higher. Indeed, it should be expected that suspended particles in the Irish Sea are well mixed

vertically: it has been shown [141] that this occurs if:

$$w_s < 0.1 \frac{A_v}{H} \tag{6.7}$$

Eddy viscosity, A_v, is of the order of 10^{-2} m^2/s and maximum depth is 55 m. Since w_s is of the order of 10^{-6} m/s, relation 6.7 is satisfied. It can be observed that one peak in suspended matter concentrations occurs for each tidal cycle. It is known [174] that if there is a horizontal concentration gradient the suspended matter exhibits a semi-diurnal signal (period 12.4 h) as it is advected backward and forward by the tide. Resuspended material exhibits a quarted-diurnal signal (period 6.2 h) as it is resuspended on both the flood and ebb. Combined with a semi-diurnal varying background, this will generate a characteristic double peak in m. Suspended matter concentration in the eastern Irish Sea exhibits a semi-diurnal signal, thus it appears to be composed principally on an advected component. Consequently, suspended matter concentrations are not dominated by erosion events. Indeed, computed

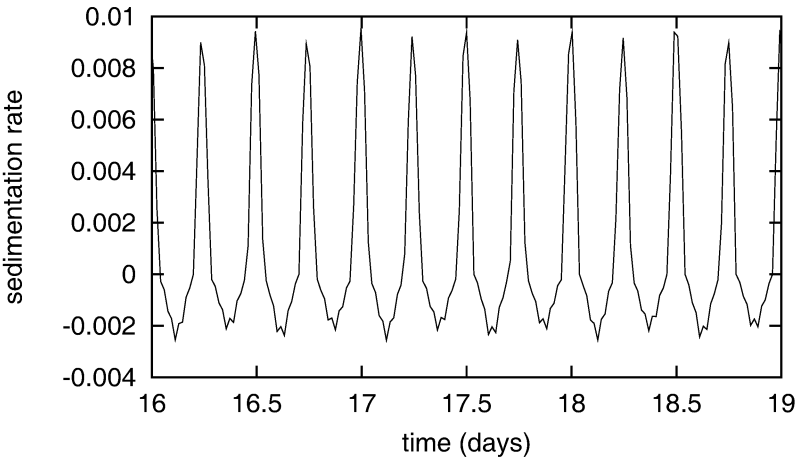

Fig. 6.2. Time evolution of computed sedimentation rate (g/cm^{2}year) at Liverpool Bay

sedimentation rates, R_S, are small. The time evolution of sedimentation rate at a point in Liverpool Bay (see map in figure 1.3) during several tidal cycles is presented in figure 6.2 as an example. It can be seen that there are erosion (negative values) and deposition (positive values) episodes. Deposition takes place during slack water and erosion takes place at the times of maximum currents.

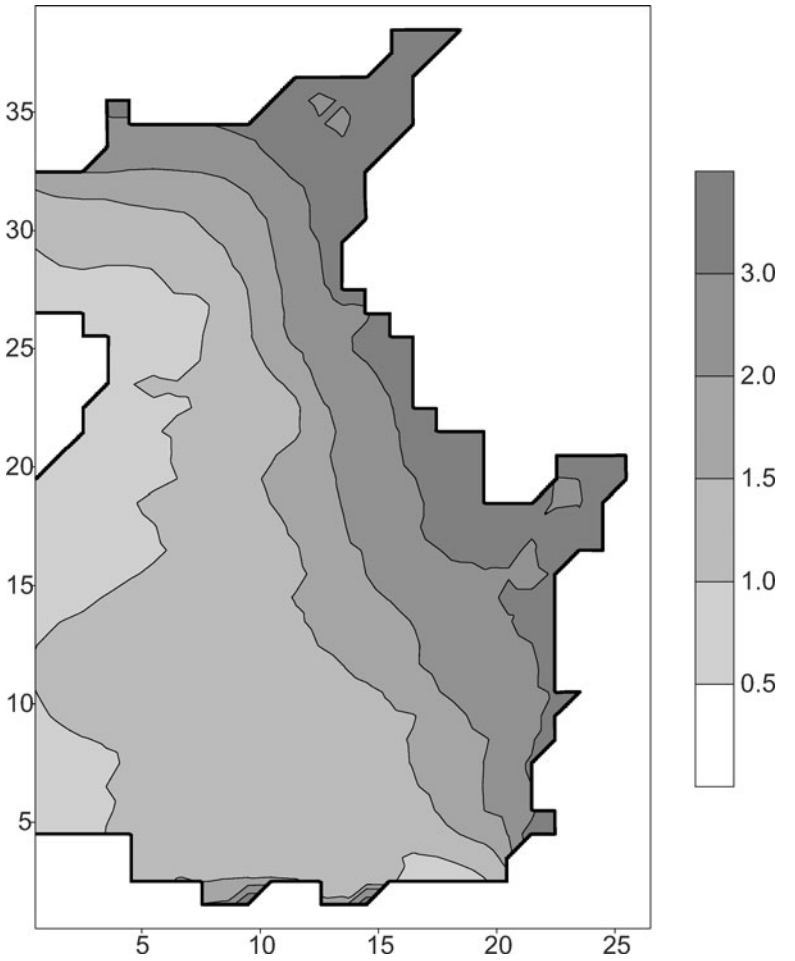

Fig. 6.3. Computed average suspended matter concentration (mg/L) in surface water

Finally, a map showing the average suspended matter concentrations at the surface is shown in figure 6.3. Maximum concentrations are obtained close to the coast due to the input of particles from runoff.

6.3 Kinetic models for uptake/release

As has already been commented, the first models for non conservative radionuclides were based upon the equilibrium distribution coefficient, k_d, or the partition coefficient. However, recent models are based on kinetic rates.

These kinetic models are more adequate since can deal with situations out from equilibrium conditions. Thus, we will directly introduce the kinetic approach for uptake/release reactions.

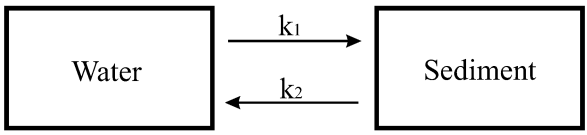

Fig. 6.4. Scheme of a water-sediment kinetic model describing exchanges of radionuclides between both phases

The simplest model for simulating uptake/release of radionuclides between water and the solid phases (suspended matter and bed sediment) considers that the exchange is governed by a first-order reversible reaction, being k_1 and k_2 the forward and backward rates respectively. It is implicitly assumed that sediment surfaces may be treated as a single entity, thereby integrating the relative importance of each component of the sediment surface [109, 27]. This approach is also used in all modelling works: rate constants express mean processes of sorption/release that may be running simultaneously with different sites in the particles. A scheme of this model may be seen in figure 6.4, where a closed water-sediment system is shown. X_w and X_s are the total activity contents in water and sediment respectively. The equations that give the time evolution of these quantities are:

$$\frac{\partial X_w}{\partial t} = -k_1 X_w + k_2 X_s \tag{6.8}$$

$$\frac{\partial X_s}{\partial t} = k_1 X_w - k_2 X_s$$

Thus, the transfer of radionuclides from one phase to the other is proportional to the activity content in the origin phase. These equations are very easily solved in finite differences using the following explicit scheme:

$$\frac{X_w^* - X_w}{\Delta t} = -k_1 X_w + k_2 X_s \tag{6.9}$$

$$\frac{X_s^* - X_s}{\Delta t} = k_1 X_w - k_2 X_s$$

An example of the solution of the equations is presented in figure 6.5. It is assumed that at $t = 0$ all the activity is dissolved, sediments being clean. The following arbitrary kinetic rates are used: $k_1 = 1.5 \times 10^{-5}$ s^{-1} and $k_2 = 2.0 \times 10^{-7}$ s^{-1}. Equations are integrated for 4 days using a time step $\Delta t = 60$ s. It can be seen how, with the kinetic rates used, essentially

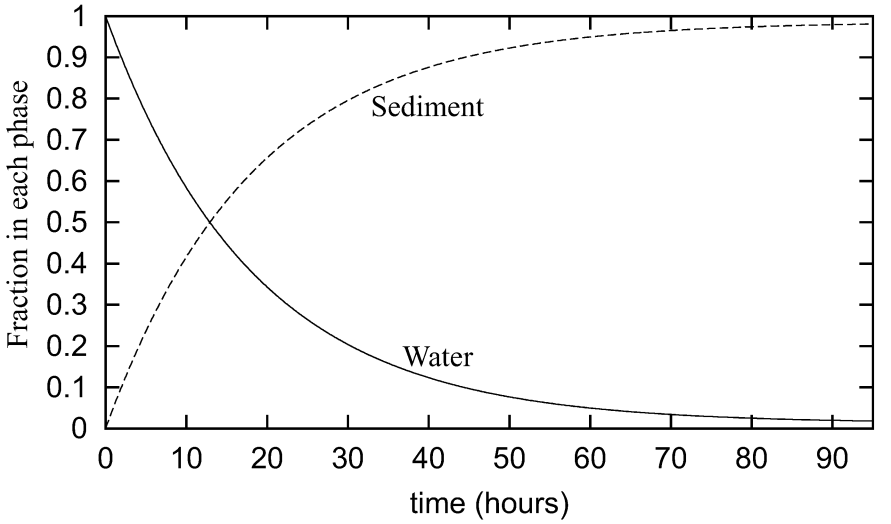

Fig. 6.5. Fraction of radionuclides in water and sediment after 4 days of contact in a closed system. All the activity is assumed to be in the dissolved phase at $t = 0$

all the activity is transferred from the dissolved to the solid phase during the simulation time. Moreover, equilibrium is not reached before than 4 days. Thus, a k_d approach would not be adequate, with these kinetic rates, if model time step in dispersion calculations is smaller.

This scheme for describing exchanges of radionuclides between the solid and dissolved phases can be easily included into the advection/diffusion dispersion equation.

The equations that describe the time evolution of radionuclide concentrations in the dissolved phase, suspended matter and bed sediment will be presented in what follows. A 2D depth averaged approach is used and, also, only a particle class is considered. These equations can be easily extended to the 3D situation and several particle classes [132, 135]. Indeed, 3D equations are summarized in appendix A.

The equation that gives the temporal evolution of specific activity in the dissolved phase, C_d (Bq/m^3), is:

$$\begin{aligned}&\frac{\partial(HC_d)}{\partial t} + \frac{\partial(uHC_d)}{\partial x} + \frac{\partial(vHC_d)}{\partial y}\\ &= \frac{\partial}{\partial x}\left(HK_D\frac{\partial C_d}{\partial x}\right) + \frac{\partial}{\partial y}\left(HK_D\frac{\partial C_d}{\partial y}\right)\\ &- k_1C_dH + k_2mC_sH + k_2A_sL\rho_sf\phi - \lambda C_dH \end{aligned} \tag{6.10}$$

where A_s and C_s are specific activity in the bed sediment and suspended matter respectively (Bq/kg), L is a mixing depth in the sediment (the dis-

tance to which the dissolved phase penetrates the sediment), ρ_s is sediment bulk density and ϕ is a correction factor that takes into account that not all the sediment is in contact with water since some particles may be partially hidden by other sediment particles. Thus it is related to sediment porosity. As commented before, f gives the fraction of small particles (diameter less than 62.5 μm). It is considered that radionuclides are fixed to these particles only. Thus, it has to be pointed out that, indeed, A_s is specific activity in the sediment fraction composed of small particles. This fraction is denoted as the active sediment. The active sediment corresponds to muddy sediments following the Wentworth scale of sediment grain size (see for instance [147]). Specific activity in the total sediment would be obtained from the following equation:

$$A_{total} = fA_s \tag{6.11}$$

Note that the third term in the right hand side of equation 6.10 is giving the transfer of radionuclides from water to suspended matter and bed sediments, the fourth term describes the transfer from suspended matter to water and the next the transfer from the bed sediment to water. The last term is radioactive decay.

The factors that appear in equation 6.10 multiplying with C_s and A_s are due to the fact that this quantities are activity concentrations, while in the definition of k_1 and k_2, through equations 6.8, X_w and X_s are total activity contents in each phase.

The adsorption process is a surface phenomenon that will depend on the surface of particles per water volume unit into the grid cell. This quantity is denoted as the exchange surface [115], that has dimensions $[L]^{-1}$. Thus, the kinetic transfer coefficient k_1 will be proportional to the exchange surface:

$$k_1 = \chi_1(S_m + S_s) \tag{6.12}$$

where the proportionality factor χ_1 has the dimensions of a velocity and is denoted as the exchange velocity [115]. It is related to the molecular velocity of dissolved radionuclides, which at the same time is related to the temperature of water (see the microscopic description of Abril [1]). S_m and S_s are, respectively, the exchange surfaces for suspended matter and bed sediments (active fraction).

As a first approach, assuming spherical particles and a step function for the grain size distribution of particles, it can be easily shown [115] that:

$$S_m = \frac{3m}{\rho R} \tag{6.13}$$

where ρ and R are density and mean radius, respectively, of suspended matter particles.

The water-sediment interface can be considered as a high suspended matter environment [88]. Thus, the exchange surface for the sediment is [115]:

$$S_s = \frac{3Lf\phi}{RH} \tag{6.14}$$

Consequently, the total k_1 coefficient appearing in equation 6.10 can be written as:

$$k_1 = \chi_1 \left(\frac{3m}{\rho R} + \frac{3Lf\phi}{RH} \right) \tag{6.15}$$

It is interesting to note that k_1 is proportional to the suspended matter concentration. Indeed, some laboratory experiments [17, 18] have shown that a direct relation between both quantities exists. Equation 6.15 is the analytical form of such a relation.

Finally, an external source of radionuclides should be added to equation 6.10 at the points where it exists.

This description of the dispersion of non conservative radionuclides has been applied to simulate the transport of ^{226}Ra, ^{238}U and ^{232}Th in the Odiel estuary [117, 118], southwest Spain. However, it has been applied to other, very different, environments. Thus, it has been applied to simulate the dispersion of ^{137}Cs and ^{239,240}Pu in the English Channel [123] and to simulate the dispersion of ^{239,240}Pu in the eastern Irish Sea [121, 124]. In this latter case, the formulation has been extended to a three dimensional description. Recently, the formulation has been applied, in a 3D form, to the Rhone River plume [132, 135]. A very similar description has also been used by other authors to simulate the dispersion of radionuclides in the sea [12, 94].

The equation for the time evolution of specific activity in suspended matter particles is:

$$\begin{aligned} &\frac{\partial(mC_sH)}{\partial t} + \frac{\partial(uHmC_s)}{\partial x} + \frac{\partial(vHmC_s)}{\partial y} \\ &= \frac{\partial}{\partial x}\left(HK_D \frac{\partial mC_s}{\partial x} \right) + \frac{\partial}{\partial y}\left(HK_D \frac{\partial mC_s}{\partial y} \right) \\ &+ k_1 C_d H - k_2 mC_s H + (\text{eros} - \text{dep}) - \lambda mC_s H \end{aligned} \tag{6.16}$$

where k_1 is given by the first term of equation 6.15, since only the transfer from water to suspended matter must be considered, and the erosion and deposition terms are given by:

$$\text{eros} = A_s Ef \left(\frac{\tau}{\tau_{ce}} - 1 \right) \tag{6.17}$$

$$\text{dep} = w_s mC_s \left(1 - \frac{\tau}{\tau_{cd}} \right) \tag{6.18}$$

Of course, there is deposition only if bed stress is smaller than the critical deposition stress and there is resuspension only if bed stress is larger than the critical erosion stress. Again, a source term should be included to equation 6.16 if there exists an external input of radionuclides fixed to solid particles.

It must be noticed that the quantity for which advection and diffusion has to be calculated is mC_s, not C_s.

The equation for the temporal evolution of specific activity in the active sediment fraction is:

$$\frac{\partial A_s}{\partial t} = k_1 \frac{C_d H}{L \rho_s f} - k_2 A_s \phi + (\text{dep} - \text{eros}) - \lambda A_S \tag{6.19}$$

In this equation, k_1 is given by the second term in equation 6.15. The erosion and deposition terms are now written in the following form:

$$\text{eros} = \frac{A_s E}{L \rho_s} \left(\frac{\tau}{\tau_{ce}} - 1 \right) \tag{6.20}$$

$$\text{dep} = \frac{w_s m C_s}{L \rho_s f} \left(1 - \frac{\tau}{\tau_{cd}} \right) \tag{6.21}$$

Again, these terms are calculated only if the conditions given above for the bed stress in relation to its critical erosion and deposition values are satisfied.

The following stability condition is introduced by the terms describing the transfers of radionuclides between the liquid and the solid phases:

$$\Delta t < \frac{1}{k_{max}} \tag{6.22}$$

where k_{max} is the maximum kinetic rate involved in the equations. It means that the activity transferred from one phase to another in a time step must be smaller than the activity content in the origin phase. This condition is more restrictive for a highly reactive radionuclide as Pu than for more conservative ones as, for instance, Cs. As a consequence, when the model described in [132] was applied to Pu, time step had to be decreased in a factor 6 with respect to the used in the application to Cs.

These equations have been given for the case in which uptake/release is described by a model consisting of a single reversible reaction (1-step model). However, there has also been evidence to suggest that uptake takes place in two stages: fast surface adsorption followed by slow migration of ions to pores and interlattice spacings [109, 170].

Recently, models involving several consecutive and/or parallel reactions between operationally defined compartments have been proposed by different authors to describe uptake/release reactions [19, 112, 21, 22, 52, 32] for a number of radionuclides (^{60}Co, ^{58}Co, ^{134}Cs, ^{54}Mn, ^{59}Fe, ^{110m}Ag, ^{109}Cd and ^{239}Pu). These models have been proposed to fit sorption and desorption laboratory experiments, so that the corresponding specific rate constants for the sediment and water used in the experiment are obtained.

Several of these models have been included in the English Channel long-term model, developed to simulate the dispersion of radionuclides released

from La Hague reprocessing plant, described in [130]. The behaviour of the models has been tested under three typical situations, which correspond to the types of source terms of radionuclides that generally can be found: an instantaneous release (would simulate a large accidental discharge), a continuous release (simulates chronic discharges due to the usual operation of the plant) and the case in which there are not releases but the sediment is initially contaminated, so that it behaves as a long-term source of previously released waste radionuclides (this would be the situation after the plant stops its operation). Tested models are a 1-step model consisting of a single reversible reaction, a 2-step model consisting of two consecutive reversible reactions and an irreversible model that consists of three parallel reactions, two reversible and one irreversible (figure 6.6). The radionuclide used for the comparisons is ^{137}Cs, which is essentially adsorbed by electrostatic attraction between Cs^+ and the negatively charged particle surfaces, and by cation exchange of Cs^+ with K^+. Nyffeler et al. [109] suggested that a 1-step model was appropriate for this radionuclide, although Ciffroy et al. [32] proposed a 2-step model and Børretzen and Salbu [22] have recently stated that the most suitable approach for this radionuclide is the irreversible model.

Equations presented through this section can be easily extended to these kinetic models [131]. A description on the behaviour of these models when applied to the situations mentioned above can also be seen in this reference. As an example, the case of redissolution of ^{137}Cs from contaminated sediments is discussed below.

To simulate redissolution, an initial specific activity of 10^5 Bq/kg was considered in the active fraction of the bottom sediment (in the slowly reversible fraction in the cases of the 2-step and the irreversible model) in compartment (26, 24), where discharges from La Hague are carried out. Such content implies a total amount of 2.25×10^{13} Bq in the entire compartment. In the rest of the Channel, sediments are assumed to be clean. The distributions of ^{137}Cs in water and sediments, after 50 days of redissolution, computed by the three models are presented in figures 6.7a to 6.7c. The three models are giving different results for both phases. Generally speaking, due to redissolution, activity goes from the contaminated sediment to the water column above it. Then radionuclides are removed from the area by advective/diffusive processes and they will contaminate initially clean sediments as traced water travels above them. The speed of the redissolution process will govern the distributions obtained in water and bottom sediments as well as activity levels.

The 1-step model produces the quickest redissolution, thus specific activities in water are also the higher ones. Since specific activities in water are high, sediments will also be considerably contaminated. Sediment halving time (which is defined as the time in which specific activity in the sediment decreases in a factor of 2 due to redissolution) obtained with the 1-step model is 7.009 ± 0.016 days. Redissolution from the sediment is so fast that its effect can be compared with an instantaneous discharge: in both cases a patch of contaminated water that moves along the French shore is obtained.

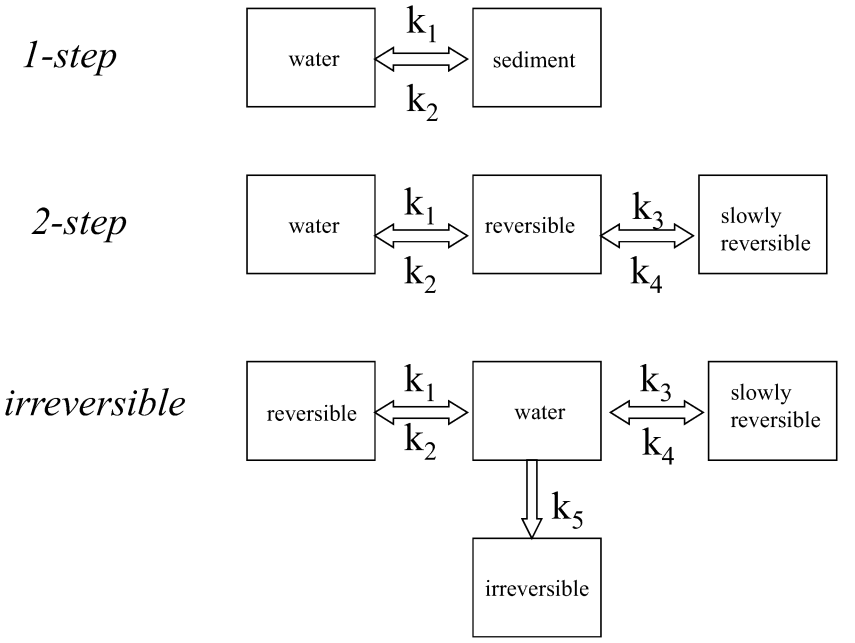

Fig. 6.6. Kinetic models describing interactions between water and sediments tested in the long-term dispersion model for the English Channel

The 2-step and irreversible models produce a slower redissolution. Sediment halving times are 793.3 ± 1.0 days and 51.477 ± 0.004 days with the 2-step and the irreversible models respectively. It can be seen that the slowest redissolution is produced by the 2-step model. As a consequence, this model also gives the lowest activity levels in water and sediments. Specific activities in water with this model are about a factor of 20 smaller than with the 1-step model. Results from the irreversible model lies between the 1-step and 2-step models: specific activities in water are a factor of 2 smaller than those obtained with the 1-step model. It is interesting to notice that, due to the decrease in the rate of redissolution, with the 2-step and irreversible models sediments are really behaving as a long-term source of waste radionuclides. Indeed, distribution maps are similar to those obtained for a continuous release: a plume extending from La Hague to the east is observed. This plume would reach Dover Strait if a longer simulation is carried out.

In general, differences between the three models are clearer when contact times between water and sediments are larger, like in the case of a continuous release from the source, and when redissolution of radionuclides from a con-

taminated sediment is the dominant process. In the case of an instantaneous release, outputs from the three models are more similar. The 1-step model produces a too fast redissolution of radionuclides from the sediments. However, this approach could be useful for models developed for decision-making purposes since it is simple, only two kinetic rates are required, and is computationally cheap. Indeed, in the case of an instantaneous release its output is similar to that of the other two models.

The irreversible model produces a continuous increase of activity in the irreversible fraction, which does not correspond to a realistic situation. This problem may be solved incorporating saturation effects in the irreversible phase (see [131] for details). However, this model also has the inconvenient that many (5) kinetic rates are required, as well as the saturation concentration. Also, initial conditions for running the model are more difficult to define since activity concentrations in three sediment phases should be given over all the model domain. Probably a 2-step model represents a compromise between ease and level of detail of the description. A more detailed discussion may be seen in [131].

Finally, it is also possible to include other processes as redox reactions. It has been done for simulating plutonium dispersion in the eastern Irish Sea. A scheme showing the exchanges of radionuclides between oxidized and reduced forms, and the dissolved and solid phases, was given in figure 2.2. Details on the equations can be seen in [124]. This redox model has also been coupled to a 2-step kinetic model for describing water-sediment interactions. Details are presented in [126, 129]. From calculations carried out, it is concluded that a 1-step kinetic model is enough to properly simulate the contamination of sediments due to a external input of radionuclides since results obtained with the 1-step and the 2-step models are essentially the same. However, if the interest consists of studying the redissolution of radionuclides from a contaminated sediment and subsequent transport, it seems clear that a 2-step model must be applied, as pointed out above. Sediment halving time computed with the 1-step model is two orders of magnitude lower than the value estimated from observations, while halving time computed with the 2-step model is of the same order of magnitude as that deduced from field observations. On the other hand, it has been found that the oxidation state of Pu in the sediment affects the redissolution process, in such a way that halving time is significantly reduced as the fraction of oxidized Pu in the sediment increases.

Examples of results can be seen in figures 6.8a and 6.8b, where the computed distributions of total (reduced plus oxidized) ^{239,240}Pu in water for year 1974 and bed sediments for 1977 are shown, together with the computed fractions of oxidized Pu in water and reduced Pu in the sediment. Computed concentrations are in good agreement with measurements in the sea. Also, the model predicts that essentially all the plutonium in the dissolved phase is in the oxidized form, in agreement with observations as well. On the other hand, plutonium in the sediment predominates in the reduced state. This is

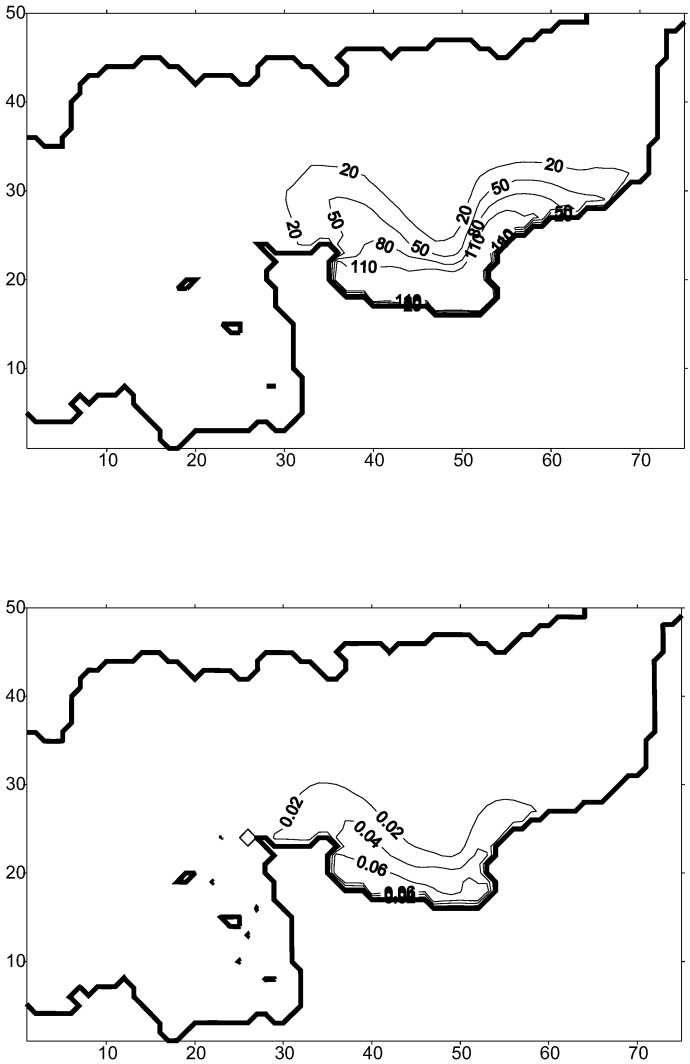

Fig. 6.7a. Distribution of ^{137}Cs in water (Bq/m^3), top, and sediments (Bq/g), bottom, computed by the 1-step model after 50 days of redissolution of ^{137}Cs from sediments of the area of La Hague

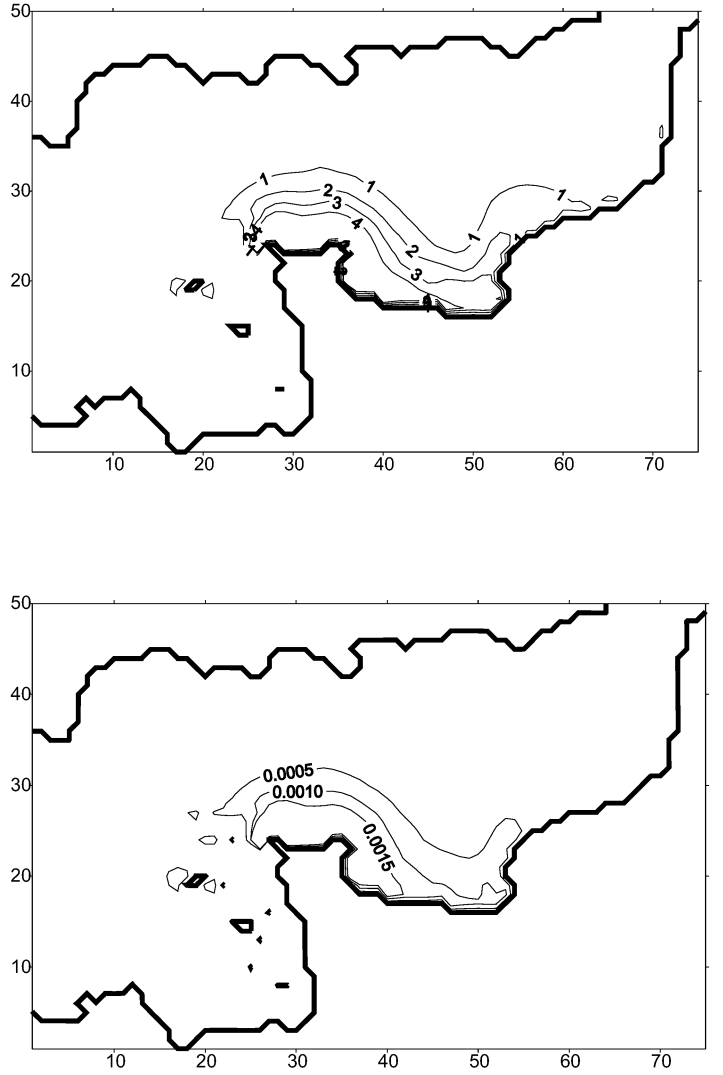

Fig. 6.7b. The same but with the 2-step model

also an expected result since reduced Pu is more reactive than the oxidized form. Nevertheless, the computed fraction of reduced Pu in the sediment is smaller than that obtained from measurements.

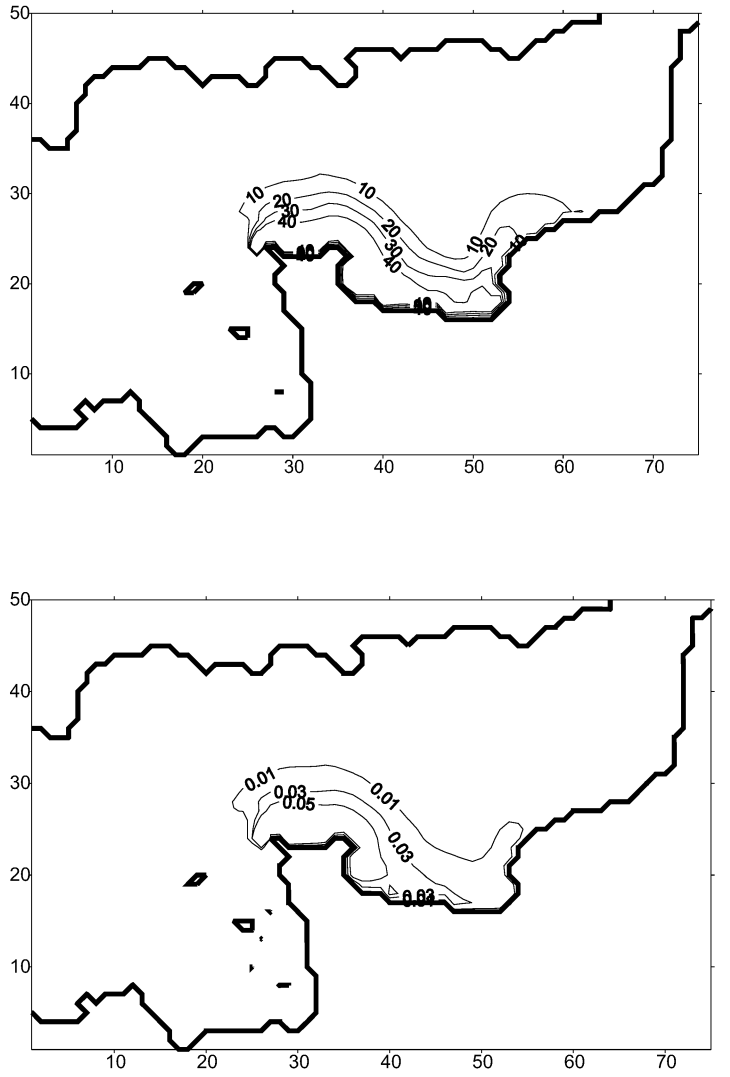

Fig. 6.7c. The same but with the irreversible model

6.4 The Rhone River plume dispersion model

Artificial radionuclides reach the Rhone River through weathering of surface soils contaminated by atmospheric fallout and through the effluents from nuclear facilities: several power plants located along the river course and, mainly, from Marcoule nuclear fuel reprocessing plant (now is not in operation but releases have continued since washing effluents are produced and discharged). In the case of the Rhone mouth, the low mixing of the discharge waters gives

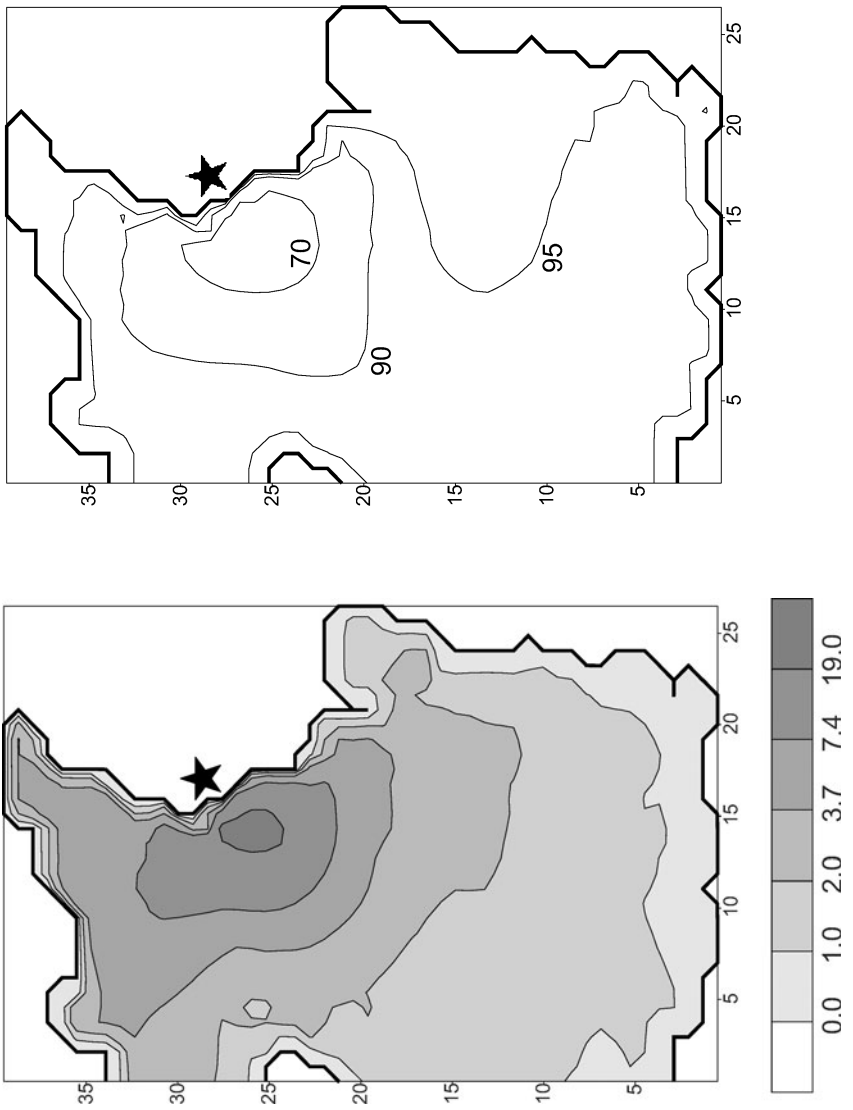

Fig. 6.8a. Computed distribution of total ^{239,240}Pu in water (Bq/m^3) for 1974 together with the computed fraction (%) of oxidized Pu. The star is Sellafield nuclear fuel reprocessing plant

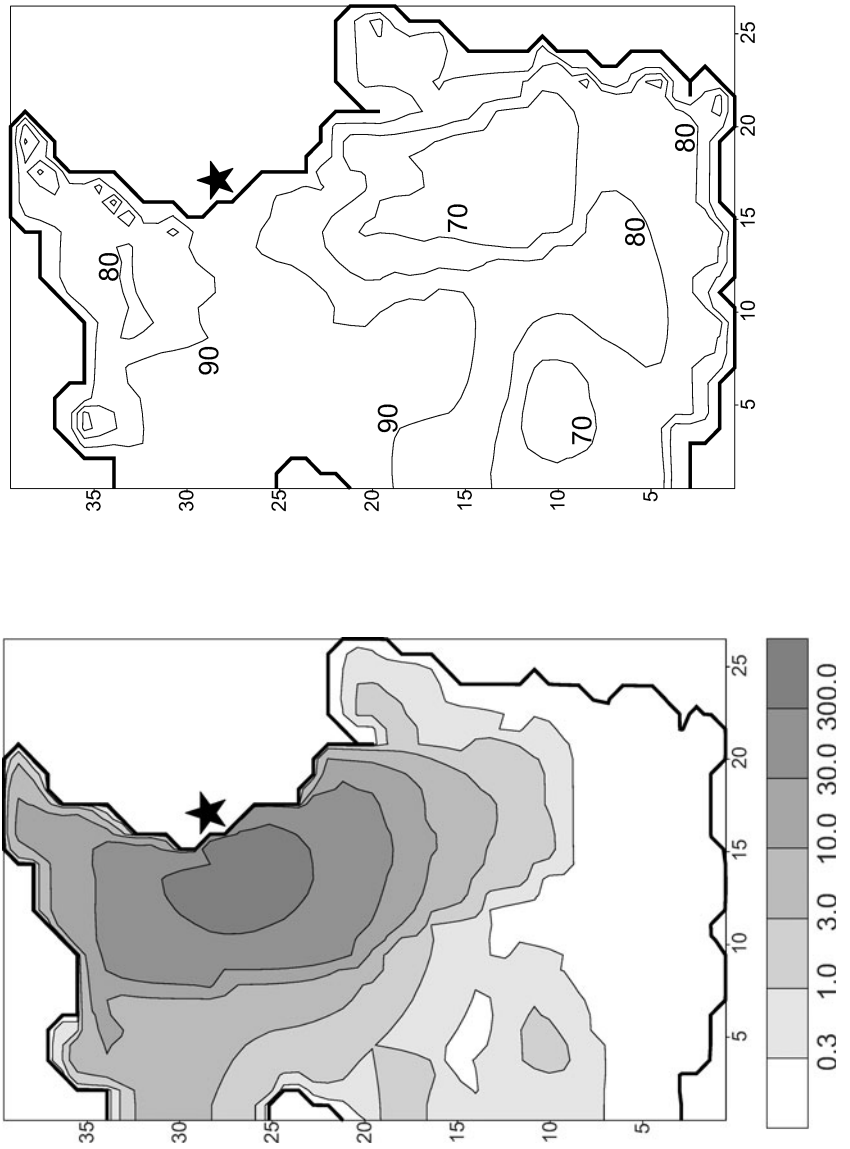

Fig. 6.8b. Computed distribution of total ^{239,240}Pu in sediments for 1977 (kBq/m^2) and computed fraction of reduced Pu (%)

place to a well-identified surface freshwater plume in which a thin upper layer (1 or 2 m) is separated from the ambient seawater by a sharp density gradient. This plume extends 20 or 30 km offshore. Numerical modelling of these plumes is a difficult task that requires the inclusion of density differences in the full 3D hydrodynamic equations. The Rhone River gives the opportunity to test the behaviour of radionuclide dispersion models, including a kinetic approach for the transfers between the liquid and solid phases, when integrated with a detailed hydrodynamic model of a complex oceanographic system as a surface river plume. The Rhone River plume model, developed at the University of Seville, is described in detail in [132, 135]. Thus, only a brief description of the model is given here and some examples of the type of results that may be obtained are presented. However, all equations are summarized in appendix A.

6.4.1 Model description

Water circulation is obtained from the full three dimensional hydrodynamic equations, including baroclinic terms that account for density gradients (see for instance [84]). Water density is related with salinity through a standard equation of state [84] and salinity is computed from an advection/diffusion equation with appropriate boundary conditions at the river mouth (zero salinity at this point). A 1-equation turbulence model is applied to determine the vertical eddy viscosity over the model domain [43].

Several suspended particle classes are considered in the model. Each particle class is governed by an advection/diffusion equation to which the settling, deposition and erosion terms are added. The settling velocity of each particle class is determined from Stokes's law applied to the average particle diameter of each class. The deposition rate is written in terms of the settling velocity of particles and their concentration just above the sea bed. The erosion term for each particle class is written using the erodability constant and the fraction of particles of the corresponding class in the bed. Critical erosion and deposition stresses are also used in the conventional form. Sedimentation rates are calculated as the balance between the deposition and erosion terms. Thus, the description for suspended sediment transport presented in this chapter, but in a 3D form, has been used. Details on the equations may be seen, however, in [135].

Bed-load transport of coarse particles has not been included since most contaminants are essentially adsorbed on the fine particles. This is also the case for radionuclides, as has been commented before.

The only difference with respect to the original model presented in the previous section is the inclusion of the explicit dependence of the kinetic coefficient k_1 with salinity, that in this application changes from freshwater to seawater values. The exchange velocity χ_1 depends on salinity as in [86]:

$$\chi_1 = \chi_1^0(1 - \delta) \tag{6.23}$$

where

$$\delta = \frac{S}{S + S_0} \tag{6.24}$$

In these equations χ_1^0 is the freshwater value of the exchange velocity and S_0 is the salinity value at which 50 % of saturation occurs [86]. It must be noted that as salinity increases, the transfer of radionuclides to the solid phase decreases due to competition effects of radionuclides with ions dissolved in water. The relations given above have been tested through laboratory experiments [86].

A 1-step kinetic model is used since, given the short time scale of the simulations that are carried out (several days), it is not expected that significant differences between the 1-step and the 2-step models appear in this case.

The hydrodynamic calculations are started from rest and an uniform salinity of 38 g/L is assumed. The effect of the large-scale circulation is neglected in the area under study, as well as tidal currents that are practically non-existing.

The hydrodynamic model is run for a given water discharge from the Rhone until a steady salinity and current amplitude pattern is obtained. Then the suspended matter model is run using such water circulation. The suspended matter model (without the erosion term) is started from a sea bottom containing no sediments. Then the accumulation of particles of each class is calculated to have a first estimation of the distribution of sediment classes over the model domain. Next, the suspended matter model is started (with erosion) from the estimated distribution of particle classes until a steady state is reached. This way a self-consistent distribution of different particle classes on the sea bed over the model domain can be obtained. This distribution is relevant to calculate the adsorption of radionuclides by the bed sediments since they adsorb radionuclides from the deepest part of the water column.

Once the water circulation, salinity distribution, suspended matter distribution for each particle class and distribution of particles in bed sediments are known and stored in files, the radionuclide dispersion model may be run using these files as input data.

The model resolution is $\Delta x = \Delta y = 1000$ m. A variable grid is used in the vertical to have enough resolution to solve the salinity gradients in the surface plume. Thus, 10 layers with $\Delta z = 1$ m are used followed by thicker layers increasing to $\Delta z = 15$ m. Time step is fixed as 5 s to solve the hydrodynamic equations due to the CFL stability condition. It is increased to 60 s to solve the suspended matter and radionuclide equations. However, when the radionuclide dispersion model was applied to plutonium, time step had to be decreased to 10 s due to the stability condition given by equation 6.22.

Four suspended matter particle classes are considered in the model according to [165]. They are shown in table 6.1. Concentrations in table 6.1 are the boundary conditions of the suspended matter model at the river mouth. The settling velocity deduced from Stokes's law for each class is also given.

Table 6.1. Average particle size for each particle class included in the model and their corresponding settling velocities. The particle concentration at the Rhone River mouth for average water discharge is also given

Average particle size (μm)	w_s (m/s)	m (mg/L)
3	7.8×10^{-6}	11.5
7	4.2×10^{-5}	9.5
20	3.5×10^{-4}	3.5
40	1.4×10^{-3}	3.5
total load		28

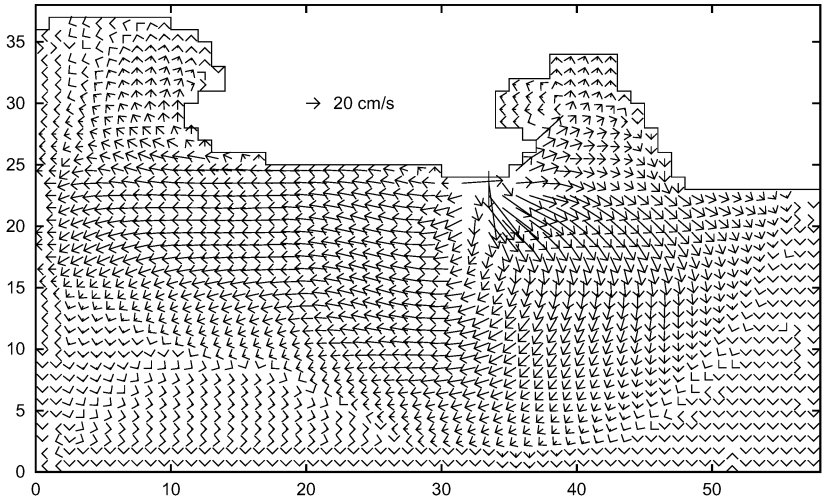

Fig. 6.9. Computed surface currents for average water discharge (1700 m^3/s) and no wind. Each unit in the x and y axis is 1 km

6.4.2 Results: some examples

The computed currents in the domain for average water discharge and no wind are presented in figure 6.9. These currents were obtained after a simulation time of 48 hours. Water discharged by the river moves in a southeast direction and then rotates towards the west due to Coriolis acceleration and moves along the coast. The salinity distribution in the surface plume can be seen in the map presented in figure 6.10. This distribution is essentially the same as that previously computed in [56, 96]. The shape of the salinity contours, together with the currents presented in figure 6.9, indicate that the plume forms a bulge of anticyclonic circulation in front of the river mouth. The circulation in the plume is baroclinic, that is, induced by the density differences.

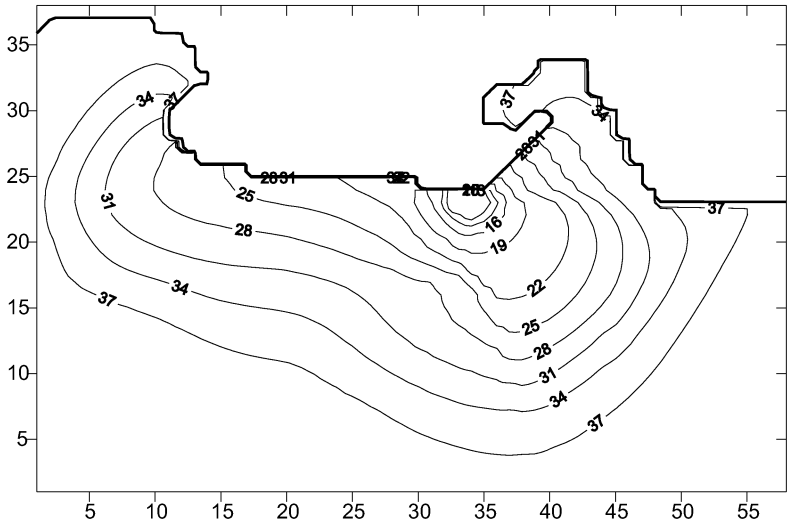

Fig. 6.10. Computed surface salinity (g/L) after a simulation time of 48 hours

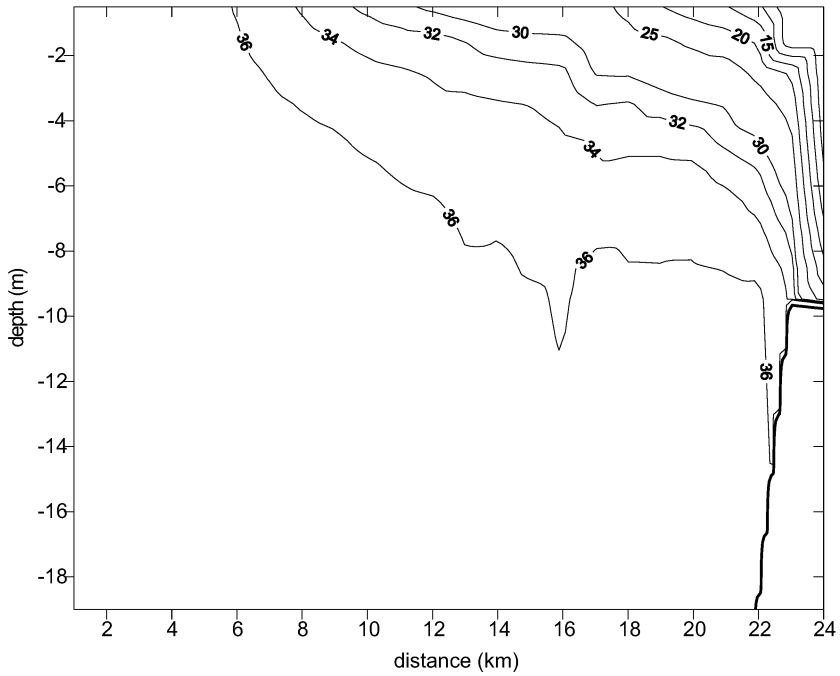

Fig. 6.11. Computed salinity (g/L) south-north vertical profile in front of the river mouth (located 24 km north from the south of the model domain) after a simulation time of 48 hours

A vertical salinity profile following a north-south transect in front of the river mouth can be seen in figure 6.11.

A map showing the total concentration of particles obtained after a computation time of three days can be seen in figure 6.12, together with measured sediment concentrations in the plume. The shape and extension of the plume is in agreement with the computations in Kondrachoff et al. [83], although in their model only one size of particles is considered, and with suspended matter concentrations obtained from satellite [83]. The plume is directed to the southwest offshore, following the water circulation.

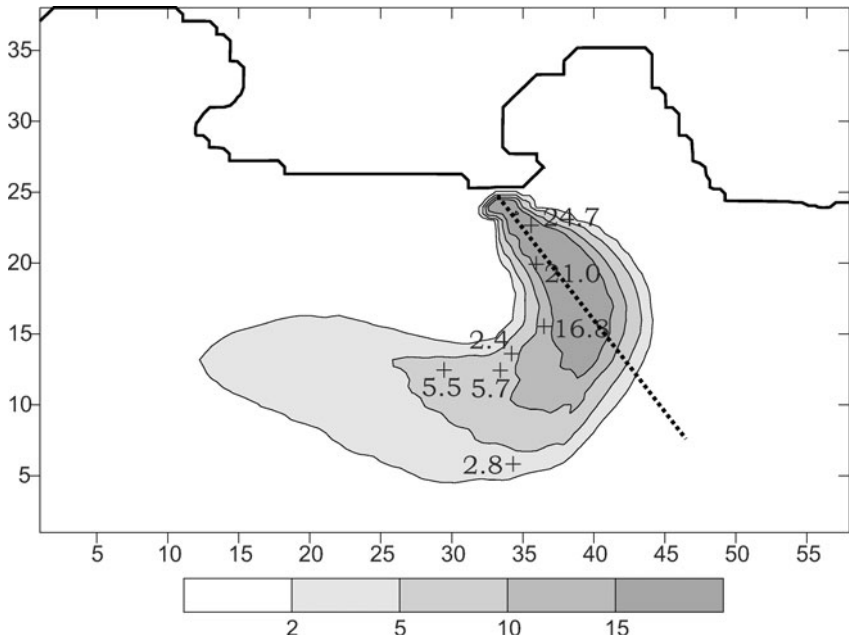

Fig. 6.12. Computed total suspended matter concentrations (mg/L) over the model domain after a computation time of three days. The dashed line indicates the axis of the plume. Measured concentrations [97, 104] are also shown

Four maps, showing the concentration of particles for each class at the surface, are presented in figure 6.13. It can also be clearly seen how the plume is mainly composed of small particles. The two largest classes settle close to the river mouth.

The computed sedimentation rates along the plume axis are shown in figure 6.14 together with the estimations presented in [148] obtained from ^{210}Pb profiles. The model underestimates the sedimentation rates. However, the following points have to be considered: estimated sedimentation rates are maximum possible values since they are calculated assuming that there is not

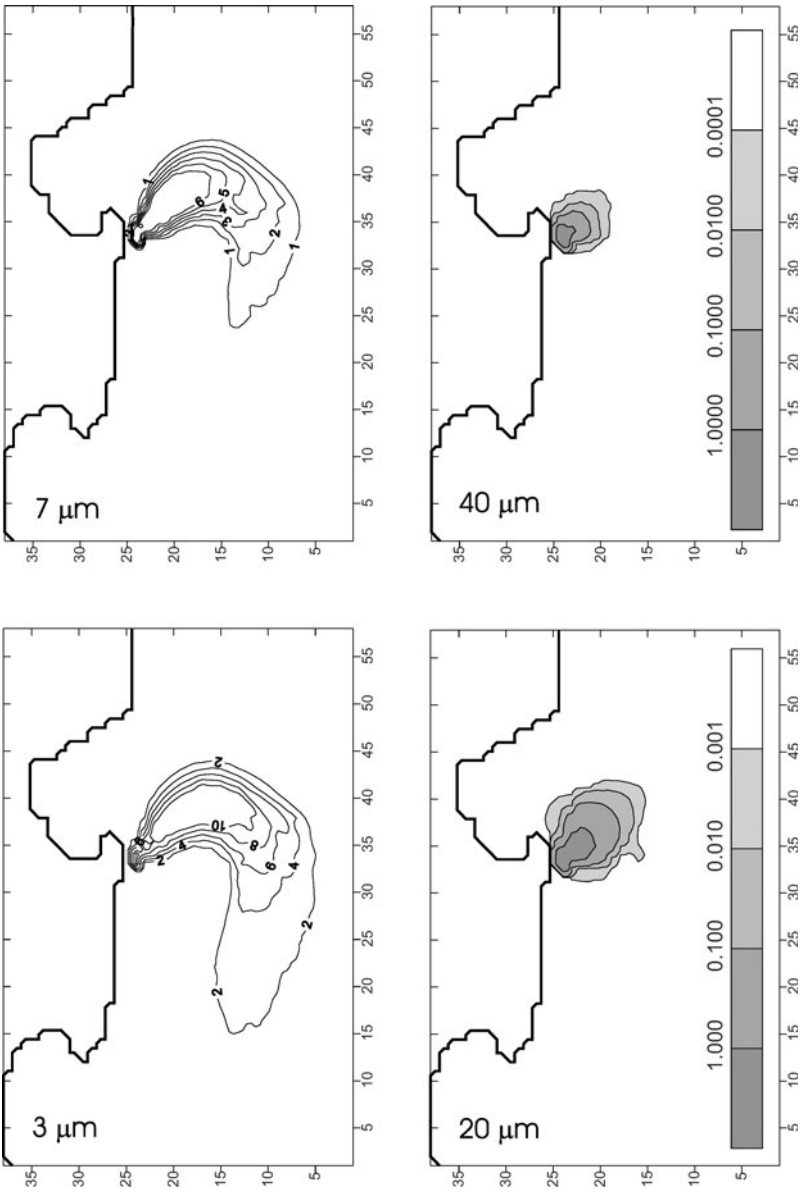

Fig. 6.13. Computed suspended matter concentrations at the surface for each particle class (mg/L)

diffusion in the sediment core. Also, the values obtained from the model are calculated for an average water discharge, and sedimentation increases during flood events when a large amount of suspended matter is discharged by the river. Finally, if must be taken into account that bed-load transport of coarse material is not included in the model. This process can also contribute to a larger sedimentation rate.

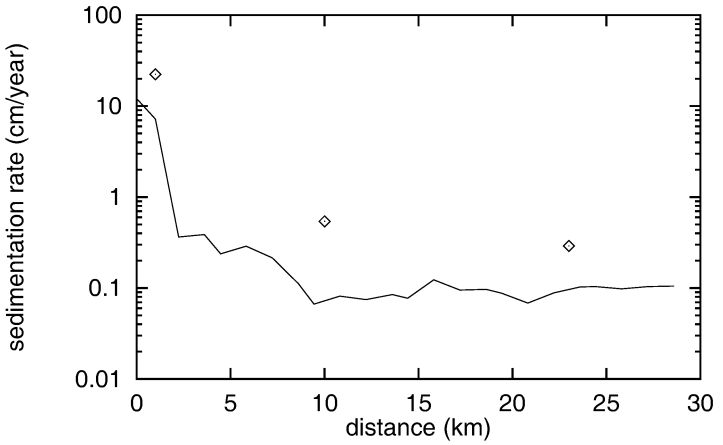

Fig. 6.14. Computed sedimentation rates along the plume axis (see figure 6.12) together with the values estimated from observations [148]. Distances are measured respect to the river mouth

Nevertheless, the model gives a realistic representation of the sedimentation process in the plume: a deposition belt is observed close to the river mouth, where sedimentation reaches values of the order of 10 cm/year, decreasing on the shelf to values of the order of 10^{-1} cm/year.

The radionuclide dispersion model consists of 9 equations expressing the time evolution of activity concentrations in the dissolved phase, the 4 suspended particle classes and the 4 bed sediment grain sizes (a summary of model equations for radionuclide dispersion is given in appendix A). Radionuclides used in the simulations are ^{137}Cs and ^{239,240}Pu. The input of radionuclides from the river in the dissolved and particulate forms has been obtained from [97]. Inputs from the river have been obtained from sampling campaigns carried out in the period 1982-1985. For this time the main source of radionuclides to the river is due to the discharges from Marcoule reprocessing plant, being fallout and watershed soil leaching negligible if compared with them. Also, no relevant radionuclide discharge variations have been found in these years [97].

The dispersion of radionuclides released from the river is calculated until a steady distribution is obtained. The radionuclide discharges are carried out assuming that the sea is initially no contaminated.

Different plutonium oxidation states have not been considered due to the lack of experimental data on Pu speciation in the Rhone area. Several studies have been carried out with respect to the transport of radionuclides in colloidal form in the plume. It has been found that Cs is not significantly fixed to colloids [57]. The fraction of colloidal Pu measured by Eyrolle and Charmasson [58] ranges from 0 % to 41 % of the dissolved phase plutonium content. Considering that over 90 % of Pu is fixed to suspended matter (see below), the fraction of colloidal Pu represents a maximum of 4 % of the total Pu content. Thus, colloids have been neglected in the case of Pu as well. Also, it seems that changes in POC (particulate organic carbon) do not affect significantly the adsorption of radionuclides [166].

Model results are compared with observations in figure 6.15, where south-north profiles in front of the river mouth of ^{137}Cs and ^{239,240}Pu in water and suspended matter (at the surface) are shown. It can be seen that computed activity levels are, in general, in agreement with observations.

The computed distribution of ^{137}Cs in bed sediments is presented in figure 6.16, together with observations obtained from [97]. It can be seen that the model gives a correct estimation of activity levels in the vicinity of the river mouth, although underestimates them away from it. It must be taken into account that sediments integrate radionuclide input variations over time. Also, episodes of high river discharge, when larger amounts of particles are released to the sea and are also transported to greater distances from the river mouth, as well as different wind conditions, are integrated in the measured concentrations. Computed concentrations are obtained for average water, suspended particles and radionuclide discharges. It is not possible to have a accurate agreement between measurements and computations with a model working in *average* conditions. Nevertheless, it seems clear that the model produces rather realistic activity levels in the area of the river mouth. Indeed, the distribution map in figure 6.16 is very similar to that presented in [30], where a sharp decrease in inventories with distance from the river mouth can be seen. Finally, it must be taken into account that measured bed concentrations include deposition from global fallout. Only sampling stations close to the river mouth in [30] present ^{137}Cs inventories clearly in excess with respect the cumulative deposit due to global fallout (Chernobyl fallout is not considered since occurred later than the time of our simulations). Thus, most of ^{137}Cs in sediments appears in a well-delimited zone in the close vicinity of the river mouth. Our simulations are in agreement with these findings.

The computed fractions of ^{137}Cs and ^{239,240}Pu fixed to suspended matter particles in surface waters of the plume are presented in figure 6.17. It can be seen that about 60 % of Cs is fixed to solid particles. This is in agreement with Calmet and Fernandez [25], that found that ^{137}Cs associated with par-

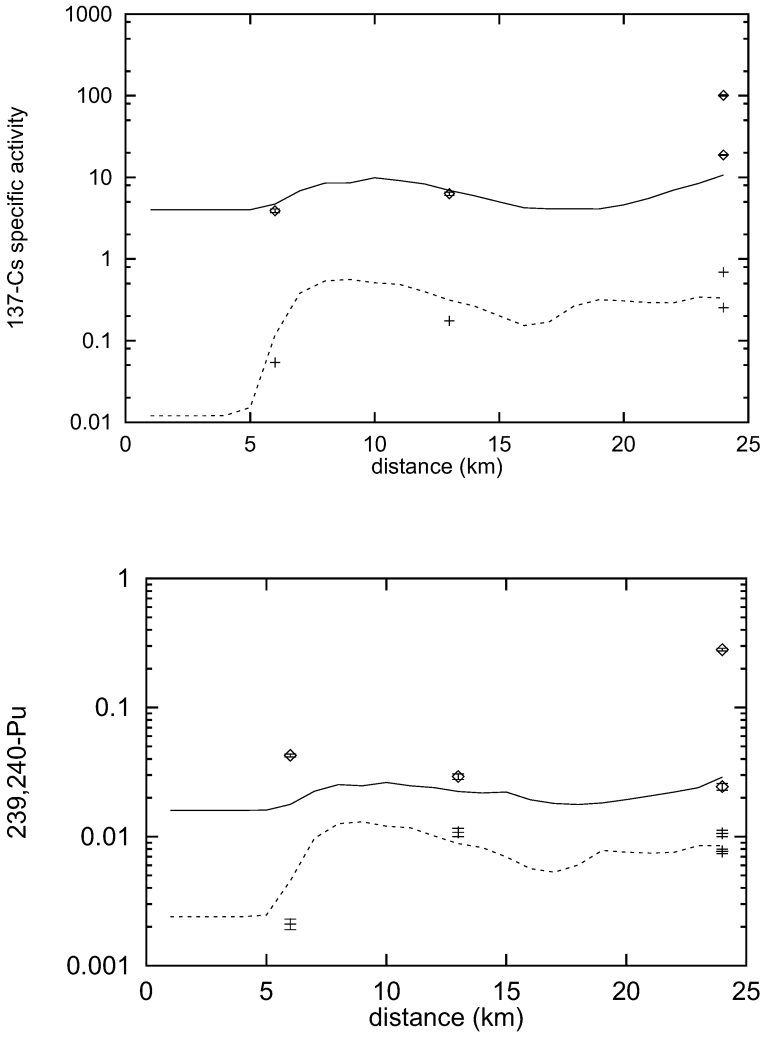

Fig. 6.15. Measured (points) and computed (lines) south-north profiles of ^{137}Cs and ^{239,240}Pu in surface water (solid line, boxes), Bq/m^3, and suspended matter (dashed line, crosses), Bq/g, in front of the river mouth. Distances are measured from the south of the model domain (the river mouth is at km 24)

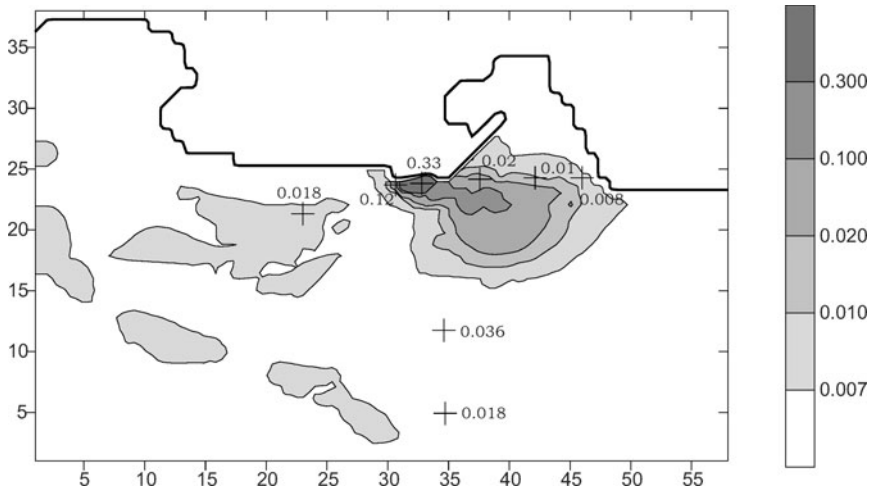

Fig. 6.16. Computed distribution of ^{137}Cs in bed sediments (Bq/g). Measured concentrations [97] are also shown

ticles represents 68 % of the Rhone input. Eyrolle and Charmasson [58] have reported that 85 % of Pu isotopes are bound to particles.

It is also possible, for instance, to obtain vertical distributions of radionuclides. k_d distribution coefficients can be calculated as well (instead of requiring them as input data). Computed ^{137}Cs suspended matter-water distribution coefficients (total suspended matter) for surface waters are presented in figure 6.18. They are of the order of 10^4 L/kg in the area of the plume, decreasing in one order of magnitude out of it and approaching the average value recommended by the IAEA [74] for Cs (3×10^3).

South-north vertical profiles of ^{137}Cs activity concentrations in suspended matter in front of the river mouth and for several particle classes are presented in figure 6.19, together with specific activity in total suspended load. It can be seen that the radionuclide content in the plume suspended load is essentially controlled by the smallest particles, since figures 6.19a and 6.19b are very similar. Coarse particles quickly sink to the bottom and, as a consequence, radionuclides are only present in a small region in front of the river mouth as can be seen in figures 6.19c and 6.19d. This is in agreement with the results of Martin and Thomas [97], who found a deposition belt close to the river mouth. It seems that this deposition belt is produced by the coarsest particles in the plume.

Vertical profiles, in front of the river mouth, of plutonium in water and total suspended matter (both in Bq/m^3), can be seen in figure 6.20. The suspended matter profile is clearly different to that of ^{137}Cs (figure 6.19). In this case, it can be appreciated, together with the surface plume, a deep layer with some Pu content which appears due to the higher reactivity of plutonium. This

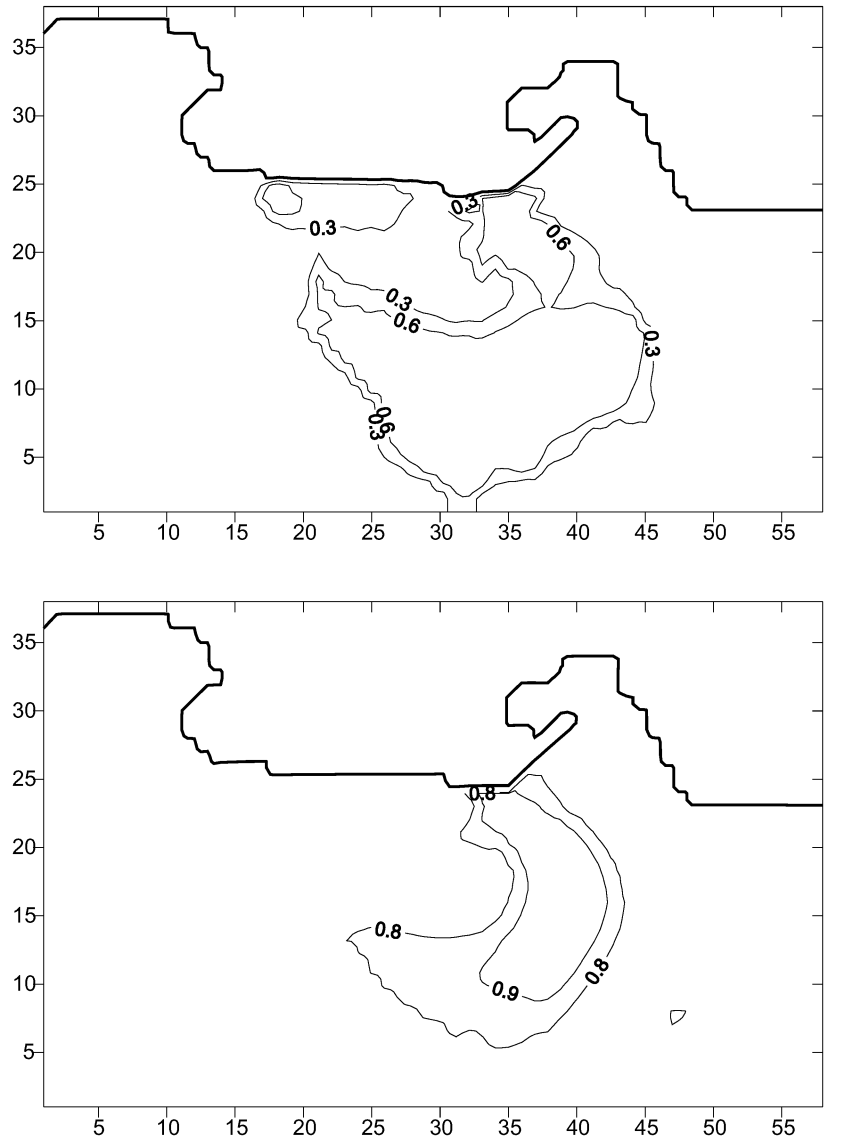

Fig. 6.17. Computed fractions of radionuclides fixed to suspended particles in surface waters for ^{137}Cs (up) and ^{239,240}Pu (down)

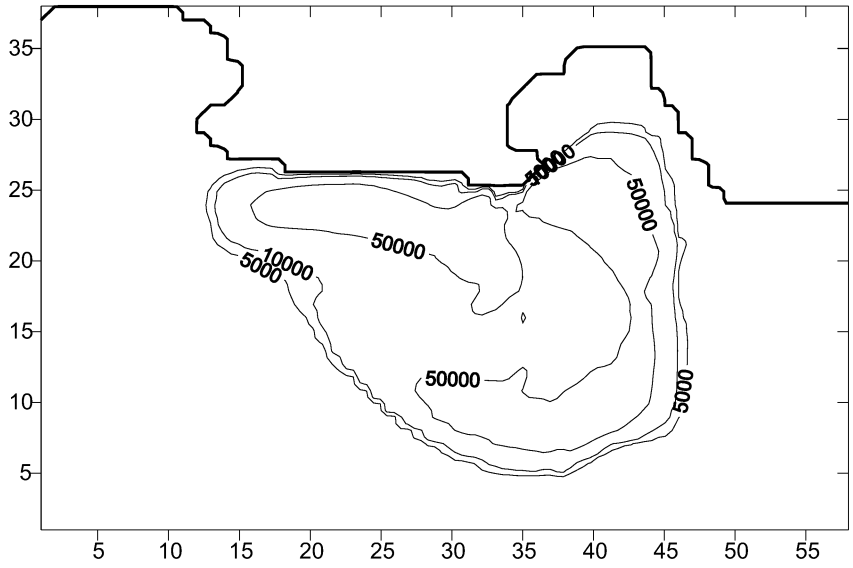

Fig. 6.18. Computed suspended matter-water k_d (L/kg) for ^{137}Cs in surface waters

deep layer is composed of the coarse particles that sink quickly after they are released from the river. When these contaminated particles penetrate the bottom waters (not contaminated by Pu discharged from the Rhone), plutonium is partially redissolved. This leads to the sub-surface layer of contaminated water that can be seen in figure 6.20. Indeed, Eyrolle and Charmasson [58] have detected some Pu coming from Marcoule reprocessing plant discharges in the bottom waters of the mixing zone.

More details about the model formulation and results may be seen in [132, 135]. Here we only pretend to present some results to show the type of information that can be obtained from these models for non conservative radionuclides.

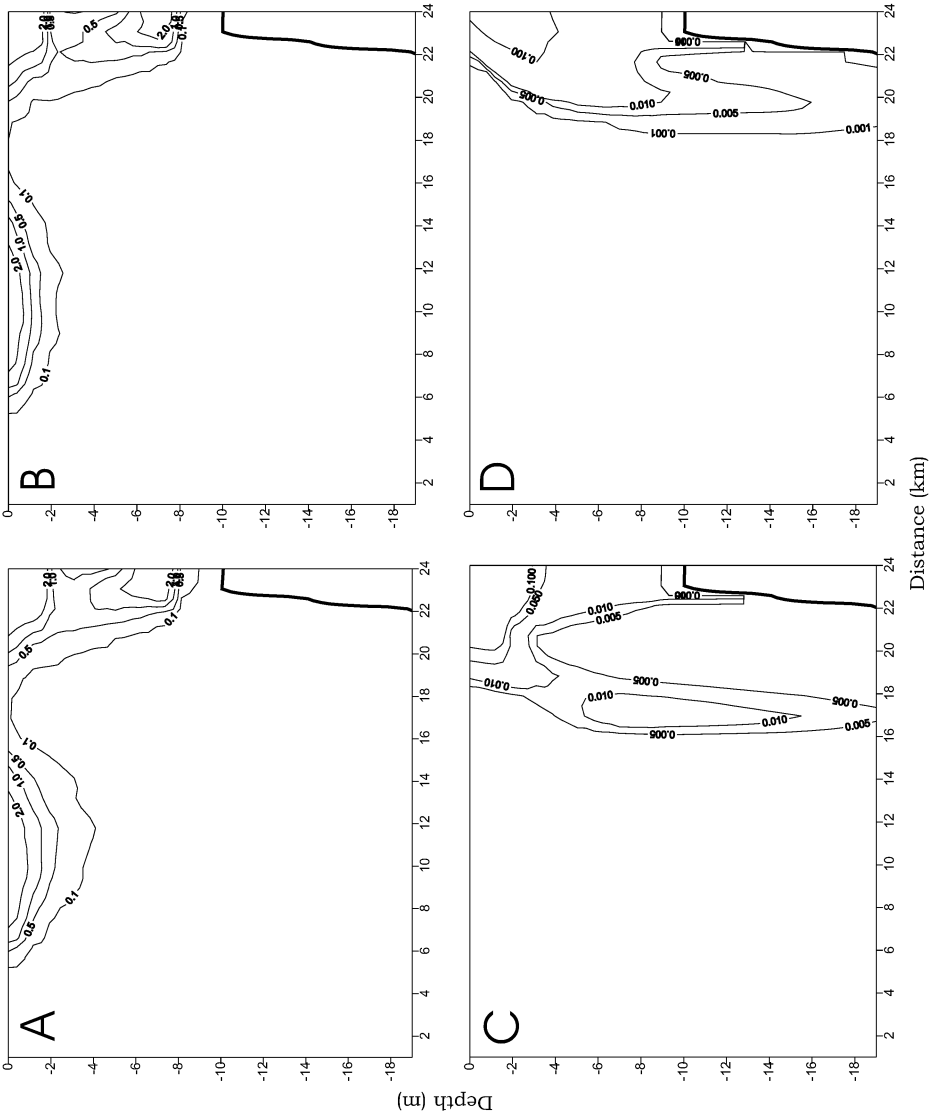

Fig. 6.19. Computed ^{137}Cs activity in suspended matter in Bq/m^3 for a south-north vertical profile in front of the river mouth. A: total suspended matter. B, C and D: 3, 20 and 40 μm particles respectively. Distances are measured from the south of the model domain. The river mouth is at km 24

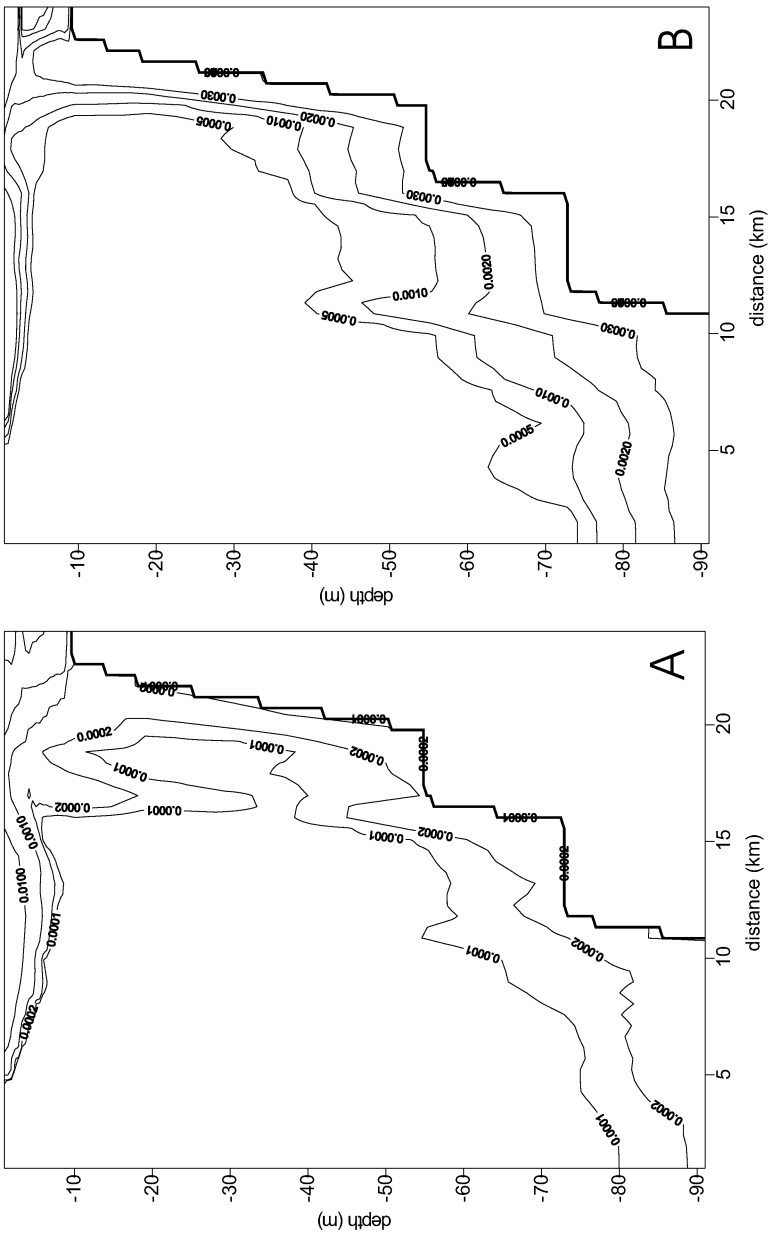

Fig. 6.20. Computed ^{239,240}Pu activity in suspended matter (A) and water (B), both in Bq/m^3, for a south-north vertical profile in front of the river mouth and for total suspended matter

7

Lagrangian dispersion models

7.1 Introduction

As has been commented before, in this type of model a release of radioactivity to the sea is modelled as a number of discrete particles, each particle being equivalent to a number of units (Bq, moles, atoms, etc...). Then the path followed by each individual particle is computed, turbulent diffusion being modelled as a three dimensional random walk (Monte Carlo) process. The density of particles per water volume unit is calculated to obtain the radioactivity concentrations at the end of the simulation.

Particle-tracking methods are well suited for problems in which high contamination gradients are involved, since they do not introduce numerical diffusion. Also, they can give very fast answers, specially if the hydrodynamic calculations are made off-line and tidal analysis and computed residuals are used to reconstruct water movements, which avoids the CFL limitations in the dispersion calculations. Thus, particle-tracking models are very useful predictive tools that can be used for assessing contamination after accidental or deliberate releases of radioactivity. Particle-tracking models have been used to simulate the dispersion of passive tracers [69, 64], radionuclides [153, 125, 102, 103], oil spills [145, 146] and even contaminated milk [55] in coastal waters.

The method to solve the essential processes (advection, diffusion and radioactive decay) in the Lagrangian approach will be presented in this chapter. Then the GISPART model (GIbraltar Strait PARticle Tracking code) is described as an example. This is a particle tracking model that simulates the dispersion of radionuclides in the Strait of Gibraltar [133]. The GISPART model is available on line at www.personal.us.es/rperianez.

Finally, a method to include the transfers of radionuclides between the dissolved and solid phases in a particle tracking approach is described [125].

7.2 Advection, diffusion and decay

The position vector of a given particle, $\mathbf{r}(t + \Delta t)$, at time $t + \Delta t$ is computed from:

$$\frac{\mathbf{r}(t + \Delta t) - \mathbf{r}(t)}{\Delta t} = \mathbf{q}(t) \tag{7.1}$$

where Δt is the time step used in the model and $\mathbf{q}$ is the current vector, of components u and v along the x and y axis respectively. Currents are generally obtained by running a hydrodynamic model in advance.

It can be observed that equation 7.1 constitutes a first order explicit approximation to an advection equation, since the water current changes continuously as the particle moves. However, for real sea dispersion calculations a first order accuracy scheme is adequate. When simulating the movement of drogues in an estuarine environment, Elliott and Clarke [54] found no improvements of results when a second order accuracy scheme was used. Indeed, the effects of turbulence will mask any small errors in the advection scheme. Thus, in practice, it is enough to obtain current components, $u(t)$ and $v(t)$, at the grid cell where the particle is located and use them directly into equation 7.1. Nevertheless, more complex interpolation algorithms may be applied as well [33, 153].

Three dimensional diffusion is simulated using a random walk method. It has been shown [145, 73] that it is a simulator of Fickian diffusion provided that the maximum size of the horizontal step given by the particle, D_h, is:

$$D_h = \sqrt{12 K_h \Delta t} \tag{7.2}$$

in the direction $\theta = 2\pi RAN$, where RAN is a random number between 0 and 1. This equation gives the maximum size of the step. In practice, it is multiplied by RAN to obtain the real size at a given time and for a given particle. Similarly, the maximum size of the vertical step is:

$$D_v = \sqrt{2 K_v \Delta t} \tag{7.3}$$

given either towards the sea surface or the sea bottom. K_h and K_v are the horizontal and vertical diffusion coefficients respectively. While there is no stability criterion equivalent to the CFL condition in the particle tracking calculations, it is wise to ensure that each particle does not move through a distance that exceeds the grid spacing during each time step.

Consider now the radioactive decay equation:

$$\frac{\partial C}{\partial t} = -\lambda C \tag{7.4}$$

where λ is the radioactive decay constant. This equation can be treated using a stochastic method if it is assumed that the probability p of removal of a particle at each time step is [145, 73]:

$$p = 1 - e^{-\lambda \Delta t} \tag{7.5}$$

In practice, a random number is generated for each particle at each time step. If $RAN \leq p$ then the particle is removed from the computation. The solution of the radioactive decay equation with this method is shown in figure 7.1 for a radionuclide with a half-life of 1 day and using 300 particles. It can be seen that the stochastic solution mimics the exact solution rather well. The agreement is getting better as the number of particles used in the calculation increases.

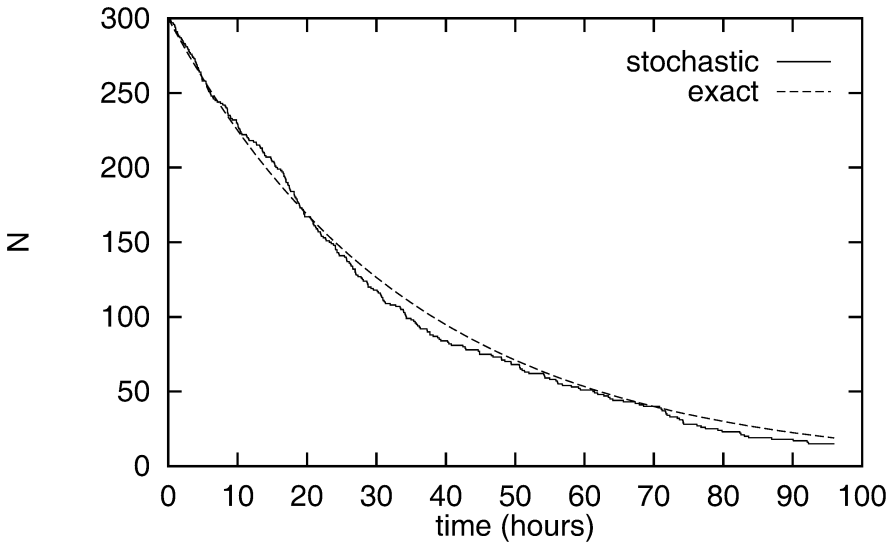

Fig. 7.1. Solution of the radioactive decay equation with the stochastic method and exact solution

The particle-tracking model is three-dimensional, but the hydrodynamic calculations are often carried out with a 2D depth averaged model. Thus they provide depth-averaged currents. In the main body of water above the logarithmic layer, the flow gradually increases in a manner which may be represented as [147]:

$$u_{z'} = u_s \left(\frac{D - z'}{D} \right)^{1/m} \tag{7.6}$$

where $u_{z'}$ is the current speed at a level z' below the sea surface and u_s is the surface flow. From observations, it has been deduced that m ranges between 5 and 7. The surface current can be deduced from the depth averaged one [147]:

$$u_s = \frac{m+1}{m}\overline{u} \tag{7.7}$$

where $\overline{u}$ is the depth averaged current. Thus, components u and v of the current at any depth can be obtained from their depth-averaged values (provided by the hydrodynamic model) applying equations 7.6 and 7.7. This current profile is used for instance in [149, 133] in a particle tracking dispersion model.

Wind is typically included in particle-tracking models assuming that the surface wind-induced current is 3 % of the wind speed measured 10 m above the sea surface [147, 145]. This current decreases logarithmically to zero at a depth z_1. This depth is generally assumed to be 20 m [53]. The wind induced current at a depth $z' < z_1$ is written as [147]:

$$u_{z'} = u_0 - \frac{u^*}{\kappa} \ln\left(\frac{z'}{z_0}\right) \tag{7.8}$$

where u_0 is the surface wind-induced current, $\kappa = 0.4$ is the von Karman constant, u^* is a friction velocity and z_0 is the sea surface roughness length, which has values between 0.5 and 1.5 mm. It has been obtained [147] that the friction velocity can be estimated as

$$u^* = 0.0012W \tag{7.9}$$

for a wide range of conditions, where W is wind speed 10 m above the sea surface. From these equations, the wind effect on the advection of particles can be calculated. Of course, the current profile is solved in the u and v components.

Some boundary conditions must be specified when computing advection and diffusion of particles. In the case of an open boundary, particles that cross it are removed from the computation. In practice, a label (for instance 1) is assigned initially to each particle. If a particle must be removed from computations at a given time (because has moved out of the domain or has decayed) the label is changed to a new value (say 0 for instance). The label of each particle is checked each time step before computing advective and diffusive transport. If the label is zero such calculations are not carried out. Of course, these particles are not considered for calculating activity concentrations from the density of particles (see below).

In addition, as with a finite difference model, flux of particles through land boundaries, sea surface and the sea bed is not allowed. If a given particle steps onto land when computing diffusion, this movement is not allowed and new random numbers are generated to repeat the particle displacement. In practice, less than five repetitions are required to obtain a valid particle displacement even in the case of a complicated topography.

The output of a particle tracking model is the position of each particle. Concentrations can be obtained by counting the density of particles (number of particles per water volume unit):

$$C = N \times R \tag{7.10}$$

where C is concentration, N is density of particles and R is the number of units (for instance Bq) that is equivalent to each particle:

$$R = \frac{I}{NP} \tag{7.11}$$

where I is the total radioactivity input and NP is the number of particles used in the simulation.

When a continuous release is simulated the number of particles that are being tracked increases linearly during the computation until the time at which the release ceases is reached. At this time (and for longer times if the computation extends beyond the end time of the release) there are NP particles in the simulation (some of which may have decayed or moved out of the region of interest) and therefore the required accuracy is achieved at the end of the simulation. At intermediate times, for example at 10 % of the way through the computation, there will only be $NP/10$ particles in the simulation and therefore the accuracy of the intermediate results will be lower than that obtained at the end of the simulation. In such circumstances the model user must decide on the simulation time at which the highest accuracy results are required. If the interest is in short time scales after the release, the model should not be run to simulate a long continuous release. However, there is no computational reason why the technique cannot be applied to releases that continue over decades and algorithms have been devised that can mimic both sporadic and long term spill scenarios.

7.3 GISPART model

GISPART is a three-dimensional particle-tracking code designed to simulate the dispersion of contaminants in the Strait of Gibraltar. All files required are into the archive GISPART.RAR, that can be downloaded from www.personal.us.es/rperianez. The model, together with instructions, is also included on the disk.

GISPART is a simple, but robust, model that may be used for decision-making purposes since gives a very fast response. It consists of two sub-models. First, a hydrodynamic module is run off-line. This provides the tidal constants and residuals that are required to reconstruct water movements in the model domain. Tidal constants and residuals are stored in files that are read by the dispersion module to compute advective transport. Once that the hydrodynamic module has been adequately calibrated and all information required by the dispersion computations is stored, it is not necessary to repeat the hydrodynamic calculations. More information on the technical aspects of the model can be seen in [133].

7.3.1 Hydrodynamic module

An important feature of the tidal flow in the Strait is that it can be considered, as a first approach, as barotropic [93, 168]. As a consequence, 2D depth-averaged models have already been applied to simulate surface tides in the Strait (see for instance [163]). In [167] a 2D barotropic model is used for simulating tides in the whole Mediterranean Sea. The success of these models indicates that the baroclinic component is of secondary importance.

The barotropic hydrodynamic equations (equations 4.1-4.3)are solved over the model domain using finite differences. Surface elevations are prescribed from observations along open boundaries and radiation conditions are used to determine the current component that is normal to the open boundary. A quadratic law for bottom friction is applied. After a calibration process, the bed friction coefficient was fixed as $k = 0.050$ and the horizontal viscosity as $A = 10\,\mathrm{m}^2/\mathrm{s}$. The spatial resolution of the hydrodynamic model is $\Delta x = \Delta y = 2500$ m. In general, good agreement between model results and observations are obtained with these values.

Hydrodynamic calculations are carried out separately for the two main tidal constituents, M_2 and S_2. Thus, spring-neap tidal cycles can be simulated. Once a stable periodic solution is achieved, standard tidal analysis is carried out and residual transport is calculated for each constituent. Tidal constants (amplitudes and phases) for each point in the domain and residual transports for each tidal constituent are stored in files to be read by the dispersion code. Results from the hydrodynamic calculations have been validated through an extensive comparison of tidal amplitudes and phases and current magnitudes and phases with observations for 16 points in the domain. As an example, a comparison of measured and computed amplitudes and phases of elevations for both tidal constituents at several locations (see map in figure 7.2) is presented in table 7.1.

Table 7.1. Observed and computed amplitudes (A, cm) and phases (g, deg) of tidal elevations at the Strait

	M_2				S_2			
station	A_{obs}	g_{obs}	A_{com}	g_{com}	A_{obs}	g_{obs}	A_{com}	g_{com}
P Gracia	64.9	49	70.5	57	22.3	74	24.8	81
P Kankoush	51.8	69	52.7	59	20.1	90	18.9	86
Tarifa	41.5	57	46.2	52	14.2	85	17.4	77
P Cires	36.4	47	38.5	56	14.1	74	14.3	82
Algeciras	31.0	48	25.0	48	11.1	74	10.0	71
P Carnero	31.1	48	25.6	46	11.5	71	10.4	69
Ceuta	29.7	50	25.0	50	11.4	76	10.0	72

7.3.2 Dispersion code

The dispersion of contaminants is calculated using a particle-tracking method. Essentially, the pollutant discharge is simulated by a number of discrete particles, each particle being equivalent to a number of units. Then the path followed by each particle is computed, turbulent diffusion being modelled as a three-dimensional random walk process. Decay of particles is also included. The density of particles per water volume unit is finally computed to obtain contaminant concentrations over the Strait at the desired time. Both instantaneous and continuous releases can be simulated. It must be noted that the particle-tracking model is three-dimensional, while the hydrodynamic module provides depth-averaged currents. Thus, the current profile described before has been used to have a 3D current distribution. Time step in the dispersion computations is $\Delta t = 600$ s. The horizontal and vertical diffusion coefficients are, respectively, $K_h = 1.7$ m^2/s and $K_v = 0.001$ m^2/s.

The effect of wind is included as usual in particle-tracking models. Thus, it is assumed that the water surface moves in the direction of wind at a speed equal to 3 % of the wind speed 10 m above the sea surface. This current decreases logarithmically to zero at a depth usually taken as 20 m.

Date and time of the discharge (and duration in the case of continuous releases) must be specified since the fate of the release will depend on the tidal state when it took place. Thus, the appropriate phase of each tidal constituent at $t = 0$ must be specified. The values used in this model correspond to the origin of time being January 1, 2003 at 0:15 hours Greenwich time.

7.3.3 Input data

The dispersion code automatically reads 6 files (table 7.2) which contain the topography of the Strait, amplitudes and phases of the two tidal constituents included in the model (M_2 and S_2), and the residual circulation. These files are provided by the hydrodynamic module that has been run off-line, as commented before.

Table 7.2. Files required by the GISPART code

File name	Content
`depth`	Strait topography
`residual.dat`	average water circulation
`gm2.dat`	phases of the M_2 constituent
`gs2.dat`	phases of the S_2 constituent
`hm2.dat`	amplitudes of the M_2 constituent
`hs2.dat`	amplitudes of the S_2 constituent

The dispersion code is started opening the file `strait.bat`. Data files are read and it is required that some information, related to the discharge characteristics, is introduced by the user. This information is the following:

- Release cell in grid coordinates (x, y). A map of the model domain is shown in figure 7.2. The computational grid was presented in figure 4.2. In this model version, it is assumed that the release occurs at the sea surface.
- Select between instantaneous/continuous release option.
- Wind speed.
- Wind direction.
- Date of release. It can be any time from January 1, 2003 on. Format must be day,month,year (for instance 25,3,2004).
- Time (UTC) of release in format hour,minute (for instance 22,45).
- Simulation time in days.
- Obtain the time evolution of NP (number of particles) at a given point (y/n)? If *yes* option is selected, it is required to introduce the grid coordinates of such point and the name of the file to write the information.
- Total amount of contaminant released. Units are arbitrary. The contaminant concentration over the domain computed at the end of the simulation from the density of particles per water volume unit is given in such arbitrary units per m^3.
- File name to write the integral of NP in each grid cell. This will be explained below.
- If the continuous release option was selected, it is required to introduce the discharge duration (hours) and the total quantity of contaminant released (again arbitrary units).

Calculations start (we can see on the screen the number of iterations). Results are written in several files described in the following section.

7.3.4 Model output

Several output files are generated. They are the following:

`conc.dat`: Contains the concentration of radionuclides in arbitrary units per m^3 at the end of the simulation in the format x, y, C where x and y are grid coordinates and C is concentration. These concentrations are obtained from the density of particles per water volume unit.

`foto1.dat` to `foto12.dat`: They contain the position of each particle at several times during the simulation in the format x, y, z, where z is particle depth below the sea surface. Thus, snap shots of particles can be drawn to study the evolution of the discharge along time. In particular, 12 snaps shots at constant intervals during the simulation are provided. These files are used by GNUPLOT plotting software to make an animation of pollutant dispersion.

The following steps are required to make an animation:

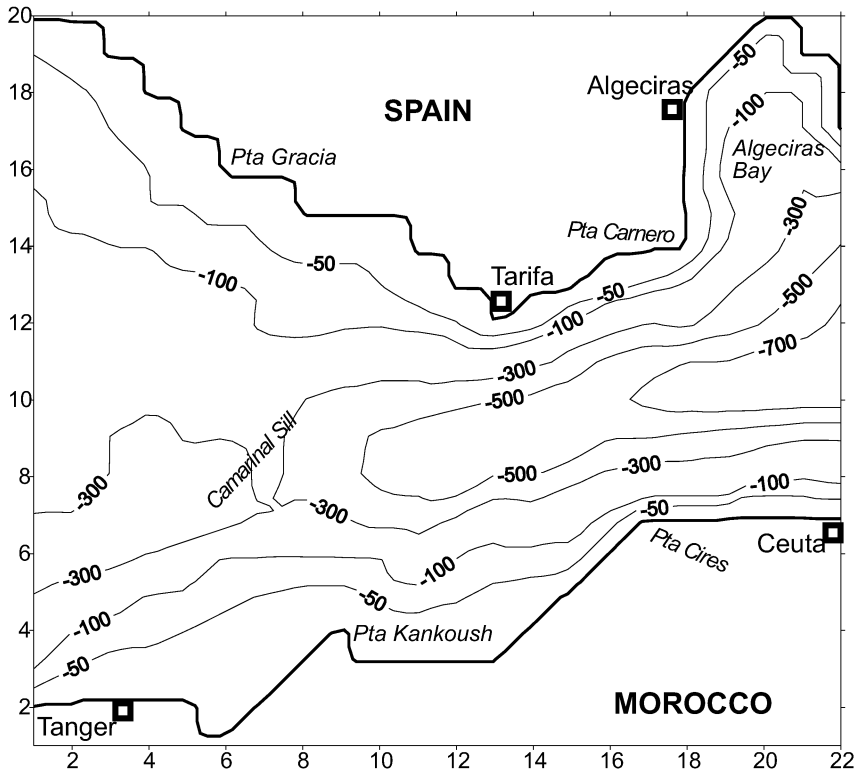

Fig. 7.2. Map of the computational domain showing some important towns (squares). Each unit in the x and y axis is the grid cell number (thus equal to 2500 m)

1. Open GNUPLOT
2. Change to the directory where GISPART is located
3. Type: `load 'film.plo'`

A name must be given to the file where the integral of NP in each grid cell is written, as was said above. That integral, $I_{i,j}$, is defined as:

$$I_{i,j} = \int_0^T NP_{i,j} dt \tag{7.12}$$

where $NP_{i,j}$ is number of particles at point i, j and T is the simulation time. Thus, $I_{i,j}$ gives the area under the curve that represents the time evolution of the number of particles at point i, j. This quantity is calculated for each point in the model domain and all $I_{i,j}$ are normalized to its maximum value. Thus, the magnitude $P_{i,j}$ is obtained as:

$$P_{i,j} = \frac{I_{i,j}}{\max\left(I_{i,j}\right)} \tag{7.13}$$

$P_{i,j}$, that ranges between 0 and 1, may be mapped over the model domain and the map is used to define the areas of the Strait with a higher probability of being affected by contamination after an accident. It must be pointed out that P does not give any absolute probability of contamination, but it can merely be used to compare different points in the Strait. The areas with lower P values will have a higher probability of remaining un-affected than the areas of higher P values. A limitation of this approach is that points in which there is an intense peak with a short temporal duration cannot be distinguished from points in which lower concentrations are obtained over longer times. Also, P does not give information about the magnitude of the peak, although this information can be obtained from the model.

The program `leo.exe`, also included with the model files, makes the normalization of the integral $I_{i,j}$, thus calculating $P_{i,j}$ and writing the result in a new file whose name must be provided. The fate of a pollutant discharge at a given point will depend on tidal state when the release took place and on wind conditions. Thus, it would be interesting to simulate an accident at a given point occurring at different tidal states or with different wind conditions to have a more general view of the areas of the Strait with higher probability of being contaminated. Thus, $P_{i,j}$ can be calculated for a single accident or for an arbitrary number of them. It is required to introduce the number of files to be read (containing the integral $I_{i,j}$), their names and the name of the file where $P_{i,j}$ is going to be written when running `leo.exe`.

In the file where the integral of NP is written, as well as in `conc.dat` and the file where $P_{i,j}$ is written after running `leo.exe`, negative values are assigned to land cells so as to distinguish them from water cells where the corresponding quantity is zero. Maps can be drawn using GNUPLOT or, for instance, Golden Software SURFER.

7.3.5 Examples

An example of the type of results that can be obtained from the particle-tracking model is presented in figure 7.3. Decay of particles is not considered. An instantaneous discharge of a radionuclide is carried out into grid cell $(7, 9)$, in the area of Camarinal Sill, during high water at Tarifa and with no wind. 3000 particles are used in the simulation, whose tracks are followed during two days. The position of each particle at four different times after the release is shown in figure 7.3 (top). The concentration of the pollutant in arbitrary units per m^3 at $t = 48$ hours is also presented in figure 7.3 (bottom). There is a net transport towards the Mediterranean Sea due to the residual currents, although the patch moves forward and backward following tidal oscillations. This can be also seen in figure 7.4, where the time evolution of the number of particles inside an arbitrary grid cell [in this case $(15, 9)$] is shown. The

patch moves three times over this point, producing three peaks in the number of particles at 21, 26 and 36 hours after the release. The highest peak, 254 particles, is observed 26 hours after the release. In this simulation 1.0×10^6 units of contaminant where released, thus the peak implies a maximum concentration equal to 9.2×10^{-5} units/m^3. For the following peak, at $t = 36$ hours, the concentration is reduced in a factor 5. From the position of the center of the patch after 48 hours, it can be estimated an average velocity of the pollutant of 17 cm/s directed towards the Mediterranean. This number can be compared with the mean speed of the Atlantic inflow equal to 23 cm/s measured in [168].

The movement of a patch is obviously influenced by wind conditions. This can be clearly seen with the help of figure 7.5. The same simulation described above has been repeated but with 15 m/s east and west winds, which are dominant in the Strait. The position of particles 28 hours after the release for both simulations is shown in figure 7.5, that can be compared with the 28 hours patch in figure 7.3. West winds, directed in the same direction as the residual circulation, produce a faster movement to the eastern part of the Strait, while east winds tend to retain particles into the Strait. Since the particle-tracking model is three-dimensional, shear diffusion is automatically simulated and the patch size increases in the direction of wind.

An example of the simulation of a continuous release is presented in figure 7.6. The release occurs at same point and tidal conditions as before (cell $(7, 9)$ and high water at Tarifa), and under calm wind. The position of particles 44 hours after the release is shown in figure 7.6. This can be compared with the 44 hours patch in figure 7.3. Now there is a plume extending from the release point to the eastern part of the Strait. It is interesting to observe that four patches with larger concentrations of particles are apparent in the plume. They correspond to particles released during slack water, that remain concentrated and move together.

The areas of the Strait with higher probability of being affected by contamination after an accident have also been estimated following the method described previously. The spread of a contaminant patch depends on the tidal state when the release occurs and on wind conditions. Thus, 4 accidents have been simulated for each point located along traffic lanes used by ships. These 4 accidents are considered to occur at high water, ebb, low water and flood. The values of $P_{i,j}$ for each of the 4 accidents occurring for several points along traffic lanes have been averaged and represented in figure 7.7. Three points along lanes have been used to simulate the four accidents. They correspond to the west, central and east Strait and have grid coordinates $(5, 8)$, $(13, 8)$ and $(18, 10)$. Three different wind conditions have also been considered: calm wind, east and west winds (which are dominant in the Strait). Thus, each map in figure 7.7 represents the average of $P_{i,j}$ over 12 values. The duration T of each simulation is long enough to allow particles to be flushed off the Strait, and ranges from 1 to 7 days.

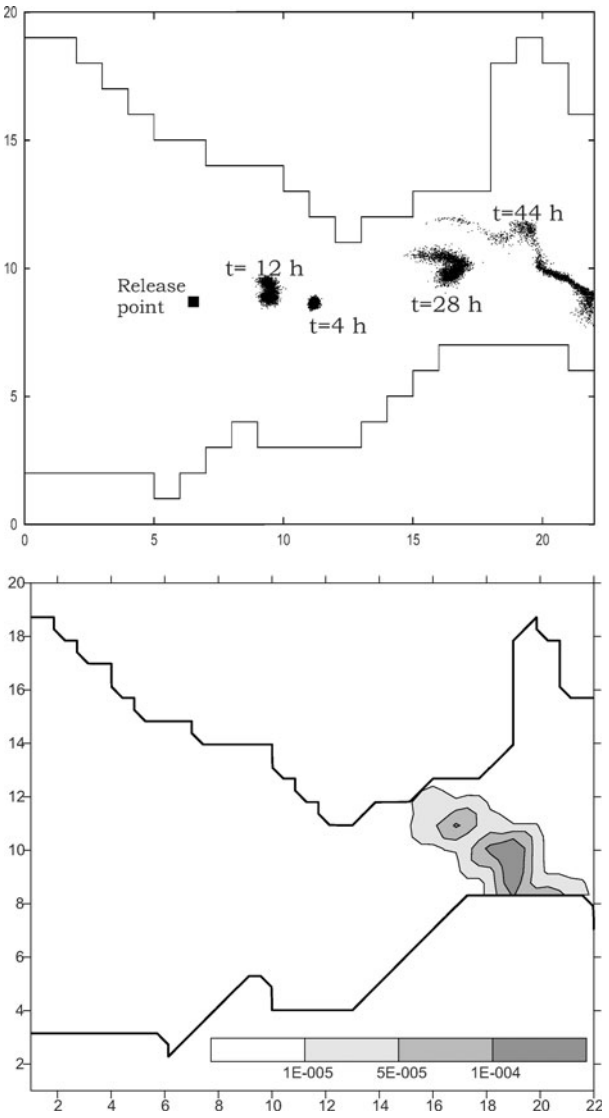

Fig. 7.3. Up: Dispersion of an instantaneous release. The position of particles at different times after the release is shown. Down: Computed surface concentration in arbitrary units per m^3 48 hours after the release. It has been obtained from the density of particles

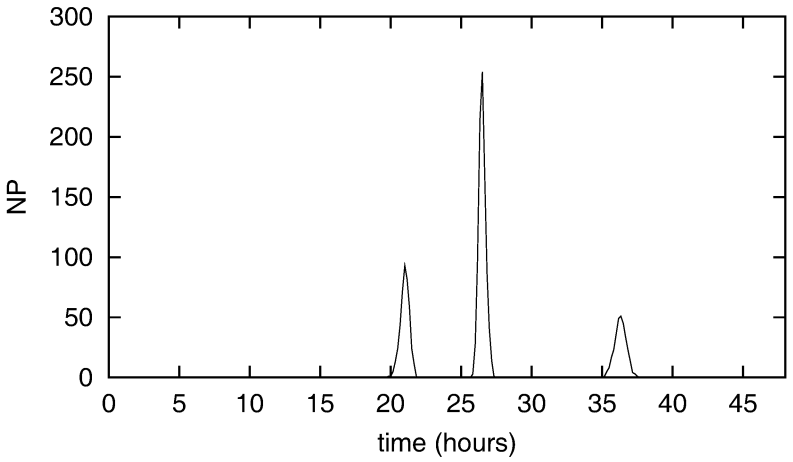

Fig. 7.4. Time evolution of the number of particles inside grid cell $(15, 9)$

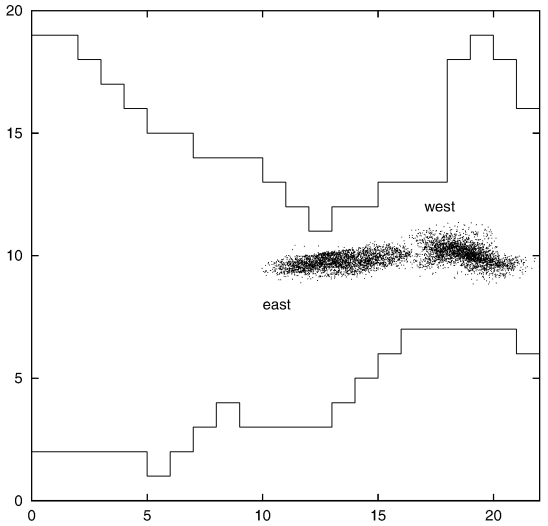

Fig. 7.5. Position of particles 28 hours after an instantaneous release at grid cell $(7, 9)$ with 15 m/s winds from the east and west

Results in figure 7.7 indicate that the area that is more affected by contamination is the central part of the Strait (shipping route). This is an obvious result, but it is interesting to note that, in general, the coast of Africa (from Pta Cires to the town of Ceuta) is more exposed to contamination than the Spanish coast. The strong west-east currents in the Strait inhibit mixing in the transverse direction, thus the coast remains relatively clean. In the case of winds blowing from the east, the wind-induced current is in the opposite direction than the residual current. Thus, contaminants are retained into the Strait for a longer time, allowing transverse mixing to occur. As a consequence, the Spanish coast is also affected, specially from Tarifa to Pta Carnero. West winds are in the same direction as the residual current and, as a consequence, produce a faster flushing of particles, but the map is essentially the same as that obtained for calm conditions.

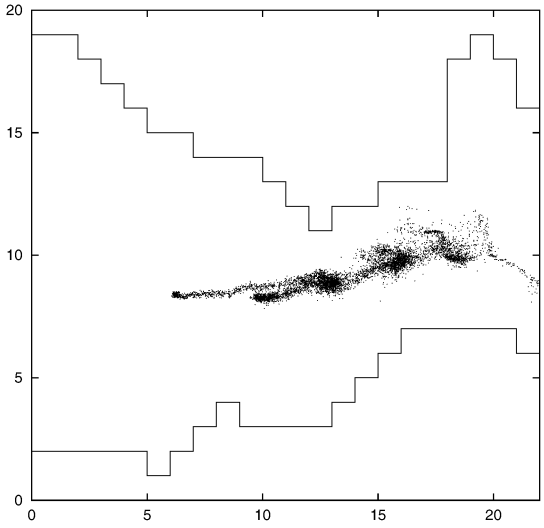

Fig. 7.6. Position of particles 44 hours after the beginning of a continuous release at grid coordinates $(7, 9)$

7.4 Water-sediment interactions

7.4.1 Formulation

The main difficulty that appears in the simulation of the dispersion of non conservative radionuclides with a particle tracking method is the treatment of adsorption and desorption: how to decide if each particle is fixed to suspended

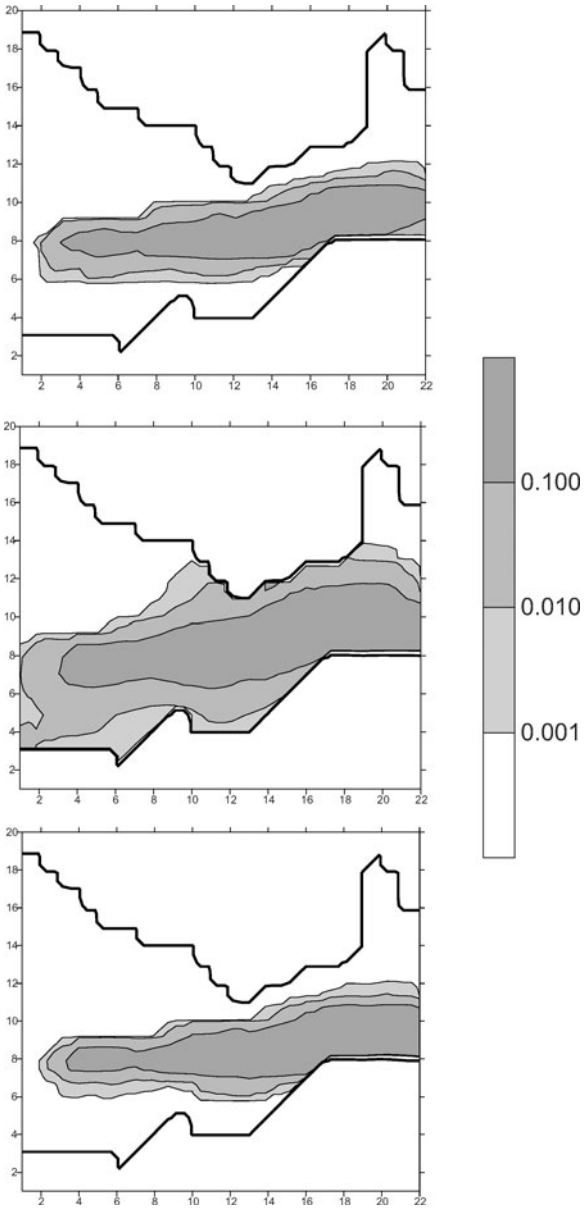

Fig. 7.7. Values of P for three different wind conditions averaged for accidents occurring at three points along traffic lanes and four tidal states for each point. Thus, each map represents an average over 12 P values for each point in the domain

matter or bottom sediments (if initially dissolved) or if it is redissolved (if initially present in the suspended matter or the bottom sediment). The method described here to solve this problem is based upon a kinetic approach and a stochastic method. It is interesting to notice that exactly the same physical parameters as in the equivalent finite difference model are used.

Let us consider the water-sediment interaction scheme described by figure 6.4 and equations 6.8. These equations are easily solved using finite differences as described in chapter 6. In particle tracking, a label is given to each particle to differentiate if it is in water or in sediment. If the particle is dissolved, the probability p_1 that the particle goes to the sediment in each time step is:

$$p_1 = 1 - e^{-k_1 \Delta t} \tag{7.14}$$

Similarly, if the particle is in the sediment, the probability that is redissolved in each time step is:

$$p_2 = 1 - e^{-k_2 \Delta t} \tag{7.15}$$

Thus, in particle tracking, the exchanges between two phases can be modelled as two decay processes with probabilities p_1 and p_2. These processes are treated as the radioactive decay process described before. If a given particle goes from one phase to the other, its label is changed and the new corresponding decay process is considered at the next time step.

This method has been compared with the finite difference solution of the system of equations 6.8. It has been considered that all radionuclides are dissolved at $t = 0$. Thus, the solution given by each method refers to the percentage of radionuclides that remain in solution at each following time step. Results obtained by both methods are presented in figure 7.8, using 200 and 10000 particles in the stochastic simulation. High fluctuations occur with 200 particles, but the finite difference solution is well modelled if 10000 particles are used in the particle tracking calculation. Of course, the exact number of particles to be used depends on the speed of calculations and accuracy required by the modeller. Accuracy increases, but the model is computationally more expensive, as the number of particles is higher.

The stochastic method can be extended to the case in which there are three different phases: water, suspended matter and bottom sediments. Equation 6.12 may be re-written as follows:

$$k_1 = \chi_1 (S_m + S_s) = k_{1m} + k_{1s} \tag{7.16}$$

Thus, k_{m1} governs the transfer of radionuclides to suspended matter particles and k_{1s} the transfer to bed sediments. Since particle tracking models are three dimensional, the equation for k_{1s} is written as:

$$k_{1s} = \chi_1 \frac{3Lf\phi}{RH} \tag{7.17}$$

but now H gives the thickness of the water layer above the sea bottom that interacts with the sediment. In a 2D depth averaged model, H would be equal to the water depth, as described before.

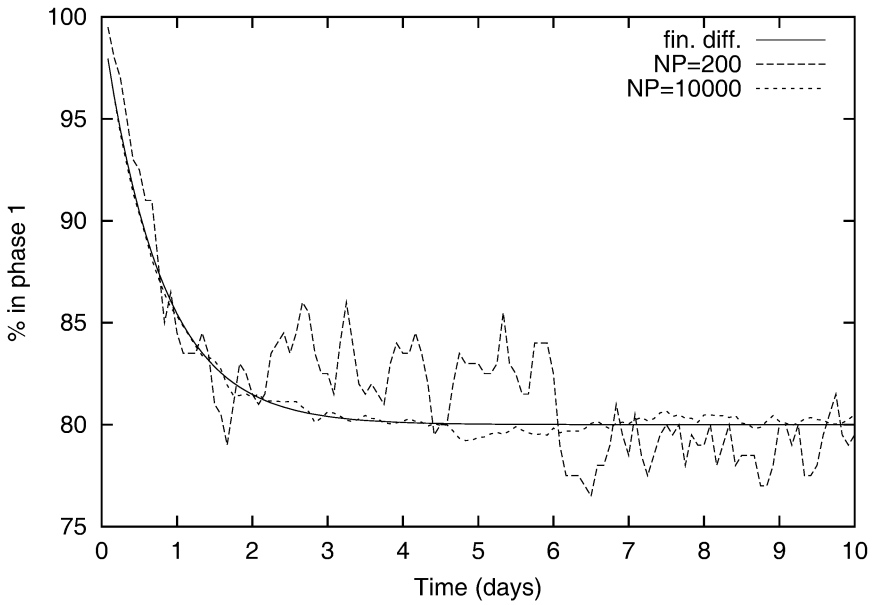

Fig. 7.8. Time evolution of the fraction of particles remaining dissolved (phase 1) calculated by finite differences and the stochastic method using 200 and 10000 particles

The decay equations that are equivalent to the differential equations that describe transfers between the three phases are:

$$\begin{aligned} \frac{\partial C_d}{\partial t} &= -(k_{1m} + k_{1s})C_d \\ \frac{\partial C_s}{\partial t} &= -k_2 C_s \\ \frac{\partial A_s}{\partial t} &= -k_2 \phi A_s \end{aligned} \tag{7.18}$$

where C_d, C_s and A_s are radionuclide concentrations in water, suspended matter and active bottom sediments respectively. A label is given to each particle to classify in which phase it is present. Depending on the label of the particle, the corresponding decay equation is treated. If the particle is in suspended matter, the probability that it goes to the dissolved phase, at each time step, is:

$$p = 1 - e^{-k_2 \Delta t} \tag{7.19}$$

Similarly, if the particle is in the bottom sediment, the probability that it is redissolved is:

$$p = 1 - e^{-k_2 \phi \Delta t} \tag{7.20}$$

If the particle is initially dissolved, and its distance to the sea bottom is smaller than H, it can go to any of the two solid phases with a probability:

$$p = 1 - e^{-(k_{1m}+k_{1s})\Delta t} \tag{7.21}$$

A random number is generated to decide if the particle is effectively removed from solution. If it is, the normalized probability that the particle goes to the sediment is calculated as:

$$p = \frac{p_s}{p_m + p_s} \tag{7.22}$$

where:

$$p_m = 1 - e^{-k_{1m}\Delta t} \tag{7.23}$$

$$p_s = 1 - e^{-k_{1s}\Delta t} \tag{7.24}$$

A second random number is then generated. If $RAN < p$ then the particle goes to the sediment. If $RAN > p$, then it goes to the suspended matter. Of course, if the distance of the particle to the sea bottom is larger than H, only the decay to suspended matter is considered since such particles cannot interact with the sediment.

A numerical experiment, described in detail in [125], was carried out to compare the finite difference solution with the stochastic solution of the equations describing transfers between the three phases. A dissolved tracer is added to a water volume containing a given amount of suspended particles and bottom sediments. The time evolution of the fraction of activity in each phase is calculated using both methods. Results from such experiment are presented in figure 7.9. The simulation shows that the stochastic method solution is in very good agreement with the finite difference solution for the three phases. Indeed, solutions corresponding to both methods cannot be distinguished in the case of water and sediment.

In real applications, it has to be considered that the kinetic coefficient k_{1m} depends on the suspended matter concentration (see equation 6.15). The particle tracking model is three dimensional, while it is possible that the suspended matter concentrations are provided by a 2D depth averaged model. Since k_{1m} should vary with water depth (as suspended particle concentration changes), a standard Rouse profile [34] may be used to resolve the vertical structure of suspended matter if a depth averaged suspended sediment model is used. The Rouse profile allows the calculation of the suspended matter concentration at height z above the bottom, m_z, from the depth averaged suspended matter concentration m:

$$m_z = m\left(1 - \frac{w_s}{\beta\kappa u_*}\right)\left(\frac{H}{z}\right)^{w_s/\beta\kappa u_*} \tag{7.25}$$

where H is water depth, κ is the von Karman constant (0.4), β is an arbitrary constant usually taken as 1 [50, 34], w_s is settling velocity of suspended particles and u_* is the scalar friction velocity:

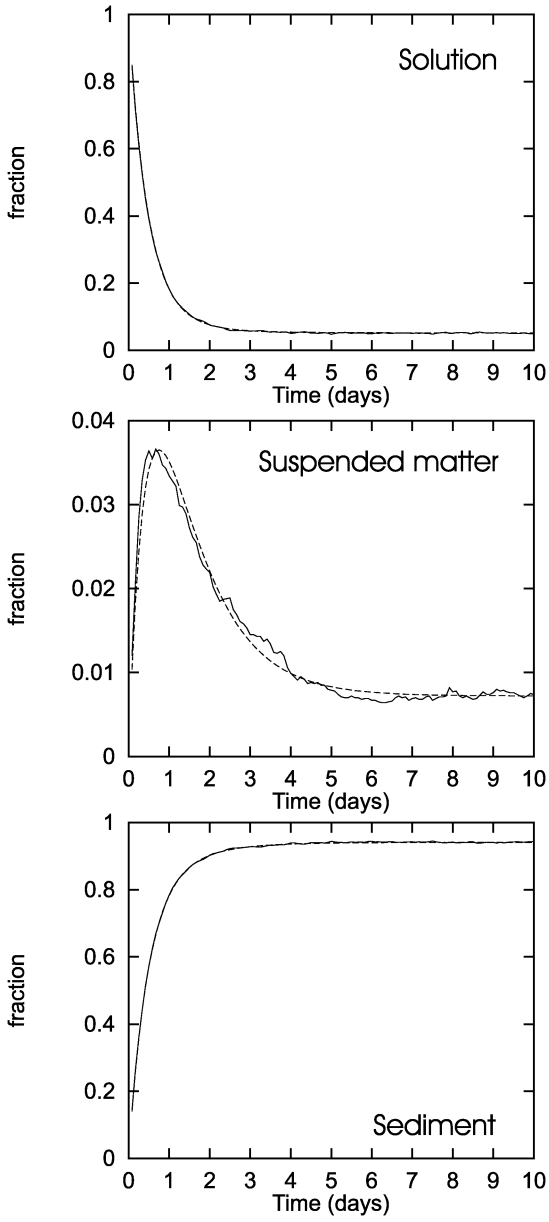

Fig. 7.9. Time evolution of the fraction of radionuclides in water, suspended matter and bottom sediments given by finite differences and by the stochastic method with 10000 particles. Solid lines correspond to the stochastic solution and dashed lines to the finite difference solution. Both lines cannot be distinguished in the cases of solution and sediment

$$u_* = \frac{\kappa|\mathbf{q}|}{\ln(H/z_0) - 1} \tag{7.26}$$

where z_0 is the bottom roughness and $\mathbf{q}$ is the water current. Typical values for the roughness length range from 0.02 cm for muds to 0.3 cm for gravels [147].

This stochastic method can also be extended to describe the erosion and settling of bed sediments [125]. Settling of suspended matter is easily described in particle tracking models by an advection equation equal to 7.1:

$$\frac{z(t + \Delta t) - z(t)}{\Delta t} = -w_s \tag{7.27}$$

If the erosion rate ER is known, for instance given by equation 6.5, the probability of erosion of a given particle may be defined as:

$$p = 1 - e^{-ER\Delta x\Delta y\Delta t} \tag{7.28}$$

Then the stochastic approach is applied as described before to decide it is effectively eroded or not.

7.4.2 Application

The modelling technique described above has been used to simulate the dispersion of non conservative radionuclides in the English Channel. An hypothetical release from La Hague nuclear fuel reprocessing plant has been simulated. Simulations have been carried out for two radionuclides with a different geochemical behaviour: the relatively soluble ^{137}Cs and the reactive ^{239,240}Pu, so as to test the stochastic model response. A finite difference model to simulate the dispersion of these radionuclides in the Channel has also been developed and validated [126]. The output from both models for the same release will be compared. A detailed description of parameter values used in the models can be seen in [125].

A hypothetical instantaneous release from La Hague of 5×10^{12} Bq of ^{137}Cs has been carried out. It is simulated by 50000 particles in the particle tracking model. A comparison between particle-tracking and finite difference results is presented in figures 7.10 and 7.11, for the dissolved phase (depth averaged) and bottom sediments. Specific activity maps have been obtained 40 days after the release from La Hague. An excellent agreement between results of both models is obtained in the dissolved phase. Results for the bottom sediments are also in good agreement. However, results for suspended matter cannot be obtained with the particle tracking model due to the low affinity of ^{137}Cs to be fixed to the solid phases. Indeed, 10.26% and 0.048% of the total activity is present in the bottom sediments and in suspended matter respectively. This implies that, if 50000 particles are used in the simulation, 5130 and 24 particles are, respectively, in the bottom sediment and in suspended matter.

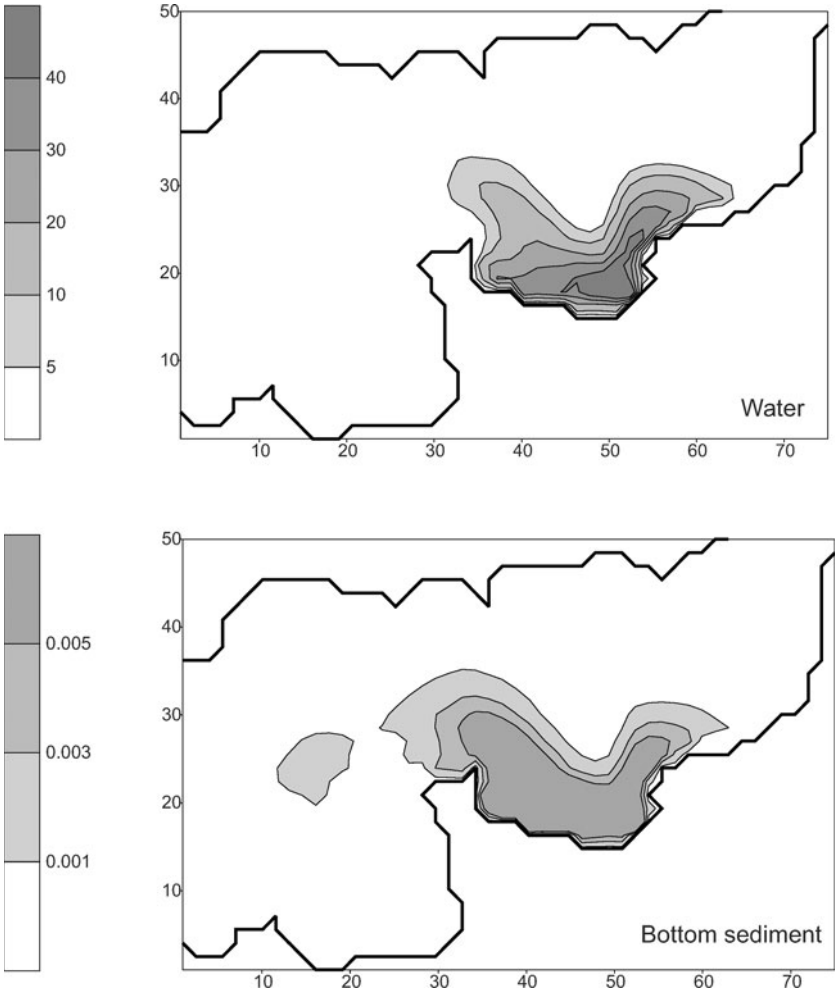

Fig. 7.10. ^{137}Cs activity concentrations in water (Bq/m^3) and sediments (Bq/g) given by the finite difference model

The number of particles in the sediment is enough to calculate the activity concentrations over the Channel from the density of particles, but this is not clearly the case with the suspended matter phase.

A similar simulation has been carried out for a release of ^{239,240}Pu. Results are presented in figures 7.12 and 7.13 for water, suspended matter and bottom sediments. They show that, due to the high reactivity of Pu, it remains essentially close to the source, as simulated by the finite difference and particle tracking models. Activity concentration levels given by the two models are, in general, in good agreement for the three phases. However, it seems that

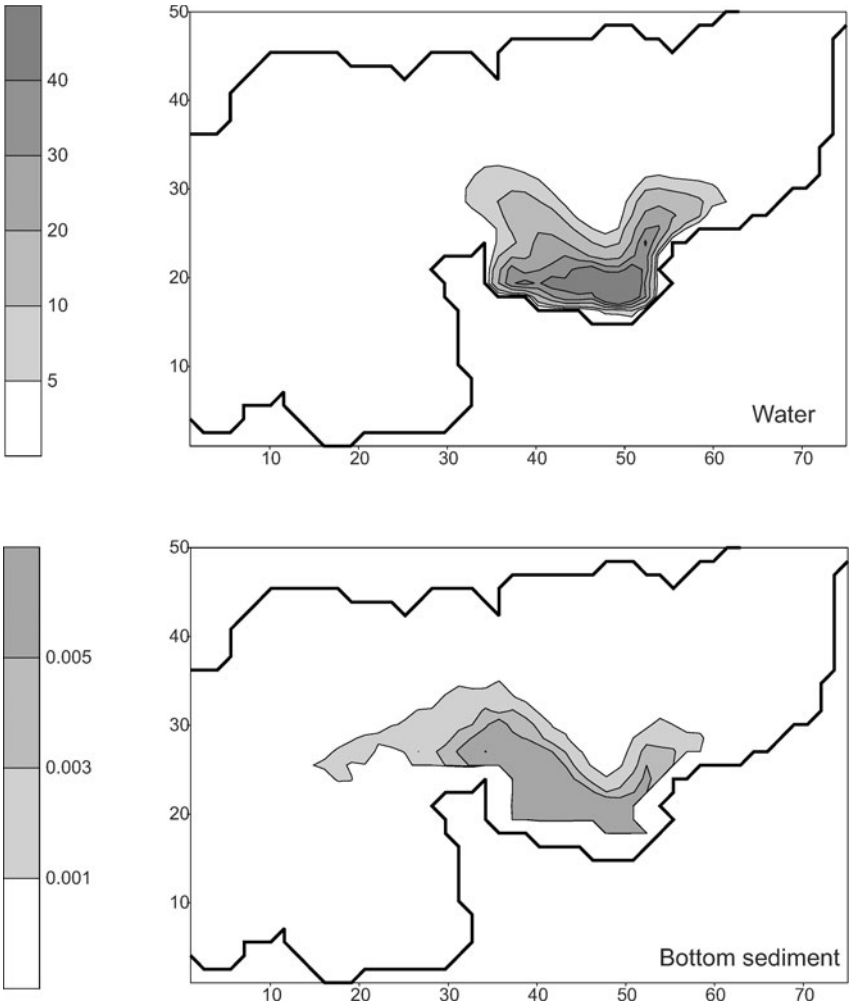

Fig. 7.11. ^{137}Cs activity concentrations in water (Bq/m^3) and active sediments (Bq/g) given by the particle tracking model

slightly higher concentrations are produced by the particle tracking model. This discrepancy may be caused by the finite difference model. Effectively, concentration gradients in the case of Pu are larger than in the case of Cs, since all the released Pu remains close to La Hague. Thus, the finite difference model introduces a numerical diffusion (even though a second order accuracy advection scheme is being used) that is more apparent than in the case of Cs. In contrast, the particle tracking method does not introduce numerical diffusion and, thus, higher concentrations are produced.

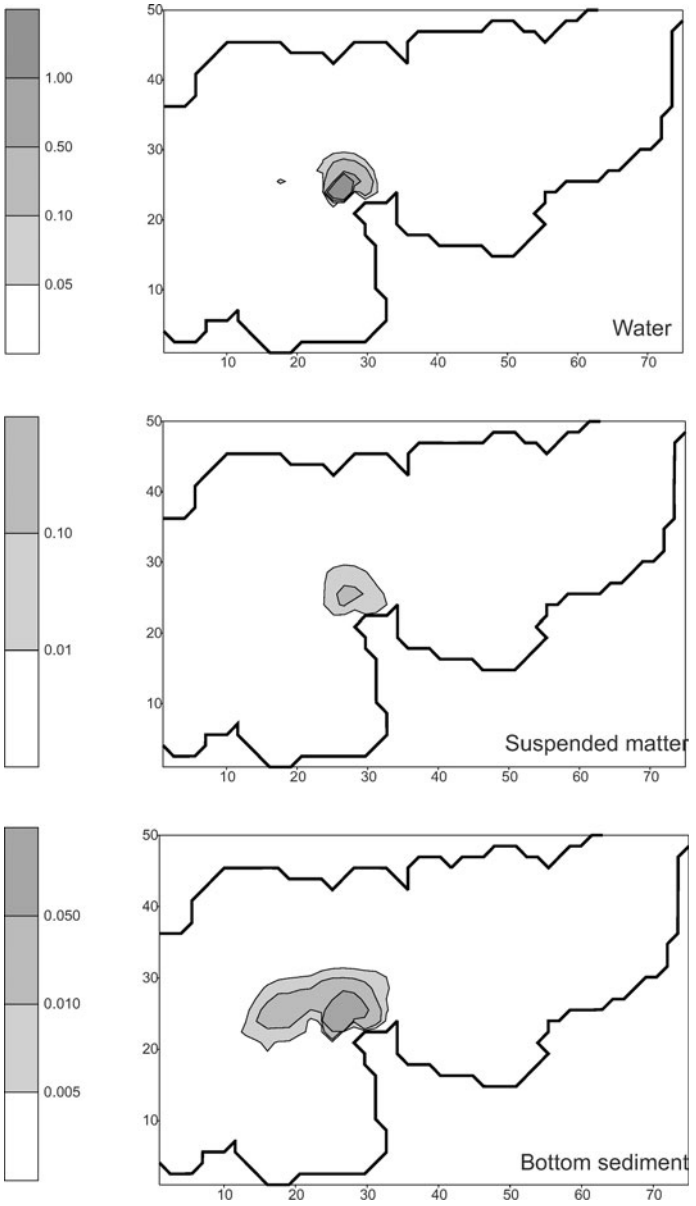

Fig. 7.12. ^{239,240}Pu activity concentrations in water (Bq/m^3), suspended matter and active sediments (Bq/g) given by the finite difference model

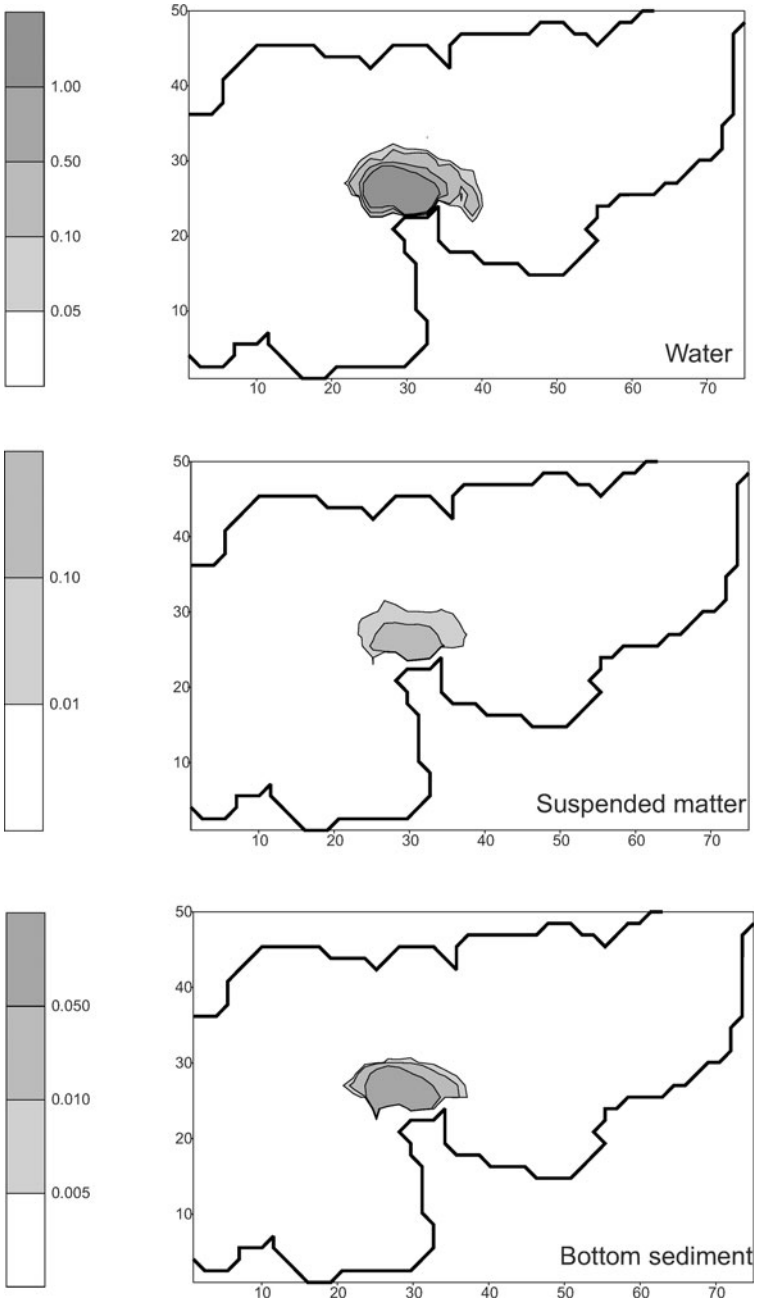

Fig. 7.13. ^{239,240}Pu activity concentrations in water (Bq/m^3), suspended matter and active sediments (Bq/g) given by the particle tracking model

In the case of Pu, it is possible to calculate activity concentrations in the three phases since 6.44%, 90.08% and 3.48% of Pu is in water, sediments and suspended matter respectively. This implies that, using 50000 particles, 3220 are in solution, 45040 in the sediment and 1740 in suspended matter. Thus, there are enough particles in each phase to calculate the corresponding densities and activity concentrations.

It can be concluded that particle tracking is a powerful tool that can be applied in the assessment of radioactive contamination following an accidental release in the marine environment. Also, the method can be applied to both conservative and non conservative radionuclides, using the same conceptual approach for the interactions between liquid and solid phases as used in finite difference models. However, it is possible that, due to the geochemical behaviour of certain radionuclides, activity concentrations in some of the phases may not be resolved. This is the case of ^{137}Cs in suspended matter.

8

Dispersion in estuaries: an example

8.1 Introduction

Estuary derives from the Latin word *estuarium*, that means tidal. An estuary is defined as a semi-enclosed coastal body of water which has a free connection with the open sea and in which sea water is mixed with freshwater. Estuaries form the transition from rivers to the sea and present a separate environment, influenced by conditions in the river and in the coastal area. Huge industrial facilities are often located along estuaries, as well as human settlements. Thus, it may be relevant to study contamination in estuaries and to develop models that simulate the dispersion of pollutants so as to assess contamination levels following potential accidental releases from the industries. In particular, this is valid for the case of radioactive contamination, which can be released to the aquatic environment not only from nuclear related industries.

The different types of estuarine circulation are presented in figure 8.1 (produced by [138] but taken from [50]). In the absence of tides (figure 8.1a), or when they are so small that tidal currents can be neglected in comparison with the river discharge, the river water flows over the sea water due to its lower density. Mixing between fresh and salt water is limited and mainly occurs because of surface waves and coastal currents. Most of the suspended matter supplied by the river settles in the area of contact between the two water masses due to the reduction in the flow velocity which usually occurs here. This is the so-called salt-wedge estuary. In tidal estuaries, two cases can be distinguished: partially mixed and fully mixed estuaries. In partially mixed estuaries (figure 8.1b) vertical mixing is incomplete and vertical density gradients occur, although they are smaller than in salt-wedge estuaries. This mixing of the fresh water discharged by the river with the incoming sea water is enhanced by turbulence induced by the tidal current. As a result, there is an entrainment of salt water into the surface seaward flow of the river, and the sea water carried out to sea in this way is replaced by a net residual flow at the bottom, directed up the estuary. The residual current in the surface is outwards because of the river water flowing out, while in the bottom

it is inwards to compensate for the outflow of sea water. The place where the upstream residual bottom flow and the downstream river flow converge is called the null point. In most estuaries the null point is associated with a turbidity maximum, where the suspended matter load may be as high as 10 kg/m^3. This area of maximum turbidity is due to the transport of sediments by the converging currents and in some cases to the flocculation of river clays because of the sudden increase of salinity. The null point and the turbidity maximum move along the estuary with spring and neap tides and with the periods of high and low river discharge: more inward during spring tides and low river discharge, and outwards during neap tides and high river discharge. In fully mixed estuaries (figure 8.1c), vertical mixing is virtually complete and the density gradients are horizontal. This occurs where the tides dominate the river outflow. Fully mixed estuaries are usually very wide when compared with their depths.

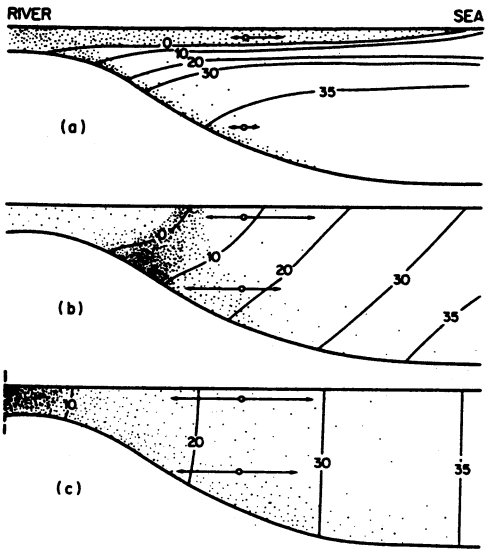

Fig. 8.1. Circulation in estuaries. Isolines represent salinity, vectors represent the residual currents and points the suspended particles. (a): salt-wedge estuary, (b): partially mixed estuary, (c): fully mixed estuary. Taken from [50]

As the estuary is narrowing and becoming shallower, interesting distortions of the tidal wave occur. The energy transported by the tidal wave is proportional to the square of the amplitude and the width of the wave front. Thus, the amplitude of the tide, A, increases as the estuary width decreases at a rate:

$$A \sim \frac{1}{\text{width}^{1/2}} \tag{8.1}$$

Of course, this relation is not exactly satisfied since energy is not constant due to friction with the estuary bed and shores. The most impressive form of tide distortion is the tidal bore. It is a breaking wall of water of about one meter that advances upstream the estuary. A large tide amplitude is required for bore generation. Some discussion may be found in [147].

The particular circulation of the estuary of interest will define the model to be used. If the estuary is fully mixed, a two dimensional depth-averaged model may be enough since there are no vertical gradients of salinity and suspended matter to be resolved. In the cases of salt-wedge and partially mixed estuaries, vertical gradients are present, so that the vertical direction must be resolved too, and a fully three dimensional model is required. In the case of narrow estuaries, another option may be to develop a two dimensional XZ model in the longitudinal and vertical directions, thus averaged in the transverse direction, if this is not relevant. An example of a XZ model applied to simulate salt transport in a Florida estuary may be seen in [31]. This kind of model is often applied in fjords as well.

Few radionuclide dispersion models for estuaries may be found in literature [127, 136], although some dispersion models for heavy metals are described [105, 89]. In contrast, hydrodynamic and suspended sediment models have been extensively developed [34, 90, 162, 16, 175, 26, 159, 59].

Nevertheless, modelling techniques are the same that have been described along the previous chapters. Dispersion is governed, as in open waters, by advection and turbulent mixing. Interactions of dissolved radionuclides with suspended particles and bed sediments are usually relevant due to the generally lower depths of estuaries and higher suspended sediment concentrations when compared to the open sea. Thus, a practical modelling study developed for a tidal estuary, Odiel-Tinto estuary in southwest Spain, that is affected by waste disposal from the phosphate fertilizer industry, is described as an example.

Some details about the Odiel-Tinto estuary are given in the following section. Next, the model is briefly described since it is based upon concepts, equations and numerical techniques described before. Finally, some examples of results are presented.

8.2 The Odiel-Tinto estuary

The Odiel and Tinto rivers, in southwest Spain, form a fully mixed estuary, with M_2 being the main tidal constituent. It is shallow (maximum water depth is ~ 10 m) and the flow of the Odiel river is low, typically ranging from 4 m^3/s (dry season) to 100 m^3/s (wet season). Tinto river flows are even smaller. A map of the estuary is presented in figure 8.2. It is surrounded by a marsh area and an industrial complex, located at the south of the town of Huelva.

The Tinto river joins the Odiel at the Punta del Sebo, and they flow together from this point to the Atlantic Ocean. Due to the low water discharge, mixing between sea and fresh water occurs north of Huelva. Thus, the water of the estuary in the area close to the industrial complex is virtually sea water.

A phosphate fertilizer processing plant is located in the industrial complex. This plant released part of its wastes directly to the Odiel river. It is well known that such wastes contain significant amounts of natural radionuclides (U, Th, Ra and their daughters) due to the fact that the phosphate rock, from which phosphoric acid is obtained, may contain U concentrations ranging from 50 to 300 ppm. During the wet processing of phosphate rock for phosphoric acid production, for instance, 86% of U and 70% of Th present in the rock appear in the phosphoric acid itself, while 80% of Ra follows the so-called phosphogypsum. This is an impure Ca sulfate that is removed as a precipitate during the process. Phosphogypsum is often discharged directly into estuaries, giving place to a clear radioactive impact. During 1990, for instance, 2×10^6 tons of phosphate rock were processed and 3×10^6 tons of phosphogypsum were produced. These wastes were partially released directly into the Odiel river (20%) and conveyed with water through a pipeline to phosphogypsum piles (remaining 80%) located by the Tinto River (see figure 8.2), where such material is stored in the open air. The gypsum piles cover some 12 km^2 of the Tinto river margin. Since 1998 wastes are not released directly into the Odiel river due to new regulations from the EU, although phosphogypsum is still being disposed in the piles by the Tinto river.

In Absi et al. [10], the time evolution of ^{226}Ra activities in water and sediments over years 1999-2002 was studied (sampling points are shown in figure 8.2). Results indicated that a self-cleaning process was taking place, as a consequence of the new waste policy, since a systematic and continuous decrease in activities was found in the water column and in bed sediments. A numerical model of the estuary was developed [136] to study quantitatively such cleaning process. The model has been initially tested through its application to simulate two dispersion scenarios. They consist of reproducing the measured ^{226}Ra concentrations resulting as a consequence of releases carried out by the fertilizer complex in the Odiel River and a discharge into the Tinto River due to an accidental release from the phosphogypsum piles. Once tested, the model is applied to simulate the cleaning process of the estuary. Some examples of results are presented along this chapter.

8.3 Model description

In this particular application only two phases are considered into each grid cell: dissolved phase and active bottom sediments. Suspended matter particles have not been considered in the model, and thus deposition processes and erosion of the sediment have been neglected. This approximation is used since previous calculations have shown that the radionuclide adsorption capacity

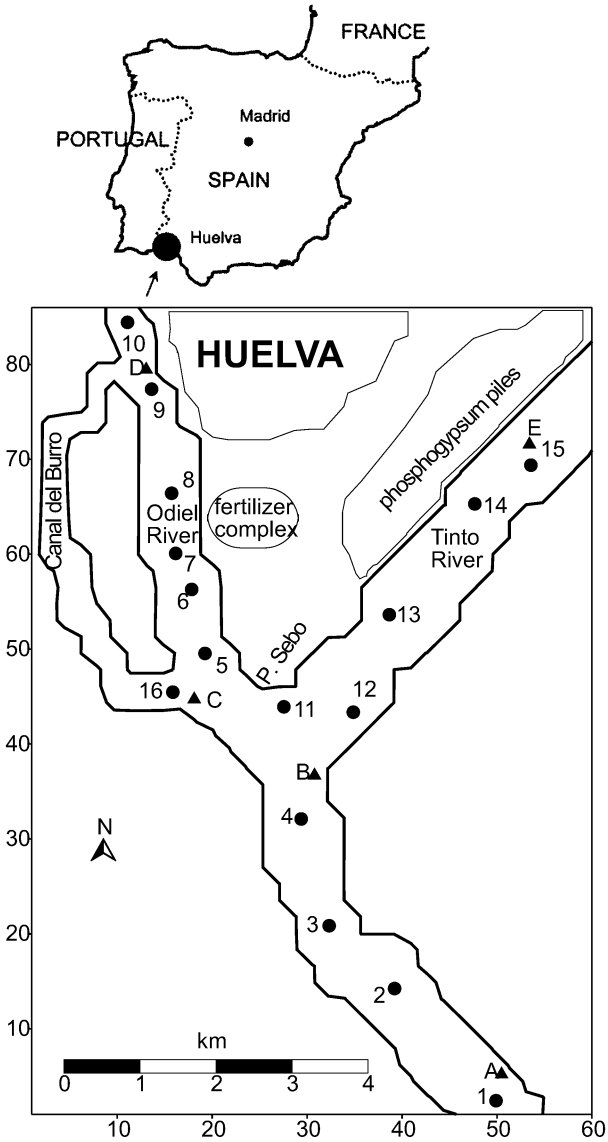

Fig. 8.2. Map of the area of the Odiel-Tinto estuary covered by the model. Numbered circles indicate the points where samples were collected. Lettered triangles indicate the points where currents measurements were available. Units on the axes give the grid cell number (each unit is equal to 125 m). The sea is approximately 1 km to the south of point 1

of suspended matter, given the typical suspended matter concentrations at the estuary, maximum concentrations of the order of 50 mg/L [116], is very small compared with that of the sediment. Moreover, the erosion-deposition rates, obtained from a suspended matter model of the estuary [116], are small (of the order of 10^{-2} g/cm^{2}year). Thus, as an approximation, it has been considered that the most important phases controlling radionuclide transport are the dissolved phase and the bottom sediment.

As was discussed in chapter 6, several kinetic models have been recently proposed to describe uptake/release of radionuclides between water and sediments. The 2-step model consisting of two consecutive reactions (figure 6.6), proposed by Ciffroy et al. [32], has been used since it is more appropriate than a 1-step model for describing both the uptake and release kinetics. Indeed, this 2-step model has already been tested in other environments, and has been shown to describe the process of redissolution of radionuclides from contaminated marine sediments [126, 129]: the rate at which radionuclides are redissolved from the bed sediments is overestimated if a 1-step model is used. However, it is in agreement with redissolution rates derived from observations if a 2-step model is applied (see references included above for more details). The 2-step model considers two successive reversible reactions. The first describes a reversible isotopic or ion exchange process between dissolved radionuclides and some non-specific sites, S_1, present on the particle surfaces. The second slower reaction represents a reversible sorption to more specific sites, S_2. They can be represented as follows:

$$R + XS_1 \rightleftharpoons_{k_2}^{k_1} RS_1 + X \tag{8.2}$$

$$S_2 + RS_1 \rightleftharpoons_{k_4}^{k_3} RS_2 + S_1 \tag{8.3}$$

where k_3 and k_4 are the kinetic transfer coefficients, or sorption and release velocities respectively, for the second reaction, R is the dissolved radionuclide, X is a competitive element that can be replaced by R on sites S_1 and RS_i is the radionuclide bound to sites S_i of the solid particle.

As already discussed in chapter 6, the kinetic rate k_1 is given by the following equation:

$$k_1 = \chi_1 \frac{3Lf\phi}{RH} \tag{8.4}$$

On the other hand, rates k_2, k_3 and k_4 are considered as constants.

The 2D depth averaged hydrodynamic equations, presented in chapter 4, are solved over the model domain using the same numerical scheme described there. The grid cell size is $\Delta x = \Delta y = 125$ m and time step is fixed as $\Delta t = 6$ s. The CFL criterion is satisfied with these selections. Water elevations are specified for each time step along the southern boundary from observations. Water depths were introduced for each grid cell from bathymetric maps.

The hydrodynamic and the dispersion models are coupled off-line (see chapter 5), and tidal analysis is used to determine tidal constants. They are stored in files that will be read by the dispersion code to determine currents

and surface elevation at each point in the domain and each instant of time. The two main tidal constituents, M_2 and S_2, are included.

The equation that gives the temporal evolution of specific activity in the dissolved phase, C_d (Bq/m^3), is:

$$\begin{aligned}&\frac{\partial(HC_d)}{\partial t}+\frac{\partial(uHC_d)}{\partial x}+\frac{\partial(vHC_d)}{\partial y}\\&=\frac{\partial}{\partial x}\left(HK_h\frac{\partial C_d}{\partial x}\right)+\frac{\partial}{\partial y}\left(HK_h\frac{\partial C_d}{\partial y}\right)\\&-k_1C_dH+k_2A_sL\rho_sf\phi\end{aligned}\tag{8.5}$$

where total depth is $H = D + z$, K_h is the diffusion coefficient, A_s (Bq/kg) is activity concentration in the non specific sites of the active sediment and ρ_s is the sediment bulk density expressed in kg/m^3. The external source of radionuclides should be added to this equation at the points where it exists.

The equation for the temporal evolution of activity concentration in the non-specific sites of the active sediment fraction is:

$$\frac{\partial A_s}{\partial t}=k_1\frac{C_dH}{L\rho_sf}-k_2A_s\phi-k_3A_s+k_4\ {}^*A_s\tag{8.6}$$

where ${}^*A_s$ is activity concentration in the specific sites of the active sediment. The equation for the specific sites is:

$$\frac{\partial {}^*A_s}{\partial t}=k_3A_s-k_4\ {}^*A_s\tag{8.7}$$

The total concentration of radionulides in the sediment, A_{tot}, is computed from:

$$A_{tot}=f(A_s+{}^*A_s)\tag{8.8}$$

The MSOU explicit scheme is used to solve the advective transport in the dispersion equation of dissolved radionuclides. It is considered that there is no flux of radionuclides through land boundaries. Along open boundaries, the boundary condition described in [120] is applied (see equation 5.25).

8.4 Examples of results

The calibration of the hydrodynamic model consisted of selecting the optimum value for the bed friction coefficient k. After some model runs, $k = 0.040$ was set for the Tinto river and $k = 0.005$ for the rest of the estuary. With these selections, a reasonable agreement between observed and computed currents has been achieved. A comparison between observed and computed magnitude and direction of the maximum currents for several locations in the estuary (see figure 8.2) is presented in table 8.1 for a situation of medium tides.

Table 8.1. Observed and computed magnitude and direction of the maximum currents for a tide of coefficient 74.4. The orientation is measured anticlockwise from east. Points are shown in figure 8.2

	computed		observed	
point	mag (m/s)	direc (deg)	mag (m/s)	direc (deg)
A	0.62	129.4	0.66	126.6
B	0.53	95.6	0.56	127.1
C	0.56	132.5	0.67	141.8
D	0.47	127.2	0.49	162.1
E	0.54	45.8	0.48	52.2

Since the dispersion model is not restricted by the CFL stability criterion, the time step in the dispersion model has been increased to 30 s. Stability conditions imposed by the dispersion equation are satisfied with this value.

Values for a number of parameters have to be defined in order to simulate ^{226}Ra dispersion. They were selected from literature values, model calibration or laboratory experiments (kinetic rates governing the first reaction). A detailed description on how values were fixed can be seen in [136] and is not included here.

As an example, the time evolution over one tidal cycle of an activity release of arbitrary magnitude carried out at high water in the Odiel River (at the point where discharges from the fertilizer complex occur) is shown in figure 8.3. It can be seen that the patch moves downstream during the ebb. After the flood starts (some 6 hours later), radionuclides enter the Tinto River, Canal del Burro and the Odiel River again. Thus, the discharged radionuclides reach the whole estuary.

The model was applied to reproduce the experimental results obtained for different sampling campaigns. The magnitudes of the external sources are not known. Thus, they had to be selected by trial and error until the model gave appropriate activity levels. On the other hand, it is known that the fertilizer plant does not release its wastes continuously, but during downstream currents that occur during the ebb tide. Thus, direct discharges are introduced only during such downstream currents. The model computes the dispersion of ^{226}Ra until stable oscillations in concentrations are obtained (because of tidal oscillations, a stationary situation is not reached). Results are extracted from the model at the same tidal state in which sampling was performed. Sampling campaigns for which model results are compared with observations were carried out in 1990 and in 1999. In the first case, the main radionuclide input to the estuary is due to direct releases from the fertilizer complex into the Odiel river. In the second case, direct releases had ceased and the source was due to runoff from the phosphogypsum piles into the Tinto river. Model results are compared with measurements (dissolved ^{226}Ra concentrations) in

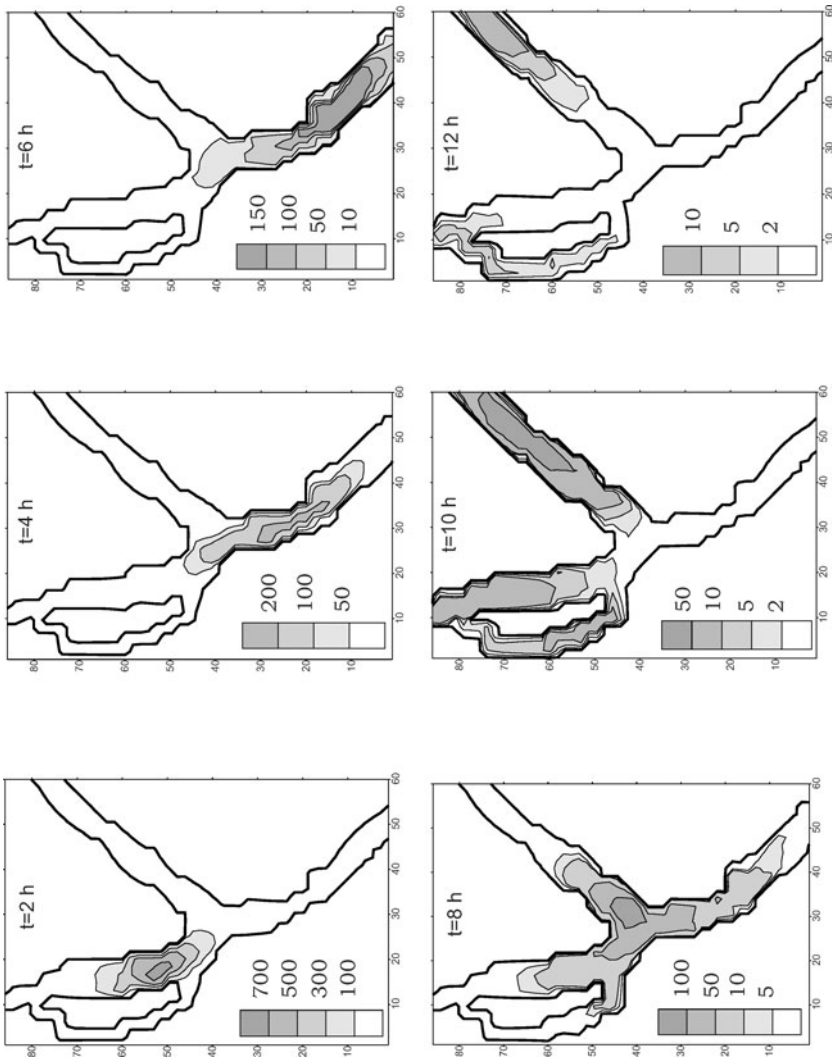

Fig. 8.3. Time evolution of dissolved concentrations resulting after an activity input of arbitrary magnitude carried out in the Odiel River during high water

figure 8.4. It can be seen that, in general, there is a good agreement between both set of data.

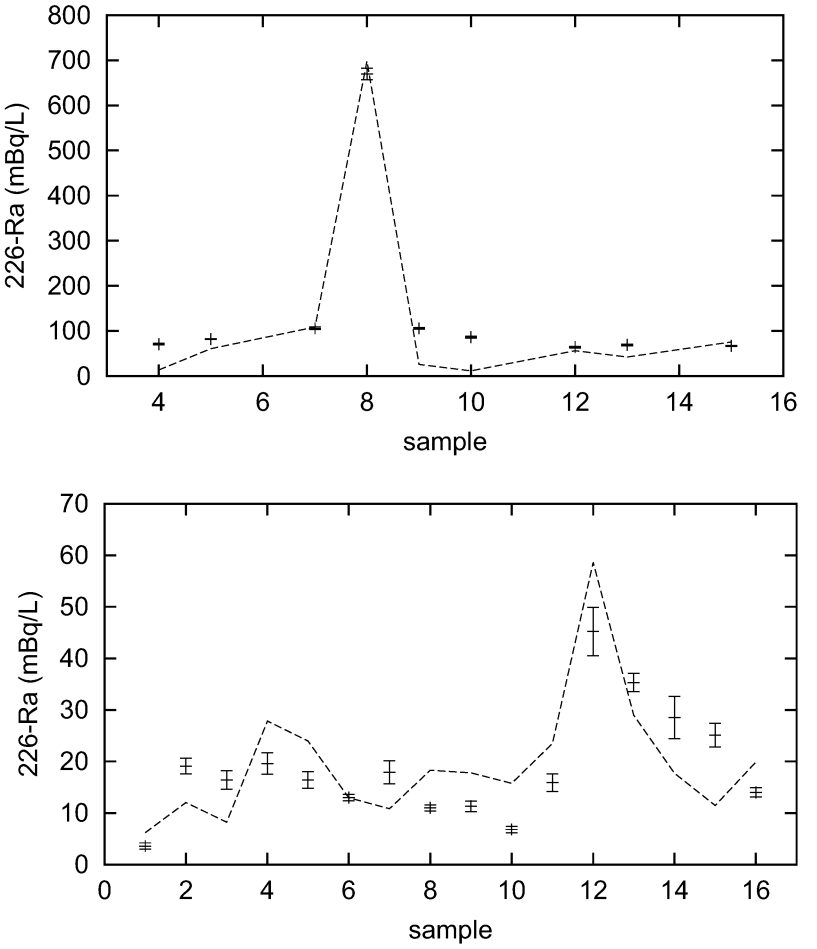

Fig. 8.4. Comparisons between measurements (points) and model results(lines) for dissolved ^{226}Ra in two sampling campaigns: top, 1990 and bottom, 1999. Sampling points are shown in the map in figure 8.2. Measurements are taken from [113] and [10] for 1990 and 1999 samples respectively

A long-term simulation has been finally carried out to compare computed and measured activity concentrations in bottom sediments. Details about this simulation may be seen in reference [136] again. Computed activity concentrations, together with measured concentrations [98], are presented in figure 8.5.

In general, the distribution of ^{226}Ra over the sediments is reproduced by the model. Maximum concentrations are obtained in the Odiel River, in the area where discharges from the fertilizer complex occur, with decreasing activities going north and south from this area. An activity peak is also measured in the Tinto River, that is not reproduced by the model. It must be taken into account that sampling was carried out during a wet season and rains may produce run-off events from the phosphogypsum piles. These run-off episodes, not included in the simulation, are probably responsible for the activity peak detected in the Tinto River. It is also interesting to note that activity gradients in the transverse direction are apparent in the Odiel River. On the other hand, the Tinto River is relatively well mixed in the transverse direction.

Once the model was tested through the comparison of measured and computed activity concentrations in the water column and bottom sediments, it has been applied to study the self-cleaning processes of the estuary after the end of discharges from the fertilizer complex. The model was started from the ^{226}Ra distribution in water and sediments obtained after the long-term simulation carried out to produce figure 8.5. The distribution of radium between the two sediment phases is also provided by the simulation: some 40 % of radium in the sediment is in the non-specific sites. These conditions are assumed to be representative of the moment at which releases ceased. A 4-year simulation is then carried out starting from these initial conditions and without external releases. This simulation provides the ^{226}Ra distribution in sediments for years 1999, 2000 and 2001 to be compared with measured distributions presented in reference [10].

The computed time evolution of ^{226}Ra inventories in bed sediments and in the water column for the whole estuary are presented in figure 8.6. It can be seen that the total radium content in the estuary bed decreases due to redissolution. The sediment halving-time (time in which activity in the sediment decreases by a factor 2) is 510 days. This number agrees relatively well with the 630 days halving-time estimated from measurements [10]. The inventory in the water column oscillates at a frequency of 15 days, which corresponds to the spring/neap tide cycles (only one year is shown in figure 8.6 to show these oscillations clearly), but halving-time for the dissolved phase is of the order of 300 days. This number, although of the same magnitude, is higher than the estimate obtained from measurements (some 130 days).

The computed distributions of ^{226}Ra in sediments corresponding to years 1999, 2001 and 2002 are presented in figures 8.7a-8.7c, together with the measured concentrations. These three maps provide a general view of the sediment cleaning process over the estuary. There are some local activity maxima in the Tinto River not reproduced by the model which are probably due to episodic release events from the phosphogypsum piles, but, in general, the decrease in ^{226}Ra concentrations is well reproduced by the model, especially in the area of the Odiel River where direct discharges took place. If these maps are compared with that presented in figure 8.5, it also seems that the cleaning process is more efficient in this region, which is the most contaminated. In the rest of

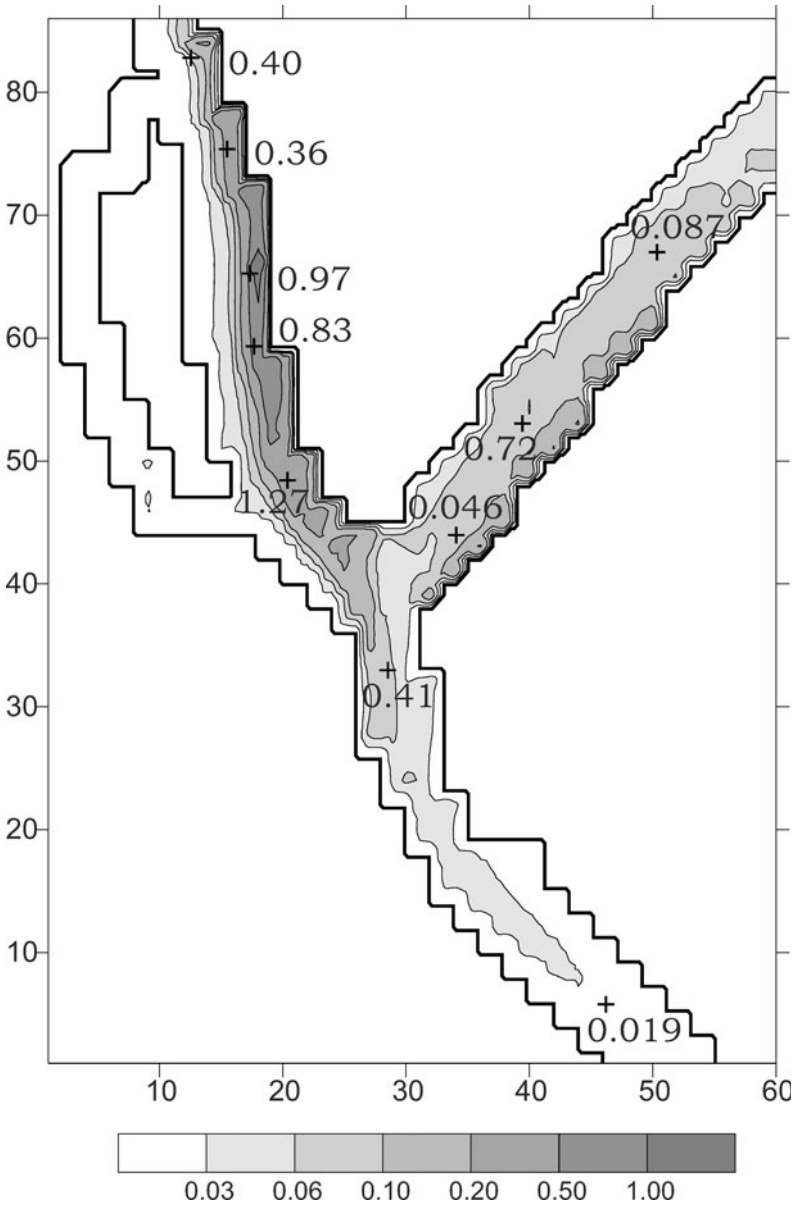

Fig. 8.5. Computed distribution of ^{226}Ra in sediments (Bq/g) and measured concentrations (from [98])

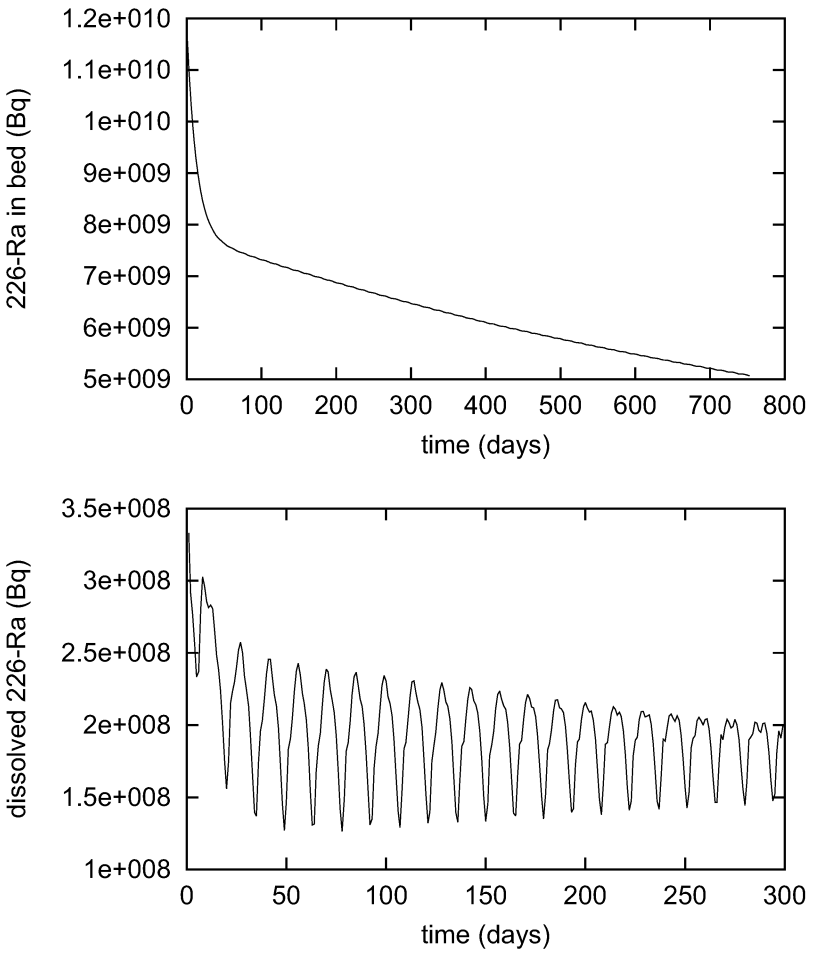

Fig. 8.6. Time evolution of the ^{226}Ra inventories for the whole estuary in bed sediments and in the water column during the self-cleaning process

the estuary, the activity concentration in the sediment decreases more slowly.

Finally, as an example of the behaviour of the 2-step kinetic model, the time evolution of radium concentration in the sediment at grid cell $(17, 60)$, that is close to the area where direct releases were carried out, is presented in figure 8.8. Radium concentrations in the non-specific sites decrease quickly due to the redissolution process. The specific sites go on absorbing radionuclides over a few days, and then concentration also decreases in this phase, although at a slower rate than in the case of the non-specific sites. Thus, Ra goes from

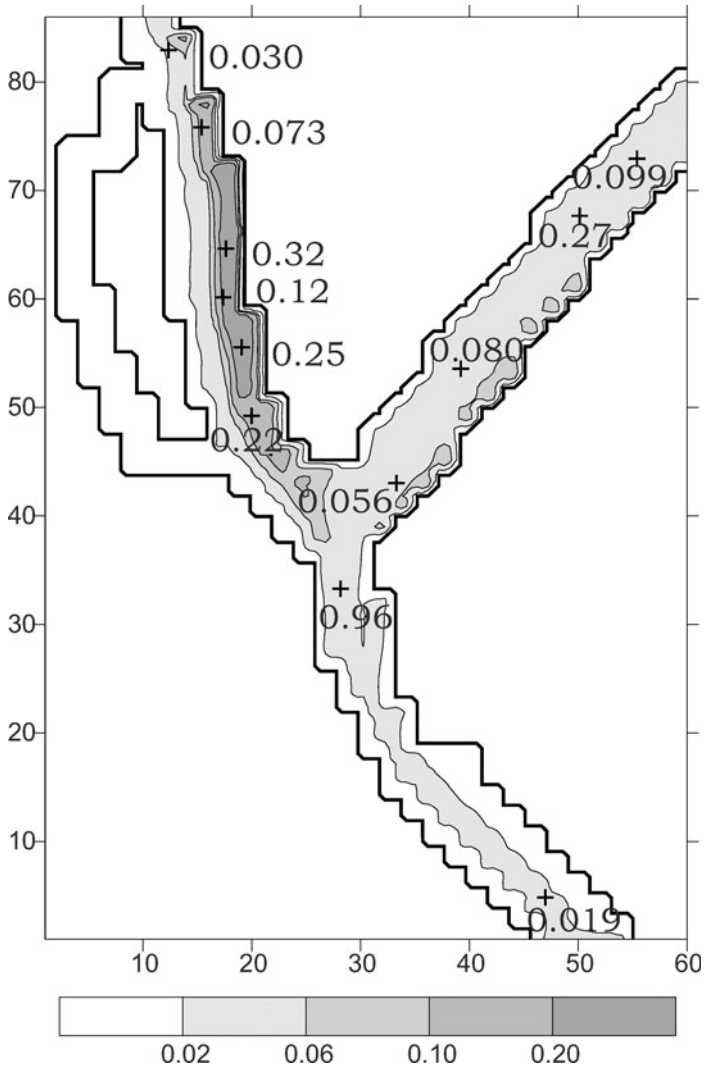

Fig. 8.7a. Computed distribution of ^{226}Ra in sediments (Bq/g) and measured concentrations for year 1999

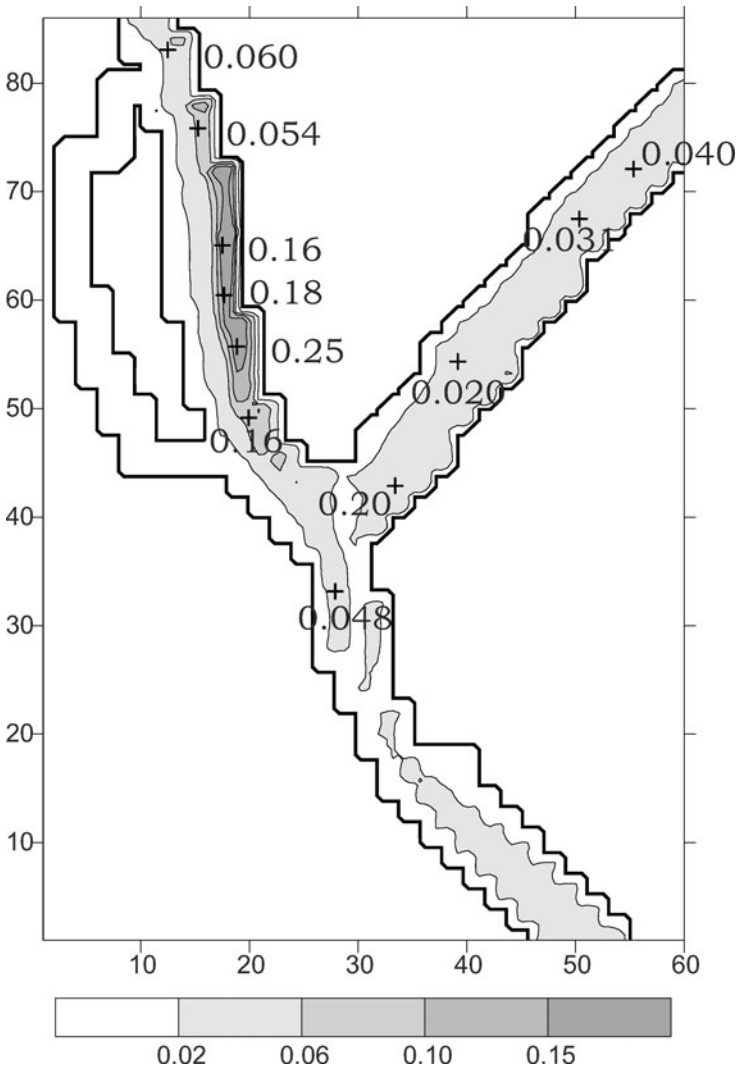

Fig. 8.7b. For 2001

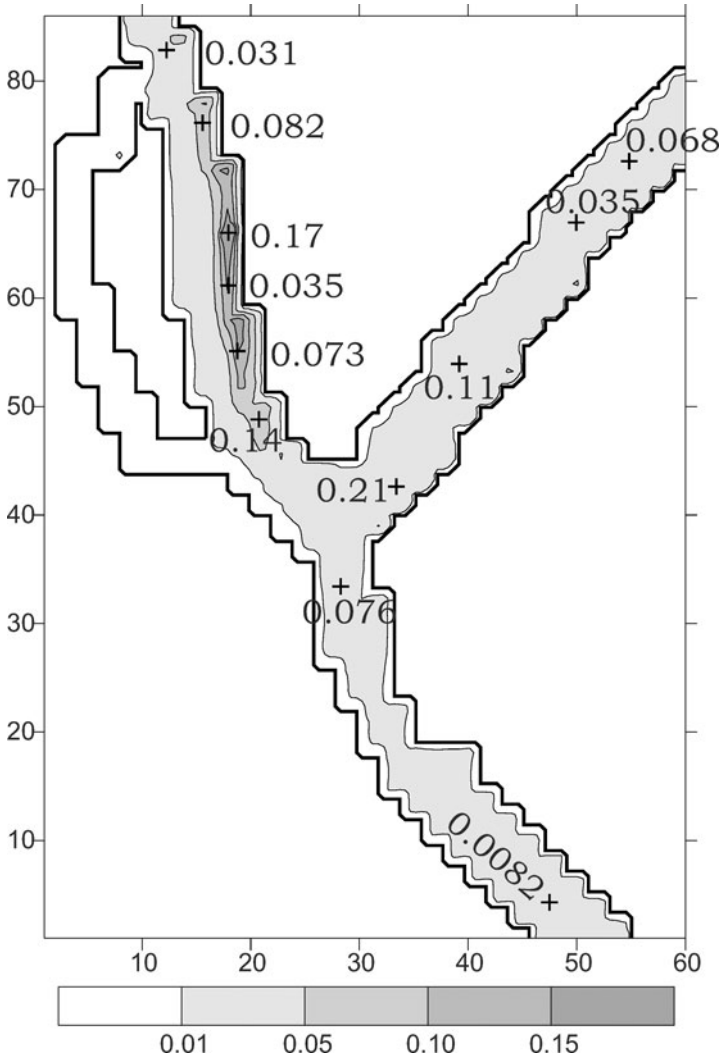

Fig. 8.7c. For 2002

the specific to the non-specific sites, and from this phase is dissolved. The time evolution of the ^{226}Ra fraction that is present in the sediment in the non-specific sites is shown in figure 8.8B. It decreases from 40 % to less than 5 %.

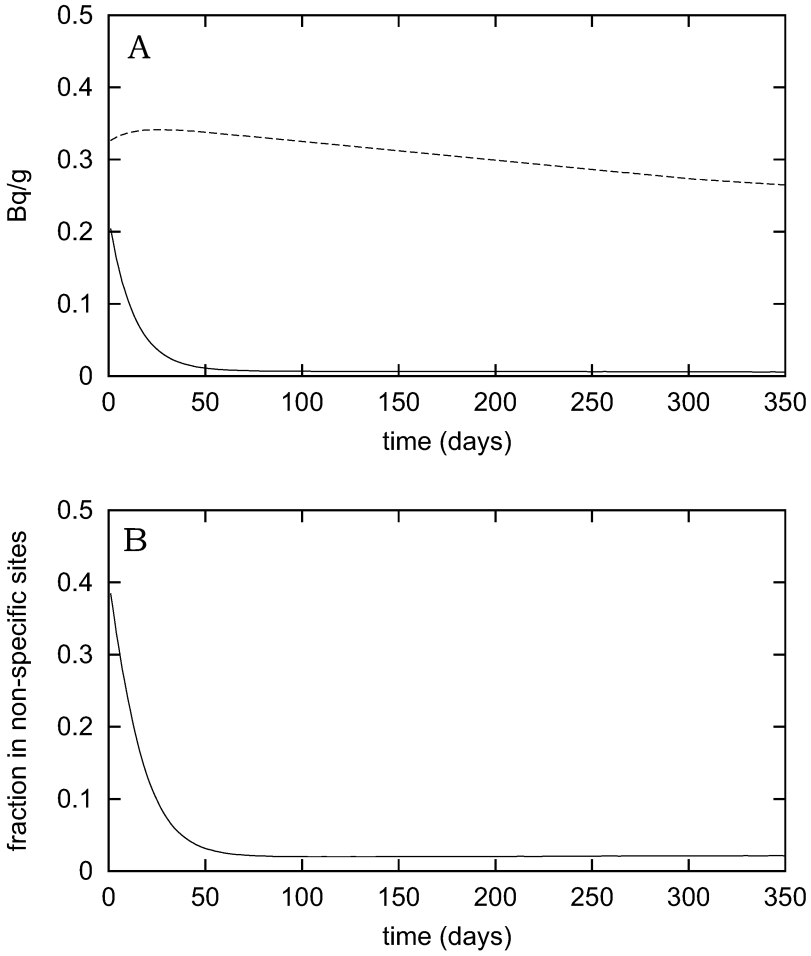

Fig. 8.8. Time evolution of the ^{226}Ra concentration in bed sediment at grid cell (17, 20) during the self-cleaning process. A: specific activity in the non-specific (solid line) and specific (dashed line) sites. B: fraction of ^{226}Ra in the non-specific sites

This chapter may serve as an example of a modelling study of radioactivity dispersion in a tidal estuary. As has been discussed previously, modelling techniques are the same as presented for the marine environment in general.

However, in the case of salt-wedge of partially mixed estuaries, where vertical salinity gradients occur, a full 3D model (now similar to that described for the Rhone River plume) should be used. In the case of a well-mixed estuary, it is also possible that horizontal salinity gradients occur in the area covered by the model (this was not the case in the Odiel-Tinto study). Thus, terms accounting for such gradients should be included in the 2D depth-averaged hydrodynamic equations (note that the depth-averaged model can still be used since gradients are in the horizontal direction; the water column is well mixed in the vertical). A description of such terms may be seen in chapter 4 and in the work by Prandle [140].

9

Sensitivity analysis

9.1 Introduction

Numerical models have been widely used to assess the effect of radioactivity releases to the environment. Model predictions may be used as the basis for important decisions on issues as emergency response and countermeasures, waste management, and environmental remediation and restoration. The consequences of such decisions may be significant in terms of human, ecological or economic costs. Thus it is essential to evaluate the reliability of the model predictions. As a consequence, the final stage in model development is the investigation of how sensitive the model predictions are to changes in the parameter values and to estimate the uncertainties on the predictions.

Model uncertainties have been typically investigated through simple sensitivity studies in which each of the parameters in the model was varied in turn, leaving the others fixed at their nominal values [117, 127, 161, 95]. Indeed, sensitivity of a model to a parameter that has a high natural variability or about which little is known can increase the uncertainty associated with model predictions. Now the Monte Carlo method has arisen as the generally most suitable approach to carry out a quantitative analysis of sensitivity and propagation of uncertainties in radionuclide transport codes [173]. It is also possible to calculate partial correlation coefficients (r_{part}) for relationships between model outputs and values of the parameters selected for analysis. Partial correlation estimates the linear correlation between an output variable and a parameter after removing the effects of the other parameters. A rank of model parameters can be obtained according to their partial correlation coefficients, which gives an indication of their relative influence on model output [173]. The effort for obtaining site-specific values for model parameters, for a given model application, should be focused on the most influential ones. A parameter with a high r_{part} may deserve more study to improve confidence in it and perhaps to reduce its uncertainty. In contrast, research on a parameter with a small r_{part} may not be useful because of the low relationship between its value and the output.

Thus, sensitivity analysis should be carried out to [154]:

- Determine the factors that mostly contribute to the output variability and require additional research to reduce the variability.
- Determine the model parameters that are not influential in the output, and which can therefore be eliminated from the final model.

Sensitivity analysis, as the final stage in model development, also contributes to a more reliable model and one whose abilities are better understood [154]: a sensitivity analysis where the uncertainty in the output is apportioned to the uncertainty in the input parameters provides an element of verification in that it ensures that the response of the computational model to the input is the expected one.

In this chapter, some examples of classical sensitivity analysis are shown. Next, a Monte Carlo based sensitivity study carried out for the English Channel long term dispersion model described in [130] is presented.

9.2 Classical sensitivity analysis

In this kind of sensitivity analysis each of the model parameters is varied in turn, leaving the other fixed at their nominal values. A model run is then made for the expected maximum and minimum values of each parameter. Thus, the model response to variations in each parameter can be assessed.

The model described in [127] simulates the dispersion of ^{226}Ra in a Spanish tidal estuary. It includes the exchanges of radionuclides between water and sediments as was presented in chapter 6, using the concept of exchange surface. As an example, we present in figure 9.1 a sensitivity analysis for parameter ϕ (correction factor, related to sediment porosity, due to the fact that not all the sediment particle surface is available for exchanges of radionuclides since may be partially hidden by other sediment particles). The nominal value of the parameter was fixed as $\phi = 0.1$. Model outputs (Ra concentrations in the water column for some points along the estuary; see figure 8.2) are presented for $\phi = 0.01$ and $\phi = 1.0$, as well as for the nominal value. An increase in ϕ implies a higher sediment-water interaction. The main source of Ra to the water column when this simulation was carried out was due to the redissolution of radium from the previously contaminated sediment. Thus, an increase in ϕ enhances redissolution and concentrations well above the measured levels are computed. On the other hand, ^{226}Ra concentrations are below observations if ϕ is reduced.

The model in [95] simulates the flux of radionuclides from an estuary contaminated after Chernobyl into the Black Sea. The model sensitivity to the water-bed sediment equilibrium k_d (that describes exchanges between these phases in the model) was investigated. In figure 9.2, the calculated flux of ^{137}Cs from the estuary to the sea (negative values) during 2 years after the accident is shown for 3 k_d values. The flux for the nominal k_d (3 m^3/kg) was

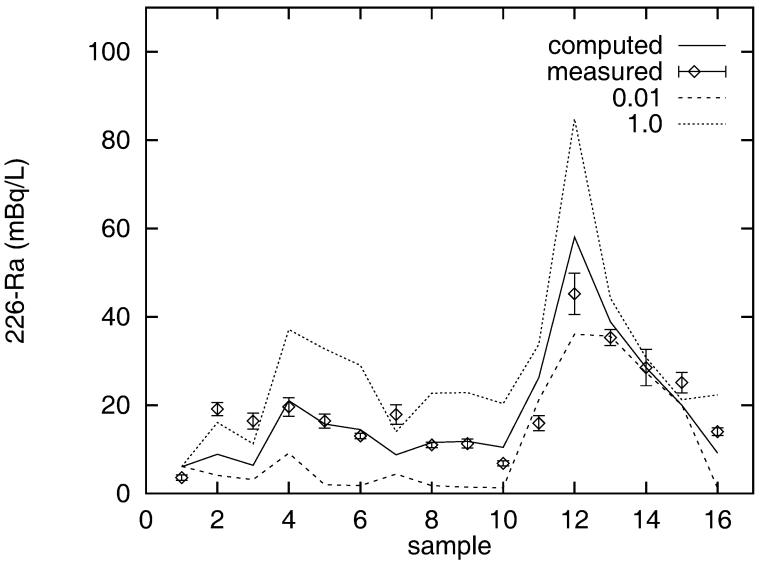

Fig. 9.1. Model sensitivity to changes in correction factor ϕ. The continuous line is model output (^{226}Ra concentrations in the water column along the estuary) for the nominal ϕ value

half than for $k_d = 0$, while differed in 10 % between $k_d = 3$ and $k_d = 5$ m^3/kg.

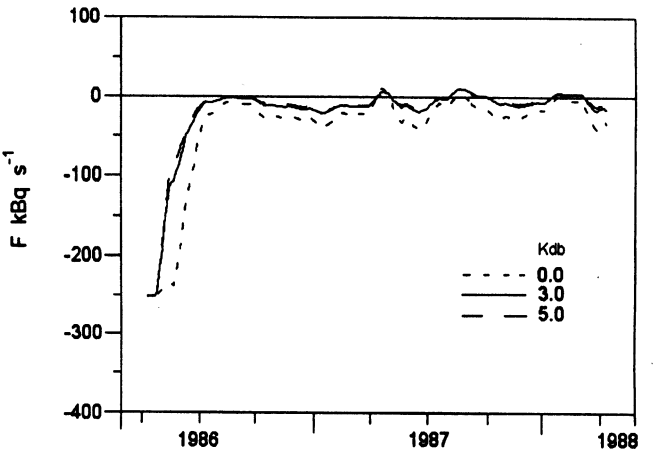

Fig. 9.2. Sensitivity of the flux of ^{137}Cs from the Dnieper-Bug estuary into the Black Sea to the sediment water distribution coefficient (from [95])

Tappin et al. [161] developed a model for metal transport in the North Sea and studied sensitivity to metal inputs from the different sources included in the model (inputs through open boundaries, rivers and atmospheric deposition). Results indicated that metal concentrations were most sensitive to concentrations in Atlantic inflows (via the Strait of Dover and the northern model boundary).

This kind of sensitivity analysis has also been carried out in the ecotoxicological model presented in [81]. Model parameters were changed, one by one, in a factor 2 above and below their nominal values. The % of change of a contaminant concentration at a target point in dissolved form, fixed to suspended particles and fixed to plankton is then given in a table.

Carroll and Harms [28] studied uncertainty in a model that simulates the dispersion of radionuclides in a shallow Artic Bay. The model uses partition coefficients to describe the distribution of radionuclides between water and suspended matter particles. Probability distributions were assigned to the suspended matter concentration and distribution coefficient k_d (parameters needed to calculate the partition coefficient). These distributions were sampled and probability distributions were then obtained for the partition coefficient. The dispersion of radionuclides was then computed for the partition coefficient probability distribution mode and for a lowest and a highest value. Thus, in this work probability distributions are used to estimate the variability of the partition coefficients, although the sensitivity analysis is carried out in the simple way presented in this section.

9.3 Monte Carlo based sensitivity study

A sensitivity analysis, based on a Monte Carlo method, of a long term marine dispersion model [130] for non conservative radionuclides previously developed and validated for the English Channel (where radionuclides are released from Cap de La Hague nuclear fuel reprocessing plant) is briefly presented here. The model is based on the computed residual transport velocity, shown in figure 4.10, obtained with the average wind on the Channel. More details on the sensitivity study may be seen in [134].

In particular, only the model sensitivity to parameters governing the exchanges of radionuclides between the liquid and solid phases (suspended matter and bottom sediments) is studied. Model sensitivity will be studied in three typical situations, which correspond to the different source terms that can generally be found: (1) the case of a hypothetical instantaneous release of radionuclides from the reprocessing plant, (2) the case of a continuous release and (3) the case in which there is not an external input of radionuclides but the bottom sediments are initially contaminated, so that they behave as a long term source of previously released waste radionuclides. Errors will be assigned to model predictions and r_{part}s will be calculated for the three situations studied. This will allow to establish a ranking of partial correlation

coefficients to analyze the relative influence of each parameter. Calculations are made for two radionuclides with different geochemical behaviour: ^{137}Cs and ^{239,240}Pu.

The sensitivity analysis has been limited to parameters governing the exchanges of radionuclides between the liquid and solid phases described before: χ_1, k_2, ρ, ρ_s, R, L, ϕ and f, as well as k_3 and k_4 in the case of redissolution (a 2-step kinetic model is used in this case. See figure 6.6).

A Gauss probability distribution is assigned to each parameter, which is defined by its average value and standard deviation. A random sampling of each distribution is carried out using a Monte Carlo method. Thus a set of model parameters is obtained, and the model is run. This process is repeated 200 times, so that a distribution of model results is obtained. The set of model results allows to be assigned uncertainties to model output and to calculate partial correlation coefficients to rank parameters. The process is summarized in figure 9.3.

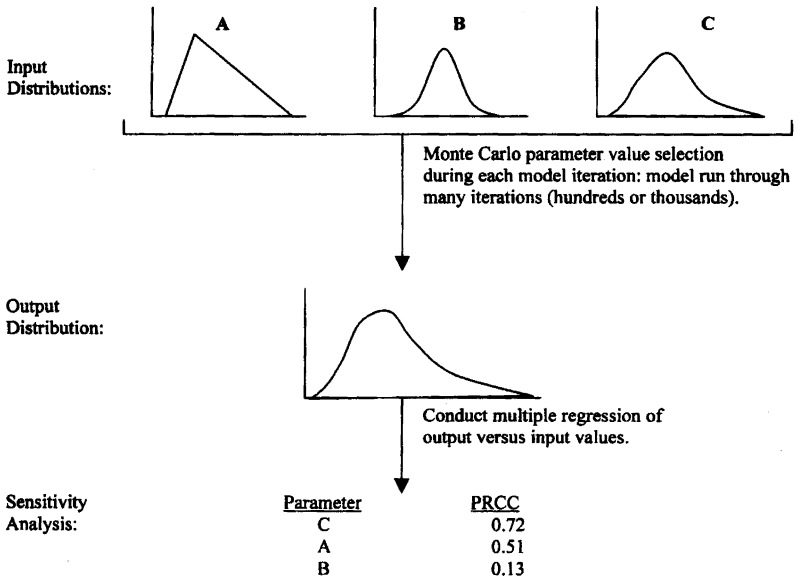

Fig. 9.3. Scheme of a Monte Carlo based sensitivity study taken from [173]

Let us see a method to carry out random sampling of a probability distribution. Consider a normalized Gauss distribution for variable x defined by its average value and dispersion, $\bar{x}$ and σ respectively:

$$P(x) = \frac{1}{\sqrt{2\pi\sigma^2}} \exp - \frac{(x-\bar{x})^2}{2\sigma^2} \tag{9.1}$$

This is distribution is going to be sampled over a 3σ distance around the average value. A random number x between $\bar{x} - 3\sigma$ and $\bar{x} + 3\sigma$ is generated in the form:

$$x = (\bar{x} - 3\sigma) + 6\sigma RAN \tag{9.2}$$

where RAN is a random number between 0 and 1. The probability P for this random x is calculated from equation 9.1. A second random number is then generated. If it smaller than P then the sampled x is accepted. If not, a new x is sampled.

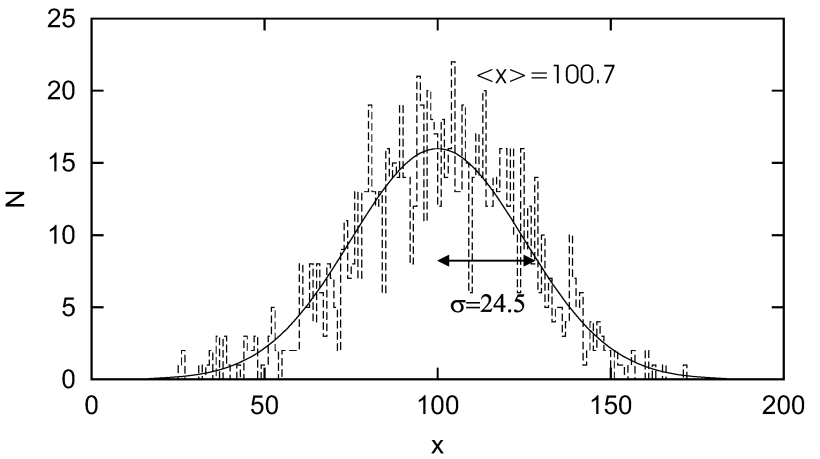

Fig. 9.4. Frequency histogram of random samples obtained from a Gauss probability distribution. The numerical fitting of this histogram to a Gauss distribution is also shown (solid line)

As an example, consider a Gauss distribution with $\bar{x} = 100$ and $\sigma = 25$. One thousand samples have been obtained from this distribution following the method described above. Results can be seen in figure 9.4, where the histogram of results is shown. This histogram has been fitted to a Gauss distribution also shown in figure 9.4. This fitted distribution has average value and dispersion equal to 100.7 ± 0.7 and 24.5 ± 0.9 respectively. Thus, the original distribution is re-obtained rather well. In other words, samples reflect very well the original probability distribution.

Partial correlation coefficients are calculated in the following way: if a set of variables $(x_1, x_2, \ldots, x_p)$ is given, the r_{part} between variables 1 and 2, for instance, is calculated obtaining the correlation coefficient in the regression

$$e_{1.34\ldots p} = A \cdot e_{2.34\ldots p} + B \tag{9.3}$$

where $e_{1.34\ldots p}$ and $e_{2.34\ldots p}$ are the residues of the multiple regression of variables 1 and 2 respectively with respect to the rest of variables $3 \ldots p$. The

correlation coefficient for regression equation 9.3 is the partial correlation coefficient between variables 1 and 2.

In the three cases analyzed, the model can produce an extensive amount of information: distribution maps of radionuclide concentrations for each phase and at any desired time, and/or temporal evolution of concentration in each phase and for each desired point of the model domain. Considering that 200 simulations are carried out for each case, the volume of data obtained would be rather difficult to handle. Thus, to simplify the model output we have fixed our attention in a given *target grid cell* and at a defined instant of time after the beginning of the simulation ($t = 0$). This target means a sensitive point in the domain, where a local population (human or not) could receive an external dose due to contamination of water and/or sediments or an internal dose due to ingestion of contaminated material, for instance. The instant of time at which results are obtained is the time required for the peak of activity to travel from La Hague to the target grid cell. Thus, the model would provide information on maximum activity levels reached in that point (in water, suspended matter and bottom sediments) so as to determine, for instance, if any kind of remedial action should be taken. For simulations carried out with ^{137}Cs, we have defined grid cell $(50, 20)$ as the target and results are obtained 40 days after the beginning of the release from La Hague or the redissolution from the sediment. In the case of ^{239,240}Pu, target grid box is $(30, 26)$. This grid box is closer to La Hague [La Hague releases are carried out at grid cell $(26, 24)$] since due to the high reactivity of plutonium, this radionuclide moves slower than Cs.

As an example, the distribution of dissolved ^{137}Cs over the model domain 40 days after the instantaneous release from La Hague is presented in figure 9.5. The position of the target grid cell (for ^{137}Cs) is also shown in the map. It can be seen that the patch of radionuclides essentially moves along the French shore and that the target grid cell effectively is in the area of the activity peak at this instant of time. In the case of a continuous release, a banded structure showing higher concentrations along the French shore is now extending from La Hague to Dover [130]. In the case of redissolution, concentrations at La Hague in water and suspended matter initially increase due to the input from the sediment and after decrease due to advective/diffusive processes. A patch extending along the French shore is then observed. Sediments are contaminated as the patch travels above them.

The values given to the parameters are presented in table 9.1 for the ^{137}Cs application. Each value, which is the nominal value previously used in this model [130], is taken as the average value for each Gauss distribution. The errors given in table 9.1 (arbitrarily taken as 20 % of the nominal values) correspond to the standard deviation of each probability distribution. The probability distribution of each parameter is sampled using a Monte Carlo method over a 3σ distance around the average value.

Initial conditions for the simulations are the following. In cases 1 and 2 the model is started from zero concentrations in water, suspended matter and

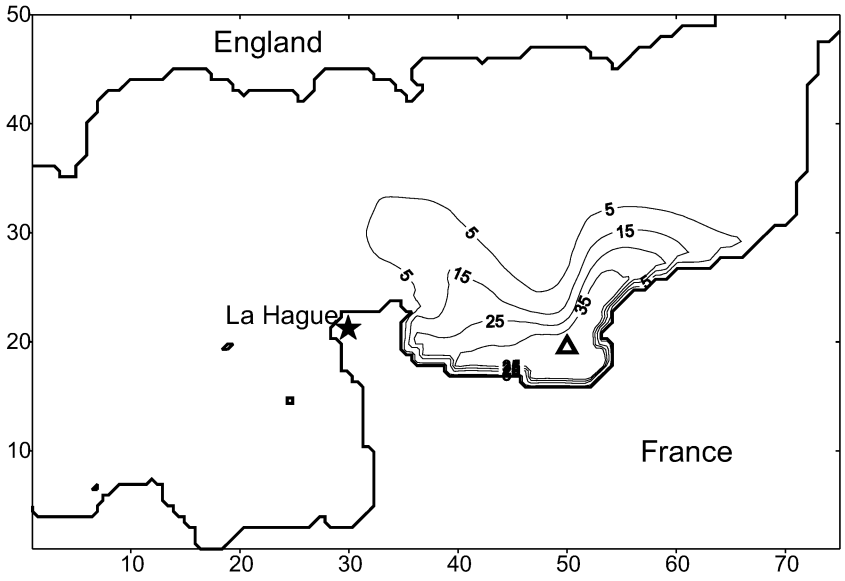

Fig. 9.5. Distribution of dissolved ^{137}Cs (Bq/m^3) 40 days after an instantaneous release at La Hague. The position of the *target grid cell* is indicated by the triangle

Table 9.1. Nominal value and error assigned to each parameter in the model for the application to ^{137}Cs

symbol	description	value
ρ	particle density	2600 ± 520 kg/m^3
ρ_s	sediment bulk density	900 ± 180 kg/m^3
χ_1	exchange velocity	$(2.1 \pm 0.4) \times 10^{-8}$ m/s
k_2	kinetic coefficient	$(1.16 \pm 0.23) \times 10^{-5}$ s^{-1}
L	sediment mixing depth	0.10 ± 0.02 m
ϕ	correction factor	0.10 ± 0.02
R	particle mean radius	15 ± 3 μm
f	active sediment fraction	0.10 ± 0.02
k_3	kinetic coefficient	$(1.16 \pm 0.23) \times 10^{-7}$ s^{-1}
k_4	kinetic coefficient	$(1.16 \pm 0.23) \times 10^{-8}$ s^{-1}

bottom sediments over all the domain. In the case of an instantaneous release, an input of 5.0×10^{12} Bq of dissolved ^{137}Cs is assumed at $t = 0$ and at grid cell $(26, 24)$, where wastes from La Hague are released. In the case of a continuous release, 5.0×10^{10} Bq are introduced each time step. In study 3 (redissolution) an initial activity concentration of 1.0×10^5 Bq/kg was considered in the active fraction of the bottom sediment in grid cell $(26, 24)$ (in the slowly reversible sediment phase), which means an inventory of 2.25×10^{13} Bq in the entire compartment. Zero concentrations are assumed for water, suspended matter and sediment (unless in the mentioned point) over all the domain.

Table 9.2. Average value ($\overline{x}$), width (w) and correlation coefficient for the numerical fitting of model results to Gauss distributions for each phase in the ^{137}Cs instantaneous release experiment. The width of the distribution is $w = 2\sigma$

phase	$\overline{x}$	w	r^2
C_d (Bq/m^3)	35.39	3.04	0.949
C_s (Bq/kg)	5.28	4.60	0.829
A_s(Bq/kg)	11.12	7.97	0.680

The frequency histograms of results have been obtained for C_d, C_s and A_s (activity concentrations in water, suspended matter and active bed sediment respectively) in the ^{137}Cs instantaneous release experiment as an example. Such histograms have been fitted to Gauss distributions. Results are presented in table 9.2, where the average value and width of the distributions are given together with the correlation coefficient of the numerical fitting. It can be seen that, in general, the fitting of the histograms to the distributions is good: Gauss distributions are obtained for the model results from the probability distributions of parameters. Uncertainty can be assigned to model results now. Thus, it can be concluded that for the target grid box 40 days after the discharge, ^{137}Cs concentrations are

$$C_d = 35.4 \pm 1.5 \quad \text{Bq/m}^3$$

$$C_s = 5.3 \pm 2.3 \quad \text{Bq/kg}$$

and

$$A_s = 11 \pm 4 \quad \text{Bq/kg}$$

for water, suspended matter and the active bottom sediment respectively (errors are 1σ). Model results are more precise in the case of the dissolved phase (relative error 4%), while uncertainties are larger for suspended matter and bottom sediments (relative errors 43% and 36% respectively). This method for estimating model uncertainties could be applied to any other modelling application.

Absolute values of the partial correlation coefficients for the three cases studied and for each parameter are presented in figure 9.6 for the case of

^{137}Cs. The most influential parameters are arbitrarily defined as those having r_{part} above 0.5 [23]. Moderately influential parameters are defined as those having r_{part} between 0.3 and 0.5.

It can be seen that all parameters are relevant in the description of the transfers between the liquid and solid phases, depending in the phase in which we are interested and in the source term. For instance, if we are interested in obtaining the activity concentration in suspended matter particles (due to any reason) it is clear that particle density, ρ, must be precisely specified for the three situations investigated ($r_{part} > 0.77$). This parameter, however, is not relevant if our interest is focused in water or bottom sediments ($r_{part} < 0.16$ in all cases). A detailed discussion may be found in [134], but is not included here since our intention is simply to show the method. However, average values of the absolute values of the partial correlation coefficients, for all phases and experiments, are presented in table 9.3, for both ^{137}Cs and ^{239,240}Pu, together with their standard deviations. The average value gives an indication of the *overall influence* of each parameter, while its dispersion indicates the variability of the parameter relevance between experiments (source terms) and phases. It seems clear that, in general for ^{137}Cs, the most influential parameters are χ_1, k_2 and R; followed by k_4 and L. The large dispersion of the average value in the remaining parameters indicates that their relevance is limited to certain phases and source terms.

Table 9.3. Average value of the partial correlation coefficients for all phases and experiments (each parameter is averaged over 9 values)

parameter	^{137}Cs	^{239,240}Pu
ρ	0.3 ± 0.4	0.3 ± 0.3
ρ_s	0.5 ± 0.4	0.23 ± 0.24
χ_1	0.80 ± 0.15	0.56 ± 0.08
k_2	0.78 ± 0.09	0.31 ± 0.25
L	0.53 ± 0.21	0.70 ± 0.11
ϕ	0.4 ± 0.3	0.29 ± 0.15
R	0.77 ± 0.13	0.51 ± 0.15
f	0.4 ± 0.3	062 ± 0.24
k_3	0.19 ± 0.24	0.18 ± 0.17
k_4	0.65 ± 0.17	0.65 ± 0.16

In the case of plutonium, χ_1 is still relevant for all phases and types of source term (although less than in the case of ^{137}Cs). This is not the case with k_2, which is only moderately influential. The most influential parameters are now L, k_4 and f, followed by χ_1 and R. The remaining parameters show similar behaviour as in the case of ^{137}Cs.

Together with uncertainties in parameters describing the exchanges of radionuclides between the liquid and solid phases, there are other sources of

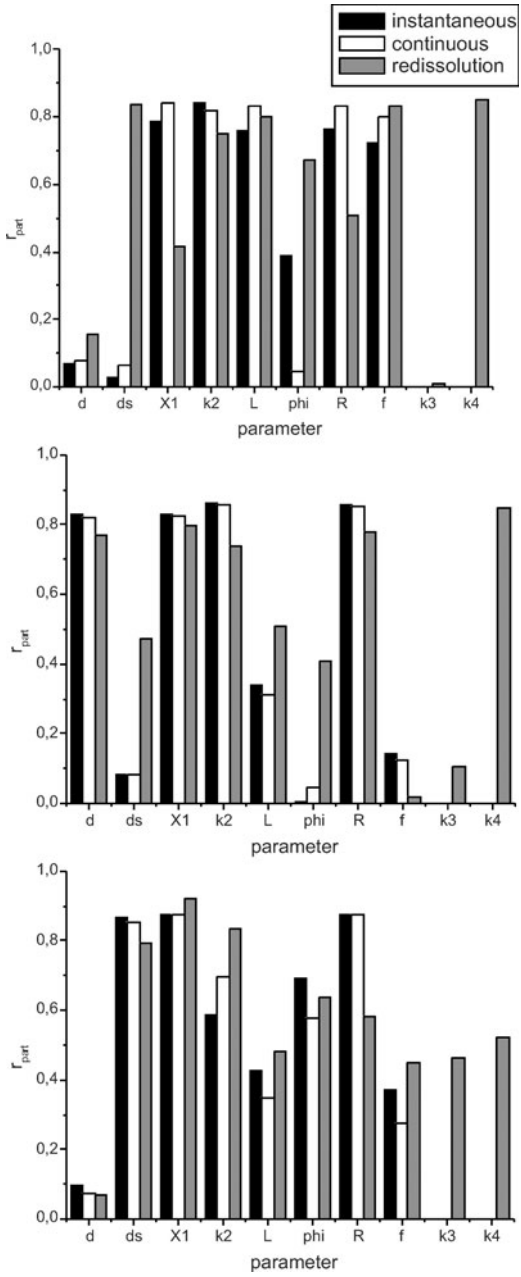

Fig. 9.6. Values of the partial correlation coefficient for the three phases and in the three situations studied (d=ρ, ds=ρ_s) in the case of ^{137}Cs. Up: water, middle: suspended matter, down: sediment

error in a model. Although the use of residual circulation to compute advection can give results very similar to those obtained by explicitly calculating tidal currents and advection, if the residual circulation field is appropriately defined [47], the use of an averaged wind speed and direction can be a source of uncertainty. Indeed, Carroll and Harms [28] have found that changing wind patterns affect the dispersion of radionuclides with low k_d (Cs and Sr). However, they have little influence on particle-reactive radionuclides. Solving the advection-diffusion dispersion equation by finite differences also introduces errors in model output since a finite difference scheme is always an approximation to the full differential equation. Open boundary conditions are often required (in our case along Dover Strait and the western boundary of the Channel). These conditions are mathematical artifacts that may introduce some errors. However, in real ocean dispersion problems, errors introduced by the finite difference scheme (if at least second order accuracy schemes are used) and boundary conditions are generally masked by turbulence.

Although results of a sensitivity analysis are specific for the particular model formulation, some general conclusions may be extracted from this study. The geochemical behaviour of radionuclides affects model sensitivity to some parameters: it is necessary to specify more carefully parameters describing sediments (L and f) when the radionuclide presents a strong non-conservative character. In contrast, model output is less sensitive to kinetic rates than in the case of a more conservative radionuclide. Also, it seems that considering several particle sizes in dispersion models can lead to an improvement in results (this is indeed the reason why 4 particle classes were considered in the Rhone River plume dispersion model described before).

10

Review of some radionuclide dispersion models

In this final chapter, some radionuclide dispersion models developed for diverse marine areas and under different approximations are briefly commented. The readers that wish more detailed information about the models can directly go to the references included along the chapter. Box models are not included since have not been discussed in the book.

10.1 The European Continental Shelf model by Prandle

This model, that may be considered as the first hydrodynamic model applied to simulate the dispersion of radioactivity in the sea, was developed by David Prandle, from the Proudman Oceanographic Laboratory (Bidston, UK), and published in 1984 [140].

The model simulates the dispersion of ^{137}Cs, considered as conservative, released from Sellafield reprocessing plant over the period 1964-1980. The model domain covers the whole north European Continental Shelf with a spatial resolution of approximately 35 km.

The 2D depth averaged hydrodynamic equations were solved specifying only the M_2 constituent along open boundaries. Once a periodic stable solution was achieved, tidal residual transport was calculated. The steady state response to two uniform wind stresses (in the x and y directions) were also calculated independently. The total average transport is then obtained by adding the tidal residual plus the two wind induced transports. Discharge rates from Sellafield were specified on a monthly basis and wind stress values averaged over three months. It is possible to calculate the wind-driven response for any particular 3-month period by suitably factoring the responses to unit values of the two components of the wind stress obtained previously. The dispersion model solves the 2D depth-averaged advection-diffusion equation over the same grid as the hydrodynamic equations. Measured and computed ^{137}Cs concentrations were, in general, in good agreement. Also, sensitivity analysis

were carried out in the classic way described in the previous chapter to study the model response to changes in the diffusion coefficient and wind forcing.

It is interesting to analyze how the diffusion coefficient values (different in the x and y directions) were selected. They were obtained from the equations:

$$\begin{aligned} K_x &= \alpha u_0 \sqrt{u_0^2 + v_0^2} \\ K_y &= \alpha v_0 \sqrt{u_0^2 + v_0^2} \end{aligned} \tag{10.1}$$

where u_0 and v_0 are the amplitudes of tidal currents in the x and y directions respectively and $\alpha = 1000$ s from model calibration. The origin of this formulation is that the major contribution to turbulent mixing arises from tides. Thus, the diffusion coefficient in a given direction increases as the corresponding tidal current component increases. However, although this formulation produces a good agreement between observed and computed ^{137}Cs concentrations, presents a conceptual objection: the diffusion coefficients depend on the axis selection. In other words, mixing in two equal channels (with the same tidal current), for instance, will be different simply if their orientations are different.

Some time parameters (age, residence time, transit time, turn over time and flushing time) were finally defined and calculated.

10.2 Ifremer long-term dispersion model for the English Channel and southern North Sea

This model was developed by M. Breton and J. Salomon and published in two papers [24, 151]. In the first, the model is described and validated through comparisons with measurements. In the second paper, the model is applied to evaluate transit times of radionuclides from La Hague to the rest of the domain.

The model works with the Lagrangian residual circulation and is 2D depth averaged. First, a hydrodynamic model is run for various combinations of winds and tides and, for each run, water particle trajectories are calculated. These are used to evaluate the Lagrangian velocity, that is related to the average geographical position of the particles as they move forward and backwards due to tides. A catalogue of residual Lagrangian velocities is then obtained. Velocity at any position for any wind condition and tide amplitude is obtained through interpolation from this catalogue. Main rivers are also considered through their average water discharges.

The dispersion model solves the usual advection-diffusion equation for real winds and tides. Water velocities are obtained from the residuals catalogue in the way mentioned above. The model has been developed for conservative radionuclides. It was applied to simulate the dispersion of dissolved ^{99}Tc and ^{125}Sb released from La Hague over a 10 year period (1983-1992).

Schonfeld [153] also developed a long term dispersion model for the English Channel and the North Sea. In this case, dispersion was solved by means of a

particle tracking method. Water currents are obtained from a 3D baroclinic model forced with meteorological data (wind, pressure, heat), supplied by a meteorological model, and 14 tidal constituents. Water currents are stored with a temporal resolution of 15 minutes. The dispersion of dissolved ^{99}Tc was simulated for a period of almost two years.

10.3 THREETOX: Three dimensional model of toxicants transport

This model has been developed at the Institute of Mathematical Machine and System problems (Kiev, Ukraine) and first published in 1997 [94, 85]. It simulates the 3D dispersion of non conservative radionuclides in stratified waters and consists of three submodels: hydrodynamics, suspended sediment transport and radionuclide transport.

The hydrodynamic model consists of the full 3D equations, including transport equations for salinity and temperature. Water density is calculated from its temperature and salt content, through a equation of state. At the sea surface, wind stress and heat flux are specified. An ice submodel is also included to provide ice thickness and drift. The suspended sediment transport is described by an advection-diffusion equation, to which settling, erosion and deposition terms are added, as has been discussed before. However, a equation used to calculate the thickness of the upper layer of contaminated sediment is also included.

The radionuclide dispersion model includes advection-diffusion of radionuclides in water and suspended sediment, as well as exchanges between water, suspended sediments and the upper sediment layer. Radionuclide transfers between suspended sediments and the upper bed layer are governed by erosion and deposition. Exchanges between water and both solid phases are described by means of a desorption rate and the equilibrium distribution coefficient. However, different rates and distribution coefficients are used for the water-suspended sediment and the water-bed sediment exchanges.

The model presentation in the above indicated references is illustrated by several case studies: ^{137}Cs dispersion at Kiev reservoir and ^{137}Cs and ^{90}Sr dispersion at the Dnieper-Bug estuary and at the Kara Sea. The model has also been applied to simulate the flux of ^{137}Cs and ^{90}Sr from the Dnieper-Bug estuary into the Black Sea [95].

A model for the whole Black Sea is described in [158]. It is a 3D baroclinic model forced with twice daily atmospheric data and river discharge. The hydrodynamic model is integrated for 40 years and a seasonal periodic solution is obtained. The dispersion model solves the advection/diffusion equation for ^{90}Sr, considered as conservative. Radionuclides are introduced through the river discharges of Danube and Dnieper after Chernobyl. Atmospheric fallout is considered negligible. Computed vertical profiles and horizontal ^{90}Sr distributions are analyzed. Details may be seen in [158].

10.4 CEFAS Irish Sea model

This model has been developed at CEFAS (Centre for Environment Fisheries and Aquaculture) at Lowestoft (UK) and published in 1998 and 2003 [12, 11]. The model resolves processes operating on tidal time scales, whilst being simple enough to run over decadal time periods. Modelled processes include transport in the water column, exchange of contaminants between dissolved and particulate phases, wave-current sediment resuspension, sediment transport and mixing of material within the seabed. Transport in the water column is by a combination of tide, wind and density driven flows. Sediment transport is based on the erosion, advection, and deposition of three sediment classes representing sand, flocculated mud/silt and fine background components. Transfer of radionuclides between the dissolved and sediment phases is implemented using rate equations. A layered seabed is incorporated, with transfers between layers representing biological and physical mixing processes.

The preparation of flow and wave fields covering thirty years (for instance), resolving tidal timescales based on measured winds and at the required grid resolution is a formidable undertaking. Therefore a less ambitious approach is used. Hydrodynamic and wind-wave models are used to produce a series of two year-long data sets with one hour temporal resolution which are stored for subsequent transport model calculations. A calculation to predict radionuclide dispersion is accomplished by taking a series of these two year-long flow and wave fields. For longer term calculations, the sequence of year-long flow fields are repeated as necessary for the duration of the run. The assumption is made that the flow and wave conditions from the years chosen are a statistically representative set of conditions. Actually, there is likely to be inter-annual variability in flow and wave conditions. Although it is expected that the repeating of a set of flow fields may introduce some bias into the model calculations, the authors believe that this approach is able to reproduce the overall long term behaviour and ascertain the dominant processes, if not to make exact year by year hindcasts.

The hydrodynamic model was run in 3D with wave-current interaction described as in [39]. For each of the two years of wind forcing, depth-averaged currents and sea surface elevations were stored at hourly intervals. Four tidal constituents are used, and equations are solved on a grid with a spatial resolution of approximately 4 km. Depth-averaged currents and surface elevations are used to solve the transport of sediments and radionuclides in a 2D form.

A spectrum of particle sizes is represented by dividing the sediment load into classes of fixed particle size. The bed is layered, with the top bed exchanging material with the water column. Transfer of sediment and associated radionuclides within the bed occurs at a fixed rate and behaves as a diffusion-like process. The total quantity of sediment and sand/mud ratio is allowed to alter during the computation as a result of sediment transport.

Radionuclide transport equations include advection/diffusion processes, exchanges by erosion and deposition and exchanges between water and the

solid phase. These are described, as in the THREETOX model, by means of a desorption rate and the distribution coefficient instead of using adsorption and desorption rates, although both formulations are equivalent. The dependence of the equilibrium distribution coefficient on the particle size is included following the formulation of Abril and Fraga [5].

The model was run for the period 1965-1996 starting from a clean water column and bed sediment. It was found a good agreement between model calculations and measured water concentrations of ^{137}Cs in the 1970s, as well as for water and seabed concentrations and inventories of ^{239,240}Pu during the whole simulated period. More details may be seen in [12].

10.5 MEAD model

This model (Marine Environment Advection Dispersion), developed at Westlakes Scientific Consulting Ltd., simulates the long term transport of non conservative radionuclides in the Irish Sea [65, 157]. It includes advection/diffusion of radionuclides in the dissolved and suspended matter phases, erosion and deposition, and adsorption/desorption reactions. Again, these processes are formulated in terms of a desorption rate and the equilibrium distribution coefficient.

The model is 2D depth-averaged, running on a grid with a spatial resolution of 2 km. The annually averaged water circulation in the Irish Sea was obtained through the application of the commercial MIKE21 [44] hydrodynamic model on the same grid. The suspended sediment field was determined using a annually averaged sediment transport model. The diffusion coefficients are written in terms of the residual velocities, mean amplitudes of tidal currents and mean water depth.

Calculations are carried out assuming a release of 1 TBq from Sellafield reprocessing plant. Radionuclide concentrations are evaluated in the three phases over the domain for a 100 years period. These distributions are stored in files and used as templates that allow the determination of activity concentrations for any specific release scenario.

In a first paper [65], the temporal evolutions of radionuclide concentrations in the three phases for the 1 TBq discharge are qualitatively analyzed during a 50 years period. Model predictions for real discharges (calculated as commented in the paragraph above) are compared with measurements in the sea, for both ^{137}Cs and ^{239,240}Pu, in a second paper [157].

10.6 Suez Canal model

This modelling study was carried out by J.M. Abril (University of Seville, Spain) after a requirement by the IAEA to evaluate the consequences of any

accidental release of radioactivity in the Canal and to investigate the dispersion of radionuclides in these tidal waters (connecting the Red and Mediterranean seas, the Suez Canal is a trade route with intense shipping activities). Details are given through four papers [9, 6, 7, 8].

The hydrodynamic of the Canal was studied by means of a 1D model (equations are described in [7]) using as boundary conditions observed water levels at the two open ends of the Canal. This was divided into 178 sectors with 800 m length each one. The effect of winds, atmospheric pressure, horizontal salinity gradients and changes in mean sea level at the south end (Red Sea) are also investigated. Water circulation in some lakes crossed by the Canal is studied by means of a 2D depth averaged model as described in chapter 4. Spatial and temporal resolutions of the 2D model are 500 m and 10 s respectively. Recorded water levels are used as open boundary conditions.

Tracing experiments in the Canal, carried out with rhodamine B, were performed to obtain information on the diffusion coefficients to be used in the dispersion model for dissolved radionuclides [9]. One dimensional and 2D depth-averaged models are again used for dispersion. Results from the tracing experiments indicate that, even in narrow and regular channels, two dimensional effects are evident due to the characteristic water velocity horizontal profile showing maximum current in the central part of the channel and minimum currents along the shores because of friction. The observed dispersion patterns could be reproduced with a 2D model.

The dispersion model was finally extended to non-conservative radionuclides [6, 8]. Exchanges of radionuclides between the liquid and solid phases were described by means of kinetic coefficients. The model was applied to simulate the dispersion of hypothetical releases of ^{137}Cs and ^{239,240}Pu, and the behaviour of these two radionuclides was compared.

10.7 The Artic Ocean environment

There has been interest in the development of radionuclide dispersion models for the Artic environment since radioactive waste was dumped here since 1959 and has continued through the early 1990s. Wastes were released as containers, whole nuclear ship reactors or barges loaded with reactor components and spent fuel. Dumping sites are small and shallow bays in the Kara Sea, but also deeper regions in the central part of the sea were used.

Ingo Harms (University of Hamburg, Germany) studied the dispersion of radionuclides released from dumping sites in the Artic in both a local and a regional scale [67]. The regional scale covers the Barents and Kara seas. The local scale is focused in the small bays where dumping occurred.

The water circulation is obtained through the application of the Hamburg Shelf Ocean Model (HamSOM), described in [14]. It is a 3D baroclinic model coupled with an ice model that provides ice growth and drift. The radionuclide dispersion model consists of the 3D advection-diffusion equation.

The distribution of radionuclides between the dissolved phase and suspended matter particles is obtained from the partition coefficient, which depends on the equilibrium distribution coefficient as discussed in chapter 2. It is also assumed that activity concentration in the surface bed sediment is equal to that of suspended particles in the water column once that a stationary radionuclide distribution in the water column is reached.

The regional scale model has a horizontal resolution of 18 km and 10 layers are used in the vertical. The dispersion model is coupled on-line with the same time step as the hydrodynamic model (15 min). The water circulation was derived using monthly mean values of wind stress and freshwater inputs from the main rivers in the region. Only the main M_2 tidal constituent was used. Two seasonal mean temperature and salinity fields (winter and summer) were also used. The model was applied to simulate the dispersion of hypothetical instantaneous releases of ^{137}Cs from dumping sites and continuous releases of ^{137}Cs and ^{239,240}Pu from these sites. Calculations extend over two and five years for the instantaneous and continuous release scenarios respectively.

In the local scale, the HamSOM model was applied to two small bays in the Kara Sea. The spatial resolution was 185 m and wind was considered as the main driving force. The hydrodynamic model was used in a barotropic mode (without density differences) and the hydrodynamic and dispersion models were coupled off-line. Temporal resolution of the dispersion model was fixed as 3 hours. The model was applied to obtain the flushing times of the bays.

These regional and local models have also been applied to estimate the radiological impacts, through calculations of doses, due to hypothetical leakage from the dumping sites [15]. Moreover, the local model has also been applied to one of the bays but including transient winds and air temperatures from monthly mean climatological data, as well as the baroclinic mode (water density differences) [68]. Only dissolved radionuclides are considered in the dispersion model. This application has been used to design a new long-term monitoring system of the bay, since the model has shown that the present approach via yearly expeditions during the ice-melting period is not effective. Details may be seen in [68].

Preller and Cheng [144] have studied the dispersion of radionuclides released from several sources with a baroclinic model, coupled with an ice model, that covers the Artic Ocean and its marginal seas. The model has a horizontal resolution ranging 17-35 km and uses 15 vertical levels. The model was forced with annually averaged climatological data corresponding to years 1986 and 1992, thus two averaged water circulation patterns are obtained. Mean outflow from the eight main rivers discharging in the Artic is also included. Radionuclide, considered as conservative, dispersion is computed for 10 years using each circulation scheme. Several numerical experiments were carried out considering a constant release rate from different sources separately: Sellafield, radionuclides in river outflow and dumped waste at several locations. Results indicate that the main contribution to activity levels detected in the Artic arises from river and Sellafield sources. Leaking of radionuclides from

dumped waste, even if is taking place, would produce activity levels lower than those observed.

Recently [80], a dispersion model for the European Continental Shelf, north Atlantic and Artic Ocean has been described. The water circulation is obtained from a 3D ice-ocean model forced with daily atmospheric data. The horizontal resolution of the model is 28 km and the dispersion model is coupled on-line. The model was applied to simulate the transport of ^{99}Tc (only advection-diffusion processes) released from Sellafield towards and into the Artic Ocean. The release of ^{99}Tc is started in 1990 and computations are carried out over 10 years. Comparisons between this model and the box model described in [75] are also provided in the paper.

A model of the Artic Ocean, including the north Atlantic as well, has been developed by Gao et al. [63]. The objective of this work consisted of studying the transport and dispersion in the Artic Ocean of coastal pollution released at Europe for the period 1950-1999, and assessing the relative contribution of Sellafield releases and fallout from bomb testing. Radionuclides considered in this study are ^{137}Cs and ^{90}Sr, both treated as perfectly conservative.

The hydrodynamic model is 3D and baroclinic, with 23 vertical layers and a horizontal resolution ranging $90 - 120$ km. It is coupled, as in [80], to an ice model. The hydrodynamic model is forced by daily atmospheric data. The dispersion model, linked on-line with hydrodynamics, consists of the advection-diffusion equation.

Computed and observed time series of radionuclide concentrations at several points were compared in the case of ^{137}Cs, but not for ^{90}Sr. Simulations have also been carried out considering only the source due to global fallout and considering both fallout and Sellafield releases.

10.8 PCFLOW3D model

This model has been developed at the University of Ljubljana (Slovenia) to simulate water circulation, sediment transport and the dispersion of radioactive pollutants. An application to the Sea of Japan is presented in Cetina et al. [29].

The hydrodynamic model is 3D and baroclinic. Simulation of the topographic stress, also known as Neptune effect, is included in the model. It is caused by an irregular topography and affects the mean circulation in such a way that the last tends to follow the topography with shallow water to the right. The dispersion model uses a particle-tracking method and the simulated radionuclides (^{137}Cs and ^{90}Sr) are considered as conservative. Thus, the sediment transport model is not used.

Radioactive wastes have been dumped in the Japan Sea, at a depth of 3000 m, by the former Soviet Union. The objective of the work described in [29] was to evaluate if radionuclides, eventually released from their containers,

would reach the surface, where they could contaminate marine organisms and fish.

Climatological data, salinity and flows through the straits connecting the Japan Sea with the Pacific Ocean, averaged for two seasons (summer and winter), were used as input data to run the hydrodynamic model. Forcing of a hydrodynamic model with salinity and temperature data directly taken from measurements often produces numerical instabilities. The authors decided to calculate the diffusion of measured temperature and salinity for three days (water velocity remaining zero over the domain). This produces a smoothing of temperature-salinity fields that eliminates instabilities when full hydrodynamic calculations are started. Thus, two average water circulation patterns (summer and winter) are obtained. These are used for the dispersion calculations, being exchanged each six months.

The spatial resolution of the model ranges from 17 to 24 km, and 15 vertical layers are used. Time step in the hydrodynamic calculations is 180 s, but it is increased to 0.5 days in the particle-tracking computations. The dispersion scenario consisted of 1 TBq (simulated by 9000 particles) released from one dumping site continuously during 90 days. Calculations extend over 30 years. Results, described in detail in [29], indicate that radionuclide concentrations over the whole sea would be two orders of magnitude smaller than the present background values. Thus, radiological effects are negligible.

A similar model, also for the Sea of Japan, is described in [82]. In this case the model was applied to simulate the dispersion of dissolved ^{241}Am released after the hypothetical accident of a nuclear submarine.

10.9 Global scale models

Some models that simulate the dispersion of radionuclides over a complete ocean basin or even the whole oceans can be found in literature.

Hazel and England [70] presented a model to simulate the dispersion of dissolved radionuclides in the South Pacific Ocean. Radionuclides are released from Moruroa Atoll, where underground nuclear weapon tests where conducted since 1975 until 1996. It is a long-term dispersion model coupled offline with the hydrodynamic model.

The hydrodynamic model is a 3D general circulation model forced with 3 days averaged wind fields. Spatial resolution depends on latitude and longitude, but is always better than 50 km. In the vertical, 20 levels are used. Monthly mean velocities are derived and used to calculate dispersion.

The dispersion model is run over 10 years with a temporal resolution of 8 hours. The objective was to evaluate the potential fate of radionuclides released from the atoll under different conditions. Thus, releases were carried out at different depths. Also, instantaneous and continuous releases were simulated. Finally, the effects of climatic conditions were also evaluated. To do this, releases were carried out over an annual mean velocity field, over two

velocity fields corresponding to summer and winter conditions and over a velocity field representing a El Niño event. A wide discussion of results may be found in [70].

A somewhat similar study was carried out earlier by Lazar and Rancher [87]. In this case, the hydrodynamic model has a spatial resolution of the order of 200 km, and 30 levels were used in the vertical. It was forced by a single climatological year (thus neglecting inter-annual variability). The dispersion model was developed for dissolved radionuclides and run over a temporal scale of 10 years. It was applied to study the effect, on the tropical Pacific Ocean, of different release depths and rates from Moruroa Atoll.

The dispersion of plutonium from the same source in the whole ocean was studied in [101]. Not many details of the hydrodynamic and dispersion models are given. However, the dispersion model uses the particle tracking method. Also, plutonium scavenging is not considered because of the clear open ocean waters. Again, consequences of releases at different depths are investigated.

Tsumune et al. [169] have described a model to simulate spatial and temporal variations of ^{137}Cs and ^{239,240}Pu in the whole ocean. Radionuclides are introduced from global fallout. Deposition of radionuclides over the oceans is considered to be proportional to precipitation, and meridional changes in radionuclide concentrations in rain water are included as well.

The 3D hydrodynamic model (45 vertical levels) provides annual mean and monthly mean flow and density fields. The dispersion model consists of the advection-diffusion equation with a scavenging term. This accounts for the fixation of radionuclides to the suspended particulate matter, that sinks with a constant velocity equal to 100 m/day. The transfer of radionuclides to suspended particles depends on the equilibrium distribution coefficient of each radionuclide and on the suspended particle concentration. This concentration is assumed to be constant and homogeneous over the whole ocean surface. An analytical function is then used to describe the variation of suspended particle concentration with depth.

The dispersion model is run for the period 1957-2000. Computed vertical profiles of radionuclides and distributions in the surface water are compared with measurements. Calculations have been repeated using both the annual and monthly mean flow and density fields. Although ^{137}Cs concentrations in the deeper layers were underestimated, model results are in generally good agreement with observations.

Other models to simulate the dispersion of radionuclides from fallout in the whole oceans have been described. Nakano and Povinec [102] developed a model to simulate dissolved ^{137}Cs dispersion in the world ocean. ^{137}Cs was introduced from both global fallout and local fallout at the Pacific Ocean. The 3D hydrodynamic model provides annually averaged velocity fields. Horizontal resolution is 225 km at the equator and 15 vertical levels are used. The dispersion model applies a particle tracking method with a time step equal to 10 days. However, time step was decreased when necessary to prevent tracking of particles over land or if a particle moves over more than two cell during

a single time step. Global fallout is simulated by 150000 particles initially distributed over the world according with latitude. Dispersion is calculated over 55 years, and particle positions are recorded every year. The local fallout component is calculated separately in the same way. In this case 55000 particles are initially distributed according with a normal distribution centered at Bikini site. Computed vertical profiles were compared with observations at 152 stations, mainly at the Atlantic and Pacific Oceans, between the 1960s and 1990s. Different combinations of horizontal and vertical diffusion coefficients were used until the best agreement between computations and measurements was obtained.

The same model was applied to simulate plutonium dispersion in the Pacific Ocean [103]. A scavenging model was added in this case. It includes transfers of plutonium between water and fine particles described by means of kinetic rates. These fine particles sink to the bottom with a constant settling velocity. The adsorption kinetic rate decreases exponentially with depth and the desorption rate is considered constant. Simultaneously, the model includes the transfer of plutonium to a fast sedimentation phase. These radionuclides are considered to reach the seabed instantaneously and are never redissolved. Contributions from global and local fallout are treated as in the previous work. Computed and measured vertical profiles are compared for 30 stations. Also, plutonium inventories in the water column and bed sediments are compared with observations. Relative contributions along the water column from global and local fallout are assessed as well.

A

Rhone River model: 3D equations

A.1 Hydrodynamic model

The full 3D hydrodynamic equations including the terms corresponding to density gradients can be written in the hydrostatic and Boussinesq approximations as [84]:

$$\frac{\partial \zeta}{\partial t} + \frac{\partial}{\partial x}\left[(h+\zeta)\int_{-h}^{\zeta} u \mathrm{d}z\right] + \frac{\partial}{\partial y}\left[(h+\zeta)\int_{-h}^{\zeta} v \mathrm{d}z\right] = 0 \tag{A.1}$$

$$\begin{aligned} &\frac{\partial u}{\partial t} + u\frac{\partial u}{\partial x} + v\frac{\partial u}{\partial y} - \Omega v + g\frac{\partial \zeta}{\partial x} + \frac{g}{\rho_0}\int_z^{\zeta} \frac{\partial \rho_w}{\partial x}\mathrm{d}z \\ &= \frac{\partial}{\partial z}\left(K\frac{\partial u}{\partial z}\right) + A\left(\frac{\partial^2 u}{\partial x^2} + \frac{\partial^2 u}{\partial y^2}\right) \end{aligned} \tag{A.2}$$

$$\begin{aligned} &\frac{\partial v}{\partial t} + u\frac{\partial v}{\partial x} + v\frac{\partial v}{\partial y} + \Omega u + g\frac{\partial \zeta}{\partial y} + \frac{g}{\rho_0}\int_z^{\zeta} \frac{\partial \rho_w}{\partial y}\mathrm{d}z \\ &= \frac{\partial}{\partial z}\left(K\frac{\partial v}{\partial z}\right) + A\left(\frac{\partial^2 v}{\partial x^2} + \frac{\partial^2 v}{\partial y^2}\right) \end{aligned} \tag{A.3}$$

where the z coordinate is measured upwards from the undisturbed sea level, h is mean water depth, ζ is the displacement of the sea surface from the undisturbed level, u and v are the two components of the water velocity along the x and y axis respectively, Ω is the Coriolis parameter, ρ_w is water density, ρ_0 is a reference density, and K and A are the vertical and horizontal eddy viscosities respectively.

The vertical component of the water velocity, w, is obtained from the continuity equation:

$$\frac{\partial u}{\partial x} + \frac{\partial v}{\partial y} + \frac{\partial w}{\partial z} = 0 \tag{A.4}$$

The water density is derived from a equation of state relating density to salinity [84]:

$$\rho_w = \rho_0(1 + \alpha S) \tag{A.5}$$

where S is salinity and $\alpha = 7.45 \times 10^{-4}$. As in [96], the effect of temperature on density is omitted for the sake of simplicity. Indeed, temperature differences between the Rhone River and the ambient seawater are small enough to consider that the bouyancy effects in the plume are represented only by the salinity gradients [96]. The reference density is taken as $\rho_0 = 998.9$ kg/m^3.

The salinity is determined from an advection-diffusion equation:

$$\frac{\partial S}{\partial t} + u\frac{\partial S}{\partial x} + v\frac{\partial S}{\partial y} + w\frac{\partial S}{\partial z} = A\left(\frac{\partial^2 S}{\partial x^2} + \frac{\partial^2 S}{\partial y^2}\right) + \frac{\partial}{\partial z}\left(K\frac{\partial S}{\partial z}\right) \tag{A.6}$$

Vertical eddy viscosity is determined from the 1-equation turbulence model described in [43]. This model has also been used in [176] to simulate a river plume. The equation for the turbulent kinetic energy E is:

$$\frac{\partial E}{\partial t} = K\left\{\left(\frac{\partial u}{\partial z}\right)^2 + \left(\frac{\partial v}{\partial z}\right)^2\right\} + \beta_0\frac{\partial}{\partial z}\left(K\frac{\partial E}{\partial z}\right) - \varepsilon + \frac{g}{\rho_0}K\frac{\partial \rho}{\partial z} \tag{A.7}$$

The first term in the right side of the equation represents generation of turbulence by the vertical shear, the second term is diffusion of turbulence and the last term is lost of turbulence by bouyancy (conversion of kinetic energy into potential energy). ε represents turbulence dissipation, that is written as:

$$\varepsilon = \frac{C_1 E^{\frac{3}{2}}}{\ell} \tag{A.8}$$

where ℓ is a mixing length and C_1 a numeric coefficient. The vertical viscosity is finally written as a function of energy as:

$$K = C_0 \ell E^{1/2} + \lambda_t \tag{A.9}$$

where C_0 is a numeric coefficient and λ_t is a background value of viscosity, that is the minimum possible value that it may have [150, 36]. The values given to the numeric constants appearing above are [43]: $\beta_0 = 0.73$, $C_0 = C^{1/4}$, $C_1 = C_0^3$ and $C = 0.046$. The background viscosity is fixed as $\lambda_t = 10^{-4}$ m^2/s, which is the same value used in [150]. Note that it has been implicitly assumed that the vertical diffusion coefficient is equal to vertical eddy viscosity.

The mixing length is derived from an algebraic expression [43]:

$$\ell = \frac{1}{1/\ell_1 + 1/\ell_2} \tag{A.10}$$

with

$$\ell_1 = \kappa(z + z_0 + h)e^{\beta_1 \frac{z+h}{h}} \tag{A.11}$$

$$\ell_2 = \kappa(z_s - z) \tag{A.12}$$

where $\kappa = 0.4$ is the von Karman's constant, $\beta_1 = -2.0$ and z_s and z_0 are the roughness lengths of the sea surface and bottom respectively. Nevertheless, other different parameterizations of vertical eddy viscosity may be used. A review on different approximations may be seen in [41, 42] (see also chapter 3).

Boundary conditions have also to be provided for sea surface elevation, currents, salinity and kinetic energy. At the sea surface and bottom there is no flux of salinity. At the surface, the internal stress is set equal to the external wind stress and at the bottom a quadratic friction law is applied. Thus, at the sea surface:

$$\rho_0 K \left(\frac{\partial u}{\partial z}\right)_{z=\zeta} = \tau_x^w \tag{A.13}$$

$$\rho_0 K \left(\frac{\partial v}{\partial z}\right)_{z=\zeta} = \tau_y^w \tag{A.14}$$

where τ_x^w and τ_y^w are the two components of the wind stress, deduced from equations 4.7 and 4.8. Similarly, at the sea bottom:

$$\rho_0 K \left(\frac{\partial u}{\partial z}\right)_{z=-h} = \tau_u \tag{A.15}$$

$$\rho_0 K \left(\frac{\partial v}{\partial z}\right)_{z=-h} = \tau_v \tag{A.16}$$

where bottom stresses are obtained, as commented above, from the quadratic friction law given by equation 4.4.

In the case of kinetic energy, the boundary condition at the sea surface is:

$$E_{z=\zeta} = \frac{\tau_w}{\rho_0 \sqrt{C_E}} \tag{A.17}$$

where τ_w is the wind stress (solved in τ_x^w and τ_y^w) and $C_E = 0.07$ [56]. If there is no wind, the flux of energy at the surface is set to zero. At the sea bottom, boundary condition is:

$$E_{z=-h} = \frac{\tau_b}{\rho_0 \sqrt{C_E}} \tag{A.18}$$

where τ_b is the bottom stress (solved in τ_u and τ_v) and $C_E = 0.07$ as in [56].

A no-flux condition is applied along land boundaries. A radiation condition in the form of Orlanski [111] is applied along open boundaries for the water velocity component that is normal to the boundary:

$$\frac{\partial \xi}{\partial t} + c\frac{\partial \xi}{\partial n} = 0 \tag{A.19}$$

where n is the direction normal to the boundary, $\xi = u, v$ is the water velocity component to which the condition is applied and c is the wave speed calculated as described in chapter 4. This condition has also been used in Marsaleix

et al. [96]. Surface elevations should be prescribed along open boundaries to propagate tides inside the computational domain. However tides can be neglected in the present model application and a radiation condition is also applied to determine water surface elevations along open boundaries.

Boundary conditions at the river mouth are:

$$S = 0 \tag{A.20}$$

that is the freshwater value and

$$q_l = \frac{Q}{ld} \tag{A.21}$$

where q_l is the water velocity in the direction of the outflow, Q is the river discharge and l and d are the width of the river mouth and the thickness of the outflow water layer respectively.

A.2 Suspended sediment model

Each particle class is represented by a concentration m_i. The equation for size i is:

$$\begin{aligned} &\frac{\partial m_i}{\partial t} + u\frac{\partial m_i}{\partial x} + v\frac{\partial m_i}{\partial y} + (w - w_{s,i})\frac{\partial m_i}{\partial z} \\ &= A\left(\frac{\partial^2 m_i}{\partial x^2} + \frac{\partial^2 m_i}{\partial y^2}\right) + \frac{\partial}{\partial z}\left(K\frac{\partial m_i}{\partial z}\right) \end{aligned} \tag{A.22}$$

where $w_{s,i}$ is the corresponding settling velocity for particle class i. The deposition and erosion terms are incorporated into the sea bed boundary condition of the equation. The deposition rate is:

$$DP_i = w_{s,i} m_i(b)\left(1 - \frac{\tau_b}{\tau_{cd}}\right) \tag{A.23}$$

where $m_i(b)$ is particle concentration of class i evaluated at the sea bottom and τ_{cd} is a critical deposition stress above which no deposition occurs since particles are maintained in suspension by water turbulence.

The settling velocity for each particle class is determined from Stokes's law:

$$w_{s,i} = \frac{\rho - \rho_w}{\rho_w}\frac{gD_i^2}{18\nu} \tag{A.24}$$

where ρ and D_i are suspended particle density and diameter respectively and ν is kinematic viscosity of water.

The erosion rate is written in terms of the erodability constant:

$$ER_i = Ef_i\left(\frac{\tau_b}{\tau_{ce}} - 1\right) \tag{A.25}$$

where E is the erodability constant, f_i gives the fraction of particles of class i in the bed sediment and τ_{ce} is a critical erosion stress below which no erosion occurs. The same values for E, τ_{cd} and τ_{ce} are used for the four particle classes. The model can also calculate sedimentation rates as the balance between the deposition and erosion terms.

Bed-load transport of coarse particles has not been included since most contaminants are essentially adsorbed on the fine particles. This is the case for radionuclides.

A.3 Radionuclide equations

The kinetic coefficient $k_{1,i}$ is written as (see chapter 6):

$$k_{1,i} = \chi_1(S_{m,i} + S_{s,i}) = k_{11,i} + k_{12,i} \tag{A.26}$$

where the exchange velocity χ_1 depends on water salinity as in equation 6.23. The kinetic coefficient k_2 is considered constant. Although a kinetic model involving 2 consecutive reversible reactions (2-step model) may be more appropriate than that consisting of a single (1-step) reversible reaction, specially for long (months) water-sediment contact times, given the time scale of simulations that are carried out (several days), it is not expected that significant differences between the 1-step and 2-step model appear. Thus a simpler 1-step model is used.

The equation that gives the time evolution of activity concentration in the dissolved phase, C_d, is:

$$\begin{aligned}
&\frac{\partial C_d}{\partial t} + u\frac{\partial C_d}{\partial x} + v\frac{\partial C_d}{\partial y} + w\frac{\partial C_d}{\partial z} \\
&= A\left(\frac{\partial^2 C_d}{\partial x^2} + \frac{\partial^2 C_d}{\partial y^2}\right) + \frac{\partial}{\partial z}\left(K\frac{\partial C_d}{\partial z}\right) \\
&- \sum_{i=1}^{N} k_{11,i} C_d + k_2 \sum_{i=1}^{N} m_i C_{s,i} \\
&+ \pi\left(k_2 \frac{L\rho_s\phi\sum_{i=1}^{N} f_i A_{s,i}}{\Upsilon} - \sum_{i=1}^{N} k_{12,i} C_d\right)
\end{aligned} \tag{A.27}$$

where $C_{s,i}$ and $A_{s,i}$ are, respectively, the concentration of radionuclides in suspended matter and bottom sediments of class i, and ρ_s is the sediment bulk density. $\pi = 0$ unless we are solving the equation for the water layer in contact with the sediment. In this case $\pi = 1$ to allow interactions between water and sediments. Υ is the thickness of the water layer above the bed sediments that interacts with them. For simplicity, it has been assumed that Υ is equal to the vertical grid size: $\Upsilon = \Delta z$.

The equation that gives the time evolution of activity concentration in each of the suspended matter classes is:

$$\begin{aligned}&\frac{\partial(m_i C_{s,i})}{\partial t} + u\frac{\partial(m_i C_{s,i})}{\partial x} + v\frac{\partial(m_i C_{s,i})}{\partial y} + (w - w_{s,i})\frac{\partial(m_i C_{s,i})}{\partial z}\\ &= A\left(\frac{\partial^2(m_i C_{s,i})}{\partial x^2} + \frac{\partial^2(m_i C_{s,i})}{\partial y^2}\right) + \frac{\partial}{\partial z}\left(K\frac{\partial(m_i C_{s,i})}{\partial z}\right)\\ &+ k_{11,i}C_d - k_2 m_i C_{s,i}\\ &+ \pi(-DPR_i + ERR_i)\end{aligned} \tag{A.28}$$

where $w_{s,i}$ is particle settling velocity, π has the same meaning as above and DPR_i is the deposition of radionuclides from the deepest water layer to the sediment evaluated according to:

$$DPR_i = \frac{w_{s,i} m_i(b) C_{s,i}(b)}{\Upsilon}\left(1 - \frac{\tau_b}{\tau_{cd}}\right) \tag{A.29}$$

Note that (b) means that the corresponding magnitude is evaluated at the deepest water layer. ERR_i is the resuspension of radionuclides due to sediment erosion:

$$ERR_i = \frac{E f_i A_{s,i}}{\Upsilon}\left(\frac{\tau_b}{\tau_{ce}} - 1\right) \tag{A.30}$$

In these equations E is the erodability constant, τ_b is bed stress and τ_{cd} and τ_{ce} are critical deposition and erosion stresses respectively, as described before. Of course, deposition of radionuclides is calculated only if $\tau_b < \tau_{cd}$ and resuspension only if $\tau_b > \tau_{ce}$. Activity concentration in the total suspended phase is calculated as:

$$C_s^{total} = \frac{\sum_{i=1}^{N} m_i C_{s,i}}{\sum_{i=1}^{N} m_i} \tag{A.31}$$

The equation for the temporal evolution of specific activity in each bed sediment particle class is:

$$\frac{\partial A_{s,i}}{\partial t} = k_{12,i}\frac{C_d \Upsilon}{L\rho_s f_i} - k_2 A_{s,i}\phi + DPR_i - ERR_i \tag{A.32}$$

where it is remembered that $\Upsilon = \Delta z$ and the deposition and erosion terms are calculated as:

$$DPR_i = \frac{w_{s,i} m_i(b) C_{s,i}(b)}{L\rho_s f_i}\left(1 - \frac{\tau_b}{\tau_{cd}}\right) \tag{A.33}$$

$$ERR_i = \frac{E A_{s,i}}{L\rho_s}\left(\frac{\tau_b}{\tau_{ce}} - 1\right) \tag{A.34}$$

Total activity concentration in bed sediments is calculated from activity concentrations in each particle class:

$$A_s^{total} = \sum_{i=1}^{N} f_i A_{s,i} \tag{A.35}$$

A.4 Numerical solution

All the equations are solved using explicit finite difference schemes. The scheme described in [60] is used to solve the hydrodynamic equations. For non-linear terms, scheme 2 described in such reference is used. It consists of calculating changes in components of the horizontal current due to advection alone and adding them to the changes caused by the other physical processes computed from the hydrodynamic equations without the advective terms. The MSOU second order scheme is used to solve the advection terms in all the dispersion equations. As was commented in chapter 6, a variable grid spacing is used in the vertical direction.

Density gradients are calculated using $\sigma_\theta = \rho_w - 1000$ instead of the density [84]. Also, the stability of the water column is checked each time step and over all the model domain. Mixing is carried out, using the algorithm described in [84], when it becomes unstable. The hydrodynamic calculations are started from rest and an uniform salinity of 38 g/L is assumed.

A.5 Normalized σ coordinates

The Rhone River plume model described above uses z coordinates in the vertical direction. This implies that the thickness of each layer is uniform over the whole model domain (although thickness is not necessarily the same for all layers, as was the case in the Rhone plume model). One problem of this coordinate system is the step like representation of the sea bed. Numerical noise may be generated near such steps. Also, the number of vertical levels must be reduced as water depth decreases. As a consequence, the model loses vertical resolution in the shallower areas of the domain.

To overcome these limitations, depth-following σ-coordinates are often used. Thus a constant number of layers is used in the vertical at each horizontal grid point and vertical resolution is not reduced in the shallower areas. The transformation to σ coordinates is (see for instance [37]):

$$\sigma = \frac{z + \zeta}{h + \zeta} \tag{A.36}$$

where h is the undisturbed depth of water, ζ is the sea surface displacement from the mean level due to tidal oscillations measured upwards from the undisturbed level and z coordinate is measured from the mean sea level to the bottom. Equations are thus transformed from the interval $-\zeta \leq z \leq h$ into the constant interval $0 \leq \sigma \leq 1$. A scheme comparing z and σ coordinates is shown in figure A.1.

The transformed barotropic hydrodynamic equations are [37]:

$$\frac{\partial \zeta}{\partial t} + \frac{\partial}{\partial x}\left[(h+\zeta)\int_0^1 u \mathrm{d}\sigma\right] + \frac{\partial}{\partial y}\left[(h+\zeta)\int_0^1 v \mathrm{d}\sigma\right] = 0 \tag{A.37}$$

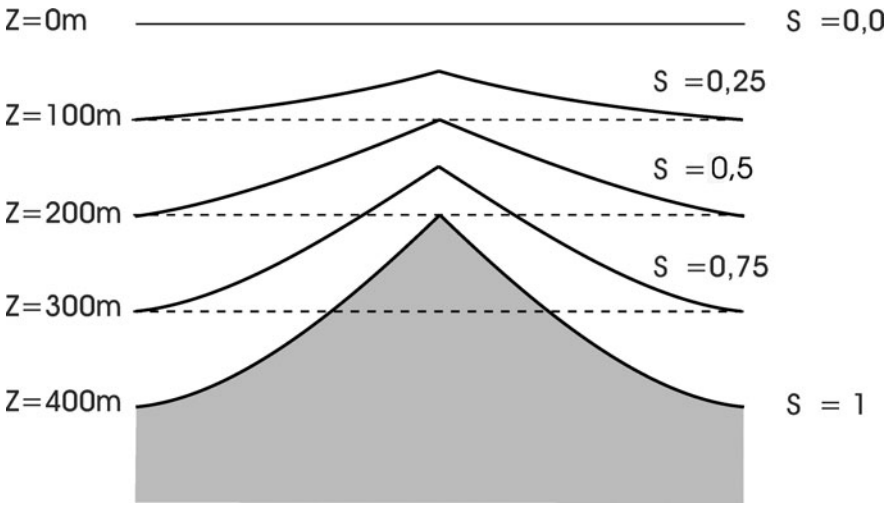

Fig. A.1. Scheme showing the depth-following σ coordinates

$$\frac{\partial u}{\partial t} + u\frac{\partial u}{\partial x} + v\frac{\partial u}{\partial y} + g\frac{\partial \zeta}{\partial x} - \Omega v = \frac{1}{(h+\zeta)^2}\frac{\partial}{\partial \sigma}\left(K\frac{\partial u}{\partial \sigma}\right) \tag{A.38}$$

$$\frac{\partial v}{\partial t} + u\frac{\partial v}{\partial x} + v\frac{\partial v}{\partial y} + g\frac{\partial \zeta}{\partial y} + \Omega u = \frac{1}{(h+\zeta)^2}\frac{\partial}{\partial \sigma}\left(K\frac{\partial v}{\partial \sigma}\right) \tag{A.39}$$

$$\begin{aligned} w^* = {} & \frac{1}{h+\zeta}\left[\frac{\partial \zeta}{\partial t}(1-\sigma)\right] + \frac{1}{h+\zeta}\frac{\partial}{\partial x}\left[(h+\zeta)\int_\sigma^1 u\mathrm{d}\sigma\right] \\ & + \frac{1}{h+\zeta}\frac{\partial}{\partial y}\left[(h+\zeta)\int_\sigma^1 v\mathrm{d}\sigma\right] \end{aligned} \tag{A.40}$$

where u, v and w^* are the components of the water velocity along the x, y and σ axis respectively. The horizontal friction terms are neglected. This form of the hydrodynamic equations has been used in the Irish Sea dispersion model described in [120, 121, 124, 126, 129].

The boundary conditions applied at the sea surface are written in σ coordinates in the following form:

$$\rho_w\left(K\frac{\partial u}{\partial \sigma}\right)_{\sigma=0} = -(h+\zeta)\tau_x^w \tag{A.41}$$

$$\rho_w\left(K\frac{\partial v}{\partial \sigma}\right)_{\sigma=0} = -(h+\zeta)\tau_y^w \tag{A.42}$$

where τ_x^w and τ_y^w denote the components of the wind stress acting on the sea surface along the x and y directions (see equations 4.7 and 4.8), and ρ_w is the water density. Similarly, at the sea bed:

$$\rho_w \left(K \frac{\partial u}{\partial \sigma} \right)_{\sigma=1} = -(h+\zeta)\tau_u \tag{A.43}$$

$$\rho_w \left(K \frac{\partial v}{\partial \sigma} \right)_{\sigma=1} = -(h+\zeta)\tau_v \tag{A.44}$$

where τ_u and τ_v are the two components of the bed stress, obtained for instance from a quadratic friction law as in equation 4.4.

One problem of σ coordinates is that levels are inclined in areas with steep bottom topography, as indeed can be appreciated in figure A.1. Any horizontal pressure gradient on these levels acquire a vertical component and thus a spurious circulation may result. Details on this problem, that is far from the scope of this book, may be seen, however, in [13, 160].

The equation for suspended sediment transport in σ coordinates is written in the following form:

$$\begin{aligned} &\frac{\partial m}{\partial t} + u\frac{\partial m}{\partial x} + v\frac{\partial m}{\partial y} + w^*\frac{\partial m}{\partial \sigma} \\ &= \frac{\partial}{\partial x}\left(K_h \frac{\partial m}{\partial x} \right) + \frac{\partial}{\partial y}\left(K_h \frac{\partial m}{\partial y} \right) + \frac{1}{(h+\zeta)^2}\frac{\partial}{\partial \sigma}\left(K_v \frac{\partial m}{\partial \sigma} \right) \\ &- \frac{1}{h+\zeta}\frac{\partial (w_s m)}{\partial \sigma} \end{aligned} \tag{A.45}$$

where m is the suspended matter concentration, K_h and K_v are the horizontal and vertical diffusion coefficients respectively and w_s is the settling velocity of suspended particles. Deposition and erosion of the sediment are incorporated into the sea bed boundary condition, as in the z coordinate model.

The advection/diffusion dispersion equation for a dissolved radionuclide, written in σ coordinates, is:

$$\begin{aligned} &\frac{\partial C_d}{\partial t} + u\frac{\partial C_d}{\partial x} + v\frac{\partial C_d}{\partial y} + w^*\frac{\partial C_d}{\partial \sigma} \\ &= \frac{\partial}{\partial x}\left(K_h \frac{\partial C_d}{\partial x} \right) + \frac{\partial}{\partial y}\left(K_h \frac{\partial C_d}{\partial y} \right) \\ &+ \frac{1}{(h+\zeta)^2}\frac{\partial}{\partial \sigma}\left(K_v \frac{\partial C_d}{\partial \sigma} \right) - \lambda C_d \end{aligned} \tag{A.46}$$

where C_d is the concentration of dissolved radionuclides and λ is the radioactive decay constant. The external source of radionuclides, where it exists, should be included to this equation. Exchanges of radionuclides between the liquid and solid phases may be described in terms of kinetic coefficients as presented in chapter 6 and in this appendix. Details may also be seen in the above mentioned references concerning the Irish Sea dispersion model.

Nevertheless, other different vertical coordinate systems may be used. A brief review is presented by Jones [78].

B

Examples of codes

These codes have been used to generate data required to draw some of the figures included in the book, and are shown as examples. All of them are written in FORTRAN.

B.1 Advection term using the upstream scheme (1D)

This code has been used to produce figure 3.2. It solves the 1D advection equation on a grid consisting of 100 cells with $\Delta x = 100$ m. Water velocity is constant and uniform ($u = 1.0$ m/s) and time step is set to $\Delta t = 10$ s. Initial concentrations are 1.0 for cells 1 to 14, being zero elsewhere. Thus, a vertical front is advected. The output consists of a file with two columns: the first is the grid cell number and the second is the computed concentration in each cell.

```
      dimension c(100),cn(100)
      data dx,dt/100.,10./
      u=1.0
      do 1,i=1,100
      cn(i)=0.0
      c(i)=1.0
      if (i.ge.15) c(i)=0.0
1     continue
      do 2,n=1,500
      do 3,i=2,99
      cn(i)=c(i)-dt*u*(c(i)-c(i-1))/dx
3     continue
      cn(1)=1.
      cn(100)=0.0
      do 4,i=1,100
      c(i)=cn(i)
```

```
4               continue
2               continue
                do 5,i=1,100
                write (1,*) i,c(i)
5               continue
                stop
                end
```

B.2 Advection term using the MSOU scheme (1D)

This code is exactly as the previous one, but the MSOU scheme is used to solve advection instead of the upstream scheme. It has been used to produce figure 3.3.

```
                dimension c(0:101),cn(0:101)
                data dx,dt/100.,10./
                u=1.0
                do 1,i=0,101
                cn(i)=0.0
                c(i)=1.0
                if (i.ge.15) c(i)=0.0
1               continue
                do 2,n=1,500
                do 3,i=2,99
                rnum=c(i+1)-c(i)
                den=c(i)-c(i-1)
                if (den.eq.0.0) then
                ri=10.
                else
                ri=rnum/den
                end if
                p=max(0,min(2.*ri,1.),min(ri,2.))
                ad1=c(i)+.5*(c(i)-c(i-1))*p
                rnum=c(i)-c(i-1)
                den=c(i-1)-c(i-2)
                if (den.eq.0.0) then
                ri=10.
                else
                ri=rnum/den
                end if
                p=max(0,min(2.*ri,1.),min(ri,2.))
                ad2=c(i-1)+.5*(c(i-1)-c(i-2))*p
                cn(i)=c(i)-dt*u*(ad1-ad2)/dx
```

```
3       continue
        cn(1)=1.
        cn(100)=0.0
        do 4,i=1,100
        c(i)=cn(i)
4       continue
2       continue
        do 5,i=1,100
        write (1,*) i,c(i)
5       continue
        stop
        end
```

B.3 Diffusion equation (1D)

This code, used to produce figure 3.4, solves a 1D diffusion problem in the same grid described before. The diffusion coefficient is constant and equal to 10 m^2/s. Initial concentrations are zero over all the grid except in cell 25. Concentrations over the grid are extracted 0.5 and 1.0 hours after the beginning of the diffusion process. The output consists of three files: concentration fields at $t = 0$, $t = 0.5$ and $t = 1.0$ hours.

```
        dimension c(100),cn(100)
        data dx,dt/100.,10./
        dh=10.
        do 1,i=1,100
        cn(i)=0.0
        c(i)=0.0
        if (i.eq.25) c(i)=1.0
1       continue
        iunit=1
        do 2,n=1,500
        do 3,i=2,99
        cn(i)=c(i)+dt*dh*(c(i+1)+c(i-1)-2.*c(i))/(dx*dx)
3       continue
        cn(1)=0.0
        cn(100)=0.0
        do 4,i=1,100
        c(i)=cn(i)
4       continue
        if (n.eq.180.or.n.eq.360) then
        iunit=iunit+1
        do 5,i=1,100
```

```
              write (iunit,*) i,c(i)
5             continue
              end if
2             continue
              stop
              end
```

B.4 Upstream scheme for a 2D problem

The 2D advection equation for a constant water depth is solved with this code, used to produce figure 5.2a. The grid consists of 75×50 cells with $\Delta x = \Delta y = 5000$ m and time step equal to 180 s. Water depth is 5 m and velocity components are considered constants(u=0.5 and v=0.15 m/s). However, as the code is written, is valid for non constant velocities of arbitrary directions. The output consists of a file with 3 columns: x and y coordinates of each cell and concentration in each cell. Initial concentrations are zero over all the grid except in cell $(5, 10)$. The equation is integrated for 100 hours.

It can be noted that the advection term is treated as a function denoted `adv`. This is very useful if several quantities are to be advected simultaneously, since the code lines have not to be written for each one.

```
              dimension u(75,50),v(75,50)
              dimension cd(0:76,0:51),cdn(0:76,0:51),d(75,50)
              data dx,dy,dt/5000.,5000.,180./
              do 1,i=1,75
              do 1,j=1,50
              u(i,j)=.5
              v(i,j)=.15
              d(i,j)=5.
1             continue
              do 60,i=0,76
              do 60,j=0,51
              cd(i,j)=0.0
              cdn(i,j)=0.0
60            continue
              cd(5,10)=1.e5
              t=-dt
c             TIME INTEGRATION
              do 10,n=1,2000
              t=t+dt
              do 20,i=2,74
              do 20,j=2,49
              if (d(i,j).eq.0.0) goto 20
```

```
      cdn(i,j)=cd(i,j)+dt*adv(cd,u,v,d,i,j)
20    continue
      do 36,i=1,75
      cdn(i,1)=cdn(i,2)
      cdn(i,50)=cdn(i,49)
36    continue
      do 37,j=1,50
      cdn(1,j)=cdn(2,j)
      cdn(75,j)=cdn(74,j)
37    continue
      do 40,i=1,75
      do 40,j=1,50
      cd(i,j)=cdn(i,j)
40    continue
10    continue
      do 100, i=1,75
      do 101, j=1,50
      write (21,*) i,j,cd(i,j)
101   continue
      write (21,*)
100   continue
      stop
      end
c     ADVECTION FUNCTION
      function adv(c,u,v,d,i,j)
      dimension u(75,50),v(75,50),d(75,50),c(0:76,0:51)
      data dx,dy/5000.,5000./
      d1=.5*(d(i,j)+d(i+1,j))
      d2=.5*(d(i,j)+d(i-1,j))
      d3=.5*(d(i,j)+d(i,j-1))
      d4=.5*(d(i,j)+d(i,j+1))
      n1=1
      n2=1
      n3=1
      n4=1
      if (u(i,j).lt.0.0) n1=0
      if (u(i-1,j).lt.0.0) n2=0
      if (v(i,j-1).lt.0.0) n3=0
      if (v(i,j).lt.0.0) n4=0
      adv1=(-n1*u(i,j)*c(i,j)-(1-n1)*u(i,j)*c(i+1,j))*d1*dy
      adv2=(n2*u(i-1,j)*c(i-1,j)+(1-n2)*u(i-1,j)*c(i,j))*d2*dy
      adv4=(-n4*v(i,j)*c(i,j)-(1-n4)*v(i,j)*c(i,j+1))*d4*dx
      adv3=(n3*v(i,j-1)*c(i,j-1)+(1-n3)*v(i,j-1)*c(i,j))*d3*dx
      adv=(adv1+adv2+adv3+adv4)/(dx*dy*d(i,j))
      return
```

```
      end
```

B.5 MSOU scheme for a 2D problem

The same advection problem described above is now solved using the MSOU scheme (figure 5.2b). It can be seen that this numerical scheme requires a considerably higher computational effort than the upstream scheme.

```
      dimension u(75,50),v(75,50)
      dimension cd(0:76,0:51),cdn(0:76,0:51),d(75,50)
      data dx,dy,dt/5000.,5000.,180./
      do 1,i=1,75
      do 1,j=1,50
      u(i,j)=.5
      v(i,j)=.15
      d(i,j)=5.
1     continue
      do 60,i=0,76
      do 60,j=0,51
      cd(i,j)=0.01
      cdn(i,j)=0.0
60    continue
      cd(5,10)=1.e5
      t=-dt
c     TIME INTEGRATION
      do 10,n=1,2000
      t=t+dt
      do 20,i=2,74
      do 20,j=2,49
      if (d(i,j).eq.0.0) goto 20
      cdn(i,j)=cd(i,j)+dt*adv(cd,u,v,d,i,j)
20    continue
      do 36,i=1,75
      cdn(i,1)=cdn(i,2)
      cdn(i,50)=cdn(i,49)
36    continue
      do 37,j=1,50
      cdn(1,j)=cdn(2,j)
      cdn(75,j)=cdn(74,j)
37    continue
      do 40,i=1,75
      do 40,j=1,50
      cd(i,j)=cdn(i,j)
```

```
40          continue
10          continue
            do 100, i=1,75
            do 101, j=1,50
            write (20,*) i,j,cd(i,j)
101         continue
            write (20,*)
100         continue
            stop
            end
c           ADVECTIVE FUNCTION
            function adv(c,u,v,d,i,j)
            dimension u(75,50),v(75,50),d(75,50),c(0:76,0:51)
            data dx,dy/5000.,5000./
            d1=.5*(d(i,j)+d(i+1,j))
            d2=.5*(d(i,j)+d(i-1,j))
            d3=.5*(d(i,j)+d(i,j-1))
            d4=.5*(d(i,j)+d(i,j+1))
            n1=1
            n2=1
            n3=1
            n4=1
            if (u(i,j).lt.0.0) n1=0
            if (u(i-1,j).lt.0.0) n2=0
            if (v(i,j-1).lt.0.0) n3=0
            if (v(i,j).lt.0.0) n4=0
            r1=10.
            if (c(i,j).ne.c(i-1,j)) r1=(c(i+1,j)-c(i,j))
            1 /(c(i,j)-c(i-1,j))
            p1=max(0.,min(2.*r1,1.),min(r1,2.))
            f1=c(i,j)+.5*p1*(c(i,j)-c(i-1,j))
            if (c(i-1,j).eq.0.0) f1=c(i,j)
            r2=10.
            if(c(i+1,j).ne.c(i,j))r2=(c(i+2,j)-c(i+1,j))/(c(i+1,j)-c(i,j))
            p2=max(0.,min(2.*r2,1.),min(r2,2.))
            f2=c(i+1,j)-.5*p2*(c(i+1,j)-c(i,j))
            if (c(i+2,j).eq.0.0) f2=c(i+1,j)
            adv1=(-n1*u(i,j)*f1-(1-n1)*u(i,j)*f2)*d1*dy
            r2=10.
            if (c(i-1,j).ne.c(i-2,j)) r2=(c(i,j)-c(i-1,j))
            1 /(c(i-1,j)-c(i-2,j))
            p2=max(0.,min(2.*r2,1.),min(r2,2.))
            f2=c(i-1,j)+.5*p2*(c(i-1,j)-c(i-2,j))
            if (c(i-2,j).eq.0.0) f2=c(i-1,j)
            r1=10.
```

```
if(c(i,j).ne.c(i-1,j))r1=(c(i+1,j)-c(i,j))/(c(i,j)-c(i-1,j))
p1=max(0.,min(2.*r1,1.),min(r1,2.))
f1=c(i,j)-.5*p1*(c(i,j)-c(i-1,j))
if (c(i+1,j).eq.0.0) f1=c(i,j)
adv2=(n2*u(i-1,j)*f2+(1-n2)*u(i-1,j)*f1)*d2*dy
r1=10.
if (c(i,j).ne.c(i,j-1)) r1=(c(i,j+1)-c(i,j))
1 /(c(i,j)-c(i,j-1))
p1=max(0.,min(2.*r1,1.),min(r1,2.))
f1=c(i,j)+.5*p1*(c(i,j)-c(i,j-1))
if (c(i,j-1).eq.0.0) f1=c(i,j)
r2=10.
if(c(i,j+1).ne.c(i,j))r2=(c(i,j+2)-c(i,j+1))/(c(i,j+1)-c(i,j))
p2=max(0.,min(2.*r2,1.),min(r2,2.))
f2=c(i,j+1)-.5*p2*(c(i,j+1)-c(i,j))
if (c(i,j+2).eq.0.0) f2=c(i,j+1)
adv4=(-n4*v(i,j)*f1-(1-n4)*v(i,j)*f2)*d4*dx
r2=10.
if (c(i,j-1).ne.c(i,j-2)) r2=(c(i,j)-c(i,j-1))
1 /(c(i,j-1)-c(i,j-2))
p2=max(0.,min(2.*r2,1.),min(r2,2.))
f2=c(i,j-1)+.5*p2*(c(i,j-1)-c(i,j-2))
if (c(i,j-2).eq.0.0) f2=c(i,j-1)
r1=10.
if(c(i,j).ne.c(i,j-1))r1=(c(i,j+1)-c(i,j))/(c(i,j)-c(i,j-1))
p1=max(0.,min(2.*r1,1.),min(r1,2.))
f1=c(i,j)-.5*p1*(c(i,j)-c(i,j-1))
if (c(i,j+1).eq.0.0) f1=c(i,j)
adv3=(n3*v(i,j-1)*f2+(1-n3)*v(i,j-1)*f1)*d3*dx
adv=(adv1+adv2+adv3+adv4)/(dx*dy*d(i,j))
return
end
```

B.6 Kinetic exchanges water-sediment

The following code is the finite difference solution of the water-sediment interaction scheme described by figure 6.4, which consists of a single reversible reaction. It has been used to produce figure 6.5. A unit concentration is initially assumed in water (cd=1) and zero concentration in the sediment (as=0). Time step is 60 s and equations are integrated for 4 days. Output consists of a file with 3 columns: time in hours, concentration in water and concentration in the sediment.

```
real k1,k2
```

```
      data k1,k2/1.5e-5,2.e-7/
      data dt/60./
      cd=1.0
      cdn=0.0
      as=0.0
      asn=0.0
      t=-dt
      do 1,n=1,5760
      t=t+dt
      cdn=cd+dt*(-k1*cd+k2*as)
      asn=as+dt*(k1*cd-k2*as)
      cd=cdn
      as=asn
      if ((t/300.).eq.int(t/300.)) write (20,*) t/3600.,cd,as
1     continue
      stop
      end
```

B.7 Stochastic method for the radioactive equation

The code solves the radioactive decay equation using the stochastic method described in chapter 7. Time step is fixed as 100 s and 300 particles are used in the simulation. The radioactive decay constant is set to 8.0×10^{-6} s^{-1}, which corresponds to a half-life equal to one day. Initially, a label equal to 1 is assigned to each particle. If a given particle decays, then the label is changed to zero. The number of particles with label 1 (have not decayed) is counted each time step. The equation is solved for 4 days and output consists of a file with two columns: time in hours and remaining particles at each time. The function used to generate random numbers, which is standard, can also be seen. This code has been used to generate figure 7.1.

```
      dimension label(1000)
      data iseed/13/
      np=300
      decay=8.e-6
      dt=100
      t=-dt
      do 3,n=1,np
      label(n)=1
3     continue
      do 1,nt=1,864*4
      t=t+dt
      do 2,n=1,np
```

```
            if (label(n).eq.0) goto 2
            p=1.-exp(-decay*dt)
            if (ran(iseed).lt.p) label(n)=0
2           continue
            cont=0.0
            do 4,n=1,np
            if (label(n).eq.1) cont=cont+1.
4           continue
            write (1,*) t/3600.,cont
1           continue
            stop
            end
c           RANDOM NUMBER GENERATOR
            function ran(idum)
            integer*4 m,ia,ic,idum,ir(97),iy,j
            parameter (m=714025,ia=1366,ic=150889,
                  rm=1.4005112e-6)
            data iff/0.0/
            if (idum.lt.0.or.iff.eq.0) then
            iff=1
            idum=mod(ic-idum,m)
            do 11,j=1,97
            idum=mod(ia*idum+ic,m)
            ir(j)=idum
11          continue
            idum=mod(ia*idum+ic,m)
            iy=idum
            end if
            j=1+97*iy/m
            if (j.gt.97.or.j.lt.1) pause
            iy=ir(j)
            ran=iy*rm
            idum=mod(ia*idum+ic,m)
            ir(j)=idum
            return
            end
```

B.8 Hydrodynamic model of the Strait of Gibraltar

This code solves the 2D depth averaged hydrodynamic equations for the M_2 tidal constituent in the Strait of Gibraltar. Tidal analysis is carried out. Thus, the output of the code consists of two files that contain tidal constants (amplitudes and phases) for this tide. The numerical filter described in [84] is also

used to smooth the solution, although in this application a very acceptable solution is obtained without it (variable `filtro` is set to zero). Horizontal and temporal resolution are 2500 m and 5 s respectively. Equations are integrated for 6 tidal cycles, time enough to obtain a stable periodic solution. Tidal analysis is carried out in the last cycle.

Model output is used by the GISPART model to simulate the dispersion of contaminants in the Strait.

```
      dimension zs(0:22,20),u(0:22,20),v(0:22,20)
      dimension un(0:22,20),vn(0:22,20),d(0:22,20)
      dimension def(22),def2(22)
      dimension ut(0:22,20),vt(0:22,20)
      dimension ys(22,20,3),yc(22,20,3),amp(22,20,3)
      dimension fase(22,20,3)
      real h1(0:23,20),h1n(0:23,20)
      real h1o(0:23,20)
      real num
      data pi/3.141592654/
      data dx,dy,dt/2500.,2500.,5./
      data rho/1027./
      data dh,f,w/10.0,8.55e-5,1.405e-4/
      data c1/0.05/
      t=-dt
      filtro=0.0
      open (1,file="depth",status="old")
      read (1,*) ((d(i,j),i=1,22),j=1,20)
      close (1)
      do 1,i=0,22
      do 1,j=1,20
      zs(i,j)=0.0
      if (d(i,j).gt.0.0) then
      h1(i,j)=d(i,j)
      else
      h1(i,j)=0.0
      end if
1     continue
      do 6,i=0,22
      do 6,j=1,20
      h1o(i,j)=h1(i,j)
      u(i,j)=0.0
      v(i,j)=0.0
      un(i,j)=0.0
      vn(i,j)=0.0
      h1n(i,j)=0.0
6     continue
```

```
      do 20,j=3,19
      def(j)=pi*(-.8125*(j-3.)+67.)/180.
20    continue
      do 212,j=8,16
      def2(j)=pi*(-.2*(j-8.)+50.)/180.
212   continue
      do 10,nci=1,6
      do 10,n=1,8944
      t=t+dt
      do 2,j=2,19
      h1n(1,j)=h1o(1,j)+.785*cos(w*t-def(j))
2     continue
      do 202, j=8,16
      h1n(22,j)=h1o(22,j)+.25*cos(w*t-def2(j))
202   continue
c     CONTINUITY EQUATION
      do 3,i=2,21
      do 3,j=2,19
      if (d(i,j).eq.0.0) goto 3
      der1=(u(i,j)-u(i-1,j))/dx
      der2=(v(i,j+1)-v(i,j))/dy
      h1n(i,j)=h1(i,j)-dt*(der1+der2)
3     continue
      do 4,i=1,22
      do 4,j=1,20
      if (d(i,j).eq.0.0) goto 4
      zs(i,j)=h1n(i,j)-h1o(i,j)
4     continue
c     U EQUATION
      do 5,i=1,21
      do 5,j=2,19
      if (d(i,j).eq.0.0) goto 5
      if (d(i+1,j).eq.0.0) goto 5
      rnonli=0.0
      if (i.ge.2.and.i.le.20) then
      s1=u(i,j)*(u(i+1,j)-u(i-1,j))/(2.*dx)
      s2=.5*(v(i,j+1)+v(i+1,j+1))*u(i,j+1)
      s3=.5*(v(i,j)+v(i+1,j))*u(i,j-1)
      rnonli=(s1+(s2-s3)/(2.*dy))/(.5*
           (h1n(i,j)+h1n(i+1,j)))
      end if
      gra=9.8*.5*(h1n(i,j)+h1n(i+1,j))*(zs(i+1,j)-
           zs(i,j))/dx
      vp=.25*(v(i,j)+v(i+1,j)+v(i+1,j+1)+v(i,j+1))
      q=sqrt(u(i,j)**2.+vp*vp)
```

```
      fri=c1*q/h1n(i,j)**2.
      cor=f*vp
      hor=0.0
      if (i.gt.1.and.i.lt.22) then
      hor=dh*(u(i+1,j)+u(i-1,j)-2.*u(i,j))/(dx*dx)+
          dh*(u(i,j+1)+u(i,j-1)-2.*u(i,j))/(dy*dy)
      end if
      ut(i,j)=(u(i,j)/dt-gra+cor+hor-rnonli)/(1./dt+fri)
5     continue
c     ORLANSKI BOUNDARY CONDITION
      do 11,j=2,19
      if (d(1,j).eq.0.0) goto 110
      den=-u(1,j)+u(2,j)
      num=ut(1,j)-u(1,j)
      cp=-num/den
      if (cp.lt.(-1.)) cp=-1.0
      if (den.eq.0.0.and.num.lt.0.0) cp=-1.0
      if (den.eq.0.0.and.num.gt.0.0) cp=0.0
      if (cp.gt.0.0) cp=0.0
      ut(0,j)=(1.+cp)*u(0,j)-cp*u(1,j)
110   continue
      if (d(22,j).eq.0.0) goto 11
      den=u(21,j)-u(20,j)
      num=ut(21,j)-u(21,j)
      cp=-num/den
      if (cp.gt.1.0) cp=1.0
      if (cp.lt.0.0) cp=0.0
      if (den.eq.0.0.and.num.gt.0.0) cp=1.0
      if (den.eq.0.0.and.num.lt.0.0) cp=0.0
      ut(22,j)=(1.-cp)*u(22,j)+cp*u(21,j)
11    continue
c     FILTER
      do 15,j=1,20
      un(0,j)=ut(0,j)
      un(22,j)=ut(22,j)
      do 15,i=1,21
      if (ut(i,j).eq.0.0) goto 15
      un(i,j)=ut(i,j)+.5*filtro*(ut(i-1,j)+
          ut(i+1,j)-2.*ut(i,j))
15    continue
c     V EQUATION
      do 7,i=1,22
      do 7,j=2,19
      if (d(i,j).eq.0.0) goto 7
      if (d(i,j-1).eq.0.0) goto 7
```

```
      rnonli=0.0
      if (i.ge.2.and.i.le.20) then
      s1=v(i,j)*(v(i,j+1)-v(i,j-1))/(2.*dy)
      s2=.5*(u(i,j)+u(i,j-1))*v(i+1,j)
      s3=.5*(u(i-1,j)+u(i-1,j-1))*v(i-1,j)
      rnonli=(s1+(s2-s3)/(2.*dx))/(.5*
     +       (h1n(i,j)+h1n(i,j+1)))
      end if
      gra=9.8*.5*(h1n(i,j)+h1n(i,j-1))*(zs(i,j)-
     +       zs(i,j-1))/dy
      up=.25*(un(i,j)+un(i-1,j)+un(i-1,j-1)+
     +       un(i,j-1))
      cor=-f*up
      q=sqrt(up*up+v(i,j)**2.)
      fri=c1*q/h1n(i,j)**2.
      hor=0.0
      if (i.gt.1.and.i.lt.22) then
      hor=dh*(v(i+1,j)+v(i-1,j)-2.*v(i,j))/(dx*dx)+
      dh*(v(i,j+1)+v(i,j-1)-2.*v(i,j))/(dy*dy)
      end if
      vt(i,j)=(v(i,j)/dt-gra+cor+hor-rnonli)/(1./dt+fri)
7     continue
c     FILTER
      do 16,j=2,19
      do 16,i=1,22
      if (vt(i,j).eq.0.0) goto 16
      vn(i,j)=vt(i,j)+.5*filtro*(vt(i,j-1)+
     +       vt(i,j+1)-2.*vt(i,j))
16    continue
      do 9,i=0,22
      do 9,j=1,20
      h1(i,j)=h1n(i,j)
      u(i,j)=un(i,j)
      v(i,j)=vn(i,j)
9     continue
c     TIDAL ANALYSIS
      if (nci.eq.6.and.int(t/600.).eq.(t/600.)) then
      ss=sin(w*t)
      cc=cos(w*t)
      seno2=seno2+ss*ss
      cose2=cose2+cc*cc
      cs=cs+cc*ss
      do 25,i=1,22
      do 25,j=1,20
      if (d(i,j).lt.0.2) goto 25
```

```
            ys(i,j,1)=ys(i,j,1)+zs(i,j)*ss
            yc(i,j,1)=yc(i,j,1)+zs(i,j)*cc
            ume=.5*(u(i,j)+u(i-1,j))/h1(i,j)
            vme=.5*(v(i,j)+v(i,j+1))/h1(i,j)
            ys(i,j,2)=ys(i,j,2)+ume*ss
            yc(i,j,2)=yc(i,j,2)+ume*cc
            ys(i,j,3)=ys(i,j,3)+vme*ss
            yc(i,j,3)=yc(i,j,3)+vme*cc
25          continue
            end if
10          continue
c           TIDAL ANALYSIS RESULTS
            det=cs*cs-seno2*cose2
            if (abs(det).lt.1.E-20) then
            write (6,*) "Not possible"
            goto 66
            end if
            do 26, i=1,22
            do 26,j=1,20
            if (d(i,j).lt.0.2) goto 26
            do 27, n=1,3
            ak=(ys(i,j,n)*cs-yc(i,j,n)*seno2)/det
            bk=(yc(i,j,n)*cs-ys(i,j,n)*cose2)/det
            amp(i,j,n)=sqrt(ak*ak+bk*bk)
            fase(i,j,n)=0.0
            if (ak.ne.0.0) fase(i,j,n)=atan2(bk,ak)*180./pi
            if (fase(i,j,n).lt.0.0) fase(i,j,n)=fase(i,j,n)+360.
27          continue
26          continue
            open (unit=10,file="h.dat",status="new")
            open (unit=11,file="g.dat",status="new")
            do 30,n=1,3
            do 30,i=1,22
            write (10,250) (amp(i,j,n),j=1,20)
            write (11,300) (fase(i,j,n),j=1,20)
30          continue
250         format (1x,20f6.3)
300         format (1x,20f6.1)
66          continue
            end
```

C

Disk contents

The disk includes:

- Codes listed on appendix B:
  - B1: upstream.f
  - B2: msou.f
  - B3: diffusion.f
  - B4: upstream2d.f
  - B5: msou2d.f
  - B6: exchanges.f
  - B7: decay.f
  - B8: barotropic-m2.f
- GISPART model: software plus required data files and instructions for installation and running.

References

1. Abril J.M. (1998). Basic microscopic theory of the distribution, transfer and uptake kinetics of dissolved radionuclides by suspended particulate matter. Part 1: theory development. Journal of Environmental Radioactivity, 41, pp 307-324
2. Abril J.M. and García-León M. (1993). A 2D 4-phases marine dispersion model for non conservative radionuclides. Part 1: conceptual and computational model. Journal of Environmental Radioactivity, 20, pp 71-88
3. Abril J.M. and García-León M. (1993). A 2D 4 phases marine dispersion model for radionuclides. Part 2: two application cases, ^{137}Cs and ^{239,240}Pu dispersion in the Irish Sea. Journal of Environmental Radioactivity, 20, pp 89-115
4. Abril J.M. and García-León M. (1994). Modelling the distribution of suspended matter and the sedimentation process in a marine environment. Ecological Modelling, 71, pp 197-219
5. Abril J.M. and Fraga E. (1996). Some physical and chemical features of the variability of k_d distribution coefficients of radionuclides. Journal of Environmental Radioactivity, 30, pp 253-270
6. Abril J.M. and Abdel-Aal M.M. (2000). Marine radioactivity studies in the Suez Canal. A modelling study on radionuclide dispersion. Journal of Environmental Radioactivity, 48, pp 279-302
7. Abril J.M. and Abdel-Aal M.M. (2000). Marine radioactivity studies in the Suez Canal. Part I: hydrodynamics and transit times. Estuarine, Coastal and Shelf Science, 50, 489-502
8. Abril J.M. abd Abdel-Aal M.M. (2000). A modelling study on hydrodynamics and pollutant dispersion in the Suez Canal. Ecological Modelling, 128, pp 1-17
9. Abril J.M., Abdel-Aal M.M., Al-Gamal S.A., Abdel-Hay F.A. and Zahar H.M. (2000). Marine radioactivity studies in the Suez Canal, part II: field experiments and a modelling studies of dispersion. Estuarine, Coastal and Shelf Science, 50, pp 503-514
10. Absi A., Villa M., Moreno H.P., Manjón G. and Periáñez R. (2004). Self-cleaning in an estuarine area formerly affected by ^{226}Ra anthropogenic discharges. Science of the Total Environment, 329, pp 183-195
11. Aldridge J.N. (1998). CSERAM: a model for prediction of marine radionuclide transport in both particulate and dissolved phases. Radiation Protection Dosimetry, 75, pp 99-103

12. Aldridge J.N., Kershaw P., Brown J., McCubbin D., Leonard K.S. and Young E.F. (2003). Transport of plutonium ($^{239/240}$Pu) and caesium (^{137}Cs) in the Irish Sea: comparison between observations and results from sediment and contaminant transport modelling. Continental Shelf Research, 23, pp 869-899
13. Auclair F., Marsaleix P. and Estournel C. (2000). Sigma coordinate pressure gradient errors: evaluation and reduction by an inverse method. Journal of Atmospheric and Oceanic Technology, 17, pp 1348-1367
14. Backhaus J.O. (1985). A three dimensional model for the simulation of shelf sea dynamics. German Journal of Hydrography, 38, pp 165-187
15. Baxter M.S., Harms I., Osvath I., Povinec P.P. and Scott E.M. (1998). Modelling the potential radiological consequences of radioactive waste dumping in the Kara Sea. Journal of Environmental Radioactivity, 39, pp 161-182
16. Bay Y., Wang Z. and Shen H. (2003). Three dimensional modelling of sediment transport and the effects of dredging in the Hayhe Estuary. Estuarine, Coastal and Shelf Science, 56, pp 175-186
17. Benes P. and Cernik M. (1992). Kinetics of radionuclide interaction with suspended solids in modelling the migration of radionuclides in rivers. Effect of the concentration of solids and temperature. Journal of Radioanalytical Nuclear Chemistry, 159, pp 187-200
18. Benes P., Cernik M. and Lam-Ramos P. (1992). Factors affecting interaction of radiocesium with freshwater solids. Contact time, concentration of solids and temperature. Journal of Radioanalytical Nuclear Chemistry, 159, pp 201-218
19. Benes P., Picat P., Cernik M. and Quinault, J.M. (1992). Kinetics of radionuclide interaction with suspended solids in modelling the migration of radionuclides in rivers. 1: parameters for two-step kinetics. Journal of Radioanalytical Nuclear Chemistry, 159, pp 175-186
20. Bolin B. and Rodhe H. (1973). A note on the concepts of age distribution and transit time in natural reservoirs. Tellus, 25, pp 58-63
21. Børretzen P. and Salbu B. (2000). Estimation of apparent rate coefficients for radionuclides interacting with marine sediments from Novaya Zemlya. The Science of the Total Environment, 262, pp 91-102
22. Børretzen P. and Salbu B. (2002). Fixation of Cs to marine sediments estimated by a stochastic modelling approach. Journal of Environmental Radioactivity, 61, pp 1-20
23. Breshears D.D., Kirchner T.B. and Whicker F.W. (1992). Contaminant transport through agroecosystems: assessing relative importance of environmental, physiological, and management factors. Ecological Applications, 2, pp 285-297
24. Breton M. and Salomon J.C. (1995). A 2D long term advection dispersion model for the Channel and southern North Sea. Part A: validation through comparisons with artificial radionuclides. Journal of Marine Systems, 6, pp 495-513
25. Calmet D. and Fernandez J.M. (1990). Caesium distribution in northwest Mediterranean seawater, suspended particles and sediments. Continental Shelf Research, 10, pp 895-913
26. Cancino L. and Neves R. (1999). Hydrodynamic and sediment suspension modelling in estuarine systems. Part I: description of the numerical models. Journal of Marine Systems, 22, pp 105-116
27. Carroll J., Boisson F., Fowler S.W. and Teyssie J.L. (1997). Radionuclide adsorption to sediments from nuclear waste dumping sites in the Kara Sea. Marine Pollution Bulletin, 35, pp 296-304

28. Carroll J. and Harms I.H. (1999). Uncertainty analysis of partition coefficients in a radionuclide transport model. Water Research, 33, pp 2617-2626
29. Cetina M., Rajar R. and Povinec P. (2000). Modelling of circulation and dispersion of radioactive pollutants in the Japan Sea. Oceanologica Acta, 23, pp 819-836
30. Charmasson S. (2003). ^{137}Cs inventory in sediment near the Rhone mouth: role played by different sources. Oceanologica Acta, 26, pp 435-441
31. Chen X. (2004). Modeling hydrodynamics and salt transport in the Alafia River estuary, Florida, during May 1999-December 2001. Esturine, Coastal and Shelf Science, 61, pp 477-490
32. Ciffroy P., Garnier J.M. and Pham M.K. (2001). Kinetics of the adsorption and desorption of radionuclides of Co, Mn, Cs, Fe, Ag and Cd in freshwater systems: experimental and modelling approaches. Journal of Environmental Radioactivity, 55, pp 71-91
33. Clarke S. (1995). Advective/diffusive processes in the Firth of Forth. PhD Thesis, University of Wales, Bangor
34. Clarke S. and Elliott A.J. (1998). Modelling suspended sediment concentrations in the Firth of Forth. Estuarine, Coastal and Shelf Science, 47, pp 235-250
35. Cheng H.P., Yeh G.T. and Cheng J.R. (2000). A numerical model simulating reactive transport in shallow water domains: model development and demonstrative applications. Advances in Environmental Research, 4, pp 187-209
36. Cugier P. and Le Hir P. (2002). Development of a 3D hydrodynamic model for coastal ecosystem modelling. Application to the plume of the Seine River. Estuarine, Coastal and Shelf Science, 55, pp 673-695
37. Davies A.M. (1985). A three dimensional modal model of wind induced flow in a sea region. Progress in Oceanography, 15, pp 71-128
38. Davies A.M. and Gerritsen H. (1994). An intercomparison of three dimensional tidal hydrodynamic models of the Irish Sea. Tellus, 46A, pp 200-221
39. Davies A.M. and Lawrence J. (1995). Modelling the effect of wave-current interaction on the three dimensional wind driven circulation on the eastern Irish Sea. Journal of Physical Oceanography, 99, pp 22665-22687
40. Davies A.M., Kwong S.C.M. and Flather R.A. (1997). Formulation of a variable function 3D model with applications to the M_2 and M_4 tide on the northwest European continental shelf. Continental Shelf Researh, 17, pp 165-204
41. Davies A.M., Jones J.E. and Xing J. (1997). Review on recent developments in tidal hydrodynamic models. I: spectral models. Journal of Hydraulic Engineering, 123, pp 278-292
42. Davies A.M., Jones J.E. and Xing J. (1997). Review on recent developments in tidal hydrodynamic models. II: turbulence energy models. Journal of Hydraulic Engineering, 123, pp 293-302
43. Davies A. and Hall P. (2000). A three dimensional model of diurnal and semidiurnal tides and tidal mixing in the North Channel of the Irish Sea. Journal of Geophysical Research, 105, pp 17079-17104
44. Danish Hydraulics Institute (1996). MIKE21 coastal hydraulics and oceanography hydrodynamic module, release 2.6
45. Dick S. and Schonfeld W. (1996). Water transport and mixing in the North Frisian Wadden Sea. Results of numerical investigations. German Journal of Hydrography, 48, pp 27-48

46. Deleersnijder E., Campin J.M. and Delhez E.J.M. (2001). The concept of age in marine modelling I: theory and preliminary model results. Journal of Marine Systems, 28, 229-267
47. Delhez E.J.M. (1996). On the residual advection of passive constituents. Journal of Marine Systems, 8, 147-169
48. Duursma E.K. and Carroll J. (1996). Environmental Compartments. Springer-Verlag, Berlin
49. Eisma D. (1981). Supply and deposition of suspended matter in the North Sea. Spec Publs int Ass Sediment, 5, pp 415-428
50. Eisma D. (1993). Suspended Matter in the Aquatic Environment. Springer-Verlag, Berlin
51. El-Ganaoui O., Schaaff E., Boyer P., Amielh M., Anselmet F. and Grenz C. (2004). The deposition and erosion of cohesive sediments determined by a multi-class model. Estuarine, Coastal and Shelf Science, 60, 457-475.
52. El-Mrabet R., Abril J.M., Manjón G. and García-Tenorio R. (2001). Experimental and modelling study of plutonium uptake by suspended matter in aquatic environments from southern Spain. Water Research, 35, pp 4184-4190
53. Elliott A.J. (1986). Shear diffusion and the spread of oil in the surface layers of the North Sea. German Journal of Hydrography, 39, pp 113-137
54. Elliott A.J. and Clarke S. (1998). Shallow water tides in the Firth of Forth. Hydrographic Journal, 87, 19-24.
55. Elliott A.J., Wilkins B.T. and Mansfield P. (2001). On the disposal of contaminated milk in coastal waters. Marine Pollution Bulletin, 42, pp 927-934
56. Estournel C., Kondrachoff V., Marsaleix P. and Vehil R. (1997). The plume of the Rhone: numerical simulation and remote sensing. Continental Shelf Research, 17, pp 899-924
57. Eyrolle F. and Charmasson S. (2001). Distribution of organic carbon, selected stable elements and artificial radionuclides among dissolved, colloidal and particulate phases in the Rhone River (France): preliminary results. Journal of Environmental Radioactivity, 55, pp 145-155
58. Eyrolle F. and Charmasson S. (2004). Importance of colloids in the transport within the dissolved phase (< 450 nm) of artificial radionuclides from the Rhone River towards the Gulf of Lions (Mediterranean Sea). Journal of Environmental Radioactivity, 72, pp 273-286
59. Falconer R.A. and Owens P.H. (1987). Numerical simulations of flooding and drying in a depth-averaged tidal flow model. Proceedings of the Institution of Civil Engineers, 83, pp 161-180
60. Flather R.A. and Heaps N.S. (1975). Tidal computations for Morecambe Bay. Geophysical Journal of the Royal Astronomical Society, 42, pp 489-517
61. Flather R.A. (1988). A numerical model investigation of tides and diurnal period continental shelf waves along Vancouver Island. Journal of Physical Oceanography, 18, pp 115-139
62. Flather R.A. (1994). A storm surge prediction model for the northern Bay of Bengal with application to the cyclone disaster in april 1991. Journal of Physical Oceanography, 24, pp 172-190
63. Gao Y., Drange H., Bentsen M. and Johannessen M. (2004). Simulating transport of non-Chernobyl ^{137}Cs and ^{90}Sr in the north Atlantic-Artic region. Journal of Environmental Radioactivity, 71, pp 1-16

64. Gomez-Gesteira M., Montero P., Prego R., Taboada J.J., Leitao P., Ruiz-Villareal M., Neves R. and Perez-Villar V. (1999). A two-dimensional particle-tracking model for pollution dispersion in A Coruña and Vigo Rias (NW Spain). Oceanologica Acta, 22, pp 167-177
65. Goshawk J.A., Clarke S., Smith C.N. and McDonald P. (2003). MEAD (Part 1)-a mathematical model of the long-term dispersion of radioactivity in shelf sea environments. Journal of Environmental Radioactivity, 68, pp 115-135
66. Hallstadius L., García-Montaño E., Nilsson U. and Boelskifte S. (1987). An improved and validated model for the North Sea and adjacent waters. Journal of Environmental Radioactivity, 5, pp 261-274
67. Harms I.H. (1997). Modelling the dispersion of ^{137}Cs and ^{239}Pu released from dumped waste in the Kara Sea. Journal of Marine Systems, 13, pp 1-19
68. Harms I.H. and Povinec P.P. (1999). The outflow of radionuclides from Novaya Zemlya bays - modeling and monitoring strategies. The Science of the Total Environment, 237/238, pp 193-201
69. Harms I.H., Karcher M.J. and Dethleff D. (2000). Modelling Siberian river runoff - implications for contaminant transport in the Artic Ocean. Journal of Marine Systems, 27, pp 95-115
70. Hazel D.R. and England M.H. (2003). Prediction of the fate of radioactive material in the south Pacific Ocean using a global high resolution ocean model. Journal of Environmental Radioactivity, 65, pp 329-355
71. Holt J.T. and James I.D. (1999). A simulation of the southern North Sea in comparison with measurements from the North Sea Project. Part 2: suspended particulate matter. Continental Shelf Research, 19, pp 1617-1642
72. Holt J.T. and Proctor R. (2001). Dispersion in shallow seas. Encyclopedia of Ocean Sciences, Academic Press, San Diego, pp 742-747
73. Hunter J.R. (1987). The application of lagrangian particle tracking techniques to modelling of dispersion in the sea. In: Numerical Modelling. Applications to Marine Systems. J. Noye (editor). Elsevier, North-Holland, pp 257-269
74. IAEA (1985). Sediment k_d and concentration factors for radionuclides in the marine environment. Technical Report Series, 247, Vienna
75. Iosjpe M., Brown J. and Strand P. (2002). A modified approach for box modelling of radiological consequences from releases into the marine environment. Journal of Environmental Radioactivity, 60, pp 91-103
76. Jensen T.G. (1998). Open boundary conditions in stratified ocean models. Journal of Marine Systems, 16, 297-322
77. Jiang W., Pohlmann T., Sundermann J. and Feng S. (2000). A modelling study of SPM transport in the Bohai Sea. Journal of Marine Systems, 24, pp 175-200
78. Jones J.E. (2002). Coastal and shelf sea modelling in the European context. Oceanography and Marine Biology: an Annual Review, 40, pp 37-141
79. Jones J.E. and Davies A.M. (1996). A high resolution three dimensional model of the M_2, M_4, M_6, S_2, N_2, K_1 and O_1 tides in the eastern Irish Sea. Estuarine Coastal Shelf Science, 42, pp 311-346
80. Karcher M.J., Gerland S., Harms I., Iosjpe M., Heldal H.E., Kershaw P.J. and Sickel M. (2004). The dispersion of ^{99}Tc in the Nordic Seas and the Artic Ocean: a comparison of model results and observations. Journal of Environmental Radioactivity, 74, pp 185-198
81. Kim D., Nakada N., Horiguchi T., Takada H., Shiraishi H. and Nakasugi O. (2004). Numerical simulation of organic chemicals in a marine environment

using a coupled 3D hydrodynamic and ecotoxicological model. Marine Pollution Bulletin, 48, pp 671-678
82. Kobayashi T., Nagai H., Chino M. and Togawa O. (2004). Development of SPEEDI-MP and its application to a hypothetical accident of a nuclear submarine at the Japan Sea. In: J. Inaba, H. Tsukada and A. Takeda (editors), Radioecology and Environmental Dosimetry. Institute of Environmental Sciences, Japan, pp 500-504
83. Kondrachoff V., Estournel C., Marsaleix P. and Vehil R. (1994). Detection of the Rhone River plume using NOAA-AVHRR data. Comparison with hydrodynamic modeling results. Oceanic Remote Sensing and Sea Ice Monitoring, 2319, pp 73-84
84. Kowalick Z. and Murty T.S. (1993). Numerical Modelling of Ocean Dynamics. World Scientific, Singapore
85. Koziy L., Maderich V., Margvelashvily N. and Zheleznyak M. (1998). Three dimensional model of radionuclide dispersion in estuaries and shelf seas. Environmental Modelling and Software, 13, pp 413-420
86. Laissaoui A., Abril J.M., Periáñez R., García-León M. and García-Montaño E. (1998). Determining kinetic transfer coefficients for radionuclides in estuarine waters: reference values for ^{133}Ba and effects of salinity and suspended load concentrations. Journal of Radioanalytical Nuclear Chemistry, 237, pp 55-61
87. Lazar A. and Rancher J. (1999). Simulation of radionuclide dispersion in the Pacific Ocean from Mururoa Atoll. Journal of Environmental Radioactivity, 43, pp 31-49
88. Li Y.H., Burkhardt L., Buchholtz M., O'Hara P. and Santschi P.H. (1984). Partition of radiotracers between suspended particles and seawater. Geochimica and Cosmochimica Acta, 48, pp 2011-2019
89. Liu Y.P., Millward G.E. and Harris J.R.W. (1998). Modelling the distributions of dissolved Zn and Ni in the Tamar estuary using hydrodynamics coupled with chemical kinetics. Estuarine, Coastal and shelf Science 47, 535-546.
90. Liu W.C., Hsu M.H. and Kuo A.Y. (2002). Modelling of hydrodynamics and cohesive sediment transport in Tanshui River estuarine system, Taiwan. Marine Pollution Bulletin, 44, pp 1076-1088
91. Liu J.T., Chao S. and Hsu R.T. (2002). Numerical modeling study of sediment dispersal by a river plume. Continental Shelf Research, 22, pp 1745-1773
92. Lumborg U. and Windelin A. (2003). Hydrography and cohesive sediment modelling: application to the Romo Dyb tidal area. Journal of Marine Systems, 38, pp 287-303
93. Mañanes R., Bruno M., Alonso J., Fraguela B. and Tejedor L. (1998). Nonlinear interaction between tidal and subinertial barotropic flows in the Strait of Gibraltar. Oceanologica Acta, 21, pp 33-46
94. Margvelashvily N., Maderich V. and Zheleznyak, M. (1997). Threetox: A computer code to simulate three dimensional dispersion of radionuclides in stratified water bodies. Radiation Protection Dosimetry, 73, pp 177-180
95. Margvelashvily N., Maderich V. and Zheleznyak M. (1999). Simulation of radionuclide fluxes from the Dnieper-Bug estuary into the Black Sea. Journal of Environmental Radioactivity, 43, pp 157-171
96. Marsaleix P., Estournel C., Kondrachoff V. and Vehil R. (1998). A numerical study of the formation of the Rhone River plume. Journal of Marine Systems, 14, pp 99-115

97. Martin J.M. and Thomas A.J. (1990). Origins, concentrations and distributions of artificial radionuclides discharged by the Rhone River to the Mediterranean Sea. Journal of Environmental Radioactivity, 11, pp 105-139
98. Martínez-Aguirre A., García-León M., Gascó C. and Travesi A. (1996). Anthropogenic emissions of ^{210}Po, ^{210}Pb, and ^{226}Ra in an estuarine environment. Journal of Radioanalytical Nuclear Chemistry, 207, pp 357-367
99. Massel S.R. (1999). Fluid Mechanics for Marine Ecologists. Springer-Verlag, Berlin
100. McKay W.A. and Pattenden N.J. (1993). The behaviour of plutonium and americium in the shoreline waters of the Irish Sea: a review of Harwell studies in the 1980s. Journal of Environmental Radioactivity, 18, pp 99-132
101. Mittelstaedt E., Osvath I., Povinec P.P., Togawa O. and Scott E.M. (1999). Transport of radionuclides from the Mururoa and Fangataufa atolls through the marine environment. The Science of the Total Environment, 237/238, pp 301-309
102. Nakano M. and Povinec P. (2003). Oceanic general circulation model for the assessment of the distribution of ^{137}Cs in the world ocean. Deep Sea Research II, 50, pp 2803-2816
103. Nakano M. and Povinec P. (2003). Modelling the distribution of plutonium in the Pacific Ocean. Journal of Environmental Radioactivity, 69, pp 85-106
104. Naudin J.J., Cauwet G., Fajon C., Oriol L., Terzic S., Devenon J.L. and Broche P. (2001). Effect of mixing on microbial communities in the Rhone River plume. Journal of Marine Systems, 28, 203-227
105. Ng B., Turner A., Tyler A.O., Falconer R.A. and Millward G.E. (1996). Modelling contaminant geochemistry in estuaries. Water Research, 30, pp 63-74
106. Nicholson J. and O'Connor B.A. (1986). Cohesive sediment transport model. Journal of Hydraulic Engineering, 112, pp 621-640
107. Nielsen S.P. (1995). A box model for North-East Atlantic coastal waters compared with radioactive tracers. Journal of Marine Systems, 6, pp 545-560
108. Nielsen S.P., Iosjpe M. and Strand P. (1997). Collective doses to man from dumping of radioactive waste in the Arctic Seas. The Science of the Total Environment, 202, pp 135-146
109. Nyffeler U.P., Li Y.H. and Santschi P.H. (1984). A kinetic approach to describe trace element distribution between particles and solution in natural aquatic systems. Geochimica Cosmochimica Acta, 48, pp 1513-1522
110. Okubo A. (1971). Oceanic diffusion diagrams. Deep Sea Research, 18, pp 789-802
111. Orlanski I. (1976). A simple boundary condition for unbounded hyperbolic flows. Journal of Computational Physics, 21, pp 255-261
112. Oughton D.H., Børretzen P., Salbu B. and Tronstad E. (1997). Mobilisation of ^{137}Cs and ^{90}Sr from sediments: potential sources to artic waters. The Science of the Total Environment, 202, pp 155-165
113. Periáñez R. and García-León M. (1993). Ra-isotopes around a phosphate fertilizer complex in an estuarine system at the southwest of Spain. Journal of Radioanalytical Nuclear Chemistry, 172, pp 71-79
114. Periáñez R., Abril J.M. and García-León M. (1994). A modelling study of ^{226}Ra dispersion in an estuarine system in southwest Spain. Journal of Environmental Radioactivity, 24, pp 159-179

115. Periáñez R., Abril J.M. and García-León M. (1996). Modelling the dispersion of non conservative radionuclides in tidal waters. Part 1: conceptual and mathematical model. Journal of Environmental Radioactivity, 31, pp 127-141
116. Periáñez R., Abril J.M. and García-León M. (1996). Modelling the suspended matter distribution in an estuarine system: application to the Odiel river in southwest Spain. Ecological Modelling, 87, pp 169-179
117. Periáñez R., Abril J.M. and García-León M. (1996). Modelling the dispersion of non conservative radionuclides in tidal waters. Part 2: application to ^{226}Ra dispersion in an estuarine system. Journal of Environmental Radioactivity, 31, pp 253-272
118. Periáñez R. and Martínez-Aguirre A. (1997). Uranium and thorium concentrations in an estuary affected by phosphate fertilizer processing: experimental results and a modelling study. Journal of Environmental Radioactivity, 35, pp 281-304
119. Periáñez R. (1998). Three-dimensional modelling of the tide induced dispersion of radionuclides in the Sea. Journal of Environmental Radioactivity, 40, pp 215-237
120. Periáñez R. (1998). A three dimensional σ coordinate model to simulate the dispersion of radionuclides in the marine environment. Ecological Modelling, 114, 59-70
121. Periáñez R. (1999). Three dimensional modelling of the tidal dispersion of non conservative radionuclides in the marine environment: application to ^{239,240}Pu dispersion in the eastern Irish Sea. Journal of Marine Systems, 22, 37-51
122. Periáñez R. and Reguera J. (1999). A numerical model to simulate the tidal dispersion of radionuclides in the English Channel. Journal of Environmental Radioactivity, 43, pp 51-64
123. Periáñez R. (2000). Modelling the tidal dispersion of ^{137}Cs and ^{239,240}Pu in the English Channel. Journal of Environmental Radioactivity, 49, pp 259-277
124. Periáñez R. (2000). Modelling the physico-chemical speciation of plutonium in the eastern Irish Sea. Journal of Environmental Radioactivity, 49, pp 11-33
125. Periáñez R. and Elliott A.J. (2002). A particle tracking method for simulating the dispersion of non-conservative radionuclides in coastal waters. Journal of Environmental Radioactivity, 58, pp 13-33
126. Periáñez R. (2002). Modelling the physico-chemical speciation of plutonium in the eastern Irish Sea: a further development. Journal of Environmental Radioactivity, 62, pp 263-276
127. Periáñez R. (2002). The enhancement of ^{226}Ra in a tidal estuary due to the operation of fertilizer factories and redissolution from sediments: experimental results and a modelling study. Estuarine, Coastal and Shelf Science, 54, pp 809-819
128. Periáñez R. (2002). Modelling the suspended matter dynamics in a marine environment using a three dimensional σ coordinate model: application to the eastern Irish Sea. Applied Mathematical Modelling, 26, pp 583-601
129. Periáñez R. (2003). Kinetic modelling of the dispersion of plutonium in the eastern Irish Sea: two approaches. Journal of Marine Systems, 38, pp 259-275
130. Periáñez R. (2003). Redissolution and long term transport of radionuclides released from a contaminated sediment: a numerical modelling study. Estuarine, Coastal and Shelf Science, 56, pp 5-14

131. Periáñez R. (2004). Testing the behaviour of different kinetic models for uptake/release of radionuclides between water and sediments when implemented in a marine dispersion model. Journal of Environmental Radioactivity, 71, pp 243-259
132. Periáñez R. (2004). The dispersion of ^{137}Cs and ^{239,240}Pu in the Rhone River plume: a numerical model. Journal of Environmental Radioactivity, 77, pp 301-324
133. Periáñez R. (2004). A particle-tracking model for simulating pollutant dispersion in the Strait of Gibraltar. Marine Pollution Bulletin, 49, pp 613-623
134. Periáñez R. (2004). On the sensitivity of a marine dispersion model to parameters describing the transfers of radionuclides between the liquid and solid phases. Journal of Environmental Radioactivity, 73, pp 101-115
135. Periáñez R. (2005). Modelling the transport of suspended particulate matter by the Rhone River plume (France). Implications for pollutant dispersion. Environmental Pollution, 133, pp 351-364
136. Periáñez R., Absi A., Villa M., Moreno H.P. and Manjón G. (in press). Self-cleaning in an estuarine area formerly affected by ^{226}Ra anthropogenic discharges: numerical simulations. Science of the Total Environment
137. Piasecki M. (1998). Transport of radionuclides incorporating cohesive/non cohesive sediments. Journal of Marine Environmental Engineering, 4, 331-365
138. Postma H. (1980). Sediment transport and sedimentation. In: E. Olausson and I. Cato (editors), Chemistry and Biogeochemistry of Estuaries. Wiley, New York, pp 153-186
139. Prandle D. (1975). Storm surges in the southern North Sea and River Thames. Proceedings of the Royal Society of London, A344, pp 509-539
140. Prandle D. (1984). A modelling study of the mixing of ^{137}Cs in the seas of the European continental shelf. Philosophical Transactions of the Royal Society, London, A310, pp 407-436
141. Prandle D. (1997). Tidal characteristics of suspended sediments concentrations. Journal of Hydraulic Engineering, 123, pp 341-350
142. Prandle D., Jago C.F., Jones S.E., Purdie D.A. and Tappin A. (1993). The influence of horizontal circulation on the supply and distributions of tracers. Philosophical Transactions of the Royal Society, London, A343, pp 405-421
143. Prandle D., Hargreaves J.C., McManus J.P., Campbell A.R., Duwe K., Lane A., Mahnke P., Shimwell S. and Wolf J. (2000). Tide, wave and suspended sediment modelling on an open coast, Holderness. Coastal Engineering, 41, pp 237-267
144. Preller R.H. and Cheng A.B. (1999). Modeling the transport of radioactive contaminants in the Artic. Marine Pollution Bulletin, 38, pp 71-91
145. Proctor R., Flather R.A. and Elliott A.J. (1994). Modelling tides and surface drift in the Arabian Gulf: application to the Gulf oil spill. Continental Shelf Research, 14, pp 531-545
146. Proctor R., Elliott A.J. and Flather R.A. (1994). Forecast and hindcast simulations of the Braer oil spill. Marine Pollution Bulletin, 28, pp 219-229
147. Pugh D.T. (1987). Tides, Surges and Mean Sea Level. Wiley, Chichester
148. Radakovitch O., Charmasson S., Arnaud M. and Bouisset P. (1999). ^{210}Pb and caesium accumulation in the Rhone Delta sediments. Estuarine, Coastal and Shelf Science, 48, pp 77-92
149. Riddle A.M. (1998). The specification of mixing in random walk models for dispersion in the sea. Continental Shelf Research, 18, pp 441-456

150. Ruddick K.G., Deleersnijder E., Luyten P.J. and Ozer J. (1995). Haline stratification in the Rhine-Meuse freshwater plume: a three dimensional model sensitivity analysis. Continental Shelf Research, 15, pp 1597-1630
151. Salomon J.C., Breton M. and Guegueniat P. (1995). A 2D long term advection dispersion model for the Channel and southern North Sea. Part B: transit time and transfer function from Cap de La Hague. Journal of Marine Systems, 6, pp 515-527
152. Sanchez-Cabeza J.A., Ortega M., Merino J. and Masque P. (2002). Long-term box modelling of ^{137}Cs in the Mediterranean Sea. Journal of Marine Systems, 33, pp 457-472
153. Schonfeld W. (1995). Numerical simulation of the dispersion of artificial radionuclides in the English Channel and the North Sea. Journal of Marine Systems, 6, pp 529-544
154. Scott E.M. (2003). Modelling Radioactivity in the Environment. Elsevier, Amsterdam
155. Segschneider J. and Sundermann J. (1998). Simulating large scale transport of suspended matter. Journal of Marine Systems, 14, pp 81-97
156. Shen J. and Haas L. (2004). Calculating age and residence time in the tidal York River using three dimensional model experiments. Estuarine, Coastal and Shelf Science, 61, pp 449-461
157. Smith C.N., Goshawk J.A., Charles K., McDonald P., Leonard K. and McCubbin D. (2003). MEAD (part 2)-Predictions of radioactivity concentrations in the Irish Sea. Journal of Environmental Radioactivity, 68, pp 193-241
158. Stanev E.V., Buesseler K.O., Staneva J.V. and Livingston H.D. (1999). A comparison of modelled and measured Chernobyl ^{90}Sr distributions in the Black Sea. Journal of Environmental Radioactivity, 43, pp 187-203
159. Stelling G.S., Wiersma A.K. and Willemse J.B.T.M. (1986). Practical aspects of accurate tidal computations. Journal of Hydraulic Engineering, 112, pp 802-817
160. Stelling G.S. and J.A.M. van Kester (1994). On the approximation of horizontal gradients in sigma coordinates for bathymetry with steep bottom slopes. International Journal for Numerical Methods in Fluids, 18, pp 915-935
161. Tappin A.D., Burton J.D., Millward G.E. and Statham P.J. (1997). A numerical transport model for predicting the distributions of Cd, Cu, Ni, Pb and Zn in the southern North Sea: the sensitivity of model results to the uncertainties in the magnitudes of metal inputs. Journal of Marine Systems, 13, pp 173-204
162. Tattersall G.R., Elliott A.J. and Lynn N.M. (2003). Suspended sediment concentrations in the Tamar estuary. Estuarine, Coastal and Shelf Science, 57, pp 679-688
163. Tejedor L., Izquierdo A., Kagan B.A. and Sein D.V. (1999). Simulation of the semidiurnal tides in the Strait of Gibraltar. Journal of Geophysical Research, 104, 13541-13557
164. Thiessen K.M., Thorne M.C., Maul P.R., Prohl G. and Wheater H.S. (1999). Modelling radionuclide distribution and transport in the environment. Environmental Pollution, 100, pp 151-177
165. Thill A., Moustier S., Garnier J.M., Estournel C., Naudin J.J. and Bottero J.Y., (2001). Evolution of particle size and concentration in the Rhone River mixing zone: influence of salt flocculation. Continental Shelf Research, 21, pp 2127-2140

166. Thomas A.J. (1997). Input of artificial radionuclides to the Gulf of Lions and tracing the Rhone influence in marine surface sediments. Deep Sea Research II, 44, pp 577-595
167. Tsimplis M.N., Proctor R. and Flather R.A. (1995). A two dimensional tidal model for the Mediterranean Sea. Journal of Geosphysical Research, 100, pp 16223-16239
168. Tsimplis M.N. and Bryden H.L. (2000). Estimations of the transports through the Strait of Gibraltar. Deep Sea Research, 47, pp 2219-2242
169. Tsumune D., Aoyama M. and Hirose K. (2003). Numerical simulation of ^{137}Cs and ^{239,240}Pu concentrations by an ocean general circulation model. Journal of Environmental Radioactivity, 69, pp 61-84
170. Turner A. and Millward, G.E. (1994). Partitioning of trace metals in a macrotidal estuary. Implications for contaminant transport models. Estuarine, Coastal and Shelf Science, 39, pp 45-58
171. Vested H.J., Baretta J.W., Ekebjærg L.C. and Labrosse A. (1996). Coupling of hydrodynamical transport and ecological models for 2D horizontal flow. Journal of Marine Systems, 8, pp 255-267
172. Vreugdenhil C.B. (1998). Numerical Methods for Shallow Water Flows. Kluwer, The Netherlands
173. Whicker F.W., Shaw G., Voigt G. and Holm E. (1999). Radioactive contamination: state of the science and its application to predictive models. Environmental Pollution, 100, pp 133-149
174. Williams J.J., Humphery J.D., Hardcastle P.J. and Wilson D.J. (1998). Field observations of hydrodynamic conditions and suspended particulate matter in the southern North Sea. Continental Shelf Research, 18, 1215-1233
175. Wu Y., Falconer R.A. and Uncles R.J. (1998). Modelling of water flows and cohesive sediment fluxes in the Humber Estuary, UK. Marine Pollution Bulletin, 37, 182-189
176. Xing J. and Davies A. (1999). The effect of wind direction and mixing upon the spreading of a bouyant plume in a non-tidal regime. Continental Shelf Research, 19, pp 1437-1483

Index